



Superior Implant Technology

SCIENTIFIC DOSSIER 2016

Published: 08 February 2016 in:

SCIENTIFIC REPORTS

01

Novel Osteogenic Ti-6Al-4V Device
For Restoration Of Dental Function
In Patients With Large Bone
Deficiencies: Design, Development
And Implementation

D. J. Cohen, A. Cheng, A. Kahn, M. Aviram, A. J.
Whitehead, S. L. Hyzy, R. M. Clohessy, B. D. Boyan
& Z. Schwartz



Superior Implant Technology

SCIENTIFIC REPORTS

OPEN

Novel Osteogenic Ti-6Al-4V Device For Restoration Of Dental Function In Patients With Large Bone Deficiencies: Design, Development And Implementation

Received: 22 September 2015

Accepted: 05 January 2016

Published: 08 February 2016

D. J. Cohen¹, A. Cheng^{2,3}, A. Kahn⁴, M. Aviram⁵, A. J. Whitehead¹, S. L. Hyzy¹, R. M. Clohessy¹, B. D. Boyan^{1,2} & Z. Schwartz^{1,6}

Custom devices supporting bone regeneration and implant placement are needed for edentulous patients with large mandibular deficiencies where endosteal implantation is not possible. We developed a novel subperiosteal titanium-aluminum-vanadium bone onlay device produced by additive manufacturing (AM) and post-fabrication osteogenic micro-/nano-scale surface texture modification. Human osteoblasts produced osteogenic and angiogenic factors when grown on laser-sintered nano-/micro-textured surfaces compared to smooth surfaces. Surface-processed constructs caused higher bone-to-implant contact, vertical bone growth into disk pores (microCT and histomorphometry), and mechanical pull-out force at 5 and 10 w on rat calvaria compared to non surface-modified constructs, even when pre-treating the bone to stimulate osteogenesis. Surface-modified wrap-implants placed around rabbit tibias osseointegrated by 6 w. Finally, patient-specific constructs designed to support dental implants produced via AM and surface-processing were implanted on edentulous mandibular bone. 3 and 8 month post-operative images showed new bone formation and osseointegration of the device and indicated stability of the dental implants.

Currently, 23% of American adults over the age of 65 are completely edentulous¹, and 37.9 million adults in the United States will have no natural teeth by 2020. Although the number of edentulous adults is expected to decrease by 10%, this is overshadowed by the 79% increase in the adult population over the age of 55². Implant supported dentures significantly improve the quality of life in comparison to removable dentures³, but many of these individuals have significant bone loss, which may be unsuitable for implant placement.

A number of strategies have been used to enable implant placement when there is insufficient bone to provide stability for individual implants. Subperiosteal implants that follow the contours of the bony ridge of the jaw have had low success rates due to their failure to osseointegrate with the bone⁴. Approaches using dentures, partial dentures, or an implant supported bridge can provide a compromise solution to restore functional dentition. In many cases, a bone regeneration strategy using various bone graft materials is used to restore bone volume prior to the placement of the implant. This requires an additional procedure, in some cases involving the use of a membrane to guide the regenerating tissues, and complications may result^{5,6}. However, in some cases, treatment using current options is not possible, particularly when the mental nerve is exposed. In these situations, a patient-specific strategy that stimulates bone regeneration to restore ridge height, protect any exposed nerve, and stabilize the device via osseointegration is needed in order to provide adequate support for rehabilitation of the dentition.

¹Department of Biomedical Engineering, Virginia Commonwealth University, Richmond, VA, U.S.A. ²Wallace H. Coulter Department of Biomedical Engineering, Georgia Institute of Technology and Emory University, Atlanta, GA, U.S.A. ³Department of Biomedical Engineering, Peking University, Beijing, China. ⁴Department of Oral and Maxillofacial Surgery, Tel Aviv University, Tel Aviv, Israel. ⁵Tipul Behiuch Private Clinic, Tel Aviv, Israel. ⁶Department of Periodontics, University of Texas Health Science Center at San Antonio, San Antonio, TX, U.S.A. Correspondence and requests for materials should be addressed to B.D.B. (email: bboyman@vcu.edu)

Our approach was to develop a one-step custom device that could be placed subperiosteally on the bone surface and by its osteogenic surface properties generate new bone, thereby becoming osseointegrated. Additive manufacturing (AM) provides a powerful method for fabricating three-dimensional (3D) metal devices based on computerized tomography (CT) of individual patients, enabling optimal fit between the implant and the contours of the patient's existing bone. To address the goal of stimulating sufficient new bone to stabilize the device via osseointegration and ultimately to support reconstruction of the dentition, we took advantage of *in vitro* and *in vivo* observations using solid titanium (Ti) and titanium-aluminum-vanadium (Ti-6Al-4V) implants manufactured via conventional machining technology followed by grit blasting and acid etching. These studies showed that osteoblast differentiation and maturation were increased when osteoprogenitor cells were cultured on surfaces with microscale and nanoscale roughness compared to smooth surfaces^{7–10}. Moreover, preclinical and clinical studies showed that peri-implant osteogenesis was enhanced when the surface had microscale and nanoscale roughness^{11–15}. Similarly, microscale roughness on 3D nanofiber mesh surfaces supported greater osteoblastic differentiation of human mesenchymal stem cells (MSCs) *in vitro*¹⁶.

Recently, we showed that 3D Ti-6Al-4V constructs could be generated by AM and then processed via grit blasting and acid etching to have microscale and nanoscale roughness¹⁷. Osteoblast-like MG63 cells exhibited differentiation in a porosity and surface-roughness dependent manner when cultured on these constructs with hierarchical surface roughness. Taken together with previous studies using conventionally manufactured Ti and Ti-6Al-4V disks and implants described above, these results suggested that a micro-/nano-textured device could be designed that would stimulate bone regeneration sufficient to support rehabilitation of the dentition in an edentulous patient.

We used a step-wise approach to test this hypothesis (Fig. S1). To verify that osteoblast differentiation was sensitive to surface micro-/nano-topography, we assessed the response of normal human osteoblasts (NHOst cells) to the surface of surface modified Ti-6Al-4V constructs as a function of osteogenic factor production. A rat cranial bone onlay model was used to analyze osseointegration of implants with a macroporous design to enhance osseointegration. We tested device osseointegration using several clinical scenarios involving pre-treatment of the calvarial bone to stimulate osteogenesis, including decalcification of the bone surface and use of a demineralized bone matrix putty (DBX). Next, implant osseointegration of surface-processed AM-fabricated custom wrap implants in a rabbit tibial bone onlay model was examined. Finally, two clinical case studies are presented that highlight the use of customized devices produced via AM and post-fabrication surface modification in edentulous patients. 3D Ti-6Al-4V constructs were fabricated by laser sintering based on computed tomography (CT) scans of the patients' mandibles and processed to create micro-/nano-textured surfaces. Follow-up radiographs at 3 and 8 months post-surgery demonstrate the successful osseointegration of the device and support of dental implants.

Results

Osteoblast response was enhanced on laser-sintered constructs with microscale and nanoscale surface roughness. We previously showed that additive manufacturing via laser sintering could be used to fabricate solid Ti-6Al-4V disks¹⁷. After modifying the surface by grit blasting and acid etching, the resulting texture had both microscale and nanoscale roughness, and was hydrophilic. We continued using these manufacturing and post-processing methods to create materials for this study.

We first examined the response of normal human osteoblasts (NHOst cells) to the surface using 2D Ti-6Al-4V disks that were produced by laser sintering using the same methods as previously described¹⁷. The Ti-6Al-4V disks had one of two surface topographies: polished surfaces had a relatively smooth micro- and nano-topography (LST-M) (Fig. 1A) compared to grit blasted and acid etched surfaces (LST-BE), which possessed both micro- and nano-roughness (Fig. 1B). More NHOst cells were present on the LST-BE surfaces based on DNA content of the cultures (Fig. 1C), but cultures on LST-BE had lower alkaline phosphatase specific activity (Fig. 1D) than cells grown on LST-M surfaces. Cells on the rougher LST-BE surfaces produced more osteocalcin (Fig. 1E), bone morphogenetic protein 2 (BMP2) (Fig. 1F), and vascular endothelial growth factor A (VEGF-A) (Fig. 1G) than NHOst cells on LST-M.

Surface treatment of calvaria did not affect bone growth into porous constructs. An initial rat cranial bone onlay study was performed to determine if osseointegration of the device would be enhanced by inclusion of through pores to facilitate migration of host osteoprogenitor cells and to increase surface area to allow for vertical bone growth from the calvarial surface through the implant. 5 mm diameter disks with twelve 0.5 mm diameter holes were laser sintered followed by grit blasting and acid etching in the manner previously described¹⁷. Clinically, etching treatments may be used on bone prior to implant placement to increase surface area, expose more bone morphogenetic protein stored in the extracellular matrix, and increase the availability of mesenchymal cells for improved osseointegration^{18,19}. Therefore, we also assessed whether pretreatment of the calvarial bone by etching would alter the extent of new bone formation. We treated male Sprague-Dawley rat calvarial bone surfaces prior to implant placement with one of two methods and examined osseointegration at 5 and 10 weeks. After elevating the periosteum, the calvarial bone cortex was perforated 15–20 times with a dental burr to expose bone marrow derived stem cells to the implant, as would be done clinically. Calvaria (6 rats per treatment group) were treated with 24% ethylene diamine tetra acetic acid (EDTA), 37% phosphoric acid, or were left untreated after perforation. The disks were then secured to the underlying bone by approximating the periosteum to the implant via resorbable suture (Fig. S2a).

MicroCT analysis revealed that the pores did improve osseointegration, but pre-treatment of the calvaria had no effect. Bone-to-implant contact (Fig. S2B) and bone in-growth (Fig. S2C) in the disk pores were not significantly different across groups at both 5 and 10 weeks after implantation. Histology supported the microCT observations at 5 and 10 weeks (Fig. S2D). Interestingly, implants were not only osseointegrated with the calvaria, but

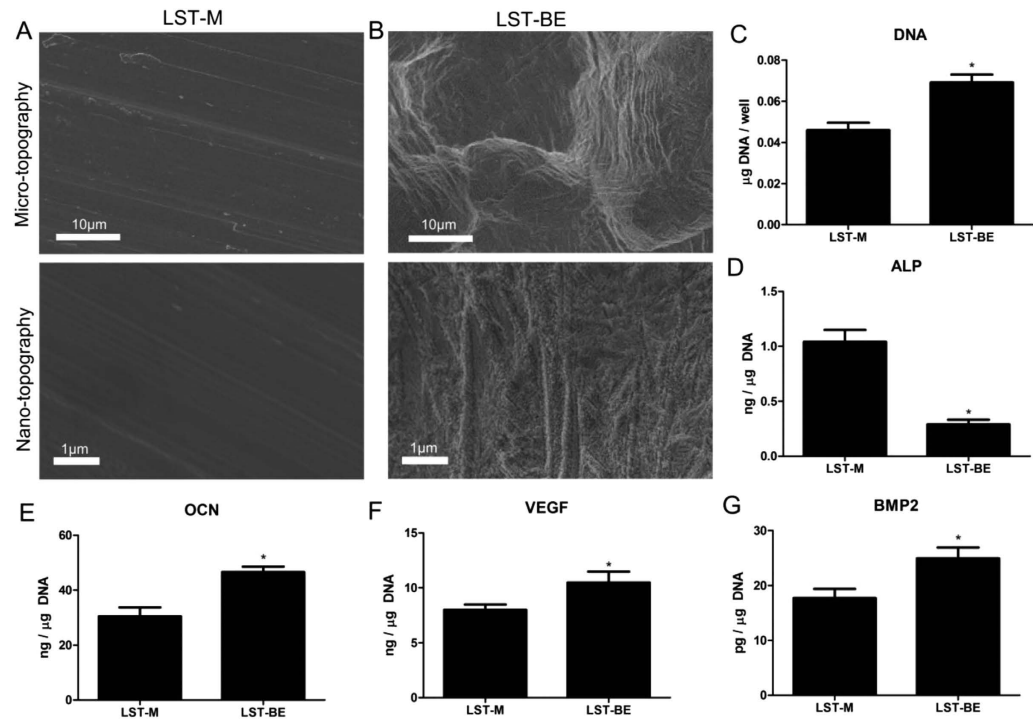


Figure 1. Cellular response to laser sintered disks with smooth or rough surfaces. Laser sintered surfaces were polished (A) or treated by blasting with calcium phosphate particles and subsequent acid etching (B) that resulted in combined micro- (top) and nano-roughness (bottom). DNA content (C), osteocalcin (D), osteoprotegerin (E), VEGF (F), and BMP2 (G) production by NHOst cells seeded on disks. Student's t-test, $p < 0.05$, *vs. LST-M.

new bone nodules were observed growing through the pores. Bone-to-implant contact determined by histomorphometry (Fig. S2E) confirmed the microCT results. Bone in-growth analyzed histomorphometrically (Fig. S2F) was higher than the microCT values, but the results still did not identify differences among treatment groups. Because analysis via microCT and histology showed no significant differences between calvarial bone growth into implants with pre-implantation treatment, no treatment was used for future studies.

Calvarial bone formation in constructs was increased in the presence of demineralized bone matrix. Demineralized bone matrix (DBM) is commonly used in clinical cases where bone regeneration is needed prior to implant placement. To determine whether inclusion of DBM would impact the osteogenic capacity of the implant design, we compared bone formation using laser sintered disks in the presence and absence of human DBM putty in hyaluronic acid (DBX®, Musculoskeletal Transplant Foundation, Edison, NJ). For these experiments, the disks were treated by grit blasting and acid etching to have the microscale and nanoscale roughness as well as the hydrophilicity described above. After elevating the periosteum, the calvarial bone cortex was perforated using a dental bur. In one-half of the athymic nude rats, the calvarial bone surface was coated with DBX prior to implant placement. After placing these implants, the implant surface was also coated with DBX. The periosteum and skin were then restored.

At 2, 4, and 10 weeks post-operatively, microCT cross-sectional analysis of the entire implant was performed to assess bone-to-implant contact and bone ingrowth in holes (Fig. 2A). Bone-to-implant contact analyzed by microCT was not significantly different between untreated and DBX-treated calvaria at 2 and 5 weeks, but DBX-treated sites had significantly higher bone-to-implant contact at 10 weeks when compared to both non-treated and DBX-treated sites at all time points (Fig. 2B). Bone in growth in implants holes supported the microCT observations, with DBX-treated sites also having a higher percent age of bone in-growth at 10 weeks when compared to non-treated and DBX-treated sites at all of the time points (Fig. 2C). Top down microCT images also confirmed bone growth into implant pores (Fig. 2D). Bone-to-implant contact determined histologically was increased in DBX-treated sites at 10 weeks compared to both non-treated and DBX-treated sites at 2 weeks (Fig. 2E). Percent bone in-growth in holes was increased in DBX-treated sites at 10 weeks compared to non-treated and DBX-treated sites at 2 weeks, and DBX-treated sites at 5 weeks (Fig. 2F). Histological sections (Fig. 2G) revealed bone growth from the bottom of non-treated sites while bone growth was achieved from both the bottom and the top of DBX-treated sites.

Surface roughness and DBX enhanced mechanical integration of bone with porous implants. To further analyze the effects of surface roughness and DBX-treatment on implant osseointegration, mechanical testing was conducted. For these experiments, the laser sintered disks were treated by grit

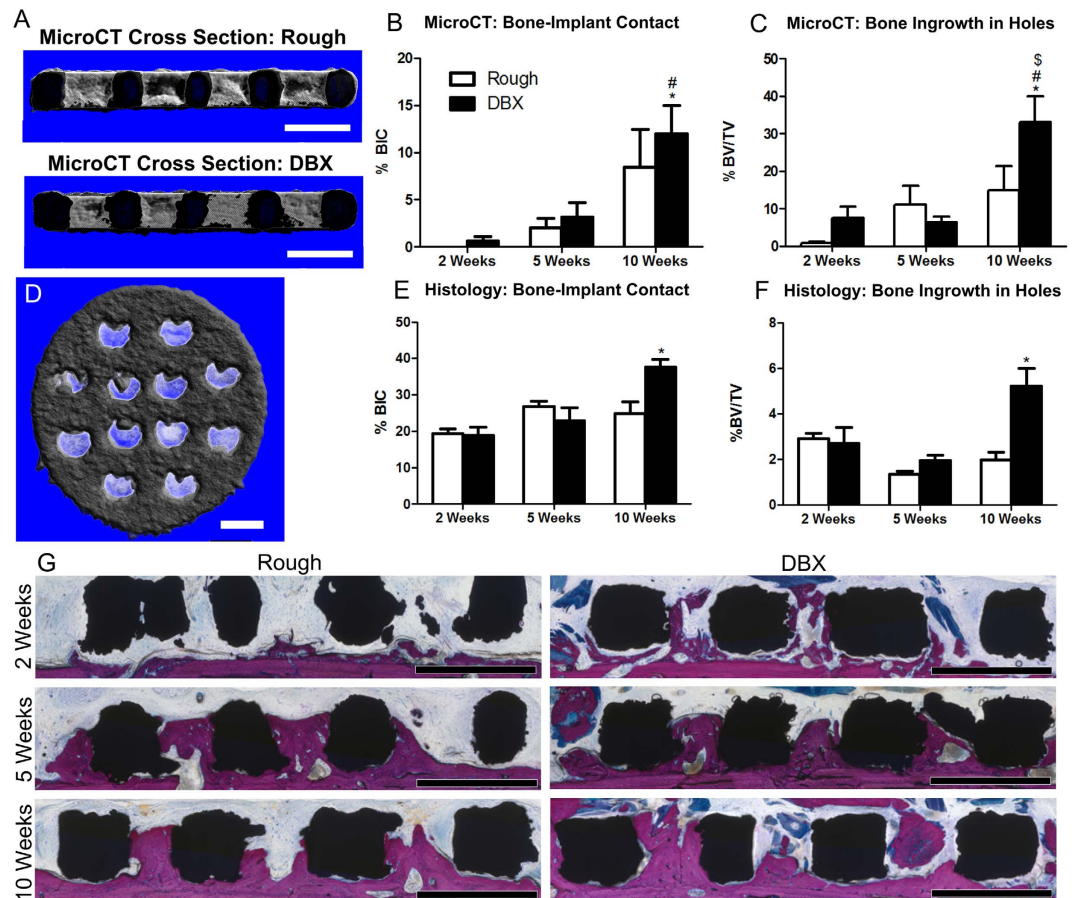


Figure 2. The effect of demineralized bone matrix on bone growth into porous disks. Disks were implanted on calvaria of athymic nude rats with and without DBX, and bone-to-implant contact was assessed after 2, 5, and 10 weeks. MicroCT cross-sectional images show sintered disks ((A), rough) implanted on calvaria of rats without ((A), rough) or with ((A), DBX) demineralized bone matrix after 10 weeks, which black indicating the implant and white indicating new bone formation. These images were analyzed for bone-to-implant contact (B) and bone ingrowth in holes (C). MicroCT top down images, thresholded to remove underlying calvaria, revealed new bone growth into pores of the disk (D). Histomorphometric analysis was conducted per implant to evaluate bone-to-implant contact (E) and bone ingrowth in holes (F). Histological images depict bone growth along sides of disk pores for both groups (G). MicroCT and histological image scale bars represent 1 mm. One-way ANOVA with Bonferroni analysis, $p < 0.05$, * vs. all groups (B,C), * vs. 2 week rough, # vs. 2 week DBX, \$ vs. 5 week DBX (E,F).

blasting and acid etching to have the microscale and nanoscale roughness as well as the hydrophilicity described above. A second set of disks was polished, producing a smooth surface. Unlike all other disks and implants used in this study, which were sterilized by gamma radiation, the polished disks were sterilized by autoclaving. Laser confocal analysis revealed significantly higher surface roughness and peak-to-valley height on rough surfaces compared to smooth surfaces (Fig. 3A). Smooth or rough implants were produced with an arch for mechanical testing (Fig. 3B). Smooth, rough or rough implants treated with DBX were placed on athymic nude rat calvaria, and microCT analysis was performed at 10 weeks.

Although bone-to-implant contact (Fig. 3C) was not significantly different across groups, bone in-growth in implant holes (Fig. 3D) was significantly increased for rough implants with DBX compared to smooth and rough implants alone. Electron and optical images of smooth implants (Fig. 3E), rough implants (Fig. 3F) and rough implants used with DBX (Fig. 3G) (top) and calvaria (bottom) after mechanical testing at 10 weeks revealed bone ingrowth into implants, with more bone observed on the rough implants regardless of DBX use compared to smooth implants. Rat calvaria with smooth implants showed bony protrusions (Fig. 3E, bottom) that were retained after implant pull-out testing, while protrusions on calvaria with rough implants with and without DBX (Fig. 3F, G bottom) were partially removed with the implant as part of mechanical testing. Force at failure of rough implants was significantly higher when DBX was included than non-treated smooth or rough implants at 10 weeks (Fig. 3H). Although the average modulus was higher for DBX-treated rough implants, no significant differences were found among groups (Fig. 3F). Pull-out testing was performed for rough implants with DBX at 5 and 10 weeks, showing higher force at failure (Fig. 3J) and modulus (Fig. 3K) at 10 weeks compared to 5 weeks.

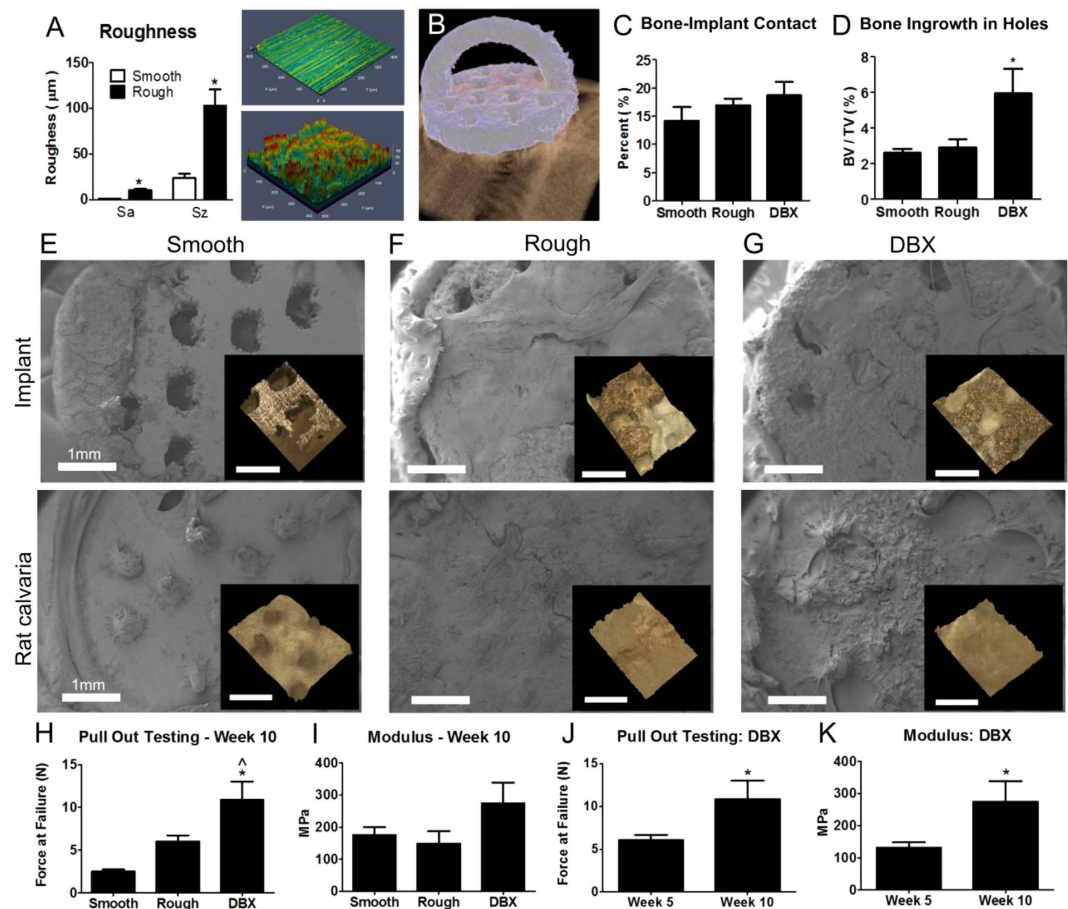


Figure 3. The effect of surface roughness and demineralized bone matrix on bone growth and mechanical properties of new bone growth into porous disks. Laser sintered implants were manufactured and polished or treated by blasting and acid etching to produce smooth and rough surfaces for calvarial implantation in rats. Laser confocal microscopy confirmed reduced surface roughness and peak to valley heights (A) of smooth surfaces (A top right) in comparison to rough surfaces (A bottom right). MicroCT image analysis (B) was conducted of calvarial implants after 10 weeks to assess bone-to-implant contact (C) and bone ingrowth in holes (D). SEM micrographs after pull-out testing of the implant ((E–G) top, with inset optical images) and calvaria ((E–G) bottom, with inset optical images) showed bone growth and attachment to implants. Pull out testing revealed force at failure (H) and modulus (I) 10 weeks after implantation. Force at failure for pull out testing (J) and modulus (K) was also compared at 5 and 10 weeks for the DBX treated group. One-way ANOVA with Bonferroni correction, $p < 0.05$, * vs. smooth or week 5, ^ vs. rough.

Custom-fit wrap implants osseointegrated with rabbit tibias. To demonstrate structural implant functionality, we analyzed osseointegration of custom-manufactured wrap implants placed around rabbit tibias. Because previous experiments in this study showed osseointegration without the use of DBX, we did not use any bone graft substitutes in this experiment in order to focus on the implant geometry. We were also able to achieve bone growth through the implant holes even without the presence of DBX, suggesting that the surface modification alone would be successful in supporting osseointegration of an implant geometry that was more clinically relevant in a larger animal model. Laser sintered wrap implants were manufactured to fit snugly around tibias of New Zealand White rabbits (Fig. 4A). Implants were secured with four screws that penetrated into the bone marrow cavity, and microCT cross sections of the entire implant were taken for analysis of osseointegration (Fig. 4B,C). MicroCT images at 1, 3 and 6 weeks showed continuous bone growth filling the void space between the tibia and the implant by 3 weeks, and even expanding beyond the implant at 6 weeks (Fig. 4D). MicroCT 3D reconstructions were able to provide better representative images of implants around tibias at 6 weeks (Fig. 4E). Quantitative analysis revealed significantly higher bone-to-implant contact values at 6 weeks compared to at 1 and 3 weeks (Fig. 4F). Histological sections of implants provided a more detailed view of bone formation (Fig. 4, S3). At 1 week, there were small gaps remaining between the implant screws and bone (Fig. 5A), with new bone (Fig. 5B) and connective tissue (Fig. 5C) forming. At 3 weeks, further bone growth was achieved (Fig. 5D), with cartilage (Fig. 5E,F) and woven bone prominent near the implant (Fig. 5G). At 6 weeks, fully formed bone was present (Fig. 5H) in contact with the inside of the implant (Fig. 5I), with bone formation occurring around the outside of the implant as well (Fig. 5J). Bone-to-implant contact analyzed from histological images showed significantly higher values at 6 weeks compared to at 1 and 3 weeks (Fig. 5K).

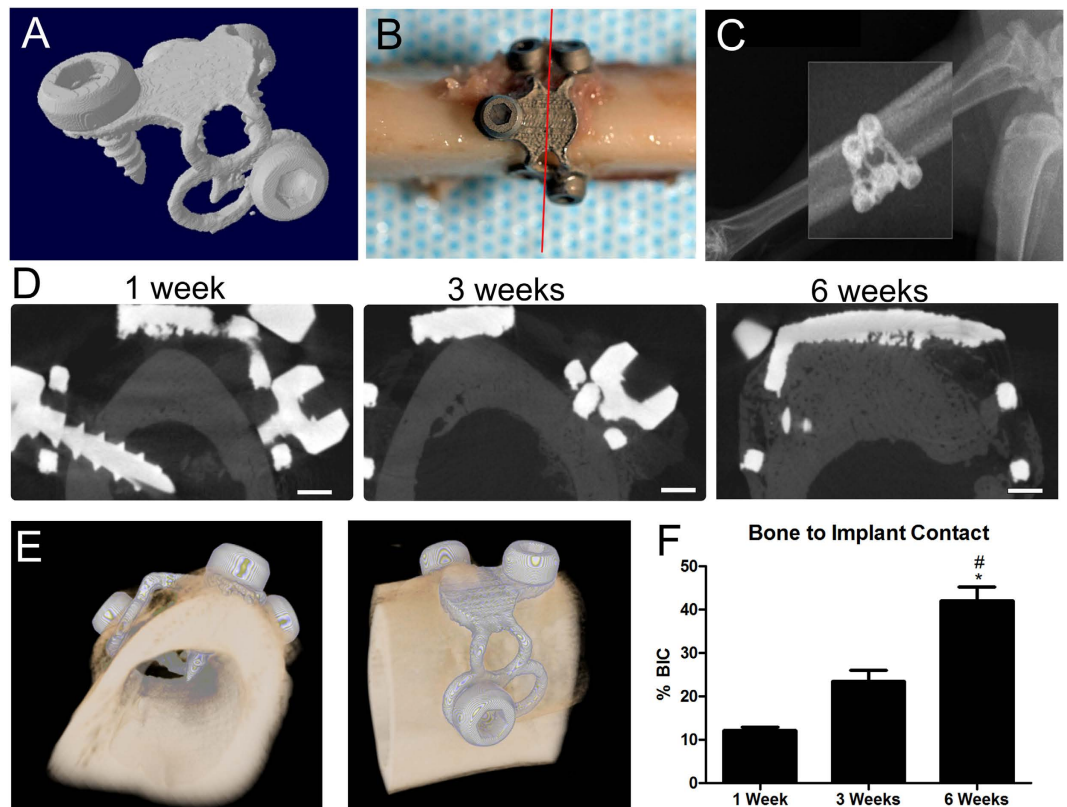


Figure 4. MicroCT analysis of endosteal wrap implants shows bone growth over 6 weeks. Wrap implants were designed and manufactured (A) for implantation around rabbit tibias (B), with the red line indicating cross sections for microCT analysis). MicroCT scans of the entire implant (C) and cross sections were taken after 1, 3, and 6 weeks after implantation (D). Reconstructed scans (E) were used for analysis of bone-to-implant contact (F). Scale bars represent 1 mm. One-way ANOVA was performed with Bonferroni's correction, $p < 0.05$, *vs. 1 week, # vs. 3 weeks.

Wrap implants were customized for dental implant placement in patients. To translate our animal studies clinically, we developed patient-specific wrap implants to induce bone regeneration with a one-step surgical procedure under a Helsinki Committee-approved protocol. Two case studies are described (Fig. 6 and Fig. S4). CT scans were taken of the patient at the site of intended implant placement (Fig. 6A), and reconstructed scans (Fig. 6B,C) were used to develop a custom, porous endosteal wrap implant (Fig. 6D) using the same laser sintering parameters and implant surface treatments as described for the disks and wrap implants above. One-piece implants included a porous base similar to the pore geometry used in rat calvaria studies, stabilizing screws as used in the rabbit studies, and implant posts to be used for eventual crown placement (Fig. 6E). Sintered implants were fit to an additively manufactured plastic mold of the patient's mandible (Fig. 6F) to ensure correct placement. Prior to perforating the bone, the implants were placed to ensure that they fit the placement site. The implants were then removed and the bone was perforated using a dental bur. The site was coated with DBX, and the implant placed and secured to the patient's mandible at the predetermined location (Fig. 6G). The secured implant was coated with DBX and the flap was passively closed. A panoramic X-ray was taken at 3 months post-surgery (Fig. 6H), and a CT scan was taken at 8 months post-surgery and 6 months post-loading (Fig. 6I). At 8 months, the implant was osseointegrated with continued functional loading and no complications reported by the patient. The implant was loaded and in function; no pain or infection was reported. The second case in which the patient received implants on both sides of the mandible is presented in Fig. S4.

Discussion

Similar to how computer aided design/computer aided manufacturing (CAD/CAM) revolutionized solid implant fabrication years ago, additive manufacturing technology is impacting the field by making the promise of precision medicine accessible to patients requiring complex reconstructive surgery^{20,21}. Here, we show that 3D Ti-6Al-4V implant surfaces can be designed that enhance osteoblast response *in vitro* and osseointegration *in vivo* compared to smooth surfaces, and that these additively manufactured and processed surfaces can be combined with DBX for osseointegration beyond the bone envelope *in vivo*. This conclusion was achieved in a stepwise process that included surface modification at the microscale and nanoscale, validation that the modified surface supported osteoblastic differentiation of normal human osteoblasts; *in vivo* demonstration that the surface modification was sufficient to support bone formation using qualitative and quantitative imaging and

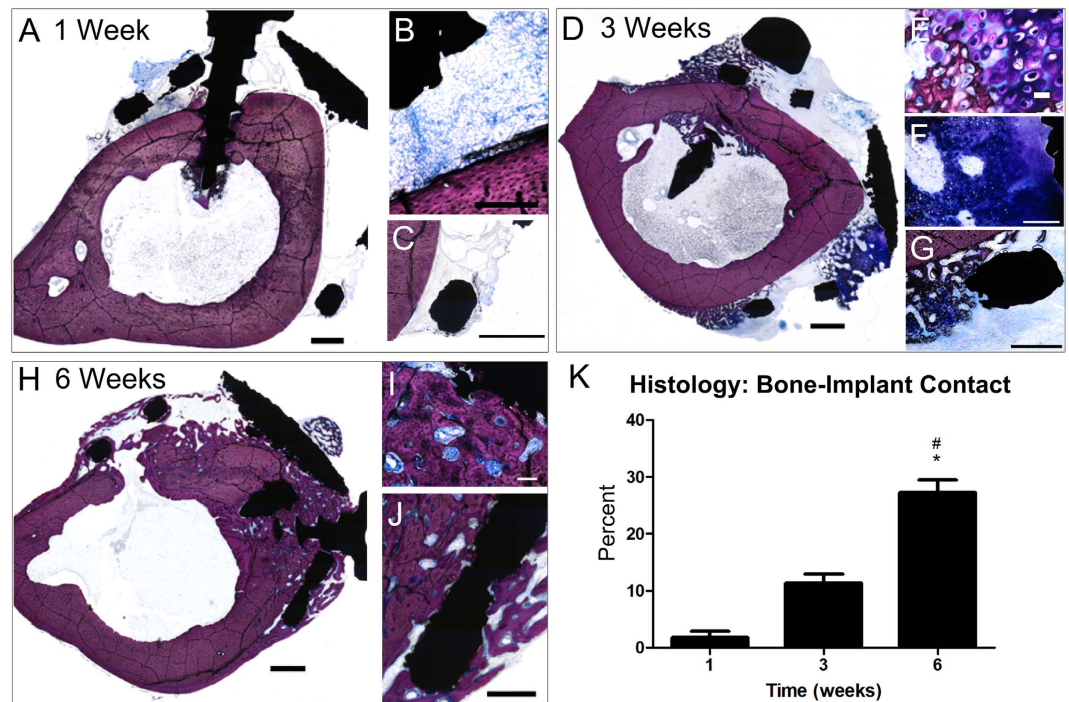


Figure 5. Bone growth into and around endosteal wrap implants on rabbit tibias. Histological sections of wrap implants stained with Steven's Blue after 1 week ((A), with enlarged (B) showing bone, and (C) showing connective tissue), 3 weeks ((D), with enlarged (E,F) showing cartilage and (G) showing woven bone), 6 weeks ((H), with enlarged (I) showing bone in contact with inside of implant and (J) showing new bone around outside of implant) and used to analyze bone-to-implant contact (K). Scale bars for (A–D,H) represent 1 mm, scale bars for (G) and (I) represent 500 μ m, scale bar for F represents 200 μ m, scale bar for (J) represents 100 μ m and scale bar for (E) represents 20 μ m. For histomorphometric analysis, one-way ANOVA was performed with Bonferroni's correction, $p < 0.05$, *vs. 1 week, # vs. 3 weeks.

biomechanical parameters, translation of the technology to a more challenging animal model, and finally use of the technology to support implant placement in two edentulous human patients with severe bone loss.

This study has shown that the implant surface can influence biological response even without the addition of exogenous factors. Surface roughness at multiple scales is necessary for increasing osteoblast response and osseointegration^{7,13,22,23}. While we did include a polished smooth surface in our initial studies to verify the superiority of implant surfaces with micro-/nano-roughness, we chose to focus on rough surfaces in our rabbit and clinical studies as they are more clinically relevant. Although we did not polish inside the implant holes, these are not the first site of contact with the calvarial bone. We believe that the large surface area of the implant underside compared to the side wall of the holes contributed more to the mechanical testing and osseointegration. In addition, this is the surface along which we measured the bone to implant contact.

In addition to the micro-texture and nano-texture of the surface, other surface parameters such as wettability have been shown to influence the biological response²⁴. Dental implants with topographies similar to those used in this study that have retained a hydrophilic surface exhibit more rapid osseointegration than implants that are hydrophobic²⁵. We did not directly compare hydrophilic implants to hydrophobic implants with identical surface morphology. However, it has been shown in other studies that autoclave sterilization results in a hydrophobic surface^{26,27}. Because we autoclave sterilized the polished disks used in the *in vivo* study, our mechanical testing experiments were only able to assess the combined effects of surface topography and hydrophilicity on cell response. Whether the relative hydrophilicity or hydrophobicity of the surface contributed in a significant way to the differences in osseointegration between the disks with smooth and rough surfaces is not known.

MicroCT evaluation of bone-to-implant contact provides a 3D analysis of implant osseointegration and new bone infiltration into the implant pores. Total implant analysis cannot be achieved with conventional histology, which evaluates osseointegration only at one cross sectional location. Previous work analyzing bone ingrowth into porous titanium implants indicated that depending on pore size and location, new bone did not form in the same manner across all pores^{28–30}, which helps explain why our bone-to-implant values achieved through microCT are different from those achieved via histomorphometry. However, the disadvantage of microCT evaluation lies in its inability to visualize non-mineralized tissue, which is easily identifiable through histological sectioning and staining³¹. Interference from the titanium can also introduce scatter and lower resolution in the image. Therefore, both methods of analysis are valuable and can contribute to evaluation of osseointegration.

In this study, we used two different animal models to focus on the scientific and clinical aspects of bone regeneration and osseointegration. We used rats to develop our surgical procedure and evaluate implant osseointegration. Before transitioning to human clinical trials, we needed to evaluate feasibility of structurally similar

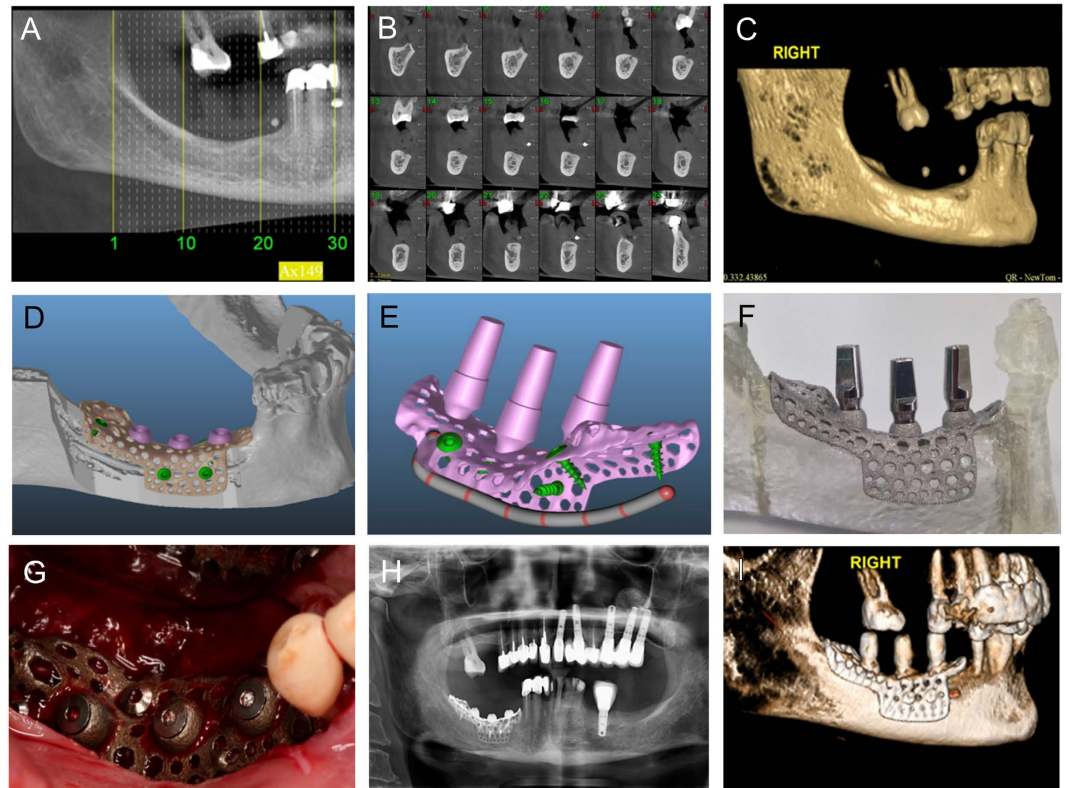


Figure 6. A patient customized endosteal implant was created to enhance bone regeneration for future dental implant placement. A CT scan was taken of the patient (A) to plan implant placement (B, C). A customized Ti-6Al-4 V implant was designed in software (D, E), with purple representing implant posts and green representing stabilizing screws. The implant was manufactured as one piece (F) and implanted in the patient (G). A follow-up panoramic X-ray was taken to evaluate osseointegration and the bone to implant contact after three months (H), and a CT scan performed after eight months (I).

constructs in a higher order animal model. We chose the rabbit tibia both as having a more geometrically comparable curvature to the human mandible compared to the rat calvaria, as well as an alternate way of showing osseointegration in the long bone. Because human maxillofacial regeneration is composed of both endochondral and intramembranous ossification, we wanted to verify endochondral bone formation in the rabbit tibia in response to the implant after observing successful intramembranous bone formation in our rat cranial only model.

One potential design concern for these one-piece custom implants is roughness at the abutment connection. Traditional dental implants leave this area polished to prevent bacterial colonization and subsequent peri-implantitis³². Studies have shown an altered bacterial attachment profile on titanium and Ti-6Al-4 V rough surfaces compared to smooth surfaces, but it is still unclear how this may affect clinical response after implantation^{33–35}. In our study at 8 months post-implantation, no complications or bacterial contamination were noted in patients. However, future studies may wish to identify post-processing methods that are able to differentially treat portions of the implant to achieve spatially disparate smooth and rough surfaces.

Although bone grafts and bone graft substitutes are commonly used in ridge augmentation, cases that require substantial vertical regeneration of bone are not predictably successful. These patients require multiple procedures and the regeneration strategy and treatment plan vary considerably from case to case³⁶. Our results, achieved through iterative *in vitro* and *in vivo* studies, suggest that additive manufacturing can be used successfully to produce implants that meet the demands of precision medicine by tailoring the shape to the individual patient's needs. The use of DBX had an osteoinductive effect, enhancing osseointegration of the roughened surface in the rat calvaria. Based on these results, we continued to use DBX with human implantation, and suggest this as a best practice for future clinical use. The combination of surface topography modification of laser sintered Ti-6Al-4 V at the microscale and nanoscale with clinical best practices can lead to osteogenesis and ultimately osseointegration of implants, even for patients with limited bone, enabling restoration of form and function. Though this study only indicates one clinical application of additive manufacturing for dentistry, we hope that others will apply our findings to bone regeneration in facial reconstruction after trauma, cancer or in other compromised cases.

Methods

Study Design. The objective of this study was to evaluate the *in vitro*, *in vivo* and human clinical performance of surfaces and implants manufactured using laser sintering with post-processing surface treatment. Our hypotheses were that laser sintered surfaces with hierarchical surface roughness could enhance osteoblast response *in*

vitro and increase osseointegration *in vivo* compared to smooth surfaces and implants. We also hypothesized that use of DBX with the implant would increase osseointegration in a rat calvaria model, and that these results would translate to rabbit and human implantation. All cell culture studies were repeated at least three times to ensure repeatability of data. Power analysis was conducted for each animal study, and animals were assigned randomly to experimental groups during surgery. Severe behavioral and physical changes in animals were considered as humane endpoints upon which to end data collection. Blind analysis was conducted for histomorphometric and microCT evaluation of bone-to-implant contact. Significance for all studies was determined using one-way analysis of variance (ANOVA) with Bonferroni's Multiple Comparison Test and a *p* value of less than 0.05. Outliers were determined and excluded based on Grubbs' extreme studentized deviate test.

Material Manufacturing. Solid disks, porous calvarial implants and tibial wrap implants and clinical implants were produced by laser sintering (EOS GmbH, Krailling, Germany). Ti-6Al-4V powder particles 25–45 μm in diameter (Advanced Powders & Coatings, Quebec, Canada) were sintered using a Ytterbium fiber laser with a scanning speed of 7 m s^{−1}, 1054 nm wavelength, 200 W continuous power and 0.1 mm spot size. Solid disks used for *in vitro* studies were 15 mm in diameter and 1 mm in height. Smooth disks and implants were polished with aluminum oxide sanding paper (P240, Norton Abrasives, Paris, France) and referred to as LST-M for solid surfaces or Smooth for porous implants. Rough disks and implants were blasted with calcium phosphate particles in a proprietary manner, then then acid etched for 90 minutes in 10% of a 1:1 ratio of maleic and oxalic acids. All materials were sterilized by gamma radiation prior to cell culture or implantation unless otherwise stated.

Material Characterization. Scanning electron microscopy (SEM, Zeiss Ultra60 FE-SEM, Oberkochen, Germany) was used to visualize surfaces, implants, and calvaria. Calvaria and implants with biological material were dehydrated in a series of ethanol: at least two hours in 15%, 30% and 45% ethanol, at least one hour in 60%, 75%, 90% and twice in 100% ethanol, 1:1 exchange in 100% ethanol and hexamethyldisilazane (HMDS), and twice for 30 minutes in HMDS. SEM was conducted with an accelerating voltage of 4 kV and working distance of 4 mm for material and 10 mm for biological samples. Before imaging, biological samples were platinum sputtered for 90 seconds at 35 μA . Smooth control disks were analyzed with confocal microscopy (Zeiss LSM 710, Jena, Germany) and scanning electron microscopy to ensure that the surfaces were significantly less rough than the test disks. Average roughness (S_a) and peak-valley height (S_z) measurements were conducted under 20 \times magnification (Plan-Apochromat 20 \times /0.8 M27 objective) over a 425 μm \times 425 μm area z-stack with a step size of 5 μm .

Cell Response. Normal human osteoblasts (NHOb cells, Lonza, Basel, Switzerland) were seeded onto disks at a density of 10,000 cells per cm² according to tissue culture polystyrene (TCPS) surface area, or 20,000 cells per well in a 24 well plate. Cells were fed with full medium (DMEM supplemented with 10% fetal bovine serum, 1% penicillin/streptomycin) 24 hours after plating, then every 48 hours until reaching confluence on TCPS. Cells were fed at confluence on TCPS and harvested 24 hours afterward for biological analysis. At harvest, medium was aliquoted and stored to analyze osteocalcin (BT-480, Alfa Aesar, Ward Hill, Massachusetts), osteoprotegerin (DY805, R&D Systems, Minneapolis, Minnesota), vascular endothelial growth factor (VEGF, DY293B, R&D Systems) and bone morphogenetic protein 2 (BMP2, 900-K255, PeproTech, Rocky Hill, New Jersey) levels. Cell layers were rinsed twice in phosphate buffered saline and then stored in 0.05% Triton X-100 at −20 °C overnight, sonicated and analyzed for DNA content (E2670, Promega, Madison, Wisconsin) and protein (23225, Life Technologies, Carlsbad, California). Alkaline phosphatase specific activity was analyzed by cleavage of *p*-nitrophenol from *p*-nitrophenylphosphate at pH 10.2. These methods are described in greater detail in references^{12,17,37}.

Rat Calvaria Experiments. 5.0 mm disks with 12 evenly spaced 0.5 mm holes were generated via additive manufacturing by laser sintering Ti-6Al-4V alloy powder. The resulting disks were grit blasted and then acid-etched to create a specific micro-surface as described previously¹⁷. Disks were subjected to a cleaning protocol¹⁷ and then sterilized via gamma radiation. Three studies were conducted using a surgical protocol where disks were implanted subperiosteally on the surface of the calvarial bone of 250–300 g 8 week old male Sprague-Dawley rats (Harlan Laboratories, Indianapolis, Indiana) or athymic (RNU/RNU) nude rats (Charles River, Wilmington, Massachusetts). All animal procedures were conducted with the institutional approval of Virginia Commonwealth University (Richmond, VA). Following the elevation of a periosteal flap, multiple 0.3 mm holes were drilled through the cortical bone into the marrow space of the left parietal bone (15 to 20 holes per calvarium). The disks were placed over the holes, and the flap was sutured over the disk.

To determine the effect of pretreating the implantation site via *in situ* decalcification, exposed bone around the holes was left untreated (*N* = 6) or treated with 24% EDTA for five minutes (*N* = 6). A third group of rats was treated with 37% phosphoric acid for 1 minute prior to drilling the holes (*N* = 6). Animals were euthanized after 5 and 10 weeks.

To determine the osteogenic capability of the disks, calvaria were not treated with either decalcification protocol prior to placing the disks. Disks were then implanted with and without the addition of demineralized bone matrix putty (DBX[®], donated by the Musculoskeletal Transplant Foundation, Edison, NJ) (*N* = 7 male athymic nude rats per group, Charles River). DBX was applied to the bone surface and the top of the disk prior to closing the periosteum. Animals were euthanized at 15, 35, and 70 days, denoted as 2, 5, and 10 weeks, respectively. Samples in both studies were analyzed by microCT and ground histology sections stained with Stevenel's Blue to determine the bone-to-implant contact and bone ingrowth into the holes of the disk via histomorphometry.

Osseointegration was also characterized as a function of the pull-out strength of the implants at 5 and 10 weeks. Implants were fabricated as above, but a handle was incorporated into the design to interface with the mechanical testing apparatus. A second set of implants was produced by additive manufacturing but the surface

was polished rather than grit blasted and acid etched. Male athymic nude rats were used for each treatment group ($N = 8$). Implants were placed using the DBX protocol. The periosteum was closed with a purse string suture, leaving the arch exposed for mechanical testing. Mechanical testing was performed at harvest as described below.

Rabbit Experiment. Male New Zealand White rabbits ($N = 30$, 3.0 to 3.2 kg each) were weighed and anesthetized with 2% isoflurane in an anesthetic chamber, then isoflurane was continually administered for the duration of the surgery via a nose mask. 50 mg/kg ketamine and 5 mg/kg xylazine were administered to sedate the rabbit. The left leg was shaved and disinfected with ethanol and chlorhexidine. The tibia was exposed and four pilot holes were drilled for placement of the implant screws. Drilling was conducted at low speed, intermittently and under a continuous stream of saline that cut through the bone fragments and cooled the drilling area. The implant was placed on the tibia and secured with screws that penetrated into the bone marrow cavity. After placing the implant, the subcutaneous tissue and skin were closed with absorbable surgical sutures. The isoflurane was removed, and the rabbit was allowed to awaken and recover on a heating pad. Rabbits were given 0.01 mg/kg buprenorphine twice daily for 3 days following surgery, and 20 mg/kg Ceporex antibiotic 7 days following surgery. Health, weight, food intake and wound state were evaluated twice daily during the first 6 days after surgery to ensure animal recovery. Rabbits were examined daily for the remaining recovery period. At 1 ($N = 3$), 3 ($N = 16$) and 6 ($N = 11$) weeks, rabbits were anesthetized with 2% isoflurane. The surgical site was re-opened to retrieve fragments of bone containing the implants. The animals were then euthanized by air embolism with a 5–50 ml/kg intravenous injection of air. Rabbit experiments were carried out at the University Lodz, approved by the Animal Ethics Committee at the University of Lodz and carried out in accordance with approved guidelines.

MicroCT. All scans were conducted on a Bruker Skyscan 1173 MicroCT, hardware version A. Images were scanned using Skyscan Control Software version 1.6 (Kontich, Belgium). Calvaria were scanned at a resolution of 2240×2240 pixels (image pixel size of $14.74 \mu\text{m}$), with x-rays of 105 kV and $65 \mu\text{A}$ using a 0.25 mm brass filter and exposure time of 500 ms and a rotation step of 0.4° . When assessing the requirement for DBX, calvaria were scanned as above using 130 kV, $61 \mu\text{A}$, exposure time of 1600 ms, and an image pixel size of $11.86 \mu\text{m}$. All calvarial implants that were not destined for mechanical testing were fixed in 10% neutral buffered formalin prior to scanning. Those calvarial implants intended for mechanical testing were scanned as fresh tissue. Rabbit tibial implants were scanned at a resolution of 1120×1120 pixels, 75 kV, $106 \mu\text{A}$, exposure time of 1200 ms, using a 0.25 mm brass filter with an image pixel size of $20.85 \mu\text{m}$ over 360° and a rotation step of 0.400° . Samples were fixed in 10% neutral buffered formalin prior to scanning. A standard Feldkamp reconstruction was performed on a subset of samples using NRecon Software version 1.6.9.17 (Kontich, Belgium) with a Gaussian smoothing kernel of zero and a beam hardening correction of 20%. Analysis of all samples was conducted with CTAn software version 1.14.4.1 (Kontich, Belgium). Bone-to-implant contact was calculated as a function of the total bone volume immediately connected to the total volume of the implant in all studies. Bone ingrowth into calvarial disk holes was calculated as a function of total bone volume within the volume of all of the disk holes of the implant.

Histology. Samples from all studies were commercially processed (Histion, Everett, WA). Briefly, samples were embedded in methyl methacrylate and one ground section was taken from each specimen, which, if possible, passed through an axis of the disk containing four holes (for rat calvaria experiments). Sections were stained with Stevenel's blue/van Gieson³⁸. Samples were photographed using Zen 2012 Blue Edition software with an AxioCam MRc5 camera and Axio Observer Z.1 microscope (Carl Zeiss Microscopy, Oberkochen, Germany). Bone-to-implant contact (BIC) in both the calvarial disk studies as well as the tibial implant study was calculated by dividing the bone contact perimeter by the total perimeter of the implant. Bone ingrowth into calvarial disk holes was calculated by dividing the bone area by the total area of each of the four holes of a sample.

Mechanical Testing. To quantitatively assess osseointegration of calvarial disks, pull out force testing was conducted using a 30 kN load cell for $N = 8$ animals per group. Ti-6Al-4 V laser sintered disks with a mounting bracket were manufactured and processed in the same way as described for surfaces used for cell culture and histological analysis. Smooth controls were prepared by sanding disks with aluminum oxide 240 grit sanding sheets (Norton Saint-Gobain, P240) and autoclaved at 121°C for 30 minutes. Smooth control implants were examined by SEM and confocal microscopy and found to be significantly less rough compared to normal implants. Surgical implantation was performed as described for the other calvarial implants, but the periosteum was closed around the base of the mechanical testing bracket.

Clinical Cases. All clinical procedures were approved by the Helsinki Committee of Tel Aviv University and the Ministry of Health of Israel and carried out in accordance with approved guidelines. Informed consent was obtained from all subjects. Two patients were screened and selected as candidates for custom wrap implant placement. For these patients, all currently known and accepted methods to rehabilitate edentulous posterior mandibles, including partial dentures, were found to be inappropriate. Initial evaluation of the implant site was performed by cone beam computed tomography (cbCT). Custom subperiosteal jaw wraps with implant posts were designed using the AB software program (AB Dental, Ashdod, Israel). Implants were fabricated by laser sintering in the same manner as described previously for implants produced for culture and animal studies, and gamma irradiated prior to implantation. Local anesthesia was administered for the surgical procedure. A crestal incision was made in the mandible, and the full flap was elevated. After examining the implant fit to the mandibular bone, bur holes were drilled along the coronal aspect and the side of the mandible to expose the bone marrow. A layer of DBX was placed on the bone surface before implant placement. The implant was placed on top of the mandibular crest as previously planned and secured with four miniscrews. Another layer of DBX was placed on top of the implant prior to closure. After placement, the gingiva was closed passively with two horizontal mattress sutures (Vicryl), and with interrupted sutures. Patients were prescribed antibiotics and local analgesics, and a final

panoramic X-Ray scan was conducted to verify implant placement. The patients were followed for 3 months with no complications noted. At 3 months post-surgery, a second panoramic X-Ray was taken and the implants were loaded. A final follow-up CT scan was taken of patients after 8 months to observe osseointegration and implant function.

References

1. Dye, B. A., Li, X. & Beltran-Aguilar, E. D. Selected oral health indicators in the united states, 2005–2008. *NCHS Data Brief*, 1–8 (2012).
2. Douglass, C. W., Shih, A. & Ostry, L. Will there be a need for complete dentures in the united states in 2020? *J. Prosthet. Dent.* **87**, 5–8 (2002).
3. Turkyilmaz, I., Company, A. M. & McGlumphy, E. A. Should edentulous patients be constrained to removable complete dentures? The use of dental implants to improve the quality of life for edentulous patients. *Gerodontology*. **27**, 3–10 (2010).
4. Albrektsson, T., Zarb, G., Worthington, P. & Eriksson, A. R. The long-term efficacy of currently used dental implants: A review and proposed criteria of success. *Int. J. Oral. Maxillofac. Implants*. **1**, 11–25 (1986).
5. Hämmerle, C. H. F. & Karring, T. Guided bone regeneration at oral implant sites. *Periodontol.* **2000**, **17**, 151–175 (1998).
6. Bodine, R. L., Yanase, R. T. & Bodine, A. Forty years of experience with subperiosteal implant dentures in 41 edentulous patients. *J. Prosthet. Dent.* **75**, 33–44 (1996).
7. Gittens, R. A. *et al.* Differential responses of osteoblast lineage cells to nanotopographically-modified, microroughened titanium–aluminum–vanadium alloy surfaces. *Biomaterials*. **33**, 8986–8994 (2012).
8. Gittens, R. A. *et al.* Superposition of nanostructures on microrough titanium–aluminum–vanadium alloy surfaces results in an altered integrin expression profile in osteoblasts. *Connect. Tissue Res.* **55**, 164–168 (2014).
9. Gittens, R. A. *et al.* The roles of titanium surface micro/nanotopography and wettability on the differential response of human osteoblast lineage cells. *Acta Biomater.* **9**, 6268–6277 (2013).
10. Gittens, R. A., Olivares-Navarrete, R., Schwartz, Z. & Boyan, B. D. Implant osseointegration and the role of microroughness and nanostructures: Lessons for spine implants. *Acta Biomater.* **10**, 3363–3371 (2014).
11. Schwartz, Z. *et al.* Effect of micrometer-scale roughness of the surface of ti6al4v pedicle screws *in vitro* and *in vivo*. *J. Bone Joint Surg. Am.* **90**, 2485–2498 (2008).
12. Lincks, J. *et al.* Response of mg63 osteoblast-like cells to titanium and titanium alloy is dependent on surface roughness and composition. *Biomaterials*. **19**, 2219–2232 (1998).
13. Gittens, R. A., Olivares-Navarrete, R., Schwartz, Z. & Boyan, B. D. Implant osseointegration and the role of microroughness and nanostructures: Lessons for spine implants. *Acta Biomater.* **10**, 3363–3371 (2014).
14. Cochran, D. L. A comparison of endosseous dental implant surfaces. *J. Periodontol.* **70**, 1523–1539 (1999).
15. Cochran, D. L. *et al.* The use of reduced healing times on iti implants with a sandblasted and acid-etched (sla) surface: Early results from clinical trials on iti sla implants. *Clin. Oral. Implants. Res.* **13**, 144–153 (2002).
16. Wang, X. *et al.* Effects of structural properties of electrospun tio2 nanofiber meshes on their osteogenic potential. *Acta Biomater.* **8**, 878–885 (2012).
17. Cheng, A., Humayun, A., Cohen, D. J., Boyan, B. D. & Schwartz, Z. Additively manufactured 3d porous ti-6al-4v constructs mimic trabecular bone structure and regulate osteoblast proliferation, differentiation and local factor production in a porosity and surface roughness dependent manner. *Biofabrication*. **6**, 045007 (2014).
18. Rezende, M. L. *et al.* Demineralization of the contacting surfaces in autologous onlay bone grafts improves bone formation and bone consolidation. *J. Periodontol.* **85**, e121–129 (2014).
19. de Rezende, M. L. *et al.* Bone demineralization with citric acid enhances adhesion and spreading of preosteoblasts. *J. Periodontol.* **86**, 146–154 (2015).
20. van Noort, R. The future of dental devices is digital. *Dent. Mater.* **28**, 3–12 (2012).
21. Parthasarathy, J. 3d modeling, custom implants and its future perspectives in craniofacial surgery. *Ann. Maxillofac. Surg.* **4**, 9–18 (2014).
22. Gittens, R. A. *et al.* The effects of combined micron-/submicron-scale surface roughness and nanoscale features on cell proliferation and differentiation. *Biomaterials*. **32**, 3395–3403 (2011).
23. Wennerberg, A. & Albrektsson, T. Effects of titanium surface topography on bone integration: A systematic review. *Clin Oral Implants Res.* **20** Suppl 4, 172–184 (2009).
24. Park, J. H. *et al.* The responses to surface wettability gradients induced by chitosan nanofilms on microtextured titanium mediated by specific integrin receptors. *Biomaterials*. **33**, 7386–7393 (2012).
25. Buser, D. *et al.* Enhanced bone apposition to a chemically modified sla titanium surface. *J. Dent. Res.* **83**, 529–533 (2004).
26. Serro, A. P. & Saramago, B. Influence of sterilization on the mineralization of titanium implants induced by incubation in various biological model fluids. *Biomaterials*. **24**, 4749–4760 (2003).
27. Park, J. H. *et al.* Effect of cleaning and sterilization on titanium implant surface properties and cellular response. *Acta Biomater.* **8**, 1966–1975 (2012).
28. Amin Yavari, S. *et al.* Bone regeneration performance of surface-treated porous titanium. *Biomaterials*. **35**, 6172–6181 (2014).
29. de Wild, M. *et al.* Bone regeneration by the osteoconductivity of porous titanium implants manufactured by selective laser melting: A histological and micro computed tomography study in the rabbit. *Tissue Eng. Part A*. **19**, 2645–2654 (2013).
30. Li, J. P. *et al.* Bone ingrowth in porous titanium implants produced by 3d fiber deposition. *Biomaterials*. **28**, 2810–2820 (2007).
31. Baril, E., Lefebvre, L. P. & Hacking, S. A. Direct visualization and quantification of bone growth into porous titanium implants using micro computed tomography. *J. Mater. Sci. Mater. Med.* **22**, 1321–1332 (2011).
32. Bollen, C. M. *et al.* The influence of abutment surface roughness on plaque accumulation and peri-implant mucositis. *Clin Oral Implants Res.* **7**, 201–211 (1996).
33. Wu, Y., Zitelli, J. P., TenHuisen, K. S., Yu, X. & Libera, M. R. Differential response of staphylococci and osteoblasts to varying titanium surface roughness. *Biomaterials*. **32**, 951–960 (2011).
34. Braem, A. *et al.* Staphylococcal biofilm growth on smooth and porous titanium coatings for biomedical applications. *J Biomed Mater Res A*. **102**, 215–224 (2014).
35. Almaguer-Flores, A. *et al.* Influence of topography and hydrophilicity on initial oral biofilm formation on microstructured titanium surfaces *in vitro*. *Clin Oral Implants Res.* **23**, 301–307 (2012).
36. McAllister, B. S. & Haghighat, K. Bone augmentation techniques. *J. Periodontol.* **78**, 377–396 (2007).
37. Zinger, O. *et al.* Differential regulation of osteoblasts by substrate microstructural features. *Biomaterials*. **26**, 1837–1847 (2005).
38. del Cerro, M., Cogen, J. & del Cerro, C. Stevenel's blue, an excellent stain for optical microscopical study of plastic embedded tissues. *Microsc. Acta*. **83**, 117–121 (1980).

Acknowledgements

The authors would like to thank Dr. Charles P. Cartin, Director of the Biomechanics Core Lab at Virginia Commonwealth University for his help in conducting the mechanical testing. Research reported in this

publication was supported by the National Institute of Arthritis and Musculoskeletal and Skin Diseases of the National Institutes of Health under Award Number AR052102. The content is solely the responsibility of the authors and does not necessarily represent the official views of the National Institutes of Health. The study was also funded by AB Dental; in addition, AB Dental supplied materials for the study. DBX was provided as a gift from the Musculoskeletal Transplant Foundation. AC is supported by a National Science Foundation Graduate Research Fellowship.

Author Contributions

Z.S. and B.D.B. contributed to the study design, implementation and writing the manuscript, D.J.C. was responsible for animal studies and contributed to writing the manuscript, A.C. contributed to materials characterization and writing the manuscript, R.M.C. was responsible for mechanical characterization, A.J.W. contributed to analysis of the animal studies and S.L.H. was responsible for cell studies. A.K. oversaw the clinical study, and M.A. performed the the rabbit surgeries.

Additional Information

Supplementary information accompanies this paper at <http://www.nature.com/srep>

Competing financial interests: ZS is a consultant for AB Dental.

How to cite this article: Cohen, D. J. *et al.* Novel Osteogenic Ti6Al4V Device for Restoration of Dental Function in Patients with Large Bone Deficiencies: Design, Development and Implementation. *Sci. Rep.* **6**, 20493; doi: 10.1038/srep20493 (2016).



This work is licensed under a Creative Commons Attribution 4.0 International License. The images or other third party material in this article are included in the article's Creative Commons license, unless indicated otherwise in the credit line; if the material is not included under the Creative Commons license, users will need to obtain permission from the license holder to reproduce the material. To view a copy of this license, visit <http://creativecommons.org/licenses/by/4.0/>

**Novel Osteogenic Ti₆Al₄V Device for Restoration of Dental Function in
Patients with Large Bone Deficiencies: Design, Development and
Implementation**

Authors: D. J. Cohen, A. Cheng, A. Kahn, M. Aviram, A. J. Whitehead, S. L. Hyzy, R. M.
Clohessy, B. D. Boyan, Z. Schwartz

SUPPLEMENTAL INFORMATION

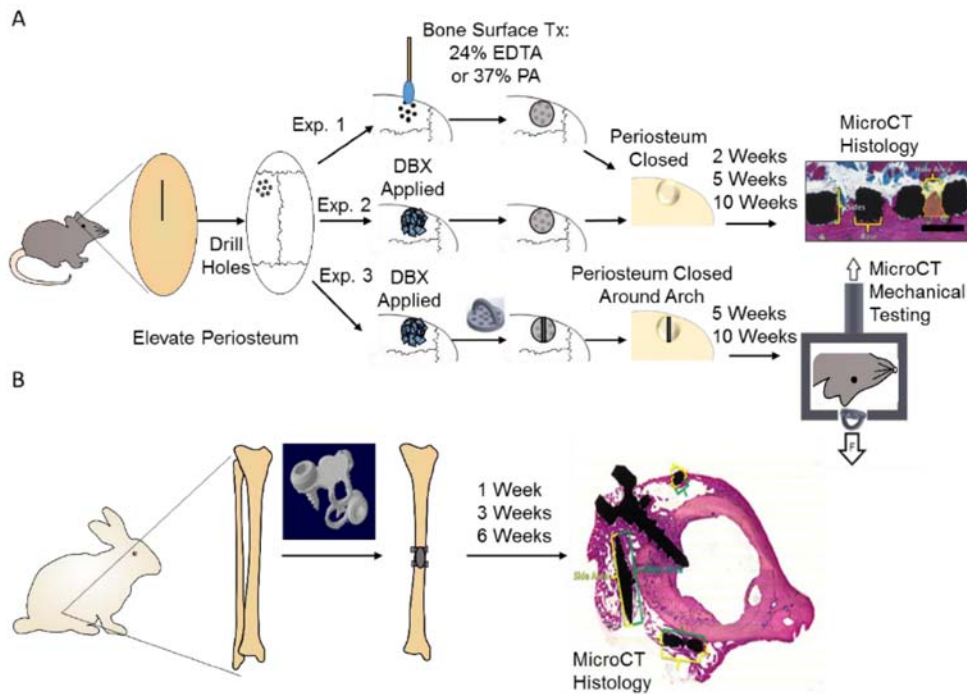


Fig. S1. Schematic of all animal experiments. The first set of experiments was conducted on rat calvaria to assess the effect of surface treatment of calvaria on implant osseointegration (A top), the second was to evaluate the effect of roughness on implant osseointegration with or without DBX (A middle) and the third was to analyze mechanical strength of osseointegrated implants with or without DBX (A bottom). Further in vivo work was conducted in a rabbit tibial model with a more clinically representative wrap implant to assess implant osteogenesis (B).

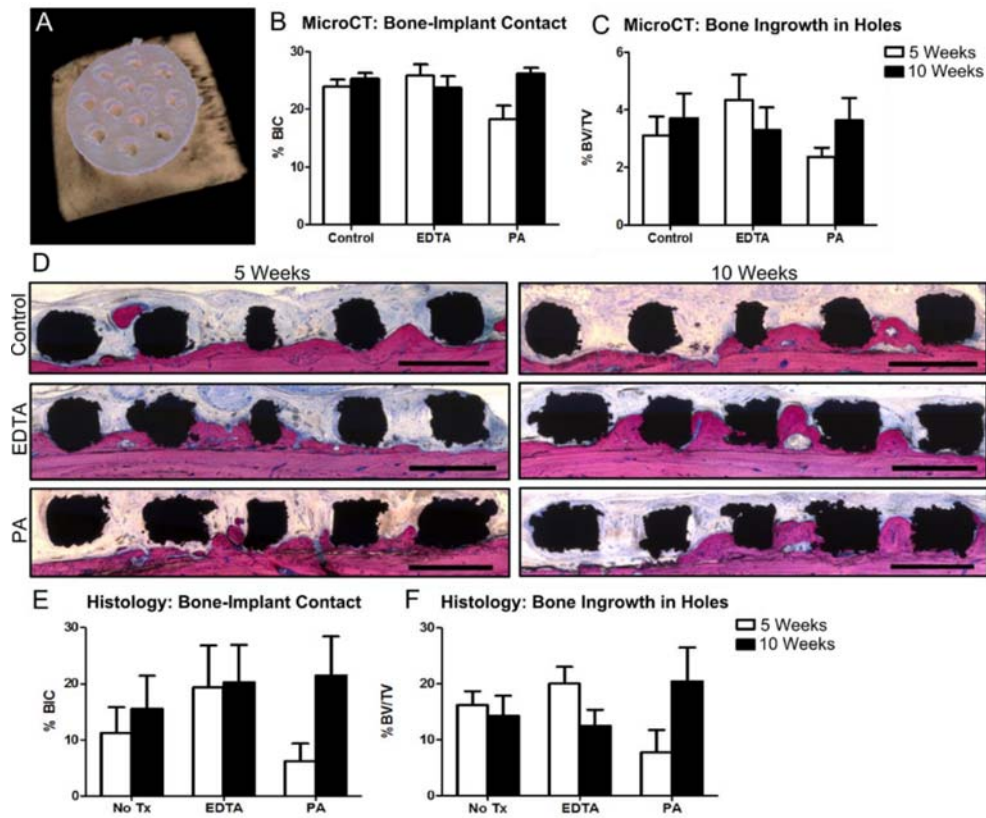


Fig. S2. The effect of pre-treatment on calvarial bone growth into porous disks. Disks were implanted on Sprague-Dawley rat calvaria with no treatment (control), EDTA, or phosphoric acid treatment prior to implantation, and bone-to-implant contact was assessed after 5 and 10 weeks. MicroCT was used to visualize disks on calvaria (A), bone-to-implant contact (B) and bone ingrowth in holes (C) was assessed in implant cross sections of the total implant. Histological sections were taken after 5 (D left) and 10 weeks (D right) for each group, and bone-to-implant contact (E) and bone ingrowth in holes (F) was measured by histomorphometry. Scale bar for histological images represents 1mm. Values were not statistically significant across treatment groups.

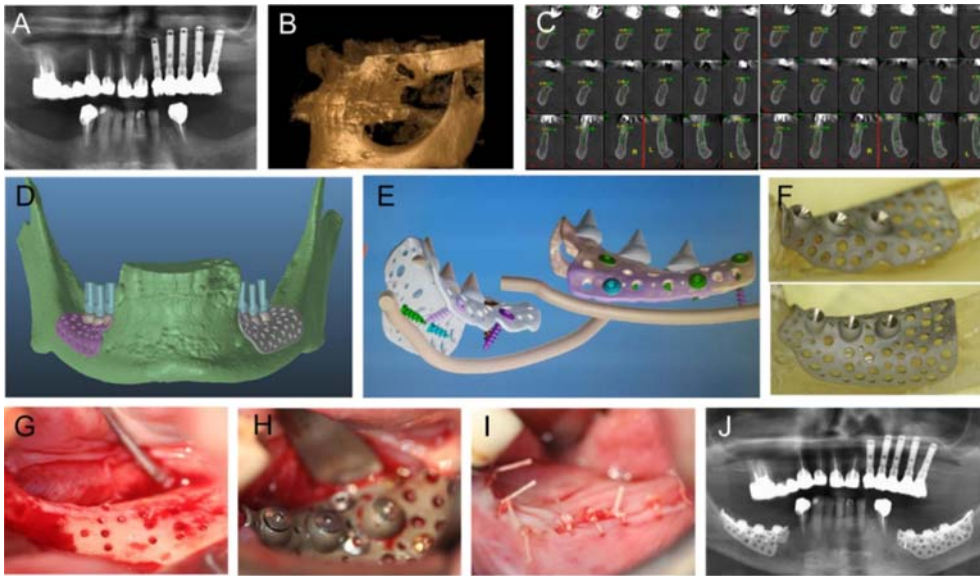


Fig. S3. A second case of a patient customized endosteal implant. A CT scan was taken of the patient (A) to plan implant placement (B, C). Customized Ti6Al4V implants were designed using software (D, E). The implants were manufactured as one piece for each side. For each implant, small holes were drilled into the patient's jaw prior to implant placement to ensure exposure to stem cells and progenitor cells (G), the implant was placed and stabilized (H) and the gum and periosteum were sutured over the implant (I). A follow-up panoramic X-ray was taken to evaluate osseointegration and the bone to implant contact after three months (J).

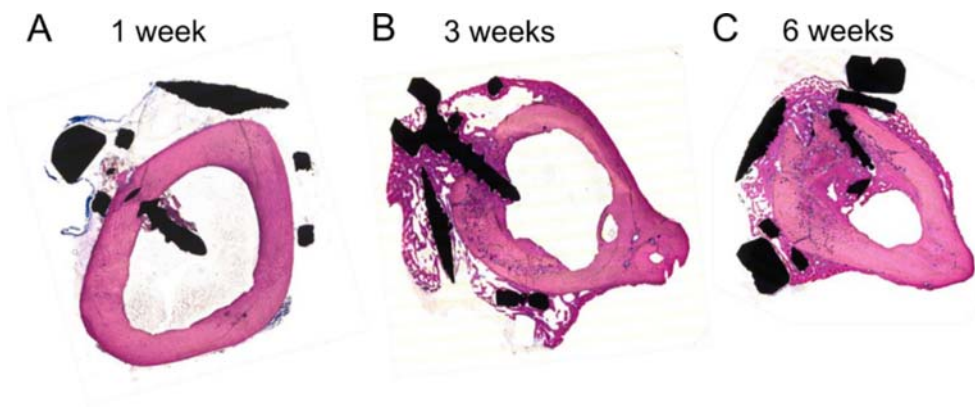


Fig. S4. Bone growth into and around endosteal wrap implants on rabbit tibias. Histological sections of wrap implants stained with Stevenel's Blue at 1 week (A), 3 weeks (B), 6 weeks (C).

Published: JBMR 2016 part A in:

**Journal of
Biomedical Materials Research**
PART A

02

Novel hydrophilic nanostructured
microtexture on direct metal laser
sintered Ti-6Al-4V surfaces enhances
osteoblast response in vitro and
osseointegration in a rabbit model

Sharon L. Hyzy, Alice Cheng, David J. Cohen,
Gustavo Yatzkaier, Alexander J. Whitehead, Ryan
M. Clohessy, Rolando A. Gittens, Barbara D.
Boyan, Zvi Schwartz



Superior Implant Technology

Novel hydrophilic nanostructured microtexture on direct metal laser sintered Ti-6Al-4V surfaces enhances osteoblast response *in vitro* and osseointegration in a rabbit model

AQ6

Sharon L. Hyzy,^{1*} Alice Cheng,^{2,3*} David J. Cohen,¹ Gustavo Yatzkaier,⁴ Alexander J. Whitehead,¹ Ryan M. Clohessy,¹ Rolando A. Gittens,⁵ Barbara D. Boyan,^{1,2} Zvi Schwartz^{1,6}

¹Department of Biomedical Engineering, Virginia Commonwealth University, Richmond, Virginia

²Department of Biomedical Engineering, Georgia Institute of Technology, Atlanta, Georgia

³Department of Biomedical Engineering, Peking University, Beijing, China

⁴Private Oral Surgery Clinic, Ashkelon, Israel

⁵Center for Biodiversity and Drug Discovery, Institute for Advanced Scientific Research and High Technology Services (INDICASAT AIP), Panama City, Panama

⁶University of Texas Health Science Center at San Antonio, San Antonio, Texas

Received 3 October 2015; revised 21 March 2016; accepted 31 March 2016

Published online 00 Month 2016 in Wiley Online Library (wileyonlinelibrary.com). DOI: 10.1002/jbm.a.35739

Abstract: The purpose of this study was to compare the biological effects *in vivo* of hierarchical surface roughness on laser sintered titanium–aluminum–vanadium (Ti-6Al-4V) implants to those of conventionally machined implants on osteoblast response *in vitro* and osseointegration. Laser sintered disks were fabricated to have micro-/nano-roughness and wettability. Control disks were computer numerical control (CNC) milled and then polished to be smooth (CNC-M). Laser sintered disks were polished smooth (LST-M), grit blasted (LST-B), or blasted and acid etched (LST-BE). LST-BE implants or implants manufactured by CNC milling and grit blasted (CNC-B) were implanted in the femurs of male New Zealand white rabbits. Most osteoblast differentiation markers and local factors were enhanced on rough LST-B and LST-BE surfaces in comparison to smooth CNC-M or LST-M surfaces for MG63 and normal human osteoblast

cells. To determine if LST-BE implants were osteogenic *in vivo*, we compared them to implant surfaces used clinically. LST-BE implants had a unique surface with combined micro-/nano-roughness and higher wettability than conventional CNC-B implants. Histomorphometric analysis demonstrated a significant improvement in cortical bone-implant contact of LST-BE implants compared to CNC-B implants after 3 and 6 weeks. However, mechanical testing revealed no differences between implant pullout forces at those time points. LST surfaces enhanced osteoblast differentiation and production of local factors *in vitro* and improved the osseointegration process *in vivo*. © 2016 Wiley Periodicals, Inc. J Biomed Mater Res Part A: 00A:000–000, 2016.

Key Words: additive manufacturing, animal model, dental implants, DMLS, laser sintering technology, titanium alloy

How to cite this article: Hyzy SL, Cheng A, Cohen DJ, Yatzkaier G, Whitehead AJ, Clohessy RM, Gittens RA, Boyan BD, Schwartz Z. 2016. Novel hydrophilic nanostructured microtexture on direct metal laser sintered Ti-6Al-4V surfaces enhances osteoblast response *in vitro* and osseointegration in a rabbit model. J Biomed Mater Res Part A 2016;00A:000–000.

INTRODUCTION

Osseointegration of implants into the jaw, hip, spine, or other bone is the ultimate clinical goal for endosseous implants. Titanium (Ti) is commonly used in bone-interfacing implants because of its desirable mechanical properties and ability to create a direct apposition with bone.^{1,2} Ti alloys such as titanium–aluminum–vanadium

(Ti-6Al-4V) are also popular and have shown success clinically.³ The five-year success rate of dental implants has increased from 93.5% to 97.1% within the past decade, with higher survival and lower complication rates.⁴ However, in dentistry and other orthopedic fields, patient and clinical variability affect implant outcomes. High variability in implant survival exists for hip replacements, with an

*These authors are Co-first Authors.

Conflict of Interest: One or more of the authors has received or will receive remuneration or other perquisites for personal or professional use from a commercial or industrial agent in direct or indirect relationship to their authorship.

Correspondence to: Barbara D. Boyan, School of Engineering, Virginia Commonwealth University, 601 West Main Street, P.O. Box 843068, Richmond, Virginia 23284-3068. e-mail: bboyan@vcu.edu

Contract grant sponsor: AB Dental and a National Science Foundation Graduate Research Fellowship (to A.C.)

Contract grant sponsor: SNI program from SENACYT, Panama (R.A.G.)

Contract grant sponsor: National Institute of Arthritis and Musculoskeletal and Skin Diseases (NIAMS) (USPHS Award Nos. AR052102 and AR068703)

AQ2

AQ1

estimated 5–20% revision rate for patients with total hip arthroplasty.⁵ Osseointegration rates are significantly lower in compromised patients including smokers, diabetics, or those with low bone density.^{6–8} In addition, an increasing number of cases require the use of custom or very specific implants. Although implants are made in a variety of shapes and sizes, the production costs and waste associated with manufacturing a single custom implant can decrease patient desire for implant therapy. Thus, a more cost-effective method of producing orthopedic and dental implants is necessary for a broad range of clinical cases and patient populations.

Much progress has been made in orthopedic and dental implant design within the past 20 years. During this time, our lab has focused on developing and characterizing new implant surfaces and understanding the physical parameters of these surfaces on biological response. Recently, the clinical implant research community has gained an interest in additive manufacturing, touting it as a “game changer” in the field.⁹ Direct metal laser sintering (DMLS) is an additive manufacturing technique that can be used to build custom orthopedic and dental implants from Ti–6Al–4V powder.¹⁰ Not only does this method save time, material, and money, but it also allows customized implants with micron-scale resolution.¹¹ Customized implants eliminate the need for further manipulation of the implanted material during surgery or piecing together multiple parts of material. Such advancements in manufacturing technology have shown positive results both *in vitro* and *in vivo*, and recently, these manufacturing methods have been implemented clinically.^{10,12–14}

From a scientific perspective, manipulating chemical and physical parameters can alter the biological response at the surface. For decades, scientists have tried to understand what factors are needed to optimize the surface for increased cell attachment, osteoblast differentiation, and ultimately osseointegration with the surrounding and new bone. Our lab has shown the importance of wettability, surface micro- and nanoroughness, and implant macrostructure in increasing osteoblast response to implant surfaces.^{15–18} These factors influence protein adsorption and cell response at the implant surface but have also been shown to affect osteoblastic differentiation and formation of an osteogenic environment at sites distal to the implant.^{18,19} In addition, various animal models used by ours and other labs continue to explore osseointegration of new surfaces *in vivo* to translate between mechanistic studies and clinical relevance.^{13,20,21}

Although small rodents are commonly used for preclinical studies due to their low price and availability, implants or surfaces must be designed with smaller dimensions to conform to these models.²⁰ Rabbits are a larger animal model that can be used with clinically relevant implant sizes, with various studies validating implant placement in rabbit tibias or femurs.^{22–24} Rabbits comprise 35% of all animal studies and are the most used model in musculoskeletal research.²⁵

In this study, we compared the biological response to Ti–6Al–4V surfaces and implants manufactured by either traditional milling using computer numerical control (CNC) technology or DMLS. We first compared osteoblast response to disks fabricated by CNC milling and then polished to yield a smooth surface (CNC-M) with disks fabricated by the laser-sintering technology (LST) followed by processing to generate smooth (LST-M), grit blasted (LST-B), and grit-blasted/acid etched (LST-BE) surfaces. To determine if LST-BE implants were osteogenic *in vivo*, we compared their osseointegration with commercially available CNC-B implants in a rabbit model. We hypothesized that laser sintered surfaces would induce osteoblast differentiation in a roughness-dependent manner and that laser sintered implants with post-fabrication surface roughness would osseointegrate in a manner comparable to, if not better than, clinically used CNC-manufactured and grit blasted implants.

MATERIALS AND METHODS

Surface manufacturing

All disks used for *in vitro* studies were 15 mm in diameter and 1 mm in height in order to fit snugly into wells in a 24-well plate. Grade 4 Ti–6Al–4V rods were cut using CNC milling and polished using aluminum oxide sandpaper (P240, Norton Abrasive, Paris, France) to yield a smooth surface (CNC-M). LST surfaces were sintered as disks as published previously.¹² Briefly, Ti–6Al–4V particles 24–45 mm in diameter were sintered with a Ytterbium fiber laser (EOS, EmbH, Munchen, Germany) using a scanning speed of 7 m s^{−1}, wavelength of 1054 nm, continuous power of 200 W, and laser size of 0.1 mm. LST-M surfaces were polished as above to produce a smooth surface. LST-B surfaces were blasted with calcium phosphate particles in a proprietary method (AB Dental, Ashdod, Israel). LST-BE surfaces were laser sintered, blasted with calcium phosphate particles and then acid etched for 90 min in 10% of a 1:1 ratio of maleic and oxalic acids (Sigma-Aldrich, St. Louis, Missouri) in distilled water. All disks and implants were generously provided as a gift from AB Dental.

Scanning electron microscopy

Scanning electron microscopy (SEM, Hitachi SU-70, Tokyo, Japan) was used to obtain low and high magnification images of surfaces and implants. Images were taken at an accelerating voltage of 4 kV, objective aperture of 30 mm, and a working distance of 4 mm. Various magnifications were used to image locations across samples and the most representative images chosen for each sample. High magnification images were used to qualitatively assess surface nano-roughness.

X-ray photoelectron spectroscopy

The surface chemical composition was determined by X-ray photoelectron spectroscopy (XPS, ThermoFisher ESCALab 250, Waltham, Massachusetts). Survey scans were taken using an Al-Kα X-ray source and a spot size of 500 nm. Six locations were surveyed for each implant, with two implants

per group analyzed for a total average across $n = 12$ locations.

X-ray dispersive spectroscopy

Chemical analysis was performed by energy dispersive X-ray spectroscopy (EDX, Hitachi SU-70, Tokyo, Japan) at an accelerating voltage of 15 kV and a working distance of 15 mm. Scans were performed for 50 s, and atomic percentages were recorded as the average of six scans per group.

Laser confocal microscopy

Laser confocal microscopy (LCM, LEXT OLS4000, Olympus, Center Valley, Pennsylvania) was used to assess average surface micro-roughness (S_a) and peak-to-valley height (S_z). Scans were taken over a $644 \mu\text{m}^2$ area with a $20\times$ objective and $0.5 \mu\text{m}$ step size. A cutoff wavelength of $100 \mu\text{m}$ was used to exclude effects of waviness. Three measurements were taken per sample, with two samples per group analyzed ($n = 6$).

Contact angle and immersion analysis

Wettability of surfaces was assessed through sessile drop contact angle. A $4 \mu\text{L}$ drop of distilled water was deposited on surfaces using a goniometer (Rame-hart model 200, Succasunna, New Jersey) and was analyzed with DROPimage (Rame-hart). For hydrophilic samples, surfaces were dried for 1 min with flowing nitrogen between measurements. Five drops were analyzed per sample, with two samples per group ($n = 10$). Reported measurements are the mean and standard deviation of the left and right contact angles for each group. Images of implant immersion into distilled water were captured to evaluate implant wettability qualitatively.²⁶

Cell culture

A cell culture model established by our lab for analyzing osteoblast response to clinically relevant surfaces was used to assess cell response to laser sintered surfaces.^{27,28} MG63 osteoblast-like cells (ATCC, Manassas, Virginia) or normal human osteoblasts (NH0st, Lonza, Walkersville, Maryland) were plated onto tissue culture polystyrene (TCPS), CNC-M, LST-M, LST-B, and LST-BE surfaces at a density of 10,000 cells/ cm^2 . MG63 cells were used before passage 15 while NH0sts were between passage 4 and 7. Cells were cultured in Dulbecco's modified Eagle's medium supplemented with 10% fetal bovine serum (Life Technologies, Carlsbad, California), 50 U/mL penicillin, and 50 $\mu\text{g/mL}$ streptomycin in a 24-well plate. Cells were fed 24 h after plating and every 48 h thereafter until cells reached confluence on TCPS (approximately 5 days after plating for MG63 cells and 7 days for NH0sts). The medium was replaced at confluence. All statistical analyses for *in vitro* studies were conducted using one-way analysis of variance (ANOVA) with Bonferroni-post-correction and a p values of <0.05 indicating significance.

Secreted factors analysis

At 24 h post-confluence, conditioned media were collected, cell monolayers were rinsed twice with PBS and lysed in 0.05% Triton X-100, and both were frozen overnight before analysis. Cell lysates were homogenized by sonication. DNA content (QuantiFluor, Promega, Madison, Wisconsin) and alkaline phosphatase specific activity (p -nitrophenol release from p -nitrophenyl phosphate at pH 10.25, normalized to the protein content of lysate) were measured.

Culture supernatants were used to quantify protein release by cells. Enzyme-linked immunosorbent assays were used to quantify osteocalcin (Alfa Aesar, Ward Hill, Massachusetts), osteoprotegerin (OPG, R&D Systems, Minneapolis, Minnesota), vascular endothelial growth factor A (VEGF, R&D Systems), fibroblast growth factor 2 (FGF2, R&D Systems) and bone morphogenetic protein 2 (BMP2, PeproTech, Rocky Hill, New Jersey) following manufacturer's instructions. Immunoassay results for each culture were normalized to total cell number.

mRNA analysis

In a separate set of culture, cells for mRNA analysis were incubated with fresh media for 12 h after cells reached confluence on TCPS. TRIzol® was used to isolate RNA according to manufacturer's instructions and reverse transcribed into cDNA (High Capacity cDNA Kit, Life Technologies, Carlsbad, California). The cDNA was used for quantitative real-time polymerase chain reaction with SYBR Green (Life Technologies). Known dilutions of cDNA were used to generate standard curves and mRNA of integrin subunits $\alpha 2$ (F: ACTGTTCAAGGAGGAGAC; R: GGTCAAAGGCTTGTTAGG) and $\beta 1$ (F: ATTACTCAGATCCAACCAC; R: TCCTCCTCA TTTCATTCATC), and were normalized to the expression of glyceraldehyde 3-phosphate dehydrogenase (GAPDH, F: GCTCTCCAGAACATCATCC; R: TGCTTCACCACCTTC TTG).

Implant manufacturing

All implants were 3.7 mm in diameter and 8 mm in length and manufactured by AB Dental. Commercially available machined implants were fabricated using a traditional CNC manufacturing process and treated with a proprietary bioresorbable blasting method (AB Dental, Ashdod, Israel) to induce surface roughness (CNC-B). LST implants were laser sintered from Ti-6Al-4V powder as described above, blasted with calcium phosphate, and subsequently acid etched in the same manner used to generate LST-BE disk surfaces. All implants were sterilized with 2.5 Mrad of gamma radiation before use.

Surgical procedure

Skeletally mature, male New Zealand white rabbits weighing 4 ± 0.25 kg were obtained from Harlan Laboratories (Rossdorf, Germany). Each rabbit received two implants: a CNC-B implant placed in its left femur and an LST-BE implant placed in its right femur. Rabbits were given full anesthesia through flowing isoflurane. A 3 cm skin incision was made laterally at the distal femur, and muscle and soft tissue were separated. Drilling was carried out at low speed and

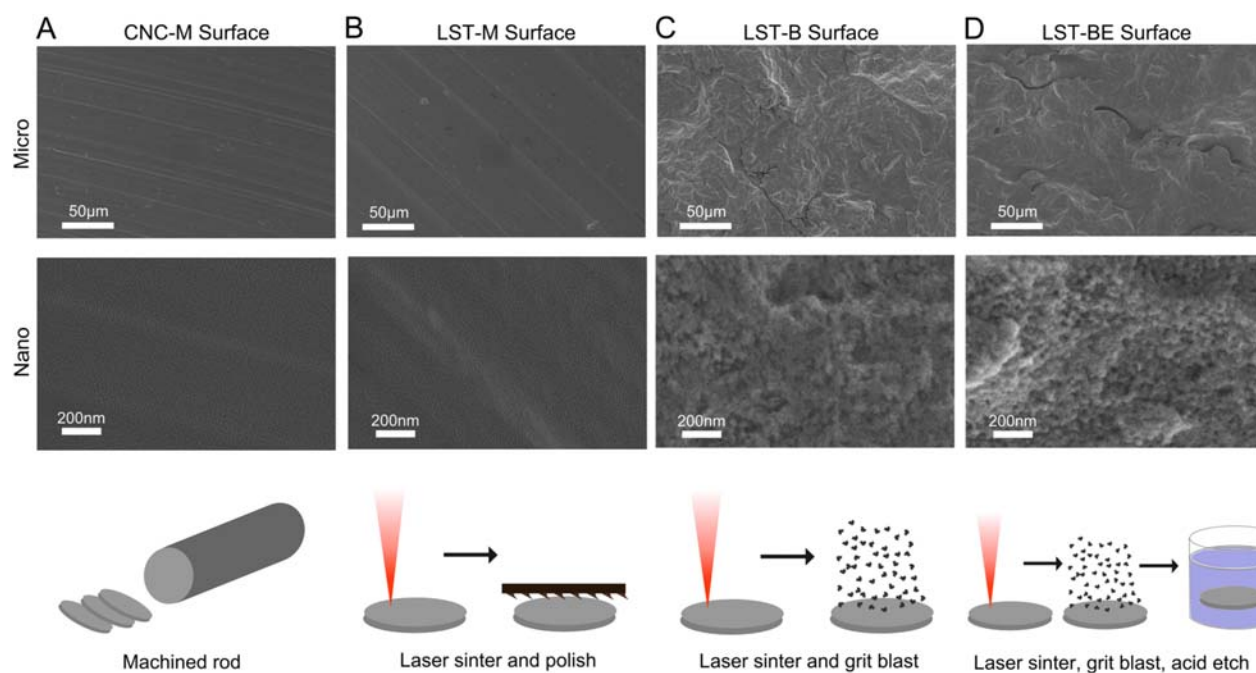


FIGURE 1. SEM micrographs of CNC-M (A), LST-M (B), LST-B (C), and LST-BE (D) surfaces used for *in vitro* studies. A low magnification view shows micro-roughness (top) and high magnification view shows nano-roughness (middle). CNC-M surfaces were cut from a rod (A, bottom), while LST-M, LST-B, and LST-BE surfaces were produced by laser sintering with further surface treatment (B–D, bottom).

was accompanied by physiological saline irrigation. CNC-B implants were placed transaxially in the distal right femur, and LST-BE implants were implanted into the contralateral (left) femur. Each rabbit received one implant in each femur, with eight animals per time point and analysis. The cover screw remained above bone level, periosteum and muscle was reapproximated, and a simple running suture technique was used to close the surgical site skin incision. Animals were euthanized 3 or 6 weeks after implantation. Implants and surrounding bone were harvested for microcomputed tomography (microCT), histomorphometry, and mechanical testing (described below). The Animal Research Committee approved animal protocols at the University of Goethe (Frankfurt, Germany) and guidelines for the care and use of laboratory animals were observed. Statistical analysis of the histologic assessment of bone-implant contact (BIC) was conducted using one-way ANOVA and Tukey's tests with a *p* values of 0.05. Student's *t* test, with a *p* values of 0.05 indicating significance was used for comparison between two groups in the histologic assessment, microCT, and mechanical testing.

Histology

Animals were euthanized at each time point, and femurs were harvested and then were fixed in 10% neutral buffered formalin. Eight implants were examined for each condition, and six implants measured for 3 week machined implants. Samples were embedded in methyl methacrylate. Histological sections longitudinal to the implant and transaxial to the animal were obtained from each sample (Histon LLC, Everett, Washington). Each section was stained using Stevenel's Blue.^{29–31}

Slides were imaged using transmitted light bright field on a Zeiss Observer Z1 (Oberkochen, Germany) microscope equipped with a 10× objective and 10× optical zoom. Images were captured by an AxioCam MRc5 camera and were analyzed with Zeiss ZEN Pro Blue Edition software. The trabecular and cortical perimeter of each implant were measured using the curve (polygon) tool; the perimeter of the implant directly adjacent to the cortical bone was measured as cortical perimeter and the remainder as trabecular bone. BIC was assessed in three measurements: trabecular BIC, cortical BIC, and total BIC. Contact percentage was found by dividing the length of contact in the cortical and trabecular regions by the cortical and trabecular perimeters, respectively. The total BIC was calculated by summing both lengths of contact and dividing by the total perimeter of the implant.

MicroCT analysis

MicroCT (Bruker SkyScan 1173, Kontich, Belgium) was performed on rabbits 3 and 6 weeks after implantation. Eight implants were examined for each condition, and six implants measured for 3 week machined implants. Samples were scanned at a resolution of 1120×1120 pixels, using a 1.0 mm aluminum filter, a source voltage of 130 kV, source current of 61 μ A, image pixel size of 18.69 μ m, exposure of 350 ms, rotation step of 0.1° , and averaging and random movement correction every 10 frames. A standard Feldkamp reconstruction was performed on a subset of samples using NRecon software (Bruker, Kontich, Belgium) with a Gaussian smoothing kernel of zero and a beam hardening correction of 12%. BIC was determined by analyzing reconstructed scans in CTA image analysis software.

TABLE I. Average Roughness and Peak-to-Valley Heights of CNC-M, LST-M, LST-B, and LST-BE Surfaces

Sample	Average (S_a) (μm)	Peak-to-valley height (S_z) (μm)
CNC-M	1.42 ± 0.10	28.59 ± 3.61
LST-M	1.71 ± 0.05	35.26 ± 11.59
LST-B	2.39 ± 0.28	49.40 ± 8.61
LST-BE	2.94 ± 0.32	57.66 ± 7.33

(Bruker, Kontich, Belgium). Sagittal cross sections were thresholded to analyze implant volume within a 25 μm radius of the inner periphery. The image was then thresholded again to remove the implant by shrink wrapping the region of interest and despeckling the image. The bone volume within a 25 μm radius of the outer implant periphery was then analyzed by thresholding and despeckling the region of interest. The quotient of the bone volume and implant volume, multiplied by 100, was calculated as the total BIC.

Mechanical testing

Pull out testing was performed as a commonly used technique for evaluating mechanical properties of implant osseointegration in a rabbit femur model (MTS Insight 30; MTS Systems Corp., Eden Prairie, Minnesota).³² In contrast to evaluating bone contact at the interface with torsional testing, pull out testing evaluates the quality of new bone formation around the implant.³³ A custom abutment fabricated by AB Dental was screwed completely into the implant and then was pulled at a crosshead speed of 5 mm/min according to ASTM standard 543-13. Axial pull-out strengths were recorded and the load was monitored for force at failure (N). Three animal-matched pairs of implants were examined 3 weeks after implantation and five pairs of implants were examined 6 weeks post-implantation.

RESULTS

Surface roughness and topography

All surfaces showed varying degrees of surface roughness. CNC-M and LST-M surfaces were smooth at both the micro- and nanoscale [Fig. 1(A,B)]. Both LST-B and LST-BE surfaces possessed similar micro-roughness and homogeneously distributed nanostructures [Fig. 1(C,D)]. LCM analysis showed increasing average surface roughness (S_a) for CNC-M

TABLE III. Sessile Drop Contact Angle of CNC-M, LST-M, LST-B, and LST-BE Surfaces

Sample	Contact angle ($^\circ$) \pm SD
CNC-M	108 ± 8
LST-M	111 ± 5
LST-B	<20
LST-BE	25 ± 7

(1.42 ± 0.10 μm), LST-M (1.71 ± 0.05 μm), LST-B (2.39 ± 0.28 μm), and LST-BE (2.94 ± 0.32 μm) (Table I). In the same manner, peak-to-valley height (S_z) increased for CNC-M (28.59 ± 3.61 μm), LST-M (35.26 ± 11.59 μm), LST-B (49.40 ± 8.61 μm), and LST-BE (57.66 ± 7.33 μm). Though blasting with calcium phosphate and acid etching both resulted in increased S_a and S_z compared to smooth surfaces, the increase of roughness on LST-B surfaces compared to LST-M was larger than the increase in roughness on LST-BE surfaces compared to LST-B surfaces.

Elemental analysis

Elemental composition analysis by EDX showed a prominence of Ti, followed by Al and V elements on all surfaces (Table II). Ti, Al, and V were present on CNC-M, LST-M, and LST-BE surfaces at similar levels. However, LST-B surfaces had reduced Ti, Al, and V and a more O compared to other surfaces.

Surface wettability

Contact angle measurements showed that LST-B had significantly lower contact angle and, therefore, higher surface wettability, compared to all other surfaces (Table III). The contact angles of CNC-M ($108 \pm 8^\circ$) and LST-M ($111 \pm 5^\circ$) were not significantly different from each other. However, micro-rough LST-B and LST-BE surfaces were hydrophilic with contact angles of $<20^\circ$ and $25 \pm 7^\circ$, respectively.

In vitro cell response

DNA was higher in MG63 cells cultured on LST surfaces than on CNC-M [Fig. 2(A)]. Alkaline phosphatase specific activity [Fig. 2(B)], osteocalcin [Fig. 2(C)], osteoprotegerin [Fig. 2(D)], FGF2 [Fig. 2(F)], and BMP2 [Fig. 2(G)] were higher in MG63 cells on LST-B and LST-BE surfaces than cells on smooth (CNC-M and LST-M) surfaces. VEGF was only higher on LST-BE surfaces in comparison to M and LST-M surfaces [Fig. 2(E)]. mRNA levels of ITGA2 [Fig. 2(H)] and ITGB1 [Fig. 2(I)] increased on LST-B and LST-BE surfaces in comparison to CNC-M surfaces, but there was no difference in expression due to the acid etched surface.

While MG63 and NH0st responded similarly on the surfaces examined, the response varied for the specific factors measured. Osteocalcin secreted by NH0st was higher on all LST surfaces in comparison to CNC-M, and was higher on LST-B and LST-BE surfaces compared to LST-M surfaces [Fig. 3(A)]. OPG was increased on LST-B and LST-BE in comparison to CNC-M and LST-M surfaces [Fig. 3(B)]. VEGF was increased on LST-B and LST-BE surfaces in comparison to CNC-M and LST-M surfaces, and was significantly higher on

TABLE II. EDX Elemental Analysis of CNC-M, LST-M, LST-B, and LST-BE Surfaces

Sample	Concentration [atomic % \pm SD]			
	Ti	Al	V	O
CNC-M	86.6 ± 1.1	9.3 ± 1.2	4.0 ± 0.2	–
LST-M	87.1 ± 1.1	8.9 ± 1.4	4.0 ± 0.3	–
LST-B	59.1 ± 1.5	5.8 ± 0.5	2.5 ± 0.1	32.6 ± 1.6
LST-BE	87.8 ± 0.5	8.3 ± 0.7	3.9 ± 0.2	–

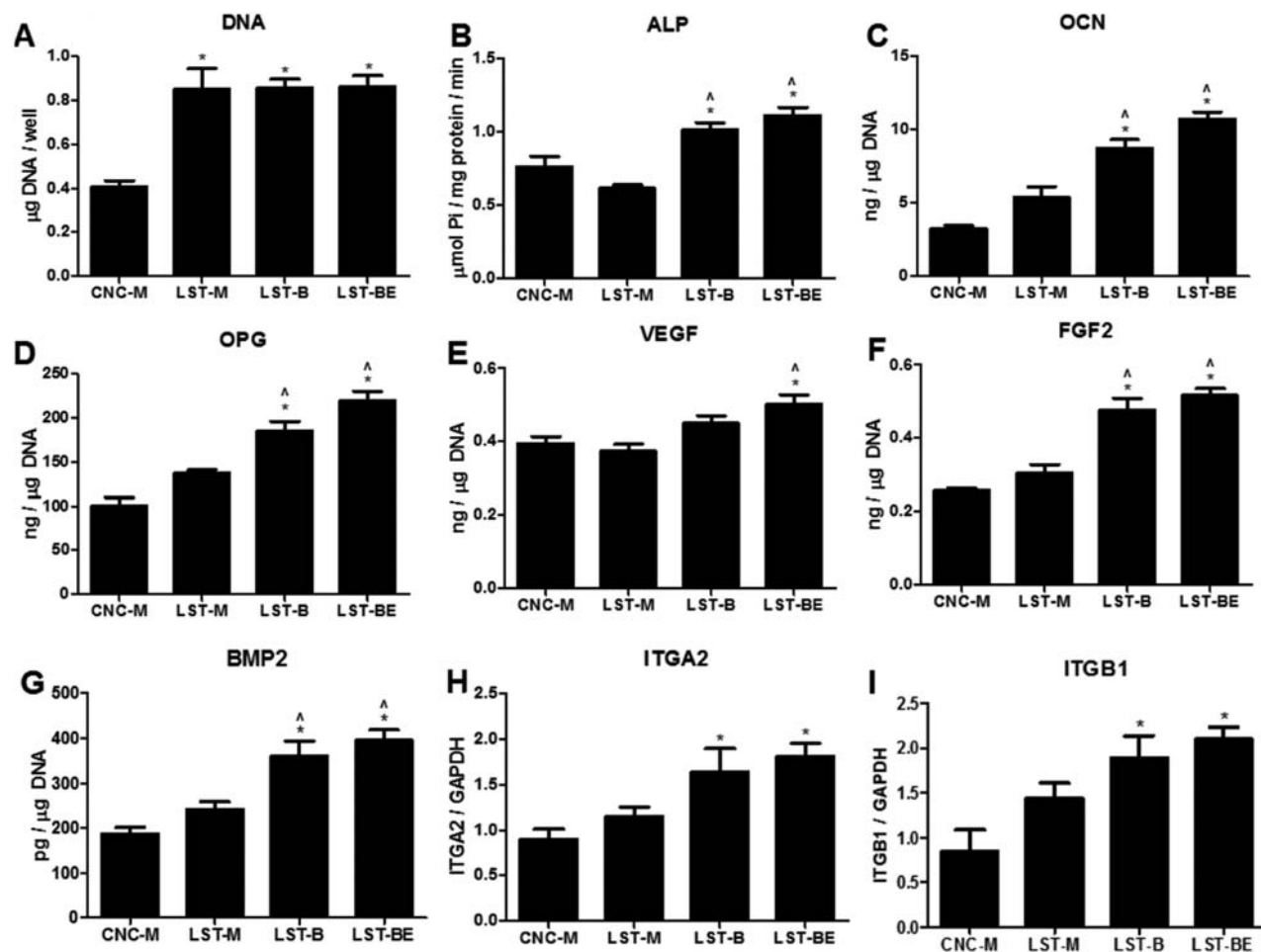


FIGURE 2. MG63 cell response to CNC-M, LST-M, LST-B, and LST-BE surfaces. DNA content (A) and alkaline phosphatase specific activity (B) were analyzed in cell lysates. Osteocalcin (C) vascular endothelial growth factor A (D), fibroblast growth factor 2 (E), and bone morphogenetic protein 2 (F) were measured in cell-conditioned media. mRNA levels of ITGA2 (G) and ITGB1 (H) were measured analyzed in cell media 24 h after confluence. $p < 0.05$, * versus CNC-M, ^ versus LST-M, # versus LST-B.

LST-BE surfaces in comparison to LST-B surfaces [Fig. 3(C)]. BMP2 was higher on LST-B and LST-BE surfaces than on M and further increased on LST-BE surfaces in comparison to LST-B surfaces [Fig. 3(D)].

Implant surface roughness

CNC-B implants were manufactured by a traditional CNC manufacturing process, and LST-BE implants were manufactured via laser sintering. CNC-B and LST-BE implants underwent different surface treatments; however, both implants possessed micro- and nano-roughness [Fig. 4(A,B)]. Although micro-roughness was similar for CNC-B and LST-BE implants, nano-roughness was quite different. LST-BE implants possessed distinct nanostructures on the surfaces while CNC-B implants did not have such distinct nanostructures.

Implant surface chemistry

Surface chemistry analysis by XPS showed mainly Ti, O, and C on implant surfaces, with <3% of F, P, Al, and Si detected on CNC-B implants only (Table IV).

Implant wettability

Sessile drop contact angle on the coronal, non-threaded portion of the implant showed a relatively more hydrophobic surface on CNC-B implants ($85 \pm 2^\circ$) compared to LST-BE implants ($<20^\circ$) [Fig. 4(C)]. Immersion of implants into distilled water showed a similar trend [Fig. 4(D)]. Water was drawn up the sides of the LST implant when immersing, indicating a hydrophilic surface. When pulling the implant out of water, more water was retained on the LST-BE implant compared to the CNC-B implant.

Histology

Histological analysis of CNC-B and LST-BE implants at 3 weeks [Fig. 5(A)] and 6 weeks [Fig. 5(B)], revealed differences in BIC values for each implant. BIC for LST implants was found to be significantly higher than in the machined implants at both the 3 week and 6 week time points [Fig. 5(C,D)]. Cortical BIC at 3 weeks was significantly lower than total or trabecular BIC for both CNC-B and LST-BE implants, although there were no differences in trabecular BIC at 3 weeks. Total BIC in the LST-BE group was statistically

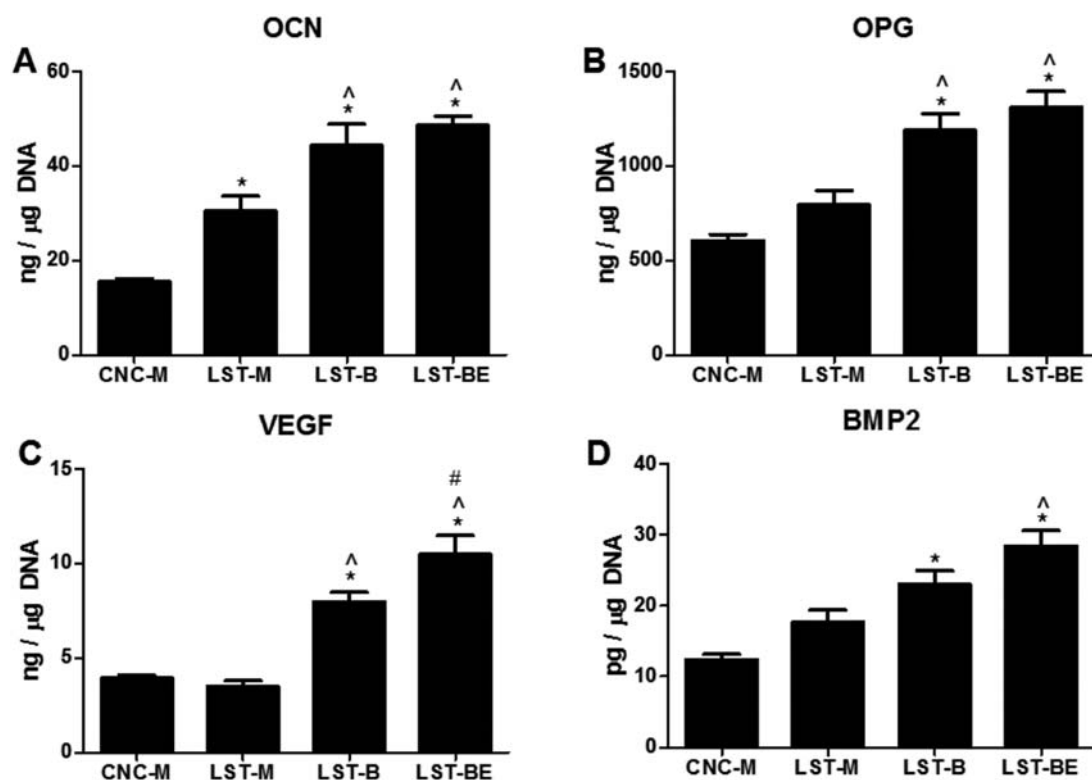


FIGURE 3. NHOst cell response to CNC-M, LST-M, LST-B, and LST-BE surfaces. Osteocalcin (A), osteoprotegerin (B), vascular endothelial growth factor (C), and bone morphogenetic proteins (D) were upregulated on LST-B and LST-BE surfaces. $p < 0.05$. * versus CNC-M, [^] versus LST-M, # versus LST-B.

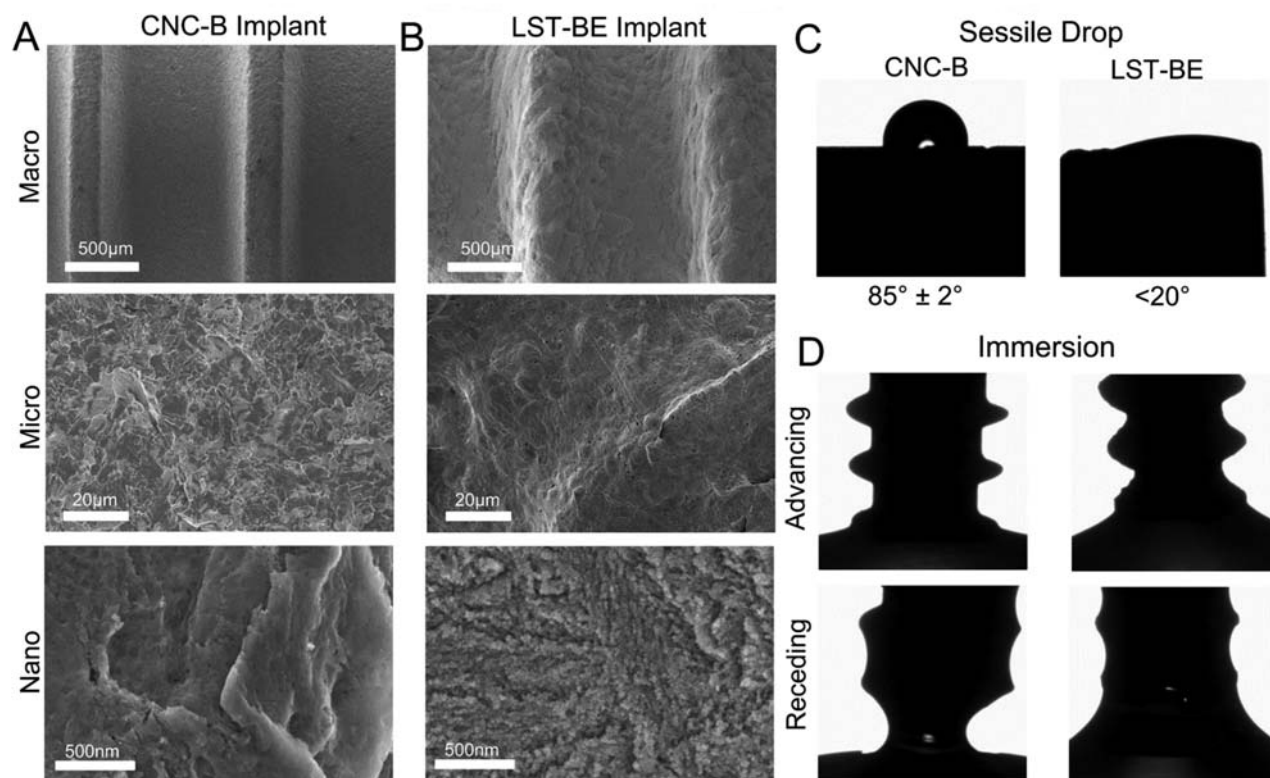


FIGURE 4. Scanning electron micrographs showing macro (top), micro (middle), and nano-roughness (bottom) of CNC-B (A) and LST-BE (B) implants. Sessile drop contact angles of CNC-M (left) and LST-BE (right) implants (C) and immersion analysis of wettability.

TABLE IV. XPS Elemental Analysis of CNC-B and LST-BE Implant Surfaces

Sample	Concentration [atomic % ± SD]						
	Ti	O	C	F	P	Al	Si
CNC-B	14.5 ± 1.2	51.1 ± 2.7	26.3 ± 4.3	2.2 ± 1.9	2.8 ± 1.4	1.7 ± 1.8	1.3 ± 1.4
LST-BE	9.4 ± 1.7	39.1 ± 1.7	39.5 ± 9.1	8.1 ± 4.2	–	–	–

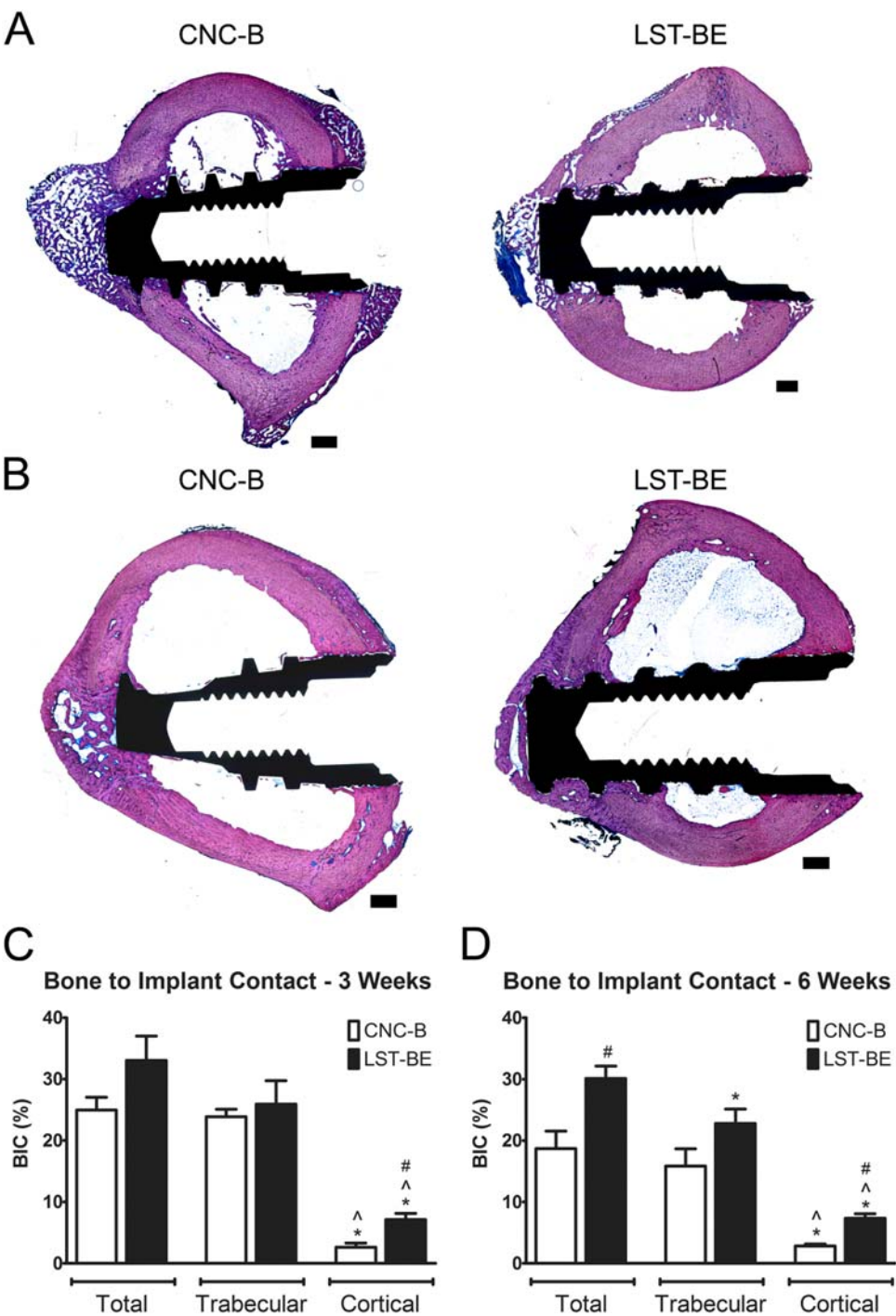


FIGURE 5. Histology stained with Stevenel's Blue of CNC-B implants (left) and LST-BE implants (right) implanted in rabbits after 3 (A, *n* = 6–8) and 6 weeks (B, *n* = 8). BIC analyzed via histology images after 3 weeks (C) and 6 weeks (D) of implantation. Scale bars are 670 μm. One-way ANOVA with Bonferroni correction, *p* < 0.05, * versus total, ^ versus trabecular. Unpaired *t* test, *p* < 0.05, # versus CNC-B implant.

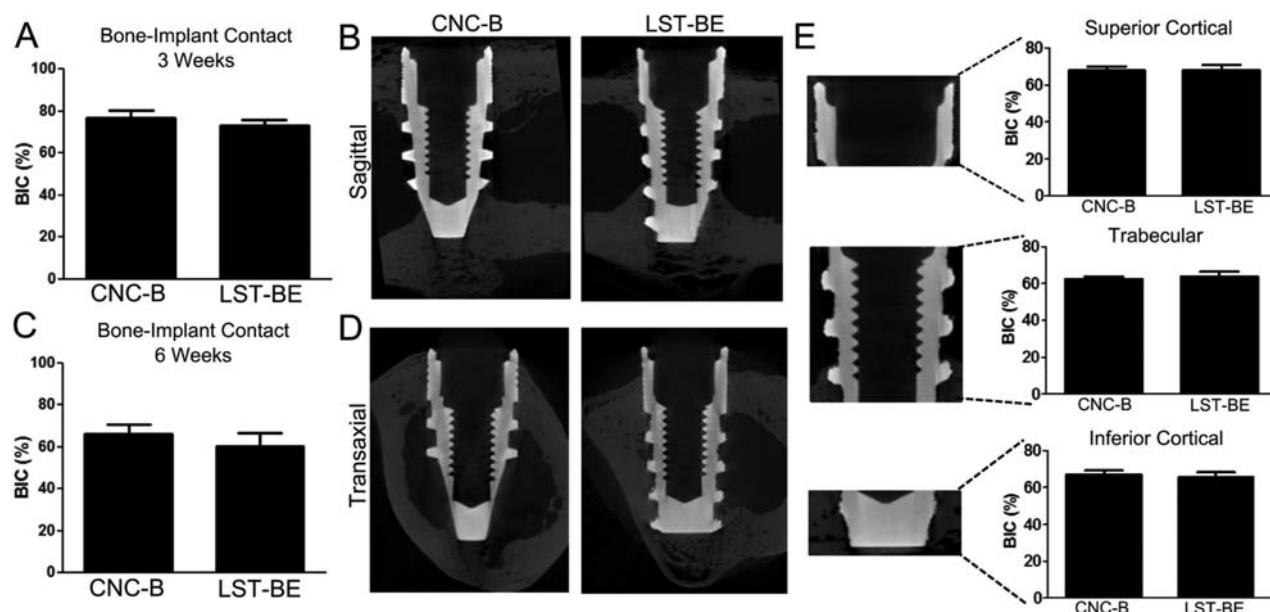


FIGURE 6. BIC values after 3 weeks (A, $n = 6-8$) and 6 weeks (C, $n = 8$) of implantation. MicroCT sagittal (B) and transaxial (D) cross sectional images of CNC-B (left) and LST-BE (right) implants after 6 weeks of implantation. Superior cortical (top), trabecular (middle), and inferior cortical (bottom) regions were analyzed for BIC as well (E).

higher than that in the machined group at 6 weeks. Trabecular BIC of LST-BE implants was significantly lower than total BIC at 6 weeks but was not significantly different from

trabecular BIC of CNC-B implants. Cortical BIC values for both CNC-B and LST-BE implants were lower than total and trabecular BIC values at 6 weeks.

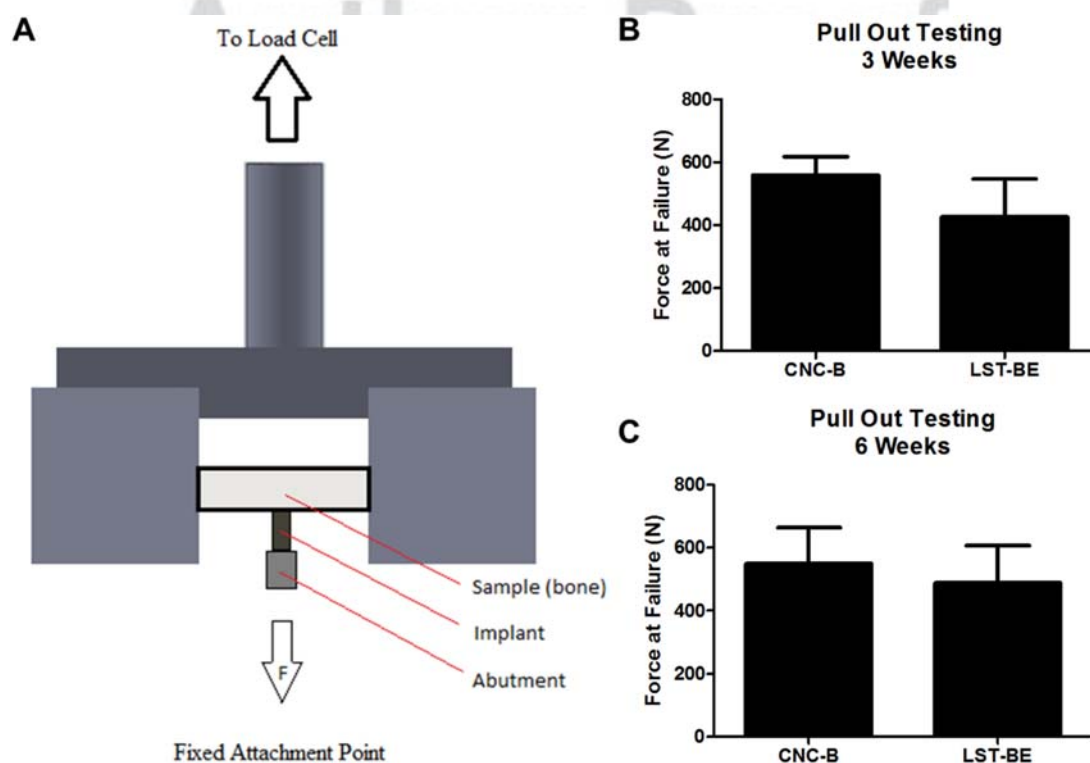


FIGURE 7. A schematic of pull out mechanical testing of implants (A). Force at failure at 3 (B, $n = 3$ implants/type) and 6 weeks (C, $n = 5$ implants/type) after surgery in rabbits. Unpaired t test showed no difference between CNC-B and LST-BE implants.

MicroCT analysis

F6

Osseointegration was achieved for both implant groups, and was compared using microCT analysis. BIC values obtained through microCT analysis were not significantly different between machined and LST-BE implants at 3 and 6 weeks [Fig. 6(A)–(D)]. Additional analysis conducted on the superior cortical, trabecular, and inferior cortical regions of implants showed no difference in BIC values between CNC-B and LST-BE implants at 6 weeks [Fig. 6(E)].

Mechanical testing

F7

The femur specimen was fixed in a custom-fabricated test device with the implant aligned to the machine axis to ensure that no bending moment was created during the test [Fig. 7(A)]. Pullout mechanical testing revealed no significant differences between failure forces for CNC-B and LST-BE implants after 3 [Fig. 7(B)] and 6 [Fig. 7(C)] weeks. Values at 3 and 6 weeks for each implant type were comparable, with strong implant to bone stability.

DISCUSSION

Advanced manufacturing technologies such as laser sintering can produce Ti-6Al-4V constructs with potential use in the dental and orthopedic implant industries. In this study, laser sintering was used in conjunction with surface treatments to produce novel Ti-6Al-4V implant surfaces and implants with hierarchical micro- and nano-roughness and hydrophilicity that increased osteoblast response *in vitro* and osseointegration *in vivo*. Our results indicate that additive manufacturing is a viable method for producing dental implants leading to enhanced biological response, even when compared to a traditionally manufactured, currently used commercial implant.

Surface characterization of disks revealed a unique hierarchical micro-/nano-roughness of LST-BE surfaces with post-processing treatments. Although both blasting (LST-B) and blasting plus acid etching (LST-BE) resulted in this roughness, LCM analysis of roughness values showed higher S_a and S_z values for LST-BE surfaces than LST-B surfaces. Because surface micro-roughness was beyond the z-limit of currently existing atomic force microscopes, nano-roughness could be observed only qualitatively via SEM images.³⁴ In this study, all laser sintered surfaces were post-processed to remove any residual particles or debris remaining from the sintering process and to create a more homogeneous surface roughness that has been shown to result in better biological response.^{10,12} The combination of micro- and nano-roughness on titanium and Ti-6Al-4V has been shown to increase osteoblast maturation, differentiation, and local factor production *in vitro*, and other studies have shown hierarchical roughness and hydrophilicity to be important for increasing osseointegration in animal models as well.^{15,27,35–39}

LST-B surface contained much higher levels of oxygen than any other surface, indicating an increased oxide layer that was a result of the calcium phosphate blasting process. Studies have shown that oxygen retention can occur during

the sintering process, even within an enclosed argon chamber.⁴⁰ Though grit blasting may have exposed these oxygen-rich sites, acid etching was able to alter the surface oxide. Traditionally, strong sulfuric and hydrochloric acids have been used to etch titanium surfaces to induce micro-roughness.⁴¹ Additional aging over time in saline solution or a second oxidation processing step was required to overlay nanostructures on existing micro-roughness.^{27,35,42} In this study, we were able to introduce both micro- and nano-roughness in just one etching step. Maleic and oxalic acids are commonly used to etch human enamel and dentin,⁴³ but this is the first report of the combination used to etch titanium. Although not characterized in this study, material mechanical properties can differ for cast and laser sintered Ti-6Al-4V.¹¹ As hardness and tensile strength can be directly affected by the thickness of the oxide layer, differences in mechanical properties may also be implicated in the biological response.⁴⁴

In vitro studies suggest that LST-BE surfaces possess unique surface characteristics that increase osteoblast differentiation and maturation at the implant site, contribute to the differentiation of cells distal to the implant surface, contribute to the bone remodeling process by decreasing osteoclast resorption, and enhance blood vessel formation to further bone formation. Our lab has pioneered the MG63 cell line as a model for evaluating osteoblast response to surface topography and wettability, showing enhanced maturation for increasing surface roughness and hydrophilicity.^{17,27,45,46} In this study, osteoblasts responded to surfaces in a maturation-dependent manner.

Osteocalcin, a late marker of osteoblast differentiation, has been shown to be regulated by both surface roughness and hydrophilicity in MG63 cells.⁴⁷ While immature osteoblast-like MG63 cells increased osteocalcin protein production on micro-/nano-rough, hydrophilic LST-B and LST-BE surfaces than on the smoother CNC-M and LST-M surfaces, the cells were not able to differentiate between the small changes in roughness between the surfaces examined. In contrast, mature NHOs were more sensitive to small roughness changes in the absence of hydrophilicity, showing increased osteocalcin production on LST-M surfaces compared to slightly smoother CNC-M surfaces. However, NHO osteocalcin production did not differ on the hydrophilic LST-B and LST-BE surfaces possessing a similar magnitude change in surface roughness.

Surface effects on OPG, a RANKL decoy receptor, for both cells were similar. Increased levels of OPG on rough surfaces suggest that surface roughness by itself can affect bone remodeling. By decreasing RANKL binding, secretion of OPG can inhibit osteoclast activity for increased net bone formation by osteoblasts. The increase in OPG on rough surfaces has been attributed to a similarity of surface micro-/nano-features with resorption pits in bone, indicating a possible explanation for the response to rough LST surfaces in our study.⁴⁸

VEGF production by NHOs showed a much more robust response to hierarchical surface roughness and hydrophilicity in comparison to VEGF production by MG63

cells. These results suggest that VEGF may play a more active role later in osteoblast maturation, contributing to continued blood vessel formation and bone integration. BMP2 expression in NHOst cells showed a differential response to small changes in roughness on hydrophilic surfaces LST-B and LST-BE while expression of MG63 cells was similar for both hydrophilic surfaces. Expression of these local factors is important for enhancing osteoblastic differentiation of mesenchymal stem cells distal to the implant, as our group has shown previously.¹⁸ Taken together, our *in vitro* results align with previous observations that a more robust response to nanotopography by mature osteoblasts in comparison to undifferentiated mesenchymal stem cells, with this effect able to be modulated by surface wettability.^{15,35}

Cell surface integrin receptors mediate cell response to biomaterials. In particular, integrin $\alpha 2 \beta 1$ has been shown to play a significant role in the osteoblast and mesenchymal response to titanium surface roughness, though different integrin profiles may play a role depending on cell lineage.^{18,49,50} In this study, we analyzed mRNA expression of $\alpha 2$ and $\beta 1$ integrin subunits, showing increased expression of both these subunits on rough LST-B and LST-BE surfaces compared to smooth CNC-M surfaces. The similar expression profiles of $\alpha 2$ and $\beta 1$ corroborate our theory that $\alpha 2 \beta 1$ is responsible for osteoblast maturation and differentiation on micro-rough surfaces. The presence of hierarchical micro-/nano-roughness on our LST-B and LST-BE suggests that $\alpha 2 \beta 1$ mediates cell response to surfaces at the nanoscale as well.

A variety of animal models have been used to study osseointegration of laser sintered implants.^{21,51,52} We opted to use a rabbit model to compare osseointegration of LST-BE implants with osseointegration of CNC-B implants, which are used clinically. Although rabbits possess differences in bone structure and remodeling in comparison to humans, including a venous plexus within the tibial cortical bone, they have shown similar responses to implant roughness that are seen clinically, and are the most commonly used model for dental implant evaluation.^{53–57} Due to faster skeletal change and bone turnover rates in rabbits compared to humans, studies have shown accelerated healing at 4 weeks.^{58,59} To address the fact that most commonly implants are used in adult humans, we used a fully mature rabbit for the present study.

We evaluated BIC values at 3 and 6 weeks to understand the effects of implant manufacturing and differences in surface roughness on early events in osseointegration. Other studies evaluating osseointegration of implants placed in a similar femoral model in rabbits show new trabecular bone formation by 4 weeks, with continued bone remodeling and growth up to 42 weeks after implantation.^{60,61} Though our study ended at 6 weeks, other studies have shown predictive osseointegration results in rabbits as early as 2 weeks after implantation.⁵⁵ It is possible that differences may have been observed at earlier time points. As with any small animal model where the implant cannot be placed directly in the jaw, mechanical loading will be different.⁵³

We believe that our model is valid for comparing osseointegration of endosseous implants and can be indicative of clinical outcomes. While BIC values showed improvement in osseointegration of LST-BE implants in comparison to CNC-B implants, further studies in disease challenged animal models or at longer time points may be necessary for elucidating the superiority of novel LST implants for improving osseointegration in compromised cases.

Although microCT evaluation of BIC has been compared to histomorphometric analysis with promising results, metal artifacts due to scattering continue to be a confounding factor in accurate microCT analysis.^{62–64} We considered BIC values from both sources and found that histomorphometric analysis was more reliable in describing bone formation during the early stages of osseointegration. Although total BIC was not significantly different between CNC-B and LST-BE implants at 3 weeks, a higher amount of cortical bone was seen in LST-BE implants compared to CNC-B implants. The change in the composition of trabecular and cortical bone between 3 and 6 weeks was evident as well, which was observed at the same time points in a similar implantation model.⁶⁵ Total BIC values were higher for LST-BE implants compared to CNC-B implants at 6 weeks, with a significantly reduced trabecular LST BIC compared to total BIC. This reduction was not seen in either implant group at 3 weeks, suggesting increased bone remodeling of LST-BE implants during the osseointegration process as compared to that of CNC-B implants.

Differences in BIC values can also be attributed to the analysis in different planes. BIC analysis was performed on sagittal cross sections throughout the entire implant for microCT, whereas analysis was carried out on transaxial cross sections for histology. Mechanical testing was performed to verify osseointegration of implants further. Similar pullout forces for both implants indicate that LST-BE implants achieved good mechanical stability, which was comparable to that of the commercially used CNC-B implant. These results suggest that LST-BE implants are similar to, if not better than traditional CNC-B manufactured implants. The enhanced biological response can be attributed to the LST-BE's unique surface properties and ability to promote osteoblast maturation and differentiation at and distal to the surface, influence bone remodeling and increase blood vessel formation for increased osseointegration.

CONCLUSION

Laser sintering is an additive manufacturing technique that can produce Ti-6Al-4V implants. The implants can be further processed to create micro-rough, nano-rough, and hydrophilic surfaces. The resulting surface with combined roughness and wettability enhanced both MG63 and NHOst cell response in comparison to smooth CNC-M and LST-M surfaces. LST-BE implants were compared to commercially available CNC-B implants in a healthy animal model, and cortical BIC was higher at 3 weeks and total BIC higher at 6 weeks than CNC implants. LST-BE and CNC-B implants had similar pullout forces at both time points examined,

indicating that LST-BE implants are as mechanically stable as clinically used implants. These results suggest that implants produced by laser sintering with combined micro-/nano-roughness and high surface energy are a suitable alternative to traditionally manufactured endosseous implants, with favorable biological response and ability to osseointegrate.

ACKNOWLEDGMENTS

The authors would like to thank AB Dental for the surfaces and implants used this study. The content is solely the responsibility of the authors; it does not necessarily represent the official views of the National Institutes of Health.

REFERENCES

1. Van Noort R. Titanium: The implant material of today. *J Mater Sci* 1987;22:3801–3811.
2. McCracken M. Dental implant materials: Commercially pure titanium and titanium alloys. *J Prosthodont* 1999;8:40–43.
3. Elias CN, Lima JHC, Valiev R, Meyers MA. Biomedical applications of titanium and its alloys. *Jom* 2008;60:46–49.
4. Pjetursson BE, Asgeirsson AG, Zwahlen M, Sailer I. Improvements in implant dentistry over the last decade: Comparison of survival and complication rates in older and newer publications. *Int J Oral Maxillofac Implants* 2014;29:308–324.
5. Corbett KL, Losina E, Nti AA, Prokopetz JJZ, Katz JN. Population-based rates of revision of primary total hip arthroplasty: A systematic review. *PLoS One* 2010;5:e13520.
6. Mellado-Valero A, Ferrer Garcia JC, Herrera Ballester A, Labaig Rueda C. Effects of diabetes on the osseointegration of dental implants. *Med Oral Patol Oral Cir Bucal* 2007;12:E38–E43.
7. Aro HT, Alm JJ, Moritz N, Makinen TJ, Lankinen P. Low bmd affects initial stability and delays stem osseointegration in cementless total hip arthroplasty in women: A 2-year RSA study of 39 patients. *Acta Orthop* 2012;83:107–114.
8. Kasat V, Ladda R. Smoking and dental implants. *J Int Soc Prev Community Dent* 2012;2:38–41.
9. McGuire MK, Wilson TG Jr. Commentary: From normal scientific progress to game changers: The impact on periodontal clinical practice. *J Periodontol* 2014;85:1001–1005.
10. Traini T, Mangano C, Sammons RL, Mangano F, Macchi A, Piattelli A. Direct laser metal sintering as a new approach to fabrication of an isoelectric functionally graded material for manufacture of porous titanium dental implants. *Dent Mater* 2008;24:1525–1533.
11. Murr LE, Quinones SA, Gaytan SM, Lopez MI, Rodela A, Martinez EY, Hernandez DH, Martinez E, Medina F, Wicker RB. Microstructure and mechanical behavior of Ti–6Al–4V produced by rapid-layer manufacturing, for biomedical applications. *J Mech Behav Biomed Mater* 2009;2:20–32.
12. Cheng A, Humayun A, Cohen DJ, Boyan BD, Schwartz Z. Additively manufactured 3D porous Ti–6Al–4V constructs mimic trabecular bone structure and regulate osteoblast proliferation, differentiation and local factor production in a porosity and surface roughness dependent manner. *Biofabrication* 2014;6:045007.
13. Amin Yavari S, van der Stok J, Chai YC, Wauthle R, Tahmasebi Birgani Z, Habibovic P, Mulier M, Schrooten J, Weinans H, Zadpoor AA. Bone regeneration performance of surface-treated porous titanium. *Biomaterials* 2014;35:6172–6181.
14. Cohen DJ, Cheng A, Kahn A, Aviram M, Whitehead AJ, Hyzy SL, Clohessy RM, Boyan BD, Schwartz Z. Novel osteogenic Ti–6Al–4V device for restoration of dental function in patients with large bone deficiencies: Design, development and implementation. *Sci Rep* 2016;6:20493.
15. Gittens RA, Olivares-Navarrete R, Cheng A, Anderson DM, McLachlan T, Stephan I, Geis-Gerstorf J, Sandhage KH, Fedorov AG, Rupp F, et al. The roles of titanium surface micro/nanotopography and wettability on the differential response of human osteoblast lineage cells. *Acta Biomater* 2013;9:6268–6277.
16. Schwarz F, Ferrari D, Herten M, Mihatovic I, Wieland M, Sager M, Becker J. Effects of surface hydrophilicity and microtopography on early stages of soft and hard tissue integration at non-submerged titanium implants: An immunohistochemical study in dogs. *J Periodontol* 2007;78:2171–2184.
17. Zhao G, Schwartz Z, Wieland M, Rupp F, Geis-Gerstorf J, Cochran DL, Boyan BD. High surface energy enhances cell response to titanium substrate microstructure. *J Biomed Mater Res A* 2005;74A:49–58.
18. Olivares-Navarrete R, Hyzy SL, Hutton DL, Erdman CP, Wieland M, Boyan BD, Schwartz Z. Direct and indirect effects of microstructured titanium substrates on the induction of mesenchymal stem cell differentiation towards the osteoblast lineage. *Biomaterials* 2010;31:2728–2735.
19. Kopf BS, Ruch S, Berner S, Spencer ND, Maniura-Weber K. The role of nanostructures and hydrophilicity in osseointegration: In-vitro protein-adsorption and blood-interaction studies. *J Biomed Mater Res A* 2015.
20. Olivares-Navarrete R, Raines AL, Hyzy SL, Park JH, Hutton DL, Cochran DL, Boyan BD, Schwartz Z. Osteoblast maturation and new bone formation in response to titanium implant surface features are reduced with age. *J Bone Miner Res* 2012;27.
21. de Wild M, Schumacher R, Mayer K, Schkommodau E, Thoma D, Bredell M, Kruse Gujer A, Gratz KW, Weber FE. Bone regeneration by the osteoconductivity of porous titanium implants manufactured by selective laser melting: A histological and micro computed tomography study in the rabbit. *Tissue Eng Part A* 2013;19:2645–2654.
22. Veltri M, Ferrari M, Balleri P. Correlation of radiographic fractal analysis with implant insertion torque in a rabbit trabecular bone model. *Int J Oral Maxillofac Implants* 2011;26:108–114.
23. He FM, Yang GL, Zhao SF, Cheng ZP. Mechanical and histomorphometric evaluations of rough titanium implants treated with hydrofluoric acid/nitric acid solution in rabbit tibia. *Int J Oral Maxillofac Implants* 2011;26:115–122.
24. Thorey F, Menzel H, Lorenz C, Gross G, Hoffmann A, Windhagen H. Osseointegration by bone morphogenetic protein-2 and transforming growth factor beta2 coated titanium implants in femora of New Zealand white rabbits. *Indian J Orthop* 2011;45:57–62.
25. Neyt JG, Buckwalter JA, Carroll NC. Use of animal models in musculoskeletal research. *Iowa Orthop J* 1998;18:118–123.
26. Rupp F, Gittens RA, Scheideler L, Marmur A, Boyan BD, Schwartz Z, Geis-Gerstorf J. A review on the wettability of dental implant surfaces I: Theoretical and experimental aspects. *Acta Biomater* 2014;10:2894–2906.
27. Gittens RA, McLachlan T, Olivares-Navarrete R, Cai Y, Berner S, Tannenbaum R, Schwartz Z, Sandhage KH, Boyan BD. The effects of combined micron-/submicron-scale surface roughness and nanoscale features on cell proliferation and differentiation. *Biomaterials* 2011;32:3395–3403.
28. Olivares-Navarrete R, Gittens RA, Schneider JM, Hyzy SL, Haithcock DA, Ullrich PF, Schwartz Z, Boyan BD. Osteoblasts exhibit a more differentiated phenotype and increased bone morphogenetic protein production on titanium alloy substrates than on poly-ether-ether-ketone. *Spine J* 2012;22:265–272.
29. del Cerro M, Cogen J, del Cerro C. Stevenel's blue, an excellent stain for optical microscopical study of plastic embedded tissues. *Microsc Acta* 1980;83:117–121.
30. Maniopoulos C, Rodriguez A, Deporter DA, Melcher AH. An improved method for preparing histological sections of metallic implants. *Int J Oral Maxillofac Implants* 1986;1:31–37.
31. Lillie RD, Conn HJ. *Biological Stains: A Handbook on the Nature and Uses of the Dyes Employed in the Biological Laboratory*. Baltimore: Williams and Wilkins; 1977.
32. Salou L, Hoornaert A, Louarn G, Layrolle P. Enhanced osseointegration of titanium implants with nanostructured surfaces: An experimental study in rabbits. *Acta Biomater* 2015;11:494–502.
33. Brånemark R, Öhrnell L-O, Nilsson P, Thomsen P. Biomechanical characterization of osseointegration during healing: An experimental in vivo study in the rat. *Biomaterials* 1997;18:969–978.
34. Hotchkiss KM, Reddy GB, Hyzy SL, Schwartz Z, Boyan BD, Olivares-Navarrete R. Titanium surface characteristics, including

AQ4

AQ5

AQ3

- topography and wettability, alter macrophage activation. *Acta Biomater* 2016;31:425–434.
35. Gittens RA, Olivares-Navarrete R, McLachlan T, Cai Y, Hyzy SL, Schneider JM, Schwartz Z, Sandhage KH, Boyan BD. Differential responses of osteoblast lineage cells to nanotopographically-modified, microroughened titanium–aluminum–vanadium alloy surfaces. *Biomaterials* 2012;33:8986–8994.
 36. Gittens RA, Olivares-Navarrete R, Schwartz Z, Boyan BD. Implant osseointegration and the role of microroughness and nanostructures: Lessons for spine implants. *Acta Biomater* 2014;10:3363–3371.
 37. Wennerberg A, Jimbo R, Stübinger S, Obrecht M, Dard M, Berner S. Nanostructures and hydrophilicity influence osseointegration: A biomechanical study in the rabbit tibia. *Clin Oral Implants Res* 2014;25:1041–1050.
 38. Olivares-Navarrete R, Hyzy SL, Gittens RAs, Schneider JM, Haithcock DA, Ullrich PF, Slosar PJ, Schwartz Z, Boyan BD. Rough titanium alloys regulate osteoblast production of angiogenic factors. *Spine J* 2013;13:1563–1570.
 39. Olivares-Navarrete R, Hyzy SL, Slosar PJ, Schneider JM, Schwartz Z, Boyan BD. Implant materials generate different peri-implant inflammatory factors: Poly-ether-ether-ketone promotes fibrosis and microtextured titanium promotes osteogenic factors. *Spine* 2015;40:399–404.
 40. Santos EC, Osakada K, Shiomi M, Kitamura Y, Abe F. Microstructure and mechanical properties of pure titanium models fabricated by selective laser melting. *Proc Inst Mech Eng C J Mech Eng Sci* 2004;218:711–719.
 41. Li D, Ferguson SJ, Beutler T, Cochran DL, Sittig C, Hirt HP, Buser D. Biomechanical comparison of the sandblasted and acid-etched and the machined and acid-etched titanium surface for dental implants. *J Biomed Mater Res* 2002;60:325–332.
 42. Wennerberg A, Svanborg LM, Berner S, Andersson M. Spontaneously formed nanostructures on titanium surfaces. *Clin Oral Implants Res* 2013;24:203–209.
 43. Fanchi M, Breschi L. Effects of acid-etching solutions on human enamel and dentin. *Quintessence Int* 1995;26:431–435.
 44. Oh JM, Lee BG, Cho SW, Lee SW, Choi GS, Lim JW. Oxygen effects on the mechanical properties and lattice strain of Ti and Ti–6Al–4V. *Met Mater Int* 2011;17:733–736.
 45. Martin JY, Schwartz Z, Hummert TW, Schraub DM, Simpson J, Lankford J, Dean DD, Cochran DL, Boyan BD. Effect of titanium surface roughness on proliferation, differentiation, and protein synthesis of human osteoblast-like cells (MG63). *J Biomed Mater Res* 1995;29:389–401.
 46. Lincks J, Boyan BD, Blanchard CR, Lohmann CH, Liu Y, Cochran DL, Dean DD, Schwartz Z. Response of MG63 osteoblast-like cells to titanium and titanium alloy is dependent on surface roughness and composition. *Biomaterials* 1998;19:2219–2232.
 47. Gittens RA, Scheideler L, Rupp F, Hyzy SL, Geis-Gerstorf J, Schwartz Z, Boyan BD. A review on the wettability of dental implant surfaces II: Biological and clinical aspects. *Acta Biomater* 2014;10:2907–2918.
 48. Zinger O, Zhao G, Schwartz Z, Simpson J, Wieland M, Landolt D, Boyan B. Differential regulation of osteoblasts by substrate microstructural features. *Biomaterials* 2005;26:1837–1847.
 49. Olivares-Navarrete R, Raz P, Zhao G, Chen J, Wieland M, Cochran DL, Chaudhri RA, Ornoy A, Boyan BD, Schwartz Z. Integrin $\alpha\beta1$ plays a critical role in osteoblast response to micron-scale surface structure and surface energy of titanium substrates. *Proc Natl Acad Sci U S A* 2008;105:15767–15772.
 50. Olivares-Navarrete R, Hyzy SL, Berg ME, Schneider JM, Hotchkiss K, Schwartz Z, Boyan BD. Osteoblast lineage cells can discriminate microscale topographic features on titanium–aluminum–vanadium surfaces. *Ann Biomed Eng* 2014;42:2551–2561.
 51. Pattanayak DK, Fukuda A, Matsushita T, Takemoto M, Fujibayashi S, Sasaki K, Nishida N, Nakamura T, Kokubo T. Bioactive Ti metal analogous to human cancellous bone: Fabrication by selective laser melting and chemical treatments. *Acta Biomater* 2011;7:1398–1406.
 52. Mangano F, Chambrone L, van Noort R, Miller C, Hatton P, Mangano C. Direct metal laser sintering titanium dental implants: A review of the current literature. *Int J Biomater* 2014;2014:461534.
 53. Mapara M, Thomas BS, Bhat KM. Rabbit as an animal model for experimental research. *Dent Res J* 2012;9:111–118.
 54. Yang GL, He FM, Yang XF, Wang XX, Zhao SF. Bone responses to titanium implants surface-roughened by sandblasted and double etched treatments in a rabbit model. *Oral Surg Oral Med Oral Pathol Oral Radiol Endod* 2008;106:516–524.
 55. Le Guehennec L, Goyenvalle E, Lopez-Heredia M-A, Weiss P, Amouriq Y, Layrolle P. Histomorphometric analysis of the osseointegration of four different implant surfaces in the femoral epiphyses of rabbits. *Clin Oral Implants Res* 2008;19:1103–1110.
 56. Götz HE, Müller M, Emmel A, Holzwarth U, Erben RG, Stangl R. Effect of surface finish on the osseointegration of laser-treated titanium alloy implants. *Biomaterials* 2004;25:4057–4064.
 57. Coelho PG, Granjeiro JM, Romanos GE, Suzuki M, Silva NRF, Cardaropoli G, Thompson VP, Lemons JE. Basic research methods and current trends of dental implant surfaces. *J Biomed Mater Res B Appl Biomater* 2009;88B:579–596.
 58. Sollazzo V, Pezzetti F, Scarano A, Piattelli A, Bignozzi CA, Massari L, Brunelli G, Carinci F. Zirconium oxide coating improves implant osseointegration in vivo. *Dent Mater* 2008;24:357–361.
 59. Pearce AI, Richards RG, Milz S, Schneider E, Pearce SG. Animal models for implant biomaterial research in bone: A review. *Eur Cell Mater* 2007;13:1–10.
 60. Suzuki K, Aoki K, Ohya K. Effects of surface roughness of titanium implants on bone remodeling activity of femur in rabbits. *Bone* 1997;21:507–514.
 61. Sennerby L, Thomsen P, Ericson LE. Early tissue response to titanium implants inserted in rabbit cortical bone. *J Mater Sci Mater Med* 1993;4:240–250.
 62. Liu S, Broucek J, Viridi AS, Sumner DR. Limitations of using micro computed tomography to predict bone-implant contact and mechanical fixation. *J Microsc* 2012;245:34–42.
 63. Butz F, Ogawa T, Chang T-L, Nishimura I. Three-dimensional bone-implant integration profiling using micro-computed tomography. *Int J Oral Maxillofac Implants* 2006;21:687–695.
 64. Vandeweghe S, Coelho PG, Vanhove C, Wennerberg A, Jimbo R. Utilizing micro-computed tomography to evaluate bone structure surrounding dental implants: A comparison with histomorphometry. *J Biomed Mater Res B Appl Biomater* 2013;101:1259–1266.
 65. Pak H-S, Yeo I-S, Yang J-H. A histomorphometric study of dental implants with different surface characteristics. *J Adv Prosthodont* 2010;2:142–147.

AQ1: Please check whether the grant info is OK.

AQ2: To Editor: Please check whether the placement is OK.

AQ3: Please provide the names of all the authors instead of others in Reference 15.

AQ4: Please provide volume and page range for Ref. 19.

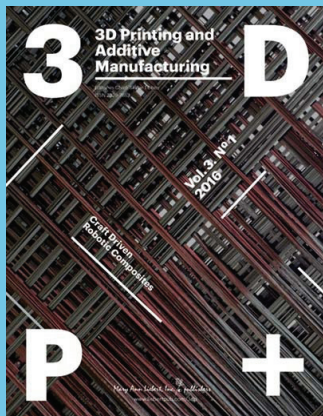
AQ5: Please provide page range for Ref. 20.

AQ6: Please confirm that given names (red) and surnames/family names (green) have been identified correctly.

Please confirm that the funding sponsor list below was correctly extracted from your article: that it includes all funders and that the text has been matched to the correct FundRef Registry organization names. If a name was not found in the FundRef registry, it may be not the canonical name form or it may be a program name rather than an organization name or it may be an organization not yet included in FundRef Registry. If you know of another name form or a parent organization name for a not found item on this list below, please share that information.

FundRef name	FundRef Organization Name (Country)	FundRef DOI	Grant IDs
AB Dental and a National Science Foundation Graduate Research Fellowship (to A.C.)	[NOT FOUND IN FUNDREF REGISTRY]		
SNI program from SENACYT, Panama (R.A.G.)	Alaska Space Grant Program Association of Schools and Programs of Public Health Australian Coal Association Research Program California Department of Alcohol and Drug Programs Canadian Child Health Clinician Scientist Program [NOT FOUND IN FUNDREF REGISTRY]		
National Institute of Arthritis and Musculoskeletal and Skin Diseases (NIAMS) (USPHS Award Nos. AR052102 and AR068703)	National Institute of Arthritis and Musculoskeletal and Skin Diseases	10.13039/1000000069	

Published: Volume 3, number 1, 2016 in:



03

Enhanced Osteoblast Response to Porosity and Resolution of Additively Manufactured Ti-6Al-4V Constructs with Trabeculae-Inspired Porosity

Alice Cheng, Aiza Humayun, Barbara D. Boyan, Zvi Schwartz



Superior Implant Technology

ORIGINAL ARTICLE

Enhanced Osteoblast Response to Porosity and Resolution of Additively Manufactured Ti-6Al-4V Constructs with Trabeculae-Inspired Porosity

Alice Cheng,¹⁻³ Aiza Humayun,⁴ Barbara D. Boyan,^{1,4,*} and Zvi Schwartz^{4,5}

Abstract

The addition of porosity to the traditionally used solid titanium metal implants has been suggested to more closely mimic the natural mechanical properties of bone and increase osseointegration in dental and orthopedic implants. The objective of this study was to evaluate cellular response to three-dimensional (3D) porous Ti-6Al-4V constructs fabricated by additive manufacturing using laser sintering with low porosity (LP), medium porosity (MP), and high porosity (HP) with low resolution (LR) and high resolution (HR) based on a computed tomography scan of human trabecular bone. After surface processing, construct porosity ranged from 41.0% to 76.1%, but all possessed micro-/nanoscale surface roughness and similar surface chemistry containing mostly Ti, O, and C. Biological responses (osteoblast differentiation, maturation, and local factor production) by MG63 osteoblast-like cells and normal human osteoblasts favored 3D than two-dimensional (2D) solid constructs. First, MG63 cells were used to assess differences in cell response to 2D compared to LR and HR porous 3D constructs. MG63 cells were sensitive to porosity resolution and exhibited increased osteocalcin (OCN), vascular endothelial growth factor (VEGF), osteoprotegerin (OPG), and bone morphogenetic protein 2 (BMP2) on HR 3D constructs than on 2D and LR 3D constructs. MG63 cells also exhibited porosity-dependent responses on HR constructs, with up to a 6.9-fold increase in factor production on LP-HR and MP-HR constructs than on HP-HR constructs. NHOs were then used to validate biological response on HR constructs. NHOs exhibited decreased DNA content and alkaline phosphatase activity and up to a 2.9-fold increase in OCN, OPG, VEGF, BMP2, and BMP4 on 3D HR constructs than on 2D controls. These results indicate that osteoblasts prefer a 3D architecture than a 2D surface and that osteoblasts are sensitive to the resolution of trabecular detail and porosity parameters of laser-sintered 3D Ti-6Al-4V constructs.

Introduction

ADDITIVE MANUFACTURING IN THE biomedical space has traditionally been limited to polymer printing through a deposition style method.¹ In contrast, methods such as laser sintering and electron beam melting manufacture from a bed of powder.² These methods allow for a bottom-up manufacturing approach for metals, opening up vast opportunities for engineering implants and devices with improved mechanical strength.

Titanium and its alloys are commonly used materials for orthopedic and dental implants because of their corrosion

resistance, high-strength-to-weight ratio, and ability to osseointegrate with the body.^{3,4} Until recently, these implants have been manufactured through a reductive process to produce a solid implant body. Although the implant body has not changed much over the past few decades, advances in surface technology have introduced micron scale, submicron scale, and nanoscale roughness as well as increased wettability on implant surfaces. These changes at the surface have helped to increase early osseointegration and implant success in patients.^{5,6} However, osseointegration rates still vary widely, especially for patients with diabetes, smokers, and

¹Department of Biomedical Engineering, Georgia Institute of Technology, Atlanta, Georgia.

²Department of Biomedical Engineering, Emory University, Atlanta, Georgia.

³Department of Biomedical Engineering, Peking University, Beijing, China.

⁴Department of Biomedical Engineering, Virginia Commonwealth University, Richmond, Virginia.

⁵Department of Periodontics, University of Texas Health Science Center at San Antonio, San Antonio, Texas.

Opposite page: High resolution microCT image of implants produced by additive manufacturing. Ti-6Al-4V construct with a 3D trabecular bone inspired porosity.

the elderly.^{7–9} In addition, mechanical mismatch in orthopedic implants between the implant bone and host bone can cause stress shielding, leading to repercussions such as increased fracture rates occurring distal to the implant.^{10,11} All these factors contribute toward a need for implants that enhance clinical success.

The introduction of porous implants by additive manufacturing has sought to address these issues. This solution is attractive for its ability not only to manufacture materials with less time and waste but also to design custom implants for patients.^{12–14} Laser sintering is one form of additive manufacturing that has been used to create bone-interfacing Ti-6Al-4V implants.¹³ Already, these laser-sintered solid implants have shown promise in clinical studies.¹⁵ Surface processing methods have been used to achieve similar surface roughness and wettability for additively manufactured Ti-6Al-4V implant materials as traditional implants.¹⁶ Previous studies have shown increased osteoblast-like response to trabecular bone-like constructs based on porosity.¹⁷ Enhanced cell response at the surface can lead to favorable clinical responses. Other porous Ti-6Al-4V implants have shown success through increased bone-to-implant contact and mechanical integration than solid implants in animal studies.^{18,19} However, as porosity of an irregular bone-like trabecular environment can be difficult to define, cell response may depend on more than just how much void space is available within the construct. The combination of well-known surface parameters such as roughness and hydrophilicity with variations in trabecular detail and porosity has not yet been explored.

In this study, we characterize and evaluate biological response to laser-sintered Ti-6Al-4V constructs with a three-dimensional (3D) trabecular bone-inspired porosity. We hypothesize that osteoblastic response will be enhanced on 3D than on two-dimensional (2D) solid constructs, and that this response is porosity and resolution dependent.

Materials and Methods

Material manufacturing and postfabrication surface processing

2D disks and 3D constructs were manufactured using laser sintering (EOS GmbH, Krailling, Germany) from Ti-6Al-4V powder as described previously.¹⁷ 2D disks were 15 mm in diameter and 1 mm in height. A computed tomography (CT) template scan was taken of human femoral trabecular bone (μ CT40; Scanco Medical, Bassersdorf, Switzerland) with a 16 μ m voxel size. Scanco software was used to rotate the template on itself 12, 24, or 36 times to create low porosity (LP), medium porosity (MP), or high porosity (HP) constructs 15 mm in diameter and 5 mm in height, which included a 1 mm solid base. In this study, resolution is defined as the amount of trabecular detail captured from the original CT scan. “High-resolution” constructs are those that captured more detail from the CT template because of higher thresholding within the capture software. “Low-resolution” constructs are those with a lower data capture threshold and resulted in less detail incorporated into the final manufactured construct. Disks and constructs were blasted with CaPO₄ particles, followed by acid etching once in 0.3N HNO₃ at 45°C and twice at 25°C for 5 min. Materials were rinsed in 97% methanol before ultrasonically cleaning three times

for 10 min in ultrapure distilled water at room temperature. Materials were then immersed for 30 min at 80°C in a 1:1 solution of 20 g/L NaOH and 20 g/L H₂O₂ and ultrasonicated again in water at room temperature. Materials were finally immersed in 65% HNO₃ for 30 min before ultrasonically cleaning in water at room temperature. All materials were allowed to dry for at least 24 h to stabilize the oxide layer, then sterilized by gamma irradiation before characterization and cell culture.

Material characterization

Scanning electron microscopy (SEM) was used to evaluate surface topography at the macro-, micro- and submicro/nanoscales (Zeiss AURIGA, Oberkochen, Germany). Images were taken using a 4 kV accelerating voltage, 30 μ m aperture, InLens detector, and 4 mm working distance.

Microcomputed tomography (microCT) was used to evaluate porosity of 3D constructs (SkyScan 1173; Bruker Corporation, Billerica, MA). An accelerating voltage of 100 kV, current of 80 μ A, 1.0 mm aluminum filter, and pixel size of 20.1 μ m were used to image constructs. Files were reconstructed in NRecon software with 100% beam hardening. Reconstructed files were analyzed in CTAn software to determine total porosity (percentage of void space within construct), surface area-to-volume ratio (SA/V), pore diameter (average spherical diameter between metal struts), and strut thickness. The average \pm standard deviation (SD) of porosity parameters was calculated for six samples per group.

Laser confocal microscopy (LCM) was used to image and quantify surface roughness (Zeiss LSM 710). Z-stacks were obtained with a Plan Apochromat 20 \times /0.8 M27 objective with a 5 \times optical zoom, 0.39 μ s pixel dwell, 25 μ m pinhole, 85 \times 85 μ m image size, and z-step of 1 μ m. A 405 nm laser with 50% strength was used in reflection mode. 3D z-stack images were captured of 2D and 3D constructs at 10 \times magnification to show differences in macroscale features. To evaluate surface roughness, z-stacks were taken at 40 \times magnification with a 5 \times optical zoom to eliminate interference from curvature. Average surface roughness (Sa) was defined as the average absolute distance in the z-plane, and peak-to-valley height (Sz) was defined as the average sum of the highest peak and the lowest valley in the z-plane. Roughness values were obtained using ZEN software (Zeiss) and shown as an average \pm SD of six samples per group.

X-ray photoelectron spectroscopy (XPS) was used to analyze surface chemistry (ThermoFisher ESCALab 250). Analysis was conducted using an XR5 gun at 15 kV with a 20 ms dwell time and 1 eV energy step size. A spot size of 500 μ m was used, with average values taken from two survey scans.

Sessile drop contact angle analysis was used to determine surface wettability on 2D disks (Ramé-Hart Instrument Co., Succasunna, NJ). A 4 μ L drop of distilled water was placed on disks, and the left and right angles were averaged every 5 s for 20 s after drop placement. A total of $n=10$ drops were analyzed across two disks.

Mechanical properties of samples were evaluated through compression testing of porous constructs (MTS Insight 30; MTS Systems Corporation, Eden Prairie, MN) at room temperature. Testing was conducted with a speed of 0.02 mm/s, data acquisition rate of 500 Hz/s, preload of 0.01 kN, preload speed of 0.025 mm/s, and strain endpoint of 80%. Testing

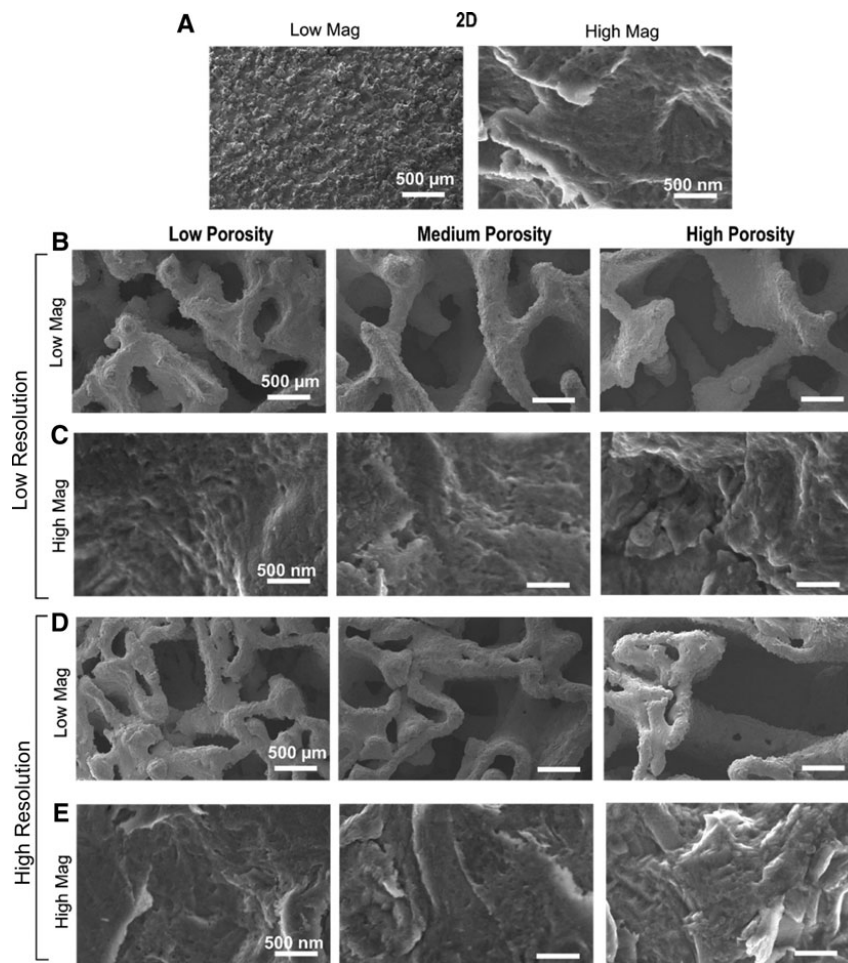


FIG. 1. Scanning electron micrographs of 2D (A), low-resolution 3D (B, C) and high-resolution 3D (D, E) constructs. Low magnification (A [left], B, D) shows macrostructure of constructs, whereas high magnification (A [right], C, E) shows micro- and nanoroughness of surfaces. 2D, two-dimensional; 3D, three-dimensional.

was conducted until failure or a 30 kN maximum load was applied.

Biological response

MG63 osteoblast-like cells (ATCC, Manassas, VA) and normal human osteoblasts (NHSt Donor 25433, Lot 336963; Lonza, Walkersville, MD) were cultured to confluence in T75 flasks before plating. 2D disks and 3D constructs were designed to fit snugly in the bottom of a 24-well plate. Cells were plated at a density of 30,000 cells/cm² according to surface area on tissue culture polystyrene, which was used as an optical control for confluence. Cells were fed with full medium (DMEM +10% FBS +1% penicillin/streptomycin) 24 h after plating. At confluence at approximately day 3, cells were

treated with fresh medium and harvested 24 h afterward for analysis of cell layer lysate and conditioned medium.

DNA content was analyzed by fluorescence using the Quanti-iT kit (Thermo Fisher Scientific, Waltham, MA). Alkaline phosphatase (ALP) specific activity of cell lysates was determined by analyzing release of para-nitrophenol from para-nitrophenolphosphate at pH 10.2. ALP was normalized to total protein content as determined by bicinchoninic acid assay (Thermo Fisher Scientific). Enzyme-linked immunosorbent assays were used to evaluate expression of osteocalcin (OCN; Alfa Aesar, Ward Hill, MA), osteoprotegerin (OPG, R&D Systems, Inc., Minneapolis, MN), vascular endothelial growth factor (VEGF, R&D Systems, Inc.), and bone morphogenetic proteins 2 and 4 (BMP2; PeproTech, Rocky Hill, NJ, and BMP4; R&D Systems, Inc.).

TABLE 1. POROSITY PARAMETERS OBTAINED BY MICROCT (AVERAGE \pm STANDARD DEVIATION)

Group	Total porosity (%)	SA/V ratio	Pore diameter (μ m)	Strut thickness (μ m)
Low resolution				
3DLP	41.0 \pm 0.3	5.1 \pm 0.1	641 \pm 9	673 \pm 10
3DMP	56.6 \pm 2.4 ^a	6.5 \pm 0.3 ^a	785 \pm 15 ^a	572 \pm 18 ^a
3DHP	76.1 \pm 0.8 ^{a,b}	8.1 \pm 0.1 ^{a,b}	1096 \pm 31 ^{a,b}	475 \pm 7 ^{a,b}
High resolution				
3DLP	52.5 \pm 2.1 ^{a-c}	10.2 \pm 0.2 ^{a-c}	461 \pm 9 ^{a-c}	311 \pm 6 ^{a-c}
3DMP	57.3 \pm 0.8 ^{a,c,d}	10.8 \pm 0.3 ^{a-d}	563 \pm 2 ^{a-d}	288 \pm 8 ^{a-d}
3DHP	70.9 \pm 0.4 ^{a-c}	11.5 \pm 0.1 ^{a-c}	872 \pm 6 ^{a-c}	267 \pm 3 ^{a-c}

One-way ANOVA with Bonferroni correction, $p < 0.05$.

^aVersus LP-LR.

^bVersus MP-LR.

^cVersus HP-LR.

^dVersus LP-HR.

^eVersus MP-HR.

LP, low porosity; MP, medium porosity; HP, high porosity; LR, low resolution; HR, high resolution.

Statistics

All material characterization results are shown as average and SD, whereas biological results are shown as average and standard error of the mean (SE). The differences between groups of three or more were measured by one-way analysis of variance (ANOVA) that was performed with a Bonferroni *post hoc* analysis. $p < 0.05$ was considered statistically significant.

Results

Material characterization

SEM images of sintered constructs showed varying macroscale topography but similar micro/submicro-/nanoscale topography after surface processing. 2D controls possessed pronounced peaks observed at low magnification, whereas microroughness with nanofeatures was evident at high magnification (Fig. 1A). Macroscale features of 3D constructs with low resolution (LR) (Fig. 1B) were significantly different than those with high resolution (HR) (Fig. 1D). 3D constructs with HR contained smaller pores and struts within larger features. However, high-magnification images of all 2D and 3D constructs across porosities and resolutions indicated similar microroughness, which included submicron and nanofeatures (Fig. 1C, E).

MicroCT analysis showed that total porosity was 41.0%, 56.6%, and 76.1% for LP-LR, MP-LR, and HP-LR constructs, respectively. Total porosity was 52.5%, 57.3%, and 70.9% for LP-HR, MP-HR, and HP-HR constructs, respectively (Table 1). Total porosity values were not significantly different than open porosity values for the same constructs (Fig. 2A). Cross-sectional images of constructs showed finer detail in HR constructs than in LR constructs, which was evident throughout the bulk of the construct (Fig. 2B). MicroCT analysis also showed that SA/V ratio and pore diameter increased and strut thickness decreased with increasing porosity for both LR and HR constructs (Table 1). SA/V ratio ranged from 5.1 to 8.1 for LR constructs and from 10.2 to

11.5 for HR constructs. Pore diameter ranged from 641 to 1096 μ m for LR constructs and from 461 to 872 μ m for HR constructs. Strut thickness ranged from 475 to 673 for LR constructs and from 267 to 311 for HR constructs.

Surface roughness was evaluated by LCM (Fig. 2C–E). Sa was not significantly different for any of the 2D or 3D construct surfaces. Peak-to-valley height values did not differ for any surfaces except for 3DHP-HR, the values of which were higher than those for 3DMP-LR.

XPS showed that a majority of elements present on the surface of 2D and 3D LR constructs were oxygen (O), carbon (C), and titanium (Ti). The levels of these three main elements did not vary significantly between 2D and 3D constructs (Fig. 3A). Differences were exhibited for lower concentration elements nitrogen (N) and sulfur (S). 2D surfaces possessed a contact angle of $62 \pm 18^\circ$ (Fig. 3B).

Compression testing showed a nonlinear decrease in compressive modulus with increasing construct porosity, with different trends for changes in porosity in LR and HR constructs (Fig. 3C). Average compressive moduli of 3.6 ± 0.083 , 3.4 ± 0.080 , and 2.6 ± 0.078 GPa decreased significantly as porosity increased for LP-LR, MP-LR, and HP-LR constructs, respectively. A similar trend was observed for LP-HR, MP-HR, and HP-HR constructs with respective compressive moduli of 4.1 ± 0.024 , 3.8 ± 0.058 , and 2.4 ± 0.15 GPa.

Cell response

MG63 cells exhibited differential responses to 2D and LR and HR 3D constructs. MG63 cells exhibited porosity- and resolution-dependent responses to 3D constructs. DNA content decreased for all 3D constructs compared with that for 2D surfaces (Fig. 4A). DNA content was further decreased for LP-HR and MP-HR constructs than for all LR constructs, and DNA content increased for HP-HR constructs than for LP-HR and MP-HR constructs. OCN was elevated on HP-LR, LP-HR, and MP-HR constructs than on 2D surfaces and LP-LR constructs (Fig. 4B). OCN for LP-HR and MP-HR constructs was additionally increased than for MP-LR and HP-LR constructs. OPG was elevated on LP-HR and LP-HR constructs than on 2D surfaces, and OPG was elevated on LP-HR than on LP-LR and MP-LR constructs (Fig. 4C). OPG was decreased on MP-HR and HP-HR constructs than on LP-HR constructs. VEGF was increased on HP-LR and MP-HR constructs than on 2D surfaces and LP-LR and MP-LR constructs, and VEGF on MP-HR was also increased than on HP-LR and LP-HR constructs (Fig. 4D). BMP2 was increased on HP-LR, LP-HR, and MP-HR constructs than on 2D surfaces, LP-LR, and MP-LR constructs and decreased on HP-HR constructs than on HP-LR, LP-HR, and MP-HR constructs (Fig. 4E).

NHOS response to 2D versus 3D constructs confirmed the MG63 cell results. Therefore, effects of porosity were only analyzed on HR constructs. NHOS grown on HR constructs exhibited less robust differences to porosity on HR constructs than MG63 cells. DNA content and ALP activity were decreased on all 3D constructs compared with those on 2D surfaces (Fig. 5A, B). Osteocalcin was significantly higher on LP-HR and MP-HR constructs than on 2D surfaces, whereas OPG, VEGF, and BMP4 were elevated on all 3D constructs compared with those on 2D surfaces (Fig. 5D, E, G). BMP2

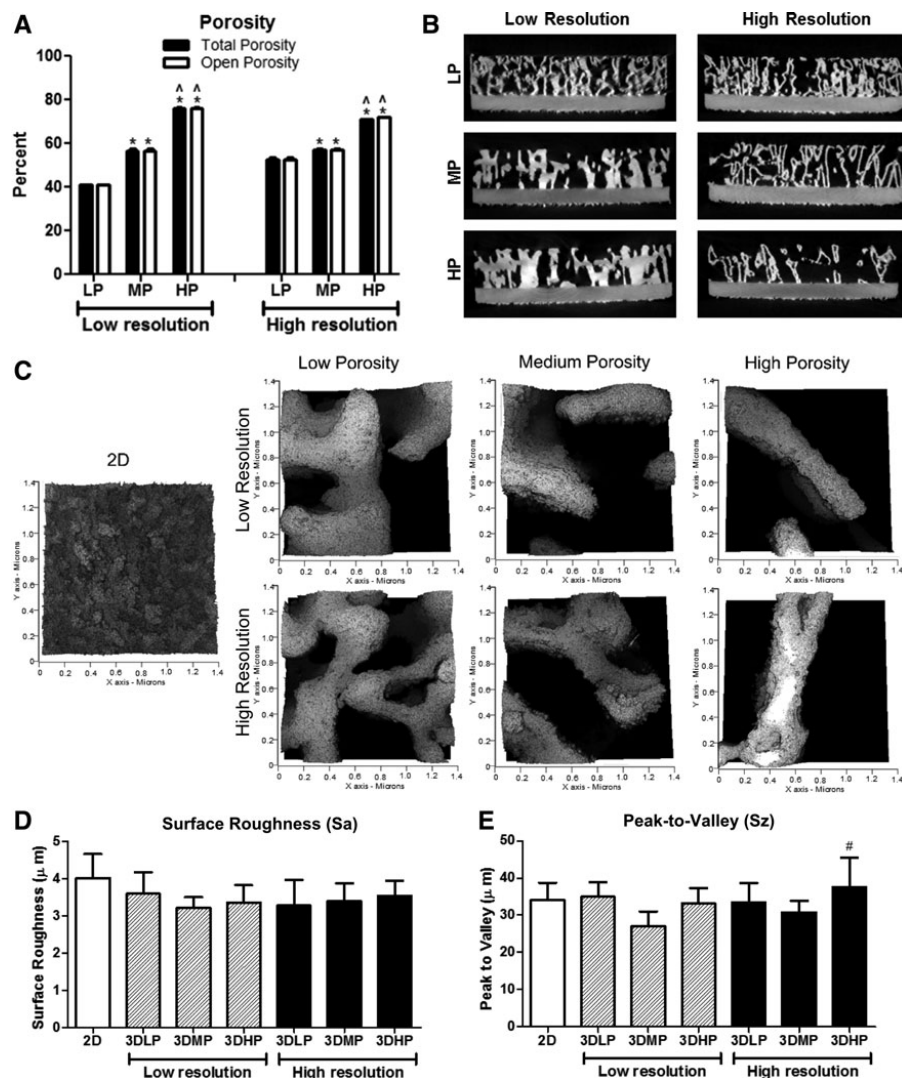


FIG. 2. Total (black) and open (white) porosity values (A) and cross-sectional views (B) of 3D constructs obtained by microCT imaging. One-way ANOVA with Bonferroni correction, $p < 0.05$, *versus LP, ^versus MP within low-and high-resolution groups. Student's *t*-test comparing total and open porosity for each group was not significant. Surface roughness images (C) and average surface roughness (D) and peak-to-valley height values (E) for 2D surfaces and 3D constructs. One-way ANOVA with Bonferroni correction, $p < 0.05$, #versus 3DMP-LR. LP, low porosity; MP, medium porosity; LR, low resolution;

was elevated on all 3D constructs compared with that on 2D surfaces but was decreased on HP-LR constructs compared with that on MP-HR constructs (Fig. 5F).

Discussion

Total and open porosity of 3D constructs did not differ, indicating that all pores were interconnected. MicroCT re-

sults corroborated qualitative SEM observations. Although MP-LR and MP-HR constructs did not have significantly different total porosity values, MP-HR constructs had a significantly higher SA/V ratio and smaller pore diameter and smaller strut thickness than 3DMP-LR constructs. This could also be observed in SEM images and was due to the incorporation of higher detail into 3DMP-HR constructs.

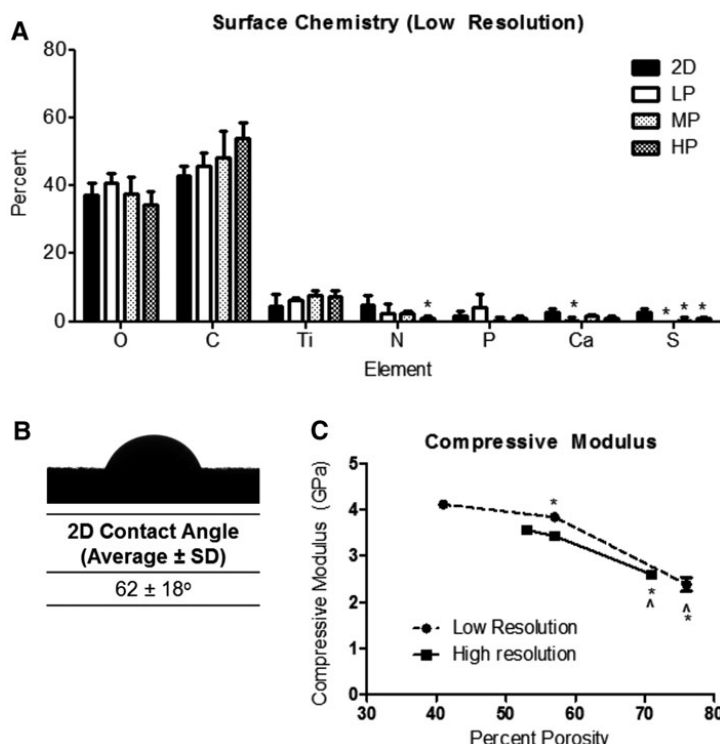


FIG. 3. Surface chemistry of 2D and 3D high-resolution constructs (A). One-way ANOVA with Bonferroni correction, $p < 0.05$, *versus 2D. Contact angle of 2D surfaces (B). Average and standard deviation of compressive modulus values for low-resolution (circles, dotted line) and high-resolution (squares, solid line) 3D constructs (C). One-way ANOVA with Bonferroni correction, $p < 0.05$, *versus low porosity, ^versus medium porosity for each type of resolution.

Although Sa did not differ for constructs, peak-to-valley heights did vary for some. This may have been because of the inability of line-of-sight surface processing techniques to evenly affect and penetrate all parts of the constructs. Although acid etching may be able to penetrate the entire construct, blasting by calcium phosphate may have been limited to certain exposed sites at the surface. Cross-sectional SEM images shown in a previous study corroborate this.¹⁷

Although high-concentration Ti, O, and C elements did not vary across constructs, the presence of low-concentration elements did differ. Variations in nitrogen may be a result of time spent during manufacturing and surface processing, as nitrogen is used in the laser sintering process as well as during etching in HNO_3 . The presence of Ca and P could be attributed to trace elements left behind during blasting with CaPO_4 . Although XPS analysis was averaged across six different areas and multiple constructs, differences in one area may contribute to a larger SD for low-concentration elements.

Contact angle analysis could not be performed on 3D constructs because of the large pores. Although contact angle was performed on 2D surfaces as a proxy, the surface roughness may have contributed to higher SD in contact angle values.²⁰ Additional methods for wettability analysis may need to be

evaluated in the future to gain a better understanding of surface energy on 3D constructs.

Optimal bone substitution materials should have similar mechanical properties to natural bone and integrate well with the surrounding tissue. In addition to their ability to osseointegrate, titanium alloys are attractive for implant materials because of their high-fracture toughness and strength.²¹ However, the high elastic modulus of titanium compared with that of bone can cause significant clinical problems for orthopedic implants. Elastic moduli for bone has been reported to range from 0.5 to 30 GPa based on trabecular or cortical areas, which differs from an elastic modulus of up to 115 GPa for titanium alloys.^{22–24} This difference in bulk material properties can lead to insufficient loading on bone distal to the implant, resulting in stress shielding and bone resorption.^{10,23} For hip implants in particular, reduced stem stiffness by incorporating porosity can decrease bone atrophy due to stress shielding.¹¹

All 3D constructs presented in this study had compressive moduli ranging from 2.4 to 4.1 GPa, which are within the lower range of moduli for bone.²³ Other studies have indicated similar mechanical properties for laser-sintered porous Ti-6Al-4V.^{17,25} Differences in mechanical properties of

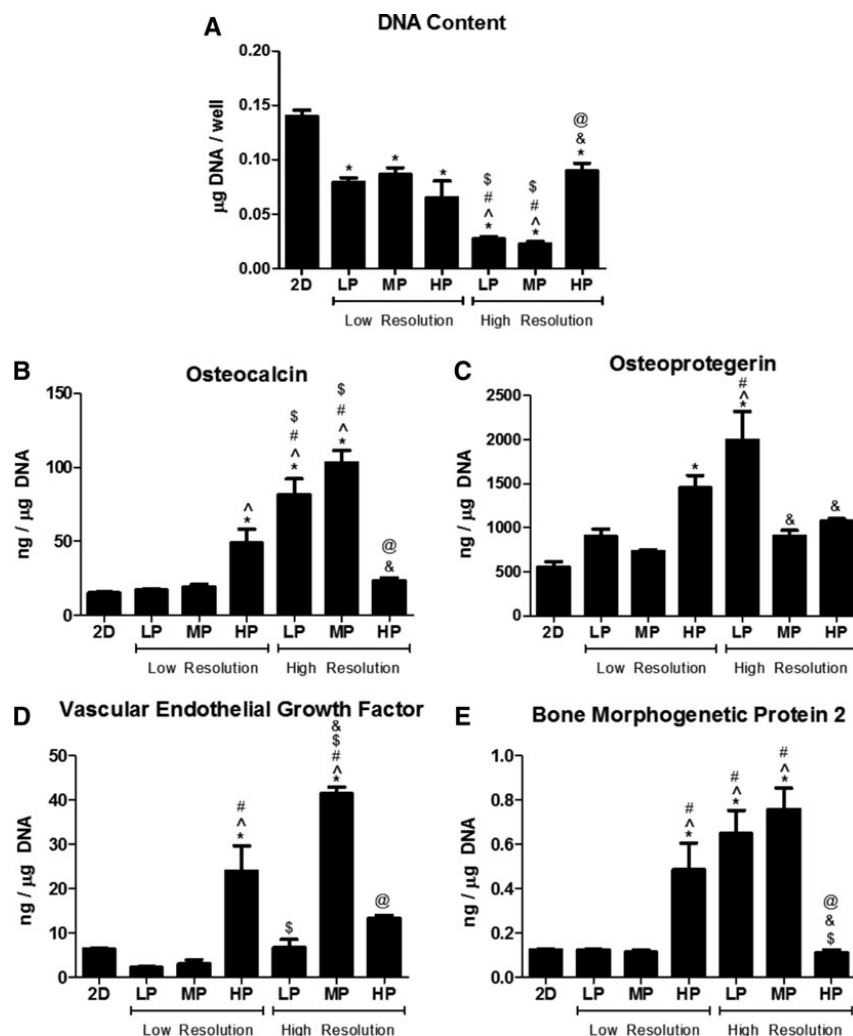


FIG. 4. MG63 cell response to 2D and low- and high-resolution 3D constructs. DNA content (A), osteocalcin (B), osteoprotegerin (C), vascular endothelial growth factor (D), and bone morphogenetic protein 2 (E). One-way ANOVA with Bonferroni correction, $p < 0.05$, *versus 2D, ^versus 3DLP-LR, #versus 3DMP-LR, \$versus 3DHP-LR, &versus 3DLP-HR, @versus 3DMP-HR.

constructs and the nonlinear correlation with total porosity can also be attributed to differences in structural parameters such as strut size and tortuosity.^{26,27} These results indicate that porosity can be tailored to alter mechanical properties for patient- and application-specific implants, with the potential to reduce stress shielding. In this study, compression testing was performed to evaluate the elastic modulus. Although tensile modulus is typically reported for materials, previous studies have shown that compressive and tensile analyses of bone yield comparable modulus values.²⁸ In addition, the load-bearing nature of bone-interfacing implants makes compression testing more clinically relevant. Because com-

pression testing was performed on constructs which included a 1 mm solid base, modulus values may be higher than for completely porous constructs. However, the values presented here may be more clinically relevant for solid implants coated with a porous exterior.

Various studies have shown increased osseointegration through volume of bone ingrowth and mechanical stability of porous implants compared with that of solid implants.^{19,29,30} Our hope is that porosity inspired by nature would yield a better biological response than human-designed porosity. We have seen this concept to be true in previous studies of surface roughness, where osteoblasts exhibit higher factor production

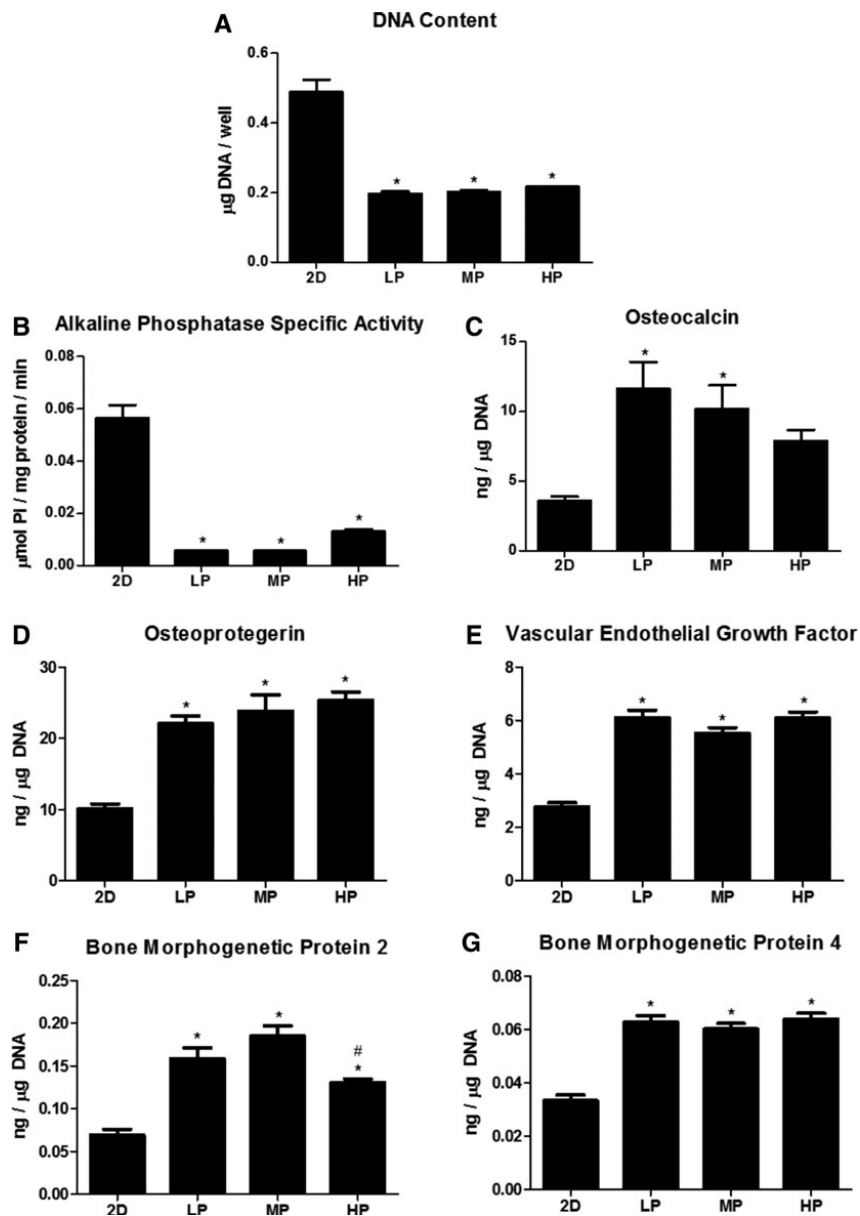


FIG. 5. Normal human osteoblast response to 2D and high-resolution 3D constructs. DNA content (A), alkaline phosphatase specific content (B), osteocalcin (C), osteoprotegerin (D), vascular endothelial growth factor (E), bone morphogenetic protein 2 (F), and bone morphogenetic protein 4 (G). One-way ANOVA with Bonferroni correction, $p < 0.05$, *versus 2D, #versus MP.

on acid-etched and grit-blasted titanium surfaces with a more natural distribution of peaks and valleys than micro-patterned substrates with predefined features.³¹ Other studies have shown the effectiveness of combined micro-/nanoroughness on titanium substrates, mimicking the natural hierarchical

surface roughness of bone, for improving osteoblast response.^{32,33} Through characterization data, we showed that our constructs had similar surface chemistry and multiscale roughness but differences in 3D porosity. Based on the differential biological response to our materials, we propose that

osteoblast response is sensitive to and dependent on changes in pore diameter and structure in 3D Ti-6Al-4V constructs.

Osteoblasts showed increased differentiation, maturation, and local factor production on 3D constructs compared to on 2D solid surfaces. In this study, we first used the MG63 cell line to screen for differences in biological response to 2D versus 3D constructs with LR and HR. The MG63 osteoblast-like cell line is commonly used to evaluate cell response to titanium surfaces. Although immortalized cell lines are attractive for their ease of culture and reduced biological variability, they cannot serve as a substitute for using primary cells. MG63 cells in particular, although acceptable for pilot testing of biomaterials, still exhibit increased proliferation, *RUNX2*, and *BGLAP* gene expression and decreased *ALPL* and *COL1A1* gene expression compared with normal human osteoblasts.³⁴ Owing to the clear preference of MG63 cells for HR constructs, we then chose NHOst as a primary osteoblast to validate MG63 results to changes in porosity only on HR constructs. Although both MG63 and NHOst cells significantly favored 3D porous constructs over 2D solid surfaces, NHOst exhibited less of a porosity-dependent response on HR constructs compared with that of MG63 cells.

This cell-dependent response to titanium surfaces has been shown previously with respect to surface roughness.^{20,35} We propose that this response is also dependent on the stage of osteoblast maturation. A heightened response to various porosities from immature osteoblast-like MG63 cells contrasts a decreased response from NHOst at a potentially different stage of maturation. Our results showed 6.9-, 6.5-, and 6.1-fold increases in OCN, VEGF, and BMP2 for MG63 cells on MP-HR constructs compared with those on 2D controls, respectively, whereas NHOst on the same constructs exhibited 2.9-, 2.0-, and 2.7-fold increases, respectively. We have previously observed that mature osteoblasts exhibit a reduced response to surface roughness as well as to 1,25-dihydroxyvitamin D3 treatment compared to less mature osteoblasts.³⁶

Age and sex are also important considerations when evaluating response of primary cells and have been shown to significantly affect response to titanium substrates.^{37,38} In this study, the NHOst donor was a 2-year-old Caucasian male. It is possible that the young age of this donor resulted in favorable responses to all 3D constructs regardless of porosity, and that an older or more compromised donor would show a more differential response based on porosity. Further studies on primary osteoblast response based on donor age, sex, and potentially health will be necessary to understand whether and how porous constructs can be tailored to certain populations.

Few studies have shown such a clear preference of osteoblasts for 3D porous Ti-6Al-4V constructs over 2D surfaces. Because all materials in this study were manufactured and processed in the same way to achieve similar roughness and chemistry, we propose that the 3D constructs provide a distinct structural advantage over 2D surfaces that increases osteoblast response. It is unclear which specific material parameter drives differentiation of osteoblasts on 3D constructs, if one at all. Previous studies by our laboratory suggest that the enhanced osteoblast response to surface roughness and 3D substrate morphology is dependent upon the $\alpha2\beta1$ integrin, a surface receptor for collagen.^{39,40} Indeed, changes in porosity may lead to variations in cell attachment and orientation, affecting extracellular matrix production and

mineralization.⁴¹ Characterization by microCT shows that total porosity, SA/V, pore diameter, and strut size all vary based on construct design and resolution. However, because of the trabeculae-inspired design of porosity, each of these parameters may change depending on the exact location of characterization. In addition, it is unclear how interconnected porosity affects cell–cell communication.

Not only can open porosity facilitate paracrine signaling but parameters such as size, shape, and tortuosity have also been shown to influence the shear stress on cells.⁴² Although mechanical transduction is not well understood in porous constructs, it is well known that changes in the mechanical stimulus of a cell or its substrate can lead to downstream effects.⁴³ In fact, it is suggested that fluid forces contribute more to osteoblast response than to strain from the substrate or extracellular matrix.⁴⁴ Although our characterization provides information on the average porosity parameters for these constructs, cells may experience a different microscale environment based on their location within the construct. Future studies may examine location-specific biological response to understand how response within individual pores contributes to overall biological response.

Conclusion

Porous Ti-6Al-4V implants have great potential in the dental and orthopedic fields. With additive manufacturing, implant porosity can be customized for the patient. In this study, laser-sintered constructs were manufactured with various porosities and resolution inspired by human trabecular bone structure. Biological response by human osteoblasts showed increased differentiation, maturation, and local factor production on 3D than on 2D solid constructs. Osteoblasts exhibited cell-type-dependent responses to construct porosity. MG63 cells produced higher local factor production on HR than on LR constructs, which incorporated finer detail from trabecular bone. NHOst cells also exhibited an enhanced response to 3D porous constructs than on 2D solids surfaces, though the response to changes in porosity was less evident than that of MG63 cells. These results suggest that incorporating trabecular-inspired porosity into bone-interfacing implants may enhance cellular response and implant osseointegration.

Acknowledgments

The authors would like to thank Dr. David J. Cohen for his help with microCT analysis, and Illya Kajan for his help with cell culture. Research reported in this publication was supported by the National Institute of Arthritis and Musculoskeletal and Skin Diseases of the National Institutes of Health under Award Number AR052102. The content is solely the responsibility of the authors' and does not necessarily represent the official views of the National Institutes of Health.

Author Disclosure Statement

Z.S. is a consultant for AB Dental. B.D.B. is a consultant for TitanSpine LLC.

References

1. Chia HN, Wu BM. Recent advances in 3d printing of biomaterials. *J Biol Eng* 2015;9:4.
2. van Noort R. The future of dental devices is digital. *Dent Mater* 2012;28:3–12.

3. Long M, Rack HJ. Titanium alloys in total joint replacement—A materials science perspective. *Biomaterials* 1998;19:1621–1639.
4. Van Noort R. Titanium: The implant material of today. *J Mater Sci* 1987;22:3801–3811.
5. Wennerberg A, Albrektsson T. Effects of titanium surface topography on bone integration: A systematic review. *Clin Oral Implants Res* 2009;20 Suppl 4:172–184.
6. Lang NP, Salvi GE, Huynh-Ba G, *et al.* Early osseointegration to hydrophilic and hydrophobic implant surfaces in humans. *Clin Oral Implants Res* 2011;22:349–356.
7. Moy PK, Medina D, Shetty V, *et al.* Dental implant failure rates and associated risk factors. *Int J Oral Maxillofac Implants* 2005;20:569–577.
8. Meldrum RD, Wurtz LD, Feinberg JR, *et al.* Does smoking affect implant survivorship in total hip arthroplasty? A preliminary retrospective case series. *Iowa Orthop J* 2005;25:17–24.
9. Jämsen E, Peltola M, Eskelinen A, *et al.* Comorbid diseases as predictors of survival of primary total hip and knee replacements: A nationwide register-based study of 96 754 operations on patients with primary osteoarthritis. *Ann Rheum Dis* 2013;72:1975–1982.
10. Oh I, Harris WH. Proximal strain distribution in the loaded femur. An in vitro comparison of the distributions in the intact femur and after insertion of different hip-replacement femoral components. *J Bone Joint Surg Am* 1978;60:75–85.
11. Sumner DR, Galante JO. Determinants of stress shielding: Design versus materials versus interface. *Clin Orthop Relat Res* 1992;274:202–212.
12. Jariwala SH, Lewis GS, Bushman ZJ, *et al.* 3D printing of personalized artificial bone scaffolds. *3D Printing Additive Manuf* 2015;2:56–64.
13. Mangano F, Chambrone L, van Noort R, *et al.* Direct metal laser sintering titanium dental implants: A review of the current literature. *Int J Biomater* 2014;2014:461534.
14. Mangano F, Bazzoli M, Tettamanti L, *et al.* Custom-made, selective laser sintering (sls) blade implants as a non-conventional solution for the prosthetic rehabilitation of extremely atrophied posterior mandible. *Lasers Med Sci* 2013;28:1241–1247.
15. Mangano C, Piattelli A, d'Avila S, *et al.* Early human bone response to laser metal sintering surface topography: A histologic report. *J Oral Implantol* 2010;36:91–96.
16. Traini T, Mangano C, Sammons RL, *et al.* Direct laser metal sintering as a new approach to fabrication of an isoelastic functionally graded material for manufacture of porous titanium dental implants. *Dent Mater* 2008;24:1525–1533.
17. Cheng A, Humayun A, Cohen DJ, *et al.* Additively manufactured 3d porous ti-6al-4v constructs mimic trabecular bone structure and regulate osteoblast proliferation, differentiation and local factor production in a porosity and surface roughness dependent manner. *Biofabrication* 2014;6:045007.
18. de Wild M, Schumacher R, Mayer K, *et al.* Bone regeneration by the osteoconductivity of porous titanium implants manufactured by selective laser melting: A histological and micro computed tomography study in the rabbit. *Tissue Eng Part A* 2013;19:2645–2654.
19. Palmquist A, Snis A, Emanuelsson L, *et al.* Long-term biocompatibility and osseointegration of electron beam melted, free-form-fabricated solid and porous titanium alloy: Experimental studies in sheep. *J Biomater Appl* 2013;27:1003–1016.
20. Gittens RA, Olivares-Navarrete R, Cheng A, *et al.* The roles of titanium surface micro/nanotopography and wettability on the differential response of human osteoblast lineage cells. *Acta Biomater* 2013;9:6268–6277.
21. Rack HJ, Qazi JI. Titanium alloys for biomedical applications. *Mater Sci Eng C Mater Biol Appl* 2006;26:1269–1277.
22. Geetha M, Singh AK, Asokamani R, *et al.* Ti based biomaterials, the ultimate choice for orthopaedic implants—A review. *Prog Mater Sci* 2009;54:397–425.
23. Krishna BV, Bose S, Bandyopadhyay A. Low stiffness porous ti structures for load-bearing implants. *Acta Biomater* 2007;3:997–1006.
24. Parthasarathy J, Starly B, Raman S. A design for the additive manufacture of functionally graded porous structures with tailored mechanical properties for biomedical applications. *J Manuf Process* 2011;13:160–170.
25. Sallica-Leva E, Jardini AL, Fogagnolo JB. Microstructure and mechanical behavior of porous ti-6al-4v parts obtained by selective laser melting. *J Mech Behav Biomed Mater* 2013;26:98–108.
26. Roque WL, Alberich-Bayarri A. Tortuosity influence on the trabecular bone elasticity and mechanical competence. In: Tavares JMRS, Natal Jorge R, editors. *Developments in medical image processing and computational vision*. Switzerland: Springer International Publishing, 2015, pp. 173–191.
27. Parthasarathy J, Starly B, Raman S, *et al.* Mechanical evaluation of porous titanium (ti6al4v) structures with electron beam melting (ebm). *J Mech Behav Biomed Mater* 2010;3:249–259.
28. Reilly DT, Burstein AH, Frankel VH. The elastic modulus for bone. *J Biomech* 1974;7:271–275.
29. Ponader S, von Wilmsky C, Widenmayer M, *et al.* In vivo performance of selective electron beam-melted ti-6al-4v structures. *J Biomed Mater Res A* 2010;92A:56–62.
30. Maniopoulos C, Pilliar RM, Smith DC. Threaded versus porous-surfaced designs for implant stabilization in bone-endodontic implant model. *J Biomed Mater Res* 1986;20:1309–1333.
31. Zinger O, Zhao G, Schwartz Z, *et al.* Differential regulation of osteoblasts by substrate microstructural features. *Biomaterials* 2005;26:1837–1847.
32. Gittens RA, McLachlan T, Olivares-Navarrete R, *et al.* The effects of combined micron-/submicron-scale surface roughness and nanoscale features on cell proliferation and differentiation. *Biomaterials* 2011;32:3395–3403.
33. Gittens RA, Olivares-Navarrete R, Schwartz Z, *et al.* Implant osseointegration and the role of microroughness and nanostructures: Lessons for spine implants. *Acta Biomater* 2014;10:3363–3371.
34. Czekanska EM, Stoddart MJ, Ralphs JR, *et al.* A phenotypic comparison of osteoblast cell lines versus human primary osteoblasts for biomaterials testing. *J Biomed Mater Res A* 2014;102:2636–2643.
35. Gittens RA, Olivares-Navarrete R, McLachlan T, *et al.* Differential responses of osteoblast lineage cells to nanotopographically-modified, microroughened titanium–aluminum–vanadium alloy surfaces. *Biomaterials* 2012;33:8986–8994.
36. Lohmann CH, Bonewald LF, Sisk MA, *et al.* Maturation state determines the response of osteogenic cells to surface roughness and 1,25-dihydroxyvitamin d3. *J Bone Miner Res* 2000;15:1169–1180.

37. Olivares-Navarrete R, Raines AL, Hyzy SL, *et al.* Osteoblast maturation and new bone formation in response to titanium implant surface features are reduced with age. *J Biomed Mater Res* 2012;27:1773–1783.
38. Olivares-Navarrete R, Hyzy SL, Chaudhri RA, *et al.* Sex dependent regulation of osteoblast response to implant surface properties by systemic hormones. *Biol Sex Differ* 2010;1:4.
39. Olivares-Navarrete R, Raz P, Zhao, G, *et al.* Integrin $\alpha 2\beta 1$ plays a critical role in osteoblast response to micron-scale surface structure and surface energy of titanium substrates. *Proc Natl Acad Sci U S A* 2008;105:15767–15772.
40. Wang X, Schwartz Z, Gittens RA, *et al.* Role of integrin $\alpha 2\beta 1$ in mediating osteoblastic differentiation on three-dimensional titanium scaffolds with submicron-scale texture. *J Biomed Mater Res A* 2015;103:1907–1918.
41. Frosch KH, Barvencik F, Lohmann CH, *et al.* Migration, matrix production and lamellar bone formation of human osteoblast-like cells in porous titanium implants. *Cells Tissues Organs* 2002;170:214–227.
42. Botchwey EA, Pollack SR, El-Amin S, *et al.* Human osteoblast-like cells in three-dimensional culture with fluid flow. *Biorheology* 2003;40:299–306.
43. Kapur S, Baylink DJ, William Lau KH. Fluid flow shear stress stimulates human osteoblast proliferation and differentiation through multiple interacting and competing signal transduction pathways. *Bone* 2003;32:241–251.
44. Owan I, Burr DB, Turner CH, *et al.* Mechanotransduction in bone: Osteoblasts are more responsive to fluid forces than mechanical strain. *Am J Physiol* 1997;273:C810–C815.

Address correspondence to:

Barbara D. Boyan
Department of Biomedical Engineering
Virginia Commonwealth University
601 West Main Street
Richmond, VA 23284

E-mail: bboyan@vcu.edu

Published: volume 6, 2014 in:

Biofabrication

04

Additively manufactured 3D porous Ti-6Al-4V constructs mimic trabecular bone structure and regulate osteoblast proliferation, differentiation and local factor production in a porosity and surface roughness dependent manner

Alice Cheng, Aiza Humayun, David J Cohen, Barbara D Boyan and Zvi Schwartz



Superior Implant Technology

Additively manufactured 3D porous Ti-6Al-4V constructs mimic trabecular bone structure and regulate osteoblast proliferation, differentiation and local factor production in a porosity and surface roughness dependent manner

Alice Cheng^{1,2}, Aiza Humayun³, David J Cohen³, Barbara D Boyan^{1,3} and Zvi Schwartz^{3,4}

¹Wallace A Coulter Department of Biomedical Engineering, Georgia Institute of Technology and Emory University, Atlanta, Georgia, USA

²Department of Biomedical Engineering, Peking University, Beijing, People's Republic of China

³Department of Biomedical Engineering, Virginia Commonwealth University, Richmond, Virginia, USA

⁴University of Texas Health Science Center at San Antonio, San Antonio, Texas, USA

E-mail: bboyan@vcu.edu

Received 16 June 2014, revised 8 August 2014

Accepted for publication 21 August 2014

Published 7 October 2014

Abstract

Additive manufacturing by laser sintering is able to produce high resolution metal constructs for orthopedic and dental implants. In this study, we used a human trabecular bone template to design and manufacture Ti-6Al-4V constructs with varying porosity via laser sintering. Characterization of constructs revealed interconnected porosities ranging from 15–70% with compressive moduli of 2579–3693 MPa. These constructs with macro porosity were further surface-treated to create a desirable multi-scale micro-/nano-roughness, which has been shown to enhance the osseointegration process. Osteoblasts (MG63 cells) exhibited high viability when grown on the constructs. Proliferation (DNA) and alkaline phosphatase specific activity, an early differentiation marker, decreased as porosity increased, while osteocalcin, a late differentiation marker, as well as osteoprotegerin, vascular endothelial growth factor and bone morphogenetic proteins 2 and 4 increased with increasing porosity. Three-dimensional (3D) constructs with the highest porosity and surface modification supported the greatest osteoblast differentiation and local factor production. These results indicate that additively manufactured 3D porous constructs mimicking human trabecular bone and produced with additional surface treatment can be customized for increased osteoblast response. Increased factors for osteoblast maturation and differentiation on high porosity constructs suggest the enhanced performance of these surfaces for increasing osseointegration *in vivo*.

Keywords: osteoblast differentiation, laser sintering, surface roughness, materials properties, custom implants, additive manufacturing



Content from this work may be used under the terms of the Creative Commons Attribution 3.0 licence. Any further distribution of this work must maintain attribution to the author(s) and the title of the work, journal citation and DOI.

(Some figures may appear in colour only in the online journal)

1. Introduction

Over two million dental implants are placed annually, and over four million hip and knee replacement surgeries are expected by the year 2030 [1, 2]. The orthopedic implant market is projected to exceed \$46 billion by the year 2017, in part due to an increasing number of elderly patients as well as increased quality of life expectations of younger patients [3]. Titanium and its alloys are still widely used in dental and orthopedic metal implants, based on the ability of bone to form in tight apposition to implants fabricated from these materials [4–6]. Titanium and titanium-aluminum-vanadium (Ti6Al4V) have a naturally occurring passive oxide layer on their surface that is biologically preferable and resists corrosion, while still maintaining strong mechanical properties and a high strength to weight ratio [7].

Implant surface roughness is one factor that has been shown to successfully increase cell response *in vitro* and osseointegration *in vivo*, and micro-rough surfaces are currently used as the industry standard in dental and many bone-interfacing orthopedic implants [8, 9]. Previous studies in our lab confirm that the combined presence of micro-/submicron-scale roughness contributes to increased osteoblast response [10, 11]. By altering only the surface microtopography and without exogenous factors in media, osteoblast differentiation can be increased on titanium surfaces [12]. This may be due in part to the protein–material interaction at the surface, which affects downstream cell response. Changes in the cytoskeleton, including integrin expression and signaling, have also been implicated in this effect [13, 14].

Although dental implant success is achieved in over 95% of healthy patients, certain risk factors still inhibit osseointegration. Osseointegration rates for diabetics and smokers are reduced tremendously [15, 16]. In addition, low bone density or osteoporosis most commonly seen in the increasing elderly population can also decrease osseointegration. Most orthopedic implants have a lifetime of only 12–15 years, requiring revision surgery that can be fatal for older patients [5, 17]. These factors contribute to the need for improving both osseointegration rates and implant longevity. Therefore, there is an existing need for implants that have the ability to increase bone formation and enhance the regeneration process.

Titanium also has desirable mechanical properties due to its low modulus of elasticity and high strength to weight ratio [18]. However, solid titanium still exceeds the stiffness of cortical bone by more than threefold, causing stress shielding and bone loss downstream of the implant [19]. 3D porous coatings and implants have been proposed to decrease stress shielding via porosity-dependent mechanical properties and increased bone interlocking, making these a promising treatment for at risk patients or younger patients who need an extended implant lifetime [20, 21].

Additive manufacturing techniques provide a layer-by-layer approach to building porous or patient-specific implants that have tailored macro structural and mechanical properties [22].

Selective laser sintering has the ability to create high resolution, porous metal constructs with positive results in both *in vitro* and *in vivo* studies [23]. There have been many studies that observe the effect of controlled porosity on *in vitro* or *in vivo* response. However, porosity in these studies was created using homogeneous strut and pore sizing, without a biological template and with limited surface modification [23–26]. Trabecular bone in the human body does not have the same pore shape, size or surface roughness. In studies where surface modification was used to induce micro-roughness, bulk porosity was limited to a user designed template [27, 28]. Thus far, the combination of macro structural parameters integrated with micro-scale surface treatment has not been studied. The purpose of this study was to replace the traditional man-made structural template with a biological template.

In this study, we used human trabecular bone as a template to laser sinter Ti6Al4V with varying porosity, and additionally modified the surfaces to obtain a combined micro-/nano-roughness. The resulting constructs were characterized for their surface, structural and mechanical properties. Cellular response to constructs with varying porosity was also performed, with the hypothesis that osteoblast response would increase on 3D constructs with increasing porosity.

2. Materials and methods

2.1. Manufacturing

2.1.1. Material manufacturing. A computed tomographic (CT) scan was taken of a human femoral head retrieved from a hip replacement (μ CT 40, Scanco Medical, Bassersdorf, Switzerland) with a 16 μ m voxel size. A template was created using Scanco software (Scanco Medical, Bassersdorf, Switzerland) and rotated and superimposed on itself 12, 24, or 36 times to create constructs with low (3DLP), medium (3DMP) and high porosity (3DHP), respectively (figure 1(A)). Generated 3D renderings were manufactured into Ti6Al4V disks 15 mm in diameter and 5 mm in height. Each disk included a 1 mm solid base upon which the remaining porous material was sintered in order to ensure mechanical stability during sintering. 2D surfaces were 15 mm in diameter and 1 mm in height (figure 1(B)). Laser sintering was performed using an Ytterbium fiber laser system (EOS, EmbH Munchen, Germany) with Ti6Al4V (grade 5) particles 25–45 μ m in diameter (Advanced Powders & Coatings, Quebec, Canada). Laser scanning speed was 7 m s^{−1} with a wavelength of 1054 nm, continuous power of 200 W and laser spot size of 0.1 mm.

2.1.2. Surface modification. After manufacturing, disks were blasted with calcium phosphate particles using proprietary technology (AB Dental, Ashdod, Israel) and then acid etched by ultrasonication in 0.3 N nitric acid (HNO₃) once for five minutes at 45 °C and twice for five minutes at 25 °C. Disks were rinsed in 97% methanol for five minutes. Final pickling

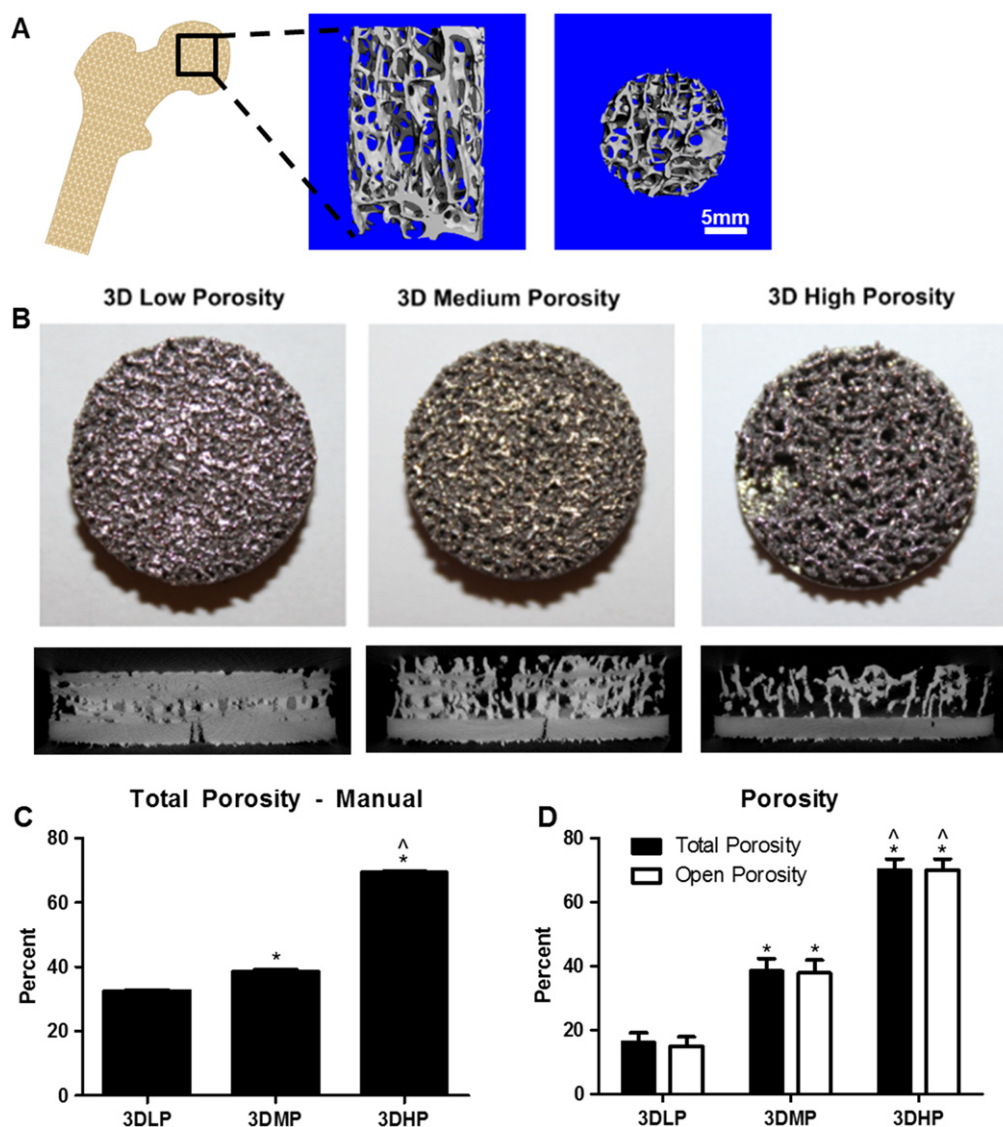


Figure 1. (Left to right) laser sintered disks were created from a CT scan conducted of human trabecular bone from the femoral head after a hip replacement. Original CT scans showing bone porosity through transverse and axial cross sections were used as a template for porous, laser sintered disks (A). Top-down camera images and micro CT cross sections of laser sintered 3D disks with (from left to right) low, medium and high porosity (B). Total porosity was calculated using a traditional method based on mass (C). Total and open porosity was calculated with micro CT (D). 1 Way ANOVA with Bonferroni's correction was performed separately for total porosity or open porosity. $p < 0.05$ is indicated by * versus 3DLP and [^] versus 3DMP. Unpair [^] porosity showed no significance between groups.

treatment was performed by ultrasonically disks thrice for 10 min in ultrapure distilled water, immersing for 30 min in 1:1 20 g L⁻¹ NaOH to 20 g L⁻¹ H₂O₂ for 30 min at 80 °C and ultrasonically in water for 10 min. Constructs were then placed in a degreaser for 12 min, immersed in 65% aqueous HNO₃, and ultrasonically thrice in water for 10 min. Surfaces were blotted with lint free tissue and allowed to dry for at least 24 h in order to stabilize the oxide layer before characterization and cell culture.

2.2. Material characterization

2.2.1. Surface chemistry. Surface chemistry was analyzed using x-ray photoelectron spectroscopy (XPS, K-Alpha, ThermoFisher Scientific, Boston, MA). Samples were

transferred to the analysis chamber at a pressure of 1e-8 mbar. An XR5 gun was used with a 500 μm spot size at 15 kV to perform survey scans with 20 ms dwelling time and 1 eV energy step size. Bulk chemistry was analyzed using energy dispersive x-ray spectroscopy (EDX, Hitachi SU-70, Tokyo, Japan).

2.2.2. Contact angle. Sessile drop contact angle was used to assess surface energy and surface wettability (Ramé-Hart goniometer, Succasunna, NJ). 2D solid laser sintered surfaces that received the same post-processing treatment as 3D constructs (figures 2(E), (F)) were used as a proxy for contact angle measurements due to difficulty in obtaining accurate contact angle measurements for porous constructs. 4 μl drops of distilled water were deposited on five predetermined

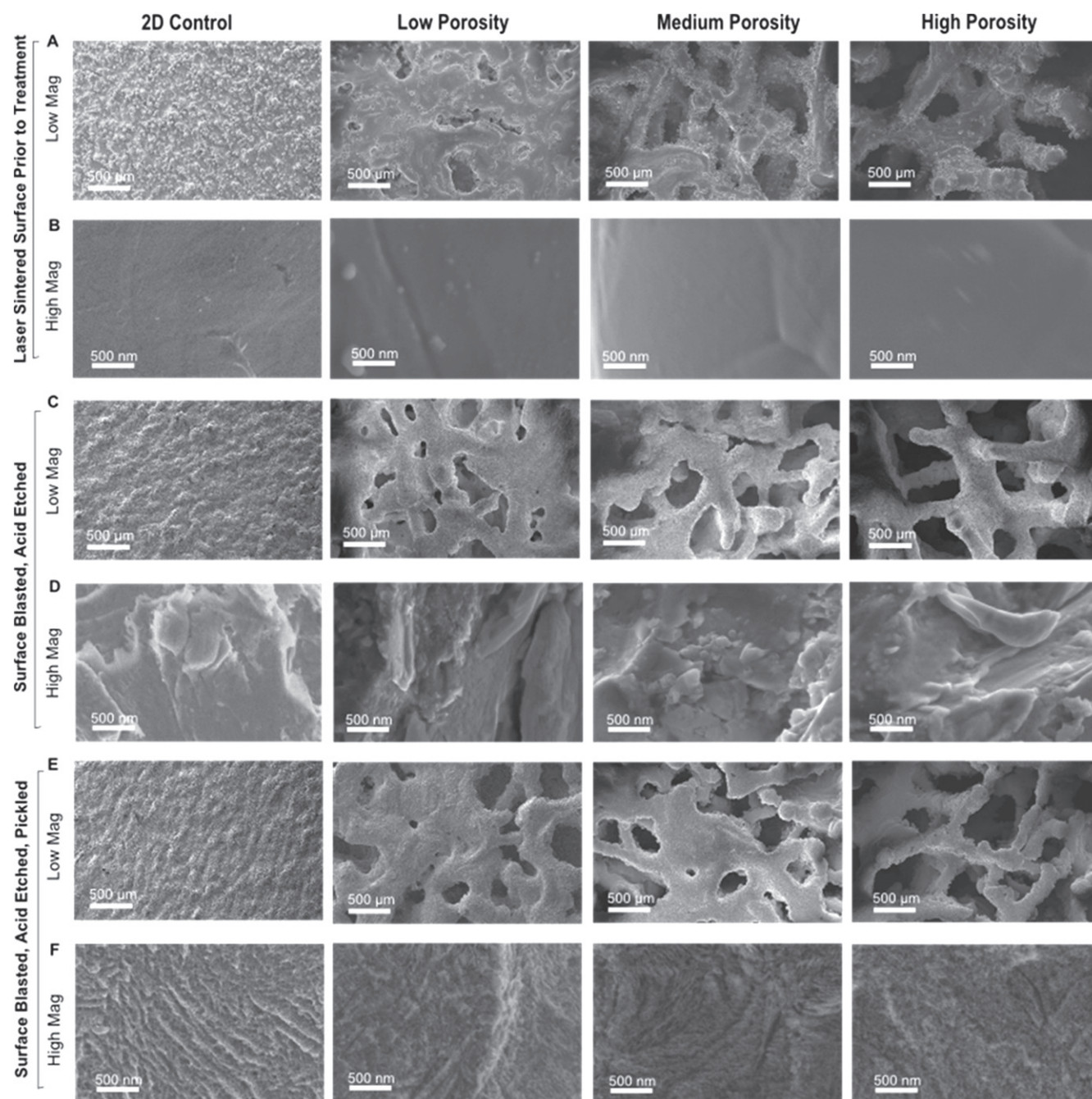


Figure 2. SEM images of (columns from left to right) 2D, 3D low, medium and high porosity disks. Low magnification images showing trabecular structure after production (A), after blasting and acid etching (B), and after pickling (C). High magnification images showing smooth surfaces after production (B), micro-roughness after blasting and acid etching (D), and nano-roughness after pickling (F).

locations per disk, with two disks per group ($n = 10$). Videos of these drops were taken and still images were used in conjunction with DROPImage software (Ramé-Hart goniometer, Succasunna, NJ) to determine the average left and right contact angle of each drop.

2.2.3. Surface topography. Surface topography was qualitatively assessed using scanning electron microscopy (SEM, Hitachi SU-70, Tokyo, Japan). Disks were secured on imaging stubs with carbon tape and imaged with 56 μ A ion current, 4 kV accelerating voltage and 4 mm working

distance. Three locations per disk were imaged to ensure homogeneous assessment, with at least two disks per group imaged.

2.2.4. Roughness. Macro- and micro-roughness were analyzed with confocal laser microscopy (LEXT OLS4000, Olympus, Center Valley, PA). Macro roughness was analyzed with a 10 \times objective, and micro-roughness was analyzed with a 20 \times objective and additional 5 \times optical zoom. After a three point correction, a cutoff wavelength of 100 μ m was used to analyze average roughness (R_a) and surface area.

2.2.5. Porosity. 3D constructs were analyzed for porosity using micro-computed tomography (micro CT) (SkyScan 1173, Micro Photonics, Allentown, PA). A volume of interest of 469 mm³, or approximately 66% of each construct's porous volume, was analyzed for total percent porosity, open porosity, pore diameter, strut size, and surface area to volume (SA/V) ratio. Scans were taken using an Al 1.0 mm filter, 100 kV voltage, 80 μ A current, 1120 \times 1120 camera pixels, 0.2° rotation step, frame averaging of 10, and random movement of 10. Post-processing included a global threshold of 100–255 and despeckling black and white speckles less than 10 voxels. We verified the validity of micro CT analysis by comparison of total porosity analyzed through a traditional method based on size and mass (figure 1(C)).

2.2.6. Mechanical testing. Compressive moduli of 3D constructs were determined using the MTS Insight 30 testing machine (MTS Systems, Minnesota, USA). A pre-load of 0.01 kN was applied at 0.025 mm s⁻¹, then a test speed of 0.02 mm s⁻¹ was used until failure or the maximum load of 30 kN was applied. Data acquisition rate was 500 Hz, and the compressive modulus was taken as the slope output of the resulting stress/strain curve. Testing was performed on 6 constructs per group (total $n=6$).

2.3. Biological response

2.3.1. Cell viability. The MG63 human osteoblast-like cell line was used as a model for osteoblast viability, proliferation and differentiation on sintered surfaces. These cells have been characterized and have been used as a model for osteoblast response to titanium surfaces with varying topography [29, 30]. Surfaces were sterilized in UV for 20 min in a biosafety cabinet prior to cell culture. Cells were cultured in tissue culture polystyrene (TCPS) flasks until confluence, then centrifuged and resuspended to yield a plating density of 30 000 cells per cm² on TCPS, or 60 000 cells per surface in a 24-well plate. Dulbecco's modified Eagle medium (DMEM) with 10% fetal bovine serum (FBS) and 1% penicillin/streptomycin was used to feed cells 24 h after plating and treat at confluence according to the TCPS control. 24 h after confluence, cells were treated with 5 μ M calcein-AM and 4 μ M ethidium homodimer-1 (LIVE/DEAD, Life Technologies, California, USA) in 1 \times Dulbecco's phosphate buffered saline (D-PBS, Life Technologies) for 20 min. Surfaces were imaged using the Zeiss LSM 710 confocal microscope (Zeiss, Oberkochen, Germany). Individual images were taken of 2D disks, while 550 μ m z-stacks were taken of 3D disks. Green (live) and red (dead) channel thresholds were optimized for each group in order to better distinguish cells. Three images were analyzed and averaged per z-stack, with at least $n=6$ total areas (z-stacks) analyzed for at least two constructs per group (total $n=12$).

2.3.2. Osteoblast proliferation and maturation. Surfaces were gamma irradiated prior to cell culture. MG63 cells were cultured as described above. Medium was changed at confluence, and cells were harvested 24 h after confluence,

rinsed twice with 1 \times PBS, then stored at -20 °C overnight for biological assays. Cell lysate was assayed for DNA content (P7589, Invitrogen) and total protein content (23225, Pierce). Alkaline phosphatase specific activity was measured as a function of *p*-nitrophenol production from *p*-nitrophenylphosphate at pH 10.2 and normalized to total protein. Medium was assayed for osteocalcin (OCN, BT-480, Biomedical Technologies), VEGF (DY293B, R&D Systems), OPG (DY805, R&D Systems), BMP2 (900-K255, PeproTech) and BMP4 (DY 314, R&D Systems). Data were normalized to total DNA content. Experiments were performed at least twice to ensure validity of the results.

2.3.3. Sample preparation for scanning electron microscopy.

One disk from each group was UV-treated for 20 min in a biological hood and plated with 60 000 MG63 cells and cultured as described above. Media were changed at confluence, and cells were fixed 24 h after confluence with 4% paraformaldehyde (electron microscopy sciences). Constructs were rinsed three times in 1 \times PBS, then dehydrated in a series of increasing ethanol concentrations: 15%, 30%, and 45% for two hours, then 60%, 75%, 90% and thrice in 100% for at least one hour. Samples were then exchanged in 1:1 100% ethanol and hexamethyldisilazane (HMDS, Sigma Aldrich) for 30 min in a chemical safety hood, then twice in 100% HMDS for 30 min. Samples were dried 24 h in a desiccator before being platinum sputtered and imaged with SEM as described above (Hitachi SU-70, Tokyo, Japan).

2.4. Statistical analysis

Surface characterization data are presented as mean \pm one standard deviation (SD) of all measurements performed across samples in the same group. Cell viability is presented as the mean of all measurements performed across samples in the same group. Cell proliferation and differentiation data are presented as mean \pm standard error of the mean (SEM) for six independent cultures. All experiments were repeated at least twice to ensure validity of observations, with results from individual experiments shown. Statistical analysis among groups was performed by analysis of variance, and significant differences between groups were compared using Bonferroni's modification of Student's *t*-test. A *p* value of less than 0.05 was considered statistically significant.

3. Results

3.1. Surface characterization

Laser sintered 3DLP, 3DMP and 3DHP constructs had 16.2 \pm 2.9%, 38.5 \pm 3.9%, and 70.0 \pm 3.5% total porosity and 15.0 \pm 2.9%, 37.9 \pm 4.0%, 70.0 \pm 3.5% open porosity, respectively (table 1). Total porosity and open porosity were not significantly different, showing complete inter-connectivity between pores (figure 1(D)). Average pore diameter was 177 \pm 22 μ m for 3DLP, 383 \pm 15 μ m for 3DMP and

Table 1. Porosity parameters.

Porosity parameters (average \pm SD)					
	Total porosity (%)	Open porosity (%)	Pore diameter (μm)	Strut thickness (μm)	SA/V Ratio
3DLP	16.2 \pm 2.9	15.0 \pm 2.9	177 \pm 22	628 \pm 150	23.5 \pm 7.4
3DMP	38.5 \pm 3.9 (*)	37.9 \pm 4.0 (*)	383 \pm 15 (*)	454 \pm 57 (*)	36.1 \pm 5.4 (*)
3DHP	70.0 \pm 3.5 (*^)	70.0 \pm 3.5 (*^)	653 \pm 22 (*^)	305 \pm 26 (*^)	56.9 \pm 5.8 (*^)

Significance * versus LP, ^ versus MP $p < 0.05$.

Table 2. Surface chemistry (XPS): elemental composition.

Element (atomic % average \pm SD)							
	O	C	Ti	N	P	Ca	Al
2D	41.6 \pm 3.7	41.8 \pm 5.4	12.6 \pm 1.5	1.3 \pm 0.6	—	—	2.5 \pm 0.5
3D-LP	44.9 \pm 4.4	36.6 \pm 7.9	6.3 \pm 1.7	5.6 \pm 1.5	3.3 \pm 3.9	2.6 \pm 1.9	—
3D-MP	54.5 \pm 1.9	20.5 \pm 20.4	6.9 \pm 1.7	4.9 \pm 0.9	9.7 \pm 1.6	3.6 \pm 1.0	—
3D-HP	51.7 \pm 3.1	29.5 \pm 2.8	13.4 \pm 1.1	3.2 \pm 0.8	1.6 \pm 1.8	—	—

Does not include trace elements less than 1%.

Table 3. Surface chemistry (EDX): elemental composition.

Element (weight % average \pm SD)				
	Ti	Al	V	C
2D	89.8 \pm 0.6	7.1 \pm 0.8	3.1 \pm 0.2	—
3D-LP	87.3 \pm 4.7	6.7 \pm 1.6	3.0 \pm 0.2	2.4 \pm 3.8
3D-MP	88.9 \pm 2.2	7.0 \pm 1.1	3.1 \pm 0.2	—
3D-HP	89.0 \pm 1.8	7.5 \pm 1.4	3.2 \pm 0.2	—

Does not include trace elements less than 1%.

653 \pm 22 μm for 3DHP constructs. Average strut thickness was 628 \pm 150 μm for 3DLP, 454 \pm 57 μm for 3DMP and 305 \pm 26 μm for 3DHP. The ratio between the analyzed construct surface area to volume ratio was 23.5 \pm 7.4 for 3DLP, 36.1 \pm 5.4 for 3DMP, and 56.9 \pm 5.8 for 3DHP disks. For all porosity parameters (total porosity, open porosity, pore diameter, strut thickness and SA/V ratio), all groups were significantly different from each other. Pore diameter, strut thickness and SA/V ratio all increased with increasing construct porosity.

Surface chemistry performed by XPS showed mostly C, O and Ti in the oxide layer, with small amounts of N, P and Ca due to processing, and Al present on 2D surfaces (table 2). EDX allows for higher penetration past the oxide layer and showed Ti, Al and V as the bulk surface composition, with a small amount of C present on 3DLP surfaces (table 3). Contact angle of 2D proxy surfaces was 92 degrees with a standard deviation of eight degrees. Compressive modulus decreased in a porosity-dependent manner (table 4). 3DLP had a modulus of 3693 \pm 27, 3DMP a modulus of 3522 \pm 52 MPa and 3DHP a modulus of 2579 \pm 106 MPa.

After manufacturing the surfaces had a very grainy topography at the macro scale, but smooth topography at the micro scale (figures 2(A), (B)). Blasting and acid etching induced micro roughness on surfaces while maintaining macro structure (figures 2(C), (D)). Pickling overlaid fine and

Table 4. Compressive modulus (MPa).

Compressive modulus (average MPa \pm SD)	
3D-LP	3693 \pm 27
3D-MP	3522 \pm 52 (*)
3D-HP	2579 \pm 106 (*^)

Significance $p < 0.05$. * versus LP, ^ versus MP.

homogenous nanofeatures on the macro surface (figures 2(E), (F)). Cross sectional, low magnification SEM images show internal pore surfaces looking similar to pretreated constructs, indicating the inability of grit blasting treatment to affect internal construct pores (figure 3). Surface roughness results revealed increasing surface roughness and area at the macro level for increasing porosity (figures 4(A), (B)). Surface micro roughness showed no difference between groups except an elevation in 3DHP surfaces, and no difference between groups for surface area at the micro level (figures 4(C), (D)).

3.2. Biological response

Live/dead analysis indicated that cells on all surfaces had high viability. No significant differences in osteoblast viability were observed across constructs with varying porosity (figure 5(A)). 2D surfaces had the highest percent viability at 99.9%. 3DLP, 3DMP and 3DHP constructs had 94.9%, 98.1% and 91.6% cell viability, respectively. Representative SEM micrographs of cells cultured on disks showed cells spread evenly across surfaces (figure 5(B)).

DNA was highest on TCPS and decreased as porosity increased (figure 6(A)). ALP, a marker of early osteoblastic differentiation, was elevated on 3DLP compared to TCPS, then decreased on 3DMP and 3DHP compared to 3DLP, and decreased significantly on 3DHP compared to TCPS (figure 6(B)). OCN increased significantly on 3DHP compared to TCPS (figure 6(C)). OPG increased on 3DMP and 3DHP compared to TCPS and 3DLP, and was also

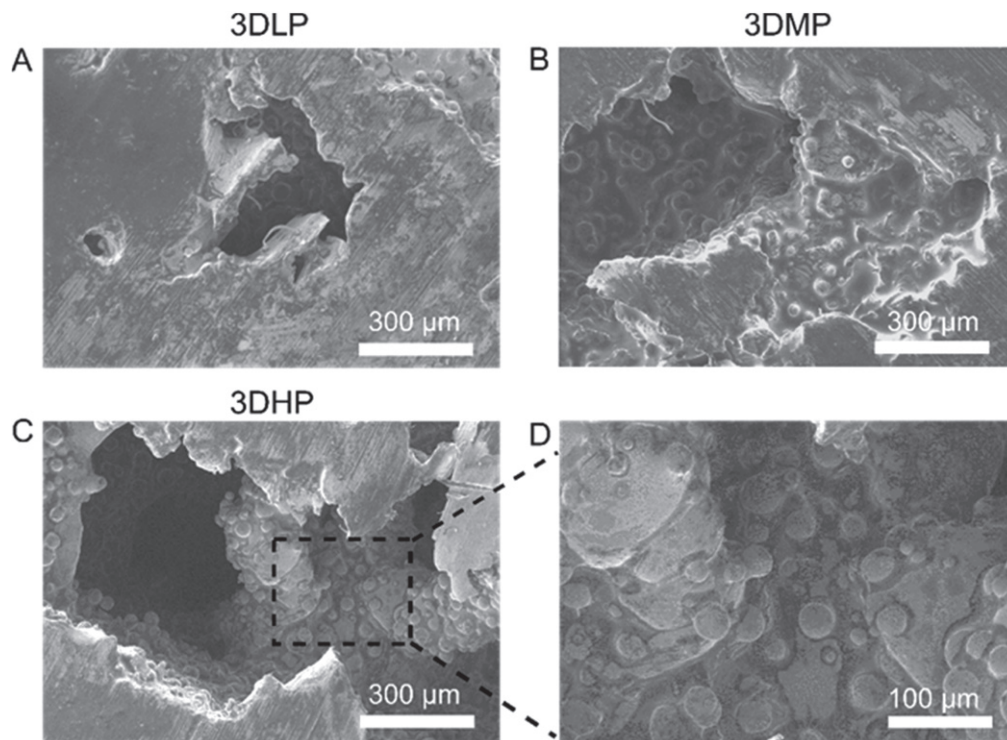


Figure 3. Cross sectional SEM images of 3DLP (A); 3DMP (B); and 3DHP (C) constructs. An enlarged image of 3DHP (D) shows an absence of surface roughness induced by grit blasting.

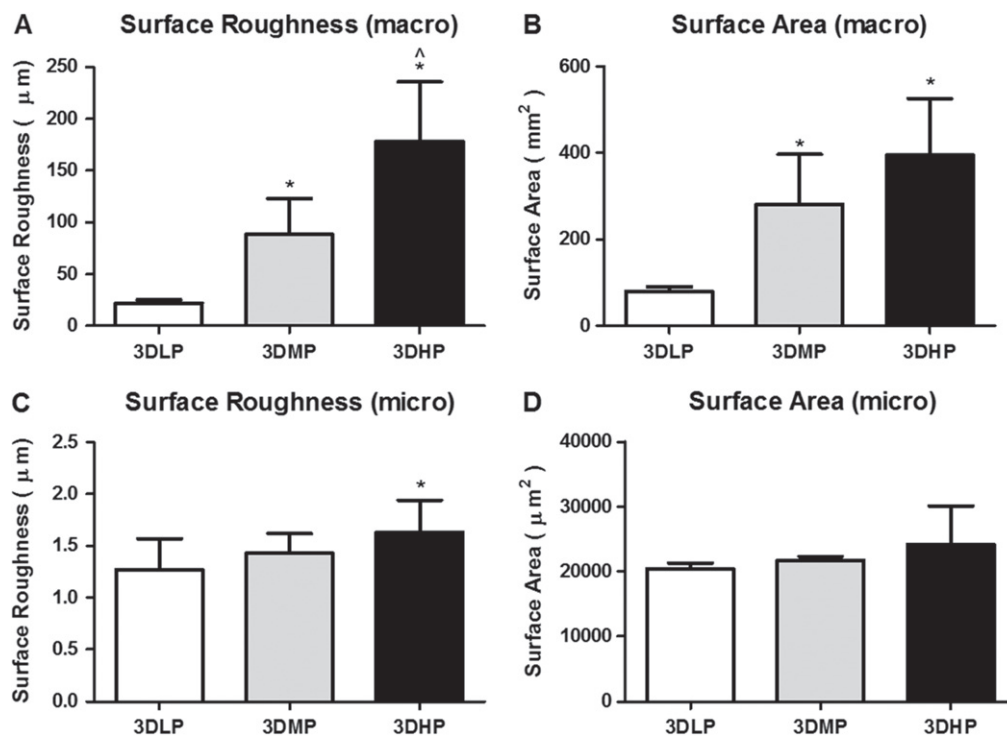


Figure 4. Macro surface roughness (A), macro surface area (B), micro surface roughness (C) and micro surface area (D) analyzed with laser confocal microscopy. 1 way ANOVA with Bonferroni's correction shows significance of $p < 0.05$ for * versus 3DLP and ^ versus 3DMP.

significantly higher on 3DHP compared to 3DMP (figure 6(D)). BMP2 on 3DLP, 3DMP and 3DHP was significantly higher than on TCPS, and 3DMP and 3DHP constructs had higher BMP2 levels compared to 3DLP

(figure 6(E)). BMP4 was elevated on 3DHP compared to TCPS only (figure 6(F)). VEGF was elevated on 3DMP and 3DHP compared to TCPS and 3DLP, and was also significantly higher on 3DHP compared to 3DMP (figure 6(G)).

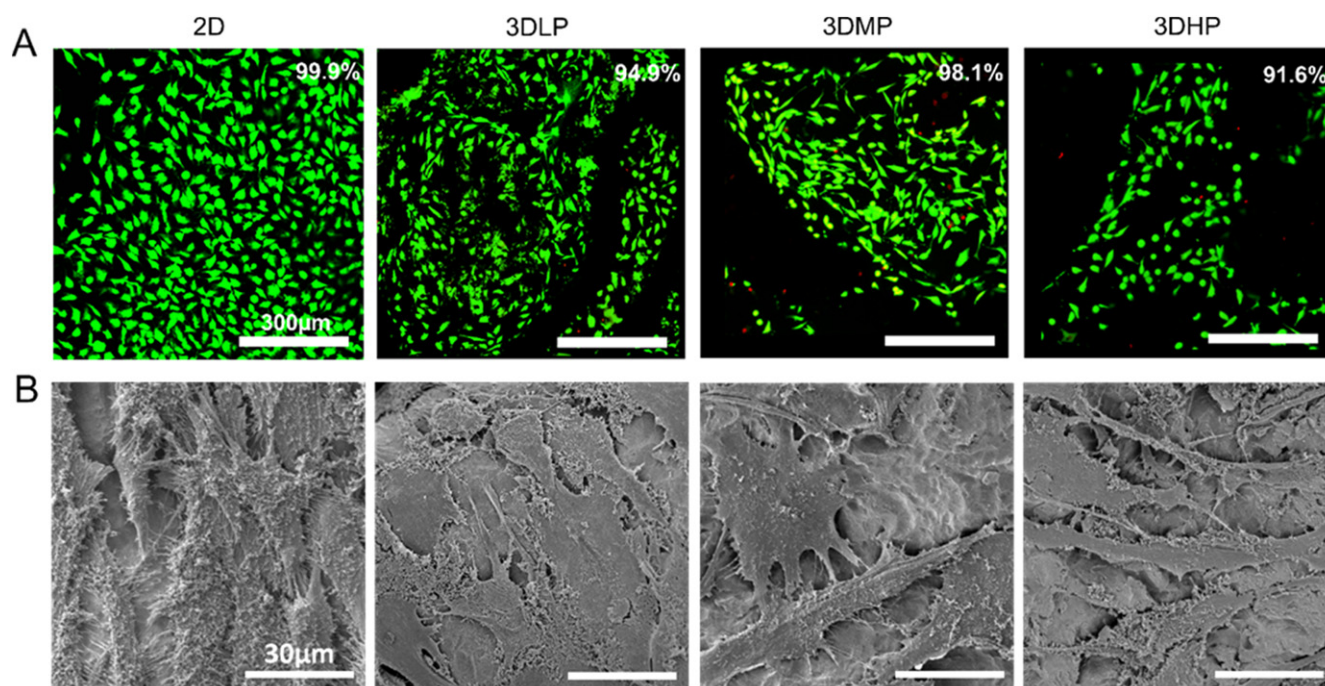


Figure 5. MG63 cell viability (live = green, dead = red) after culturing until confluence on TCPS (A). No differences were found among groups using 1 way ANOVA with Bonferroni's correction, $p < 0.05$. SEM micrographs revealing well-spread cell morphology on surfaces (B).

4. Discussion

Increased implant failure due to lack of osseointegration is a problem in compromised patients, which creates the need for better bone integration and mechanical properties of Ti and Ti alloy implants [16]. Although studies have pointed toward 3D porous implants as a possible solution, these surfaces have not been optimized for porosity or combined with desired surface roughness features.

Various additive manufacturing methods such as direct beam melting and laser sintering have come to the forefront of customized and porous implant manufacturing. The sintering system we use in this study has a theoretical resolution of 100 microns according to the laser size; however, limited studies have been performed on the homogeneity of laser strength within that diameter. Scan speed and wavelength can all have an effect on the manufactured structure's density and therefore mechanical properties, but with higher resolution comes increased time of production.

Previous studies have observed increased sintering density of over 97% with decreasing scan speeds to 50 mm s^{-1} [24]. Our qualitative evaluations using SEM and quantitative analysis using micro CT point toward a close approximation of our construct structure with that of human trabecular bone, even at high density. Although the optimal pore diameter for porous implants has been debated in literature, most studies observe increased cell infiltration or bone ingrowth for pores larger than $100 \mu\text{m}$ in diameter [31–33]. Pore sizes of $200\text{--}400 \mu\text{m}$ have been thought to increase osteoblast attachment, migration and proliferation via activation of mechanoreceptors [34]. We observed pore sizes upwards of $300 \mu\text{m}$

in our disks, which has been suggested as a minimum for new bone and capillary formation [33]. Pore diameter has been suggested to have higher influence on bone ingrowth when compared to total percent porosity alone, although we were not able to isolate these two variables in our constructs [35].

Similar processing methods have previously been shown to successfully manufacture surfaces with stable mechanical properties and good *in vitro* results [27]. The effect of roughness at both the micro- and nano-scales on osteoblast differentiation has been well documented [10, 29, 36], and our results show that traditional methods such as blasting and acid etching are effective at inducing a homogeneous combined micro-/nano-roughness on additively manufactured surfaces. Due to the high interconnectivity between pores, acid treatment and pickling solutions were able to access the entire surface area of constructs to create a unique, homogeneous nanostructured surface. However, our results show that blasting was not able to significantly alter the internal pores of the constructs. Despite this, cell response still increased significantly for high porosity constructs, suggesting that macro-structural effects of 3D porous constructs may play a larger role in cell response compared to surface roughness alone.

Human trabecular bone from the mandible has a porosity range of 70–90%, which varies with location and patient factors [37–39]. In this study, we created porous structures ranging from 20–70% to determine the optimal percent porosity for cells. Our compressive moduli decrease with increasing porosity, which has been corroborated for both synthetic constructs and human bone [20, 38]. Compressive testing on human trabecular bone has shown a compressive

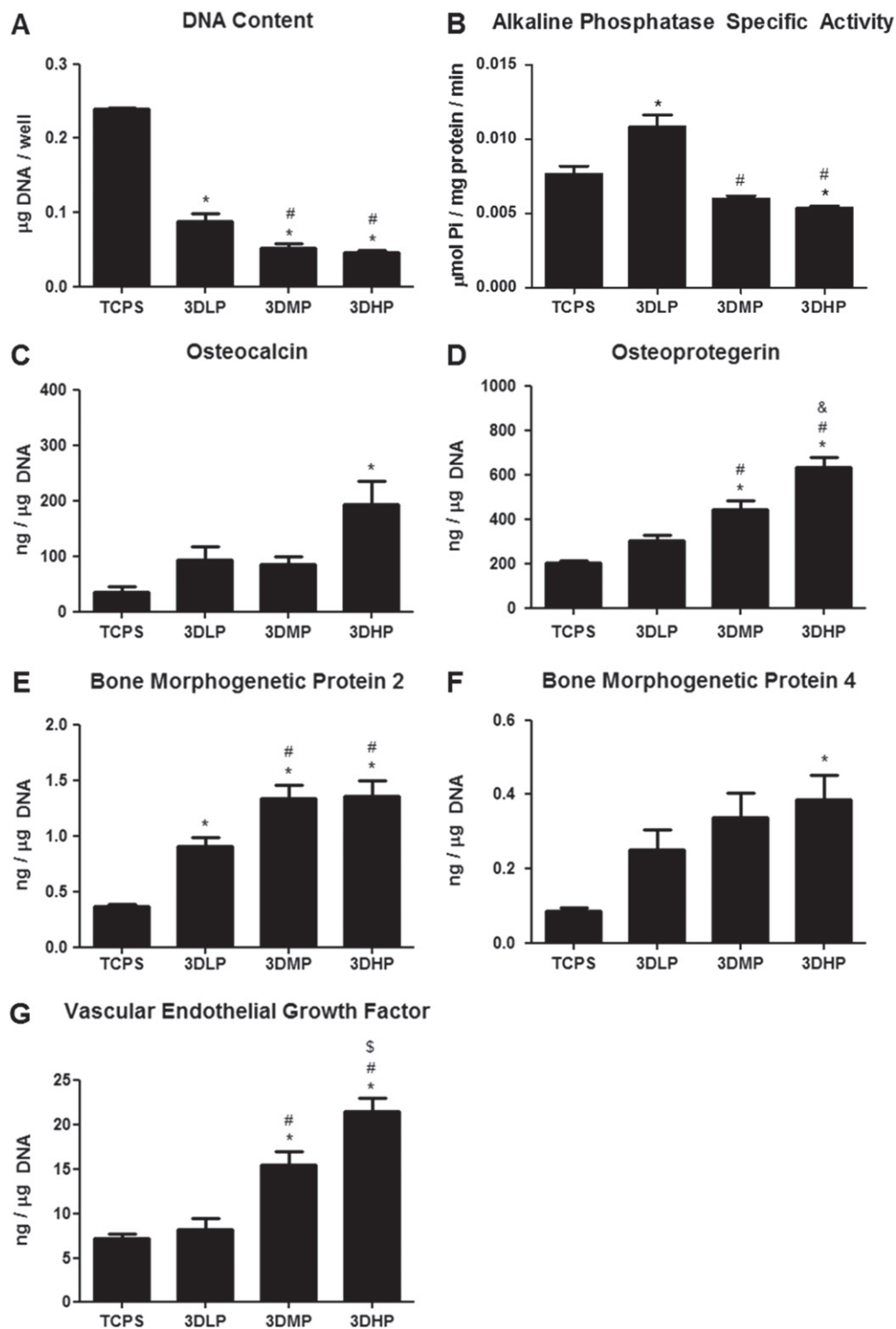


Figure 6. MG63 cell response to laser sintered, porous surfaces 24 h after confluence. DNA content (A), alkaline phosphatase specific activity (B), osteocalcin (C), osteoprotegerin (D), bone morphogenetic protein 2 (E), bone morphogenetic protein 4 (F), and vascular endothelial growth factor (G). Significance determined with 1 way ANOVA with Bonferroni's post-correction, $p < 0.05$ for * versus TCPS, ^ versus 2D, # versus 3DLP and \$ versus 3D-MP.

modulus of 1.08 GPa [40]. A study encompassing 160 human trabecular bone samples with compressive moduli ranging from approximately 300–900 MPa showed that bone-volume fraction (density), surface-to-volume ratio, trabecular thickness (strut thickness) and spacing (pore diameter) all

contributed significantly to differences in mechanical properties [41]. The direction of loading can also impact mechanical output, which is especially true due to the anisotropic properties of bone [25]. In this study, we performed testing on porous constructs with a 1 mm solid base, which

may have contributed to a higher modulus than just the porous component alone.

Surface chemistry of disks with varying porosity contained mainly elements of Ti, O and C, although bulk chemistry confirmed the presence of Ti, Al and V in the alloy. Previous surface analysis of Ti6Al4V surfaces has also shown the presence of Al in the oxide layer, which may have been masked by Ca and P after blasting [42]. Contact angle on 2D proxy surfaces was neither super-hydrophilic nor hydrophobic. These 2D surfaces underwent the same surface treatment as 3D constructs, although the effect of strut curvature and differences in internal surface roughness on wettability for 3D constructs could not be determined. Surface roughness and area at the micro level were not different among groups except for an elevated roughness on 3DHP, which may have been due to the decreased strut thickness and increased curvature at sites of analysis.

Cell viability was high and not significantly different among surfaces. A qualitative observation of a decrease in cell number with increasing porous constructs suggests that cells had infiltrated pores and distributed over a larger surface area. Previous studies on additively manufactured porous surfaces also showed high cell viability and cell infiltration into pores [43], which were confirmed by our SEM images. We assume high cell viability exists for cells that have infiltrated to the pores; however, we were not able to visualize all the way to the bottom of the disks to fully verify cell infiltration. Viability results were limited to the first 550 μm , a limitation of the imaging equipment.

The decrease in ALP specific activity and the increase in OCN point toward a porosity-dependent maturation response. Previous reports of ALP activity on roughened surfaces noted a significant difference in cell layer activity versus isolated cells, suggesting increased matrix vesicle production [44]. These results also correspond to the decreased DNA content on 3DHP constructs, indicating a preference toward osteoblast maturation instead of proliferation. OPG, a decoy receptor for RANKL and involved in the bone remodeling process, was increased on 3DMP and 3DHP constructs. This increase in OPG blocks osteoclast differentiation in a protective effect to enhance bone growth, and has been implicated in osteoblast-osteoclast communication [45]. An increase of BMP2 and BMP4, especially on 3DHP surfaces, corroborates previous studies that observe increased BMP production on constructs with 300–400 μm pore diameters [46]. Although our pore diameters are larger, the irregular porosity of trabecular bone may contribute differently to local factor production than in other studies with user-defined geometries. The increase of BMP local factor production indicates that our porous constructs have the potential to regulate the induction of bone inside the construct, as well as induce bone distally. The increased levels of VEGF on 3DHP constructs also point toward this trend, indicating that highly porous constructs of trabecular bone structure are inductive for blood vessel formation as part of supporting new bone formation and bone regeneration.

As percent porosity increased, so did the surface area to volume ratio, indicating an increased surface area for cell

interaction. It has previously been shown that rough titanium surfaces enhance osteoblastic differentiation and increase local factor production, so the increased cell response in this study may well be attributed to the varying material properties of our surface [30]. In this study, the combination of the three dimensional macro-structure, increase in surface area and combined micro-/nano-surface modification enhanced the osteoblast phenotype. Increased curvature on 3D surfaces with higher porosity may exert higher mechanical forces on a cell, which has been shown to direct cells toward osteoblast differentiation [47]. This response could be mediated by cell-surface integrin proteins. In particular, $\alpha 5$ has been implicated in osteoblast attachment and proliferation, and $\alpha 2\beta 1$ in osteoblast morphology and differentiation via its binding to collagen in the extracellular matrix [13, 48].

The role of confluence may contribute to cell response, and has been previously discussed with regard to TCPS versus rough titanium surfaces [49]. Although decreased DNA was shown on Ti6Al4V surfaces compared to TCPS controls, previous studies on pre-confluent cultures have also shown a different maturation profile of osteoblasts on the Ti alloy surfaces compared to TCPS, suggesting that our resulting cell response was also surface specific and not confluence dependent [34].

Increased bone growth in response to additively manufactured implants has been shown in various animal models, including rats and sheep [28, 50]. Previous work has shown highest calcium content and *in vivo* response to materials with 75% porosity compared to higher porosities [51]. Further work in an animal model will be essential to assess the success of bone growth into individual pores and osseointegration capability of the entire porous construct.

5. Conclusion

In this study, we used additive manufacturing to produce Ti6Al4V materials with varying porosity that structurally mimicked human trabecular bone, and further created a desirable surface for osteoblasts by inducing combined micro-/nano-roughness. Our results indicate that a high porosity construct mimicking trabecular bone structure is capable of stimulating osteoblast differentiation when compared to 2D and low porosity constructs. Additive manufacturing is a scalable manufacturing method that has the potential to create structurally complex, patient-specific orthopedic and dental implants and scaffolds for increased osseointegration. Although trabecular orientation may vary across individuals and locations in the body, this study suggests that osteoblast cells actually do prefer one type of porosity and structure. In addition, this study reveals the possibility for creating patient-specific implants, which may accelerate the fields of dental and orthopedic implants.

Acknowledgments

The authors would like to thank AB Dental (Ashdod, Israel) for funding this study. The authors also recognize the support

of the National Science Foundation (AC) and the National Institutes of Health (US PHS Grant AR052102, BDB).

References

- [1] Kurtz S, Ong K, Lau E, Mowat F and Halpern M 2007 Projections of primary and revision hip and knee arthroplasty in the United States from 2005 to 2030 *J. Bone Joint Surg. Am.* **89** 780–5
- [2] American Dental Association 2007 *The 2005–06 Survey of Dental Services Rendered* (Chicago, IL: American Dental Association)
- [3] Orthopedic implants - a global market overview. industry experts 2011
- [4] Van Noort R 1987 Titanium: the implant material of today *J. Mater. Sci.* **22** 3801–11
- [5] Rack H and Qazi J 2006 Titanium alloys for biomedical applications *Mater. Sci. Eng. C.* **26** 1269–77
- [6] Long M and Rack H J 1998 Titanium alloys in total joint replacement—a materials science perspective *Biomaterials* **19** 1621–39
- [7] Textor M, Sittig C, Frauchiger V, Tosatti S and Brunette D M 2001 Properties and biological significance of natural oxide films on titanium and its alloys *Titanium in Medicine* (Berlin: Springer) pp 171–230
- [8] Zhao G, Zinger O, Schwartz Z, Wieland M, Landolt D and Boyan B D 2006 Osteoblast-like cells are sensitive to submicron-scale surface structure *Clin. Oral Implants Res.* **17** 258–64
- [9] Zinger O et al 2005 Differential regulation of osteoblasts by substrate microstructural features *Biomaterials* **26** 1837–47
- [10] Gittens R et al 2011 The effects of combined micron-/submicron-scale surface roughness and nanoscale features on cell proliferation and differentiation *Biomaterials* **32** 3395–403
- [11] Zhao G, Raines A L, Wieland M, Schwartz Z and Boyan B D 2007 Requirement for both micron-and submicron scale structure for synergistic responses of osteoblasts to substrate surface energy and topography *Biomaterials* **28** 2821–9
- [12] Olivares-Navarrete R et al 2010 Direct and indirect effects of microstructured titanium substrates on the induction of mesenchymal stem cell differentiation towards the osteoblast lineage *Biomaterials* **31** 2728–35
- [13] Olivares-Navarrete R et al 2008 Integrin $\alpha 2\beta 1$ plays a critical role in osteoblast response to micron-scale surface structure and surface energy of titanium substrates *Proc. Natl. Acad. Sci.* **105** 15767–72
- [14] Keselowsky B G, Wang L, Schwartz Z, Garcia A J and Boyan B D 2007 Integrin $\alpha 5$ controls osteoblastic proliferation and differentiation responses to titanium substrates presenting different roughness characteristics in a roughness independent manner *J. Biomed. Mater. Res. A.* **80A** 700–10
- [15] Bain C A and Moy P K 1993 The association between the failure of dental implants and cigarette smoking *Int. J. Oral Maxillofacial Implants* **8** 1–13
- [16] Moy P K, Medina D, Shetty V and Aghaloo T L 2005 Dental implant failure rates and associated risk factors *Int. J. Oral Maxillofacial Implants* **20** 569–77
- [17] Mahomed N N et al 2003 Rates and outcomes of primary and revision total hip replacement in the united states medicare population *J. Bone Joint Surg.* **85** 27–32
- [18] Lautenschlager E P and Monaghan P 1993 Titanium and titanium alloys as dental materials *Int. Dental J.* **43** 245–53
- [19] Sumner D, Turner T M, Igloria R, Urban R M and Galante J O 1998 Functional adaptation and ingrowth of bone vary as a function of hip implant stiffness *J. Biomech.* **31** 909–17
- [20] Parthasarathy J, Starly B, Raman S and Christensen A 2010 Mechanical evaluation of porous titanium (Ti6Al4V) structures with electron beam melting (EBM) *J. Mech. Behav. Biomed. Mater.* **3** 249–59
- [21] Sumner D and Galante J O 1992 Determinants of stress shielding: design versus materials versus interface *Clin. Orthop. Relat. Res.* **274** 202–12
- [22] van Noort R 2012 The future of dental devices is digital *Dental Mater.* **28** 3–12
- [23] Warnke P H et al 2009 Rapid prototyping: porous titanium alloy scaffolds produced by selective laser melting for bone tissue engineering *Tissue Eng. C Methods.* **15** 115–24
- [24] Bertol L S, Júnior W K, Silva F P D and Aumund-Kopp C 2010 Medical design: direct metal laser sintering of Ti–6Al–4V *Mater. Des.* **31** 3982–8
- [25] Heintz P, Müller L, Körner C, Singer R F and Müller F A 2008 Cellular Ti–6Al–4V structures with interconnected macro porosity for bone implants fabricated by selective electron beam melting *Acta Biomater.* **4** 1536–44
- [26] Ryan G, Pandit A and Apatsidis D P 2006 Fabrication methods of porous metals for use in orthopaedic applications *Biomaterials* **27** 2651–70
- [27] Traini T, Mangano C, Sammons R, Mangan F, Macchi A and Piettelli A 2008 Direct laser metal sintering as a new approach to fabrication of an isoelastic functionally graded material for manufacture of porous titanium dental implants *Dental Mater.* **24** 1525–33
- [28] Amin Yavari S et al 2014 Bone regeneration performance of surface-treated porous titanium *Biomaterials* **35** 6172–81
- [29] Lincks J et al 1998 Response of MG63 osteoblast-like cells to titanium and titanium alloy is dependent on surface roughness and composition *Biomaterials* **19** 2219–32
- [30] Schwartz Z et al 2008 Effect of micrometer-scale roughness of the surface of Ti6Al4V pedicle screws *in vitro* and *in vivo* *J. Bone Joint Surg.* **90** 2485–98
- [31] Xue W, Krishna B V, Bandyopadhyay A and Bose S 2007 Processing and biocompatibility evaluation of laser processed porous titanium *Acta Biomater.* **3** 1007–18
- [32] Jones A C, Arns C H, Sheppard A P, Huttmacher D W, Milthorpe B K and Knackstedt M A 2007 Assessment of bone ingrowth into porous biomaterials using MICRO-CT *Biomaterials* **28** 2491–504
- [33] Karageorgiou V and Kaplan D 2005 Porosity of 3D biomaterial scaffolds and osteogenesis *Biomaterials* **26** 5474–91
- [34] Boyan B D, Hummert T W, Dean D D and Schwartz Z 1996 Role of material surfaces in regulating bone and cartilage cell response *Biomaterials* **17** 137–46
- [35] Gauthier O, Bouler J-M, Aguado E, Pilet P and Daculsi G 1998 Macroporous biphasic calcium phosphate ceramics: influence of macropore diameter and macroporosity percentage on bone ingrowth *Biomaterials* **19** 133–9
- [36] Martin J Y et al 1995 Effect of titanium surface roughness on proliferation, differentiation, and protein synthesis of human osteoblast-like cells (MG63) *J. Biomed. Mater. Res.* **29** 389–401
- [37] Misch C E, Qu Z and Bidez M W 1999 Mechanical properties of trabecular bone in the human mandible: implications for dental implant treatment planning and surgical placement *J. Oral Maxillofacial Surg.: Official J. Ame. Assoc. Oral Maxillofacial Surg.* **57** 700–6
- [38] McCalden R W, McGeough J A, Barker M B and Court-Brown C M 1993 Age-related changes in the tensile properties of cortical bone. The relative importance of changes in porosity, mineralization, and microstructure *J. Bone Joint Surg.* **75** 1193–205

- [39] Seeman E 2002 Pathogenesis of bone fragility in women and men *The Lancet*. **359** 1841–50
- [40] Sevilla P, Aparicio C, Planell J A and Gil F J 2007 Comparison of the mechanical properties between tantalum and nickel–titanium foams implant materials for bone ingrowth applications *J. Alloys Compd.* **439** 67–73
- [41] Ding M, Odgaard A, Danielsen C C and Hvid I 2002 Mutual associations among microstructural, physical and mechanical properties of human cancellous bone *J. Bone Joint Surg. British Vol.* **84** 900–7
- [42] Gittens R A *et al* 2012 Differential responses of osteoblast lineage cells to nanotopographically-modified, microroughened titanium–aluminum–vanadium alloy surfaces *Biomaterials* **33** 8986–94
- [43] Hollander D A *et al* 2006 Structural, mechanical and *in vitro* characterization of individually structured Ti–6Al–4V produced by direct laser forming *Biomaterials* **27** 955–63
- [44] Kieswetter K, Schwartz Z, Dean D D and Boyan B D 1996 The role of implant surface characteristics in the healing of bone *Crit. Rev. Oral Biol. Med.: Off. Publ. Am. Assoc. Oral Biol.* **7** 329–45
- [45] Boyce B F and Xing L 2007 Biology of RANK, RANKL, and osteoprotegerin *Arthritis Res. Ther.* **9** Suppl 1:S1
- [46] Tsuruga E, Takita H, Itoh H, Wakisaka Y and Kuboki Y 1997 Pore size of porous hydroxyapatite as the cell-substratum controls BMP-induced osteogenesis *J. Biochem.* **121** 317–24
- [47] Kilian K A, Bugarija B, Lahn B T and Mrksich M 2010 Geometric cues for directing the differentiation of mesenchymal stem cells *Proc. Natl. Acad. Sci.* **107** 4872–7
- [48] Lai M *et al* 2014 Role of $\alpha 2 \beta 1$ integrins in mediating cell shape on microtextured titanium surfaces *J. Biomed. Mater. Res. A* doi:10.1002/jbm.a.35185 (epub ahead of print)
- [49] Kieswetter K *et al* 1996 Surface roughness modulates the local production of growth factors and cytokines by osteoblast-like MG-63 cells *J. Biomed. Mater. Res.* **32** 55–63
- [50] Stubinger S *et al* 2013 Histological and biomechanical analysis of porous additive manufactured implants made by direct metal laser sintering: a pilot study in sheep *J. Biomed. Mater. Res. B: Appl. Biomater.* **101** 1154–63
- [51] Bandyopadhyay A, Espana F, Balla V K, Bose S, Ohgami Y and Davies N M 2010 Influence of porosity on mechanical properties and *in vivo* response of Ti6Al4V implants *Acta Biomater.* **6** 1640–8

Published: Volume 26, issue 10, October
2015, pages 1143-1149 in:

CLINICAL ORAL IMPLANTS RESEARCH WILEY

05

Accuracy of computer-guided implantation in a human cadaver model

Gustavo Yatzkaier, Alice Cheng, Stan Brodie, Eli
Raviv, Barbara D. Boyan and Zvi Schwartz



Superior Implant Technology

Gustavo Yatzkair
 Alice Cheng
 Stan Brodie
 Eli Raviv
 Barbara D. Boyan
 Zvi Schwartz

Accuracy of computer-guided implantation in a human cadaver model

Authors' affiliations:

Gustavo Yatzkair, Private Clinic, Jerusalem, Israel
 Alice Cheng, Barbara D. Boyan, Department of Biomedical Engineering, Georgia Institute of Technology and Emory University, Atlanta, GA, USA

Alice Cheng, Department of Biomedical Engineering, Peking University, Beijing, China
 Stan Brodie, AB Dental, Ashdod, Israel
 Eli Raviv, Department of Dentistry, Jewish General Hospital, Montreal, QC, Canada
 Barbara D. Boyan, Zvi Schwartz, Department of Biomedical Engineering, School of Engineering, Virginia Commonwealth University, Richmond, VA, USA

Zvi Schwartz, Department of Periodontology, University of Texas Health Science Center at San Antonio, San Antonio, TX, USA

Corresponding author:

Zvi Schwartz, DMD, PhD
 601 West Main Street
 PO Box 843067
 Richmond, VA 23284-3067, USA
 Tel.: 804 828 5824
 Fax: 804 828 9866
 e-mail: zschwartz@vcu.edu

Key words: computer-guided, dental implant, navigation, surgical guides

Abstract

Objectives: To examine the accuracy of computer-guided implantation using a human cadaver model with reduced experimental variability.

Materials and methods: Twenty-eight (28) dental implants representing 12 clinical cases were placed in four cadaver heads using a static guided implantation template. All planning and surgeries were performed by one clinician. All radiographs and measurements were performed by two examiners. The distance of the implants from buccal and lingual bone and mesial implant or tooth was analyzed at the apical and coronal levels, and measurements were compared to the planned values.

Results: No significant differences were seen between planned and implanted measurements. Average deviation of an implant from its planning radiograph was 0.8 mm, which is within the range of variability expected from CT analysis.

Conclusions: Guided implantation can be used safely with a margin of error of 1 mm.

More than 2 million dental implants are inserted into patients in the United States annually, and this number is expected to increase each year (American Dental Association 2007). As dental implants become the preferred choice for patients to restore missing teeth, methods for improving implant surgery have also been developed (Cibirka et al. 1997; Esposito et al. 2012; Vogel et al. 2013).

The development of cone-beam computed tomography (CBCT) has allowed dentists to plan surgical procedures based on a three-dimensional (3D) model of the patient's mouth. A major advantage that 3D imaging offers in planning procedures is preventing disruption of anatomic structures, in particular the lower mandibular nerve and upper sinus Schneiderian membrane (Brief et al. 2005). Compared with traditional CT imaging, CBCT has similar resolution but with lower radiation dosage (Liang et al. 2010). However, manual placement of implants with prior CBCT planning is still limited by the ability to insert the implant in the correct position and angulation. Manual implantation also requires an open flap surgery that results in alveolar crest bone loss from a

decrease in suprapariosteal blood supply during surgery (Rousseau 2010).

The introduction of computer-guided surgery templates allows for minimally invasive flapless surgery and immediate loading, resulting in reduced postoperative pain for the patient (Hultin et al. 2012). Guided surgery has gained much popularity with a mean implant survival rate of 96% after 36 months (Valente et al. 2009). The technology can also be used to reduce the number of bone augmentation and sinus lifts. Implants can be inserted into a narrow ridge; angulated implants can be used, and the insertion of an implant into non-bony tissues such as nerve can be avoided. Other advantages of computer-guided implantation include a reduced surgical time of <1 h, better alignment between implants, and the ability to plan more precisely for implants (Balshi et al. 2006; Jabero & Sarment 2006). The use of guided implantation has been concluded to be more accurate than freehand insertion (Park et al. 2009). In a direct comparison study between guided implant placement vs. manual freehand placement, use of CBCT and an implant guide resulted in significantly smaller variation between the treatment plan

Date:
 Accepted 6 August 2014

To cite this article:

Yatzkair G, Cheng A, Brodie S, Raviv E, Boyan BD, Schwartz Z. Accuracy of computer-guided implantation in a human cadaver model
Clin. Oral Impl. Res. 00, 2014, 1–7.
 doi: 10.1111/clr.12482

and the actual clinical placement (Nickenig et al. 2010). Deviation at the implant shoulder ranging from 0 to 4.5 mm was detected with use of an implant guide, while manual placement resulted in a much larger deviation ranging from 0 to 7.0 mm.

The accuracy of computer-guided implantation varies between studies due to different clinical and experimental setups (Hultin et al. 2012). A review of surgical template accuracy provides different values and ranges for *in vitro*, *ex vivo*, and clinical studies (D'Haese et al. 2012). It has also been shown previously that the experience level of the clinician can result in significant differences in accuracy (Van de Velde et al. 2008). Because error can arise from various steps in the process, it is unclear whether deviation of the resulting implant location from the planned location was a result of the guiding template (resolution from CBCT or template manufacturing) or environmental factors. The experience of the surgeon, regional location in the mouth, type of software and template, and transfer of information between entities can all contribute to deviation from the initially planned implant location.

The purpose of this study was to analyze accuracy of computer-guided dental implantation in a reduced-variability environment. We hypothesized that using computer-guided implantation with reduced human variability will increase accuracy of implant insertion and the implanted location will not be statistically different than the planned implant location. In this study, 12 clinical cases with 28 implants were implanted in human cadaver heads. All CT scans were performed in the same machine and by the same operator, and surgical procedures were planned by one clinician and executed by one surgeon. Measurements were made and analyzed by two examiners and were compared to the original plans for each implant.

Material and methods

Four whole human cadaver heads were retrieved and their mouths were examined. An impression of both jaws was taken, and a cast was made. The specimens were obtained from the USA bone bank for research only, and the study was performed in Israel under approval by the Ministry of Health. A specific CT guide with facial markers was created and used for pre-implantation scans of each cadaver head. The CT scan was used with a specific setup to obtain the CBCT radiographic scans, which allowed for scan-

ning the heads before and after implantation without altering alignment.

AB Guided Service (Ashdod, Israel) was used to plan the insertion of each implant using guided implantation. The treatment plan for each case and the plan of the AB Guide models were approved by one clinician. The AB Guided models were ordered using the AB Denpax software program. AB Guided surgical templates, an AB Guided surgical kit, and suggested implants and crowns were provided as a gift by AB Dental and were used for implantation.

Twelve (12) implantation cases were planned in four cadaver heads, with a total of 28 implants (Table 1). Cases were planned in edentulous areas only, with each cadaver head accommodating 2–4 cases. Implant length and diameter were planned according to anatomic structures on the CBCT scan. Implants were placed in the incisive, premolar, and molar areas of the mouth, covering both the upper and lower jaws (Table 2). The implantation of all implants was performed by one clinician according to the original plan. The guide was inserted and stabilized by pins, and the implant was inserted through the gingiva according to the company's guidance to the appropriate depth.

After implantation, CBCT scans were re-taken. Measurements between the location of implants in CT at the time of planning and after implantation were made at the coronal and apical levels to determine the distance between the implant and buccal bone, lingual bone, and adjacent (mesial) implant/teeth by two independent examiners, which were previously calibrated (Fig. 1). All

CBCT scans were performed by the same individual to reduce user variation.

Statistical analyses: Paired *t*-test was used to compare between planned and implanted groups, while unpaired *t*-test was used for comparison between regional implant location and across groups. All planned vs. implanted analyses were performed on different CBCT scans and analyzed separately to be considered independent. One way analysis of variance with Bonferroni post-test correction was used to compare across three groups, with significance for all statistical analyses set at $P < 0.05$. All cases were planned and implanted by the same clinician. All calibration, measurements, and analyses were performed by two examiners (data combined together) after calibration between them.

Results

Two of the twelve cases are presented as case studies in Figs 2 and 3. In the first case (Fig. 2), teeth 24–26 were extracted and the plan to rehabilitate this area with three implants can be seen in the panoramic figure obtained from the CT scan in Fig. 2a. The location of the implants on the CT at the coronal occlusal plane can be seen in Fig. 2c, and on the apical plane in Fig. 2d. A cross section of the CT shows the three implants in Fig 2g–i. The surgery guide was then produced and can be seen in the buccal view in Fig. 2m, and occlusal view in Fig. 2n. The superposition of the planned and inserted implants is presented in panoramic, occlusal (coronal and apical), and cross-sectional

Table 1. Cases and implants per case for each cadaver head

Case no.	Head no.	Implant site	Anterior	Posterior	Length (mm)	Diameter (mm)
1	1	44 45 46		3	13 10 8	3.2 3.2 3.75
2	1	36		1	11.5	3.75
3	1	11	1		13	3.2
4	1	24 25 26		3	13 13 11.5	3.75 3.75 4.2
5	2	46 47		2	13 13	4.2 4.2
6	2	35 36 37		3	13 13 13	3.75 4.2 5
7	2	24		1	13	3.75
8	3	36 37		2	10 8	3.2 3.75
9	3	46		1	8	3.75
10	4	34 35 36 37		4	13 10 10 8	4.2 3.2 3.75 3.75
11	4	45 46 47		3	11.5 10 8	3.2 3.75 4.2
12	4	11 15 21 25	2	2	13 16 11.5 16	3 3.2 3 3.2

Table 2. Total number of cases, implants, and regional placement

No. of case	No. of implant	No. of implant incisive	No. of implant premolar	No. of implant molar	No. of implant upper jaw	No. of implant lower jaw
12	28	3	11	14	9	19

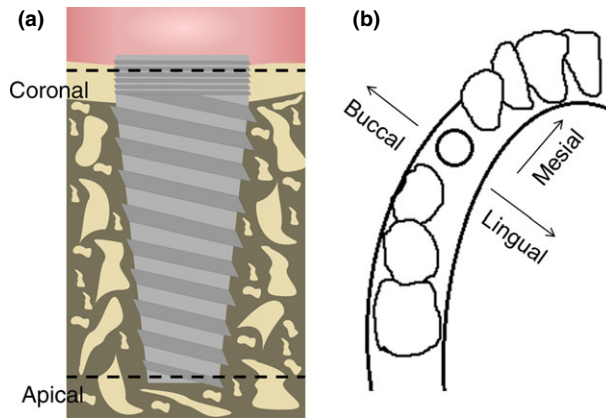


Fig. 1. Apical and coronal direction of the implant (a) and buccal, lingual, and mesial direction of analysis from implant (b).

views in Fig. 2b,e,f,j,k,l, respectively. The implant restoration bridge was examined first in the model in Fig. 2o and then inserted in the mouth for implantation as shown in Fig. 2p.

In the second case (Fig. 3), teeth 46–47 were extracted and the rehabilitation plan for this area with two implants can be seen in the panoramic figure obtained from the CT scan in Fig. 3a. The location of the implants

on the CT at the coronal-occlusal plane can be seen in Fig. 3c, and the apical plane in Fig. 3d. A cross section of the CT shows the two implants in Fig 3g,h. The surgery guide was produced and can be seen in buccal view in Fig. 2k and occlusal view in Fig. 2l. The superposition of the planned and inserted implants are present in panoramic, occlusal (coronary and apically) and on cross sectional views in Fig. 2b,e and 2f,i, and 2j, respectively.

To reduce statistical bias, analyses were performed by case and by implant. Analyses per case revealed no significant differences between planned and implanted locations in buccal, lingual, and mesial directions, both at the coronal and apical levels (Fig. 4, Table 3). Although the deviation in distance was higher at the apex compared to the coronal plane, deviation from each direction was not statistically significant in either plane.

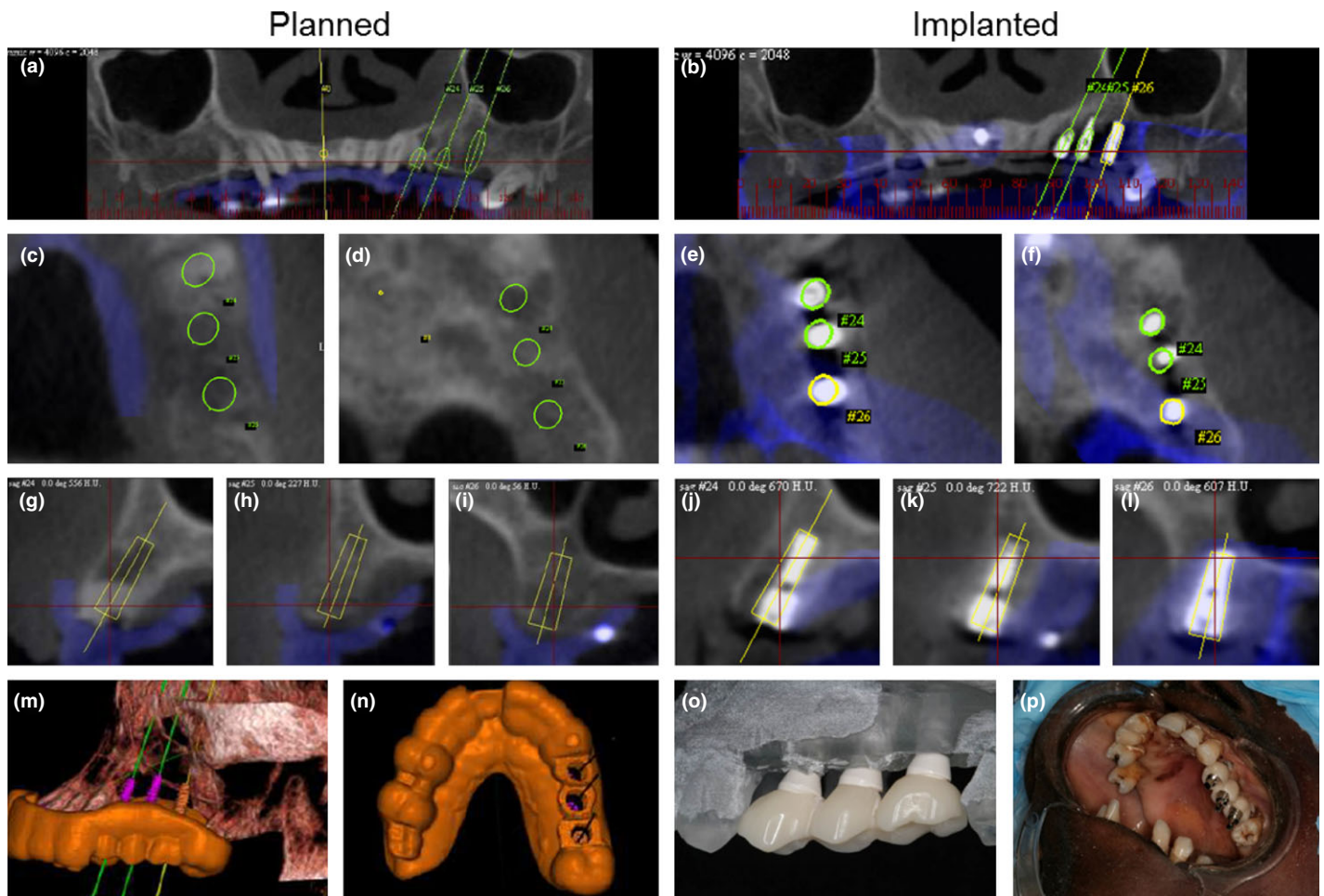


Fig. 2. Case showing planned (a, c, d, g, h, i, m, n) and implanted (b, e, f, j, k, l, o, p) images of guided implant placement in the maxilla. CBCT scans were taken of patients before (a) and after (b) implant placement, showing outline of planned implant (a, b) and location of the actual implant (b). Cross-sectional slices for location analysis were performed for planned (c, d) and implanted (e, f) implants at the coronal (c, e) and apical (d, f) levels. Close-up images of each implant placed from original CBCT scans (a, b) are shown before (g–i) and after implantation (j–l). A 3D reconstructed view of the maxilla with surgical guide (m, n) was used for implant placement. A model of the maxilla with planned implants (o) was used in selection of appropriate crown size that transferred to each finished case (p).

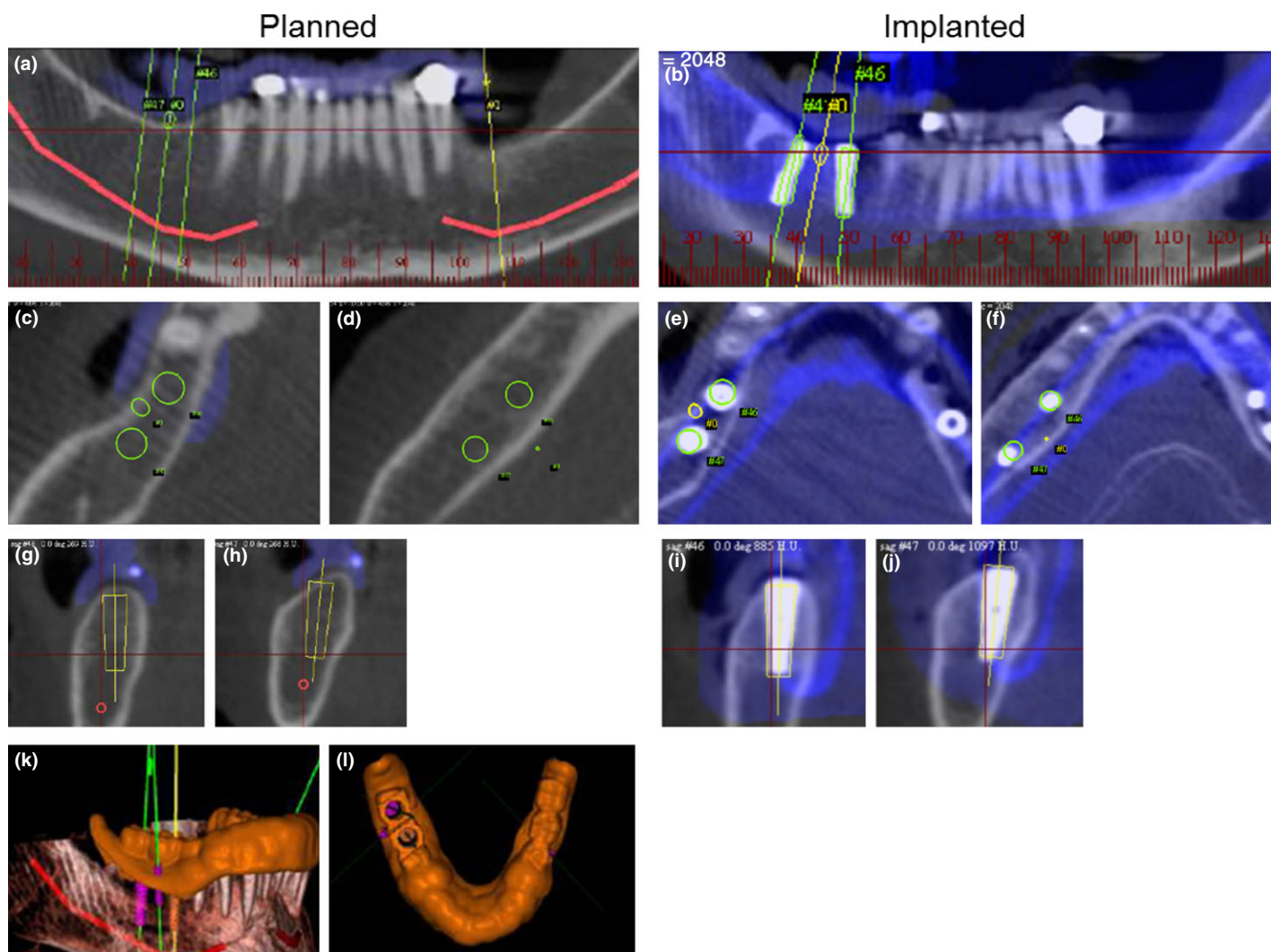


Fig. 3. Case showing planned (a, c, d, g, h, k, l) and implanted (b, e, f, i, j) images of guided implant placement in the mandible. CBCT scans were taken of patients before (a) and after (b) implant placement, showing outline of planned implant (a, b) and location of actual implant (b). Cross-sectional slices for location analysis were performed for planned (c, d) and implanted (e, f) implants at the coronal (c, e) and apical (d, f) levels. Close-up images of each implant placed from original CBCT scans (a, b) are shown before (g, h) and after implantation (i, j). A 3D reconstructed view of the mandible with surgical guide (k, l) was used for implant placement.

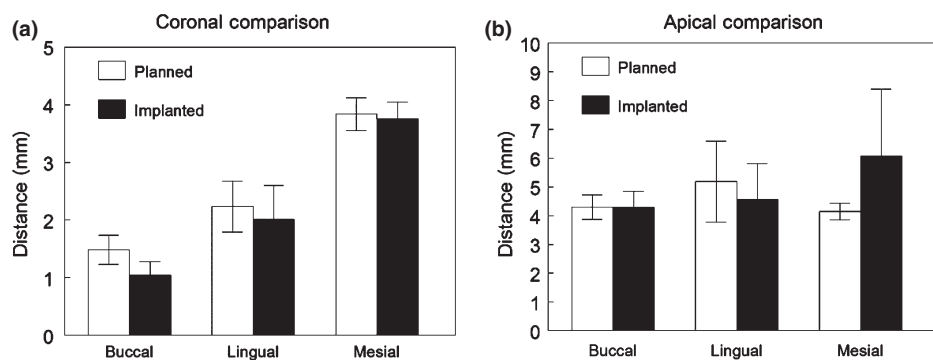


Fig. 4. Coronal and apical location analysis by case. Implant location was analyzed at the coronal (a) and apical (b) levels for planned and implanted sites. Student's *t*-test across planned and implanted locations showed no significant differences between groups.

Analyses per implant also showed no significant differences between planned and implanted locations in any direction (Fig. 5). Per implant analysis revealed a higher range

of deviation from planned locations, but deviations were not significantly different in buccal, lingual, or mesial directions. Apical deviation in the mesial direction was the

highest compared with buccal and lingual directions and the coronal plane.

Analyses per implant comparing implant locations between the premolar and molar areas did not show significant deviation from planned locations in the coronal plane (Fig. 6). Analyses were not performed for the incisive area due to the low number of implants that were placed in the region. Molar implant placement was characterized by a high standard deviation in the mesial direction. Analyses per implant comparing locations between the upper and lower jaw also did not show statistical significance from planned locations in the coronal plane.

The overall average error was 0.8 mm across all directions. The average error and standard deviation per case was 0.8 ± 0.1 mm and per implant was 0.9 ± 0.1 mm. The range of deviation between implanted and planned locations

Table 3. Difference between planned and implanted locations

Difference between measurement (mm)		Buccal			Lingual			Mesial		
		Mean	SEM	Median	Mean	SEM	Median	Mean	SEM	Median
Case	Apical	0.70	0.19	0.65	0.86	0.26	0.88	1.13	0.42	0.98
Case	Coronal	0.74	0.13	0.55	0.78	0.22	0.78	0.41	0.09	0.59
Implant	Apical	0.72	0.12	0.48	0.82	0.20	0.98	2.1	1.10	1.76
Implant	Coronal	0.78	0.10	0.69	0.89	0.25	0.69	1.06	0.54	0.86

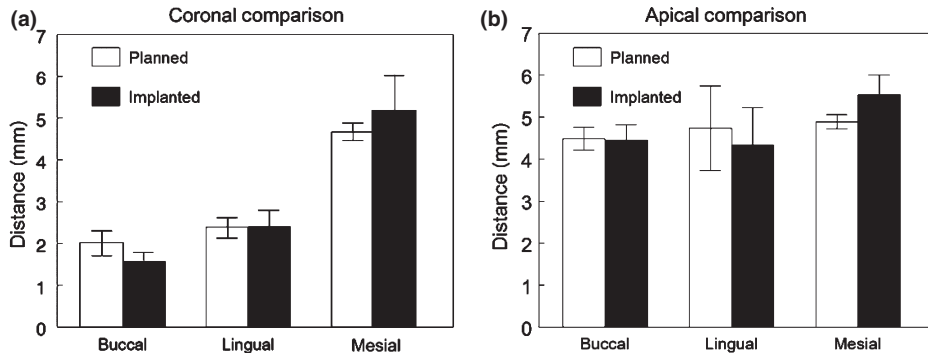


Fig. 5. Coronal and apical location analysis by implant. Implant location was analyzed at the coronal (a) and apical (b) levels for planned and implanted sites. Student's *t*-test across planned and implanted locations showed no significant differences between groups.

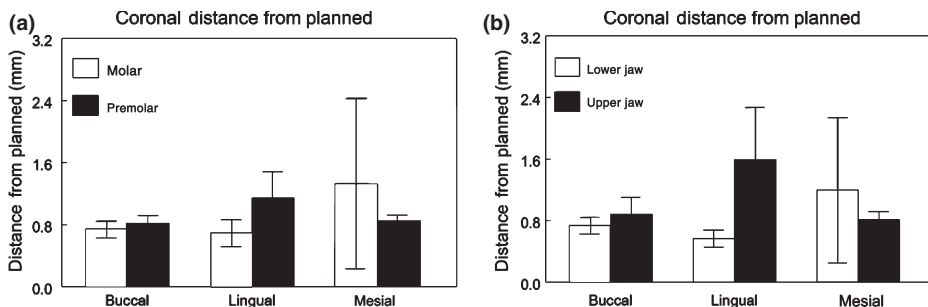


Fig. 6. Regional analysis by implant. Distance from buccal and lingual bone and mesially to adjacent tooth/implant was evaluated for planned and inserted implants in the molar and premolar regions (a) and lower and upper jaw (b). Student's *t*-test across molar vs. premolar and lower vs. upper jaw showed no significance differences between groups.

was greater mesially, as indicated by higher standard deviations in Figs 4d, 5b,d, 6a,b.

Discussion

With an increasing number of dental implant guides being used, it is important to analyze the accuracy of these systems in a controlled clinical environment. To reduce experimental variability while still remaining biologically relevant, we assessed placement accuracy for implants that were planned and performed consistently by the same clinician. Our results show that when using this guided implant system, final implant locations are not statistically different from planned locations, corroborating our original hypothesis.

Our novel cadaveric model provides a clinically relevant analysis of implant placement error resulting from the use of surgical guides, while upholding scientific rigor by reducing experimental variance.

In this study, average deviation was 0.8 mm, which is well accepted and within the lower range of error in the literature. It was also observed that the range of deviation was higher at the apex compared to the coronal plane. This has also been observed in the literature, and is due to changes in the placement angle, which was not measured in this study (Ersoy et al. 2008; Schneider et al. 2009; Van Assche et al. 2012). It has also been suggested that higher error in the apical plane could be attributed to the type of drill (cylindrical or tapered) being using (Arisan

et al. 2010). Careful planning can help ensure an appropriate implant length to prevent damage to the maxillary sinus or mandibular nerve.

The number and distribution of remaining teeth as well as the number of steps in producing and using the template can contribute to error (Behneke et al. 2012). In addition, implants placed with the same guide are not independent from each other and errors are interactive and possibly cumulative (Widmann & Bale 2006). It has been shown that error occurring during image acquisition and data processing ranges from 0.5 to 1 mm (Reddy et al. 1994; Abad-Gallego et al. 2011). A comparison study of linear measurement error between CBCT scans and direct measurements in an *ex vivo* porcine model found that overestimation occurred in 36% of the sites when using CBCT, with 0.8% of sites having an overestimation error of over 0.5 mm (Kurtz et al. 2007). Error during surgical template production can be up to 0.2 mm for transfer of the computer-assisted design to guide manufacturing axes (Champleboux et al. 1998). Error can also occur during template positioning and be increased if there is movement during drilling.

In addition, mechanical error caused by the bur-cylinder gap can lead to deviations up to 1 mm at the apex in surgical templates (Valente et al. 2009). However, this is less than axial deviation caused by freehand drilling (Nickenig et al. 2010). Axial deviation could also occur from human error, such as setting the bur at the incorrect position. Because tolerance is dependent on bone mass and location to critical anatomic structures, among other patient factors, there are no universal tolerance values established for dental implant placement. With the ability of errors to compound, it is important to still maintain safety margins when planning implant placement.

In this study, experimental variability was reduced significantly by allowing only one clinician to plan and perform all surgeries in the same surgical environment. In contrast to other studies on guided implantation accuracy using human cadaver jaws, this study was performed on whole human cadaver heads (Van Assche et al. 2007; Ruppini et al. 2008). Another study using two whole human cadaver jaws was performed only in the maxilla and could not provide quantitative assessments of accuracy for different regions in the mouth (van Steenberghe et al. 2002). The *ex vivo* use of entire cadaver heads allows a more clinical representation of surgical conditions while being able to eth-

ically control for environmental variability. However, due to preservation, cadaveric bone can be softer than live bone. In this study, limited bone was observed in the posterior mandible in one cadaver. This contributed to the large placement difference and deviation seen in Fig. 5d. We believe that this deviation was specific to the cadaver and would not translate to a healthy patient clinically. Although there may be slight biological differences between an *ex vivo* cadaver model and an *in vivo* clinical study, using this model allows us to much better control for other more important clinical variables. To the best of our knowledge, this is the first instance of a qualitative guided implant accuracy study in which an entire cadaver head was used.

In clinical studies, the most frequent problem encountered is limited access in posterior areas (Schneider et al. 2009). However, reducing the surgical guide occlusogingival height from 8 to 4 mm did not significantly affect implant placement (Park et al. 2009). The cadaver head model used in the present

study enables assessment of surgical guide design with respect to accuracy, but it cannot determine postoperative complications and see trends based on patient variability over time.

Conclusion

With the emergence and refinement of new technologies, the accuracy and popularity of computer-guided implantation will continue to grow. Before the advent of guided templates, safety margins of 2 mm were recommended to reduce damage to vital structures during implantation (Worthington 2004). Within the past 10 years, guided implantation has increased implant accuracy to 1.07 mm at the entry point and <0.5 mm in vertical deviation (Schneider et al. 2009).

In this study, we took a unique approach to analyzing guided implant placement accuracy through a biological model while controlling for clinician experience, hospital setting, equipment usage, and other

experimental variability. This effective experimental model was able to isolate the true error of guided implant systems from the general compounded error due to clinical variation. The average deviation of placed from planned implants in this study was 0.8 mm, which is well accepted within the literature for computer-guided implantation. No statistical differences were found between the planned and implanted locations. To factor in clinician variability and patient type, the authors advise that implant planning with 3D and guided templates should include a safety distance of 1 mm. This study suggests that guided implantation can be used safely in difficult cases near anatomic structures.

Acknowledgements: The authors would like to acknowledge contributions from Eitan Krause and Nataniel Agour. This research was supported by a grant from AB Dental (Ashdod, Israel).

References

- Abad-Gallego, M., Gomez-Santos, L., Sanchez-Garcés, M.A., Pina-Penalva, M., Freixes-Gil, J., Castro-Garcia, A. & Gay-Escoda, C. (2011) Complications of guided surgery and immediate loading in oral implantology: a report of 12 cases. *Medicina Oral Patología Oral y Cirugía Bucal* **16**: 220–224.
- American Dental Association (2007) 2005–06 Survey of Dental Services Rendered. Chicago, IL: American Dental Association.
- Arisan, V., Karabuda, Z.C. & Ozdemir, T. (2010) Accuracy of two stereolithographic guide systems for computer-aided implant placement: a computed tomography-based clinical comparative study. *Journal of Periodontology* **81**: 43–51.
- Balshi, S.F., Wolfinger, G.J. & Balshi, T.J. (2006) Surgical planning and prosthesis construction using computed tomography, CAD/CAM technology, and the Internet for immediate loading of dental implants. *Journal of Esthetic and Restorative Dentistry*, **18**: 312–323. discussion 324–315.
- Behneke, A., Burwinkel, M. & Behneke, N. (2012) Factors influencing transfer accuracy of cone beam CT-derived template-based implant placement. *Clinical Oral Implants Research* **23**: 416–423.
- Brief, J., Edinger, D., Hassfeld, S. & Eggers, G. (2005) Accuracy of image-guided implantology. *Clinical Oral Implants Research* **16**: 495–501.
- Champleboux, G., Fortin, T., Buatois, H., Coudert, J.L. & Blanchet, E. (1998) A fast, accurate and easy method to position oral implant using computed tomography. *Medical Image Computing and Computer-Assisted Intervention* **1496**: 269–276.
- Cibirka, R.M., Razzoog, M. & Lang, B.R. (1997) Critical evaluation of patient responses to dental implant therapy. *The Journal of Prosthetic Dentistry* **78**: 574–581.
- D'Haese, J., Van De Velde, T., Komiyama, A.I., Hultin, M. & De Bruyn, H. (2012) Accuracy and complications using computer-guided stereolithographic surgical guides for oral rehabilitation by means of dental implants: a review of the literature. *Clinical Implant Dentistry & Related Research* **14**: 321–335.
- Ersay, A.E., Turkyilmaz, I., Ozan, O. & McGlumphy, E.A. (2008) Reliability of implant placement with stereolithographic surgical guides generated from computed tomography: clinical data from 94 implants. *Journal of Periodontology* **79**: 1339–1345.
- Esposito, M., Maghazeh, H., Grusovin, M.B., Zio-unas, I. & Worthington, H.V. (2012) Soft tissue management for dental implants: what are the most effective techniques? A cochrane systematic review. *European Journal of Oral Implantology* **5**: 221–238.
- Hultin, M., Svensson, K.G. & Trulsson, M. (2012) Clinical advantages of computer-guided implant placement: a systematic review. *Clinical Oral Implants Research* **23**: 124–135.
- Jabero, M. & Sarment, D.P. (2006) Advanced surgical guidance technology: a review. *Implant Dentistry* **15**: 135–142.
- Kurtz, S., Ong, K., Lau, E., Mowat, F. & Halpern, M. (2007) Projections of primary and revision hip and knee arthroplasty in the United States from 2005 to 2030. *The Journal of Bone & Joint Surgery* **89**: 780–785.
- Liang, X., Jacobs, R., Hassan, B., Li, L., Pauwels, R., Corpas, L. & Lambrechts, I. (2010) A comparative evaluation of Cone Beam Computed Tomography (CBCT) and Multi-Slice CT (MSCT): Part I. On subjective image quality. *European Journal of Radiology* **75**: 265–269.
- Nickenig, H.-J., Wichmann, M., Hamel, J., Schlegel, K.A. & Eitner, S. (2010) Evaluation of the difference in accuracy between implant placement by virtual planning data and surgical guide templates versus the conventional free-hand method – a combined in vivo – in vitro technique using cone-beam CT (Part II). *Journal of Cranio-Maxillofacial Surgery* **38**: 488–493.
- Park, C., Raigrodski, A.J., Rosen, J., Spiekerman, C. & London, R.M. (2009) Accuracy of implant placement using precision surgical guides with varying occlusogingival heights: an in vitro study. *Journal of Prosthetic Dentistry* **101**: 372–381.
- Reddy, M.S., Mayfield-Donahoo, T., Vandervan, F.J. & Jeffcoat, M.K. (1994) A comparison of the diagnostic advantages of panoramic radiography and computed tomography scanning for placement of root form dental implants. *Clinical Oral Implants Research* **5**: 229–238.
- Rousseau, P. (2010) Flapless and traditional dental implant surgery: an open, retrospective comparative study. *Journal of Oral and Maxillofacial Surgery* **68**: 2299–2306.
- Ruppin, J., Popovic, A., Strauss, M., Spuntrup, E., Steiner, A. & Stoll, C. (2008) Evaluation of accuracy of three different computer-aided surgery systems in dental implantology: optical tracking vs. stereolithographic splint systems. *Clinical Oral Implants Research* **19**: 709–716.
- Schneider, D., Marquardt, P., Zwahlen, M. & Jung, R.E. (2009) A systematic review on the accuracy and the clinical outcome of computer-guided

- template-based implant dentistry. *Clinical Oral Implants Research* **20**: 73–86.
- van Steenberghe, D., Naert, I., Andersson, M., Brajnovic, I., Van Cleynenbrugel, J. & Suetens, P. (2002) A custom template and definitive prosthesis allowing immediate implant loading in the maxilla: a clinical report. *International Journal of Oral & Maxillofacial Implants* **17**: 663–670.
- Valente, F., Schioli, B. & Sbrenna, A. (2009) Accuracy of computer-aided oral implant surgery: a clinical and radiographic study. *The International Journal of Oral & Maxillofacial Implants* **24**: 234–242.
- Van Assche, N., Van Steenberghe, D., Guerrero, M.E., Hirsch, E., Schutyser, F., Quirynen, M. & Jacobs, R. (2007) Accuracy of implant placement based on pre-surgical planning of three-dimensional cone-beam images: a pilot study. *Journal of Clinical Periodontology* **34**: 816–821.
- Van Assche, N., Vercruyssen, M., Coucke, W., Teughels, W., Jacobs, R. & Quirynen, M. (2012) Accuracy of computer-aided implant placement. *Clinical Oral Implants Research* **23**: 112–123.
- Van de Velde, T., Glor, F. & De Bruyn, H. (2008) A model study on flapless implant placement by clinicians with a different experience level in implant surgery. *Clinical Oral Implants Research* **19**: 66–72.
- Vogel, R., Smith-Palmer, J. & Valentine, W. (2013) Evaluating the health economic implications and cost-effectiveness of dental implants: a literature review. *International Journal of Oral & Maxillofacial Implants* **28**: 343–356.
- Widmann, G. & Bale, R.J. (2006) Accuracy in computer-aided implant surgery – a review. *International Journal of Oral & Maxillofacial Implants* **21**: 305–313.
- Worthington, P. (2004) Injury to the inferior alveolar nerve during implant placement: a formula for protection of the patient and clinician. *International Journal of Oral & Maxillofacial Implants* **19**: 731–734.

Published in Quintessence International
magazine, volume 41, number 7, July-
August 2010



06

Short dental implants in reduced alveolar bone height

Eli Raviv, DMD; Antony Turcotte, DMD; Mili Harel-
Raviv, DMD



Superior Implant Technology

Short dental implants in reduced alveolar bone height

Eli Raviv, DMD¹/Antony Turcotte, DMD²/Mili Harel-Raviv, DMD³

Reduced alveolar bone height is very common in the posterior jaws. The current treatment modality to replace the missing teeth with an implant-retained fixed partial denture includes sinus bone grafting in the maxilla and onlay bone graft in the mandible. These procedures are invasive and require more time and cost. Short dental implants are used as an alternative treatment modality to bone grafting procedures. To enhance success rate, certain principles should apply. Short implants could provide comparable results to those of longer implants. The present article reviews the current literature on the use of short implants, discusses the biomechanical considerations when utilizing short implants, and presents a case. (*Quintessence Int* 2010;41:xxx-xxx)

Key words: alveolar bone, fixed partial denture, PFM-FPD, porcelain-fused-to-metal, short implant[Au: additions ok?]

Clinicians often face challenges when placing implants in an area of reduced alveolar bone height. This is seen in both the maxilla and mandible due to alveolar bone resorption, pneumatization of maxillary sinuses, and the presence of anatomical structures (eg, inferior alveolar nerve). The accepted treatment for this condition has been conventionally to perform a sinus lift and bone grafting procedure. Despite good predictability and success rate of grafting procedures, patients are often reluctant to undergo the surgery because of the risks, morbidities, cost of the procedure, and the stress of undergoing an invasive procedure. Short implants (≤ 8 mm) have been introduced recently as a potential alternative treatment to

bone grafting procedures in patients with limited alveolar bone height in the posterior maxilla and mandible.¹⁻⁵

This article reviews the current literature on the use of short implants and presents a case treated with short implants.

CASE REPORT

A 47-year-old white female in good general health presented with porcelain fracture on a three-unit porcelain-fused-to-metal fixed partial denture (PFM-FPD) replacing the maxillary right first molar. The porcelain fracture was limited to the pontic area with metal exposed. Clinical examination revealed wear facets on the occlusal aspects of all teeth. The attrition of the teeth was compatible with bruxism. The parafunction could be the etiologic factor for the porcelain fracture. In addition to the clinical examination, periapical radiograph showed excellent marginal adaptation of the retainers (second premolar and second molar) (Fig 1). The patient was not aware of the parafunction and never had a nightguard prescribed.

¹Associate Professor, Faculty of Dentistry; Director of Prosthodontics, Department of Dentistry, Sir Mortimer B. Davis Jewish General Hospital, McGill University, Montreal, Canada

²Resident in the MDR[Au: Please expand.] program, Department of Dentistry, Sir Mortimer B. Davis Jewish General Hospital, Montreal, Canada.

³Department of Dentistry, Sir Mortimer B. Davis Jewish General Hospital, Montreal, Canada.

Correspondence: Dr Eli Raviv, Director of Prosthodontics, Department of Dentistry, Sir Mortimer B. Davis Jewish General Hospital, 3750 Cote des neiges, Montreal, Qc. Canada H3S 1Y9. Email: raviv.eli@gmail.com

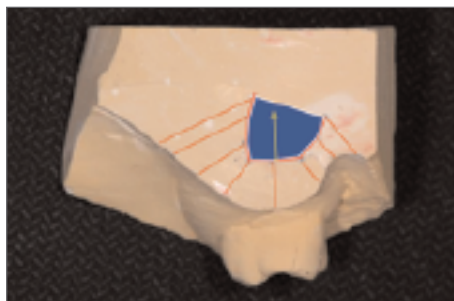
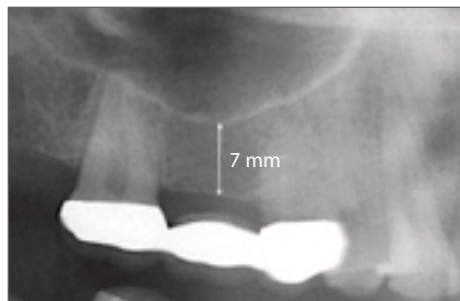


Fig 1 (left) Pretreatment radiograph, showing limited bone height.

Fig 2 (center) Clinical ridge mapping.

Fig 3 (right) Schematic illustration of an A. B. short implant.



Fig 4 (left) Postsurgical clinical presentation of the healing screw.

Fig 5 (center) Radiograph obtained after the placement of an I5, 6 × 6 mm implant with healing abutment. [Au: what is I5?]

Fig 6 (right) Clinical occlusal view of the implant restorative platform.

Three treatment options were presented to the patient: (1) replacement of the PFM-FPD with a new PFM-FPD; (2) to section the pontic, keep the retainers on the second premolar and second molar intact, and replace the missing first molar with an endosseous implant-retained crown; and (3) removal of the remaining porcelain from the pontic and casting of a PFM single onlay (U shape) to address the esthetic and functional deficiencies.

Because of lower sinus location and lack of alveolar bone height for placement of an implant of conventional length, sinus lift procedure was introduced to the patient as an adjunct to the implant surgery. Being a health care provider and working as a nurse in a hospital, she was reluctant to accept the sinus lift procedure, as for her it was an invasive procedure that she did not approve. The idea of keeping the two crowns intact was appealing to the patient. The option of placing a short-length implant was presented to the patient and discussed with her. The patient accepted the short implant option.

Before implant placement, alveolar bone volume was measured using panoramic and periapical radiographs and clinical ridge mapping. Bone volume was found to be 7 mm in height and 8 mm in width (see Figs 1 and 2).

A short, tapered, wide-diameter implant (A. B. Dental Devices, I-5 6 × 6 mm)[Au: What is "I-5"? Legend used "I5."] was placed in the edentulous site (Fig 3). This self-tapping implant design consists of very sharp and deep threads, which increase the implant surface area, resulting in an improved primary stability. The implant was torqued to 32 Ncm.

According to a single-stage procedure (nonsubmerged), a healing screw was connected (Fig 4). Periapical radiograph was taken to confirm implant orientation, which was found to engage the cortical bone of the sinus floor (Fig 5). The healing process was within normal limits. No adverse effects were reported.

Six months postimplantation the healing screw was removed (Fig 6). Final impression



Fig 7 (left) Close-tray, press-fit, hex-locked impression coping in place.

Fig 8 (right) Final impression obtained.

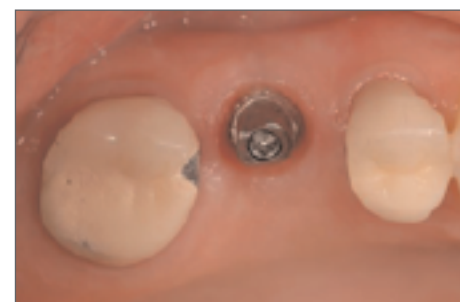


Fig 9a (left) Hex-locked abutment on model with a resin jig for proper placement.

Fig 9b (center) Abutment positioned in the mouth with a resin jig.

Fig 9c (right) Final abutment in place.

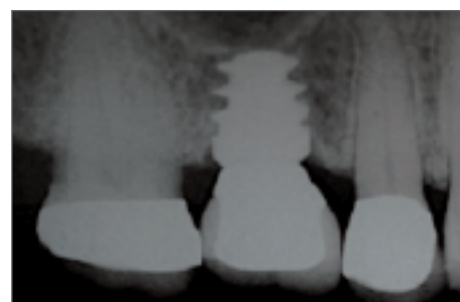


Fig 10 (left) PFM crown, temporarily cemented with Tempbond.

Fig 11 (right) Posttreatment radiograph of the implant, abutment, and crown.

was taken using a press-fit, hex-locked impression coping (A. B. Dental Devices) (Fig 7).

Polyether, heavy-body impression material, Impregum, [Au: Who is the manufacturer?] and light-body material, Permadyne (3M ESPE Pentamix) were used to pick up the impression coping (Fig 8). A straight hex-locked abutment was placed, using a resin jig for its ideal orientation (GC Pattern Resin LS, GC) (Fig 9).

A PFM crown was fabricated and temporarily cemented (Tempbond-Ne, Kerr) [Au: Please confirm product/mfr names. confirm

use of "Ne."] (Fig 10). A postinsertion radiograph was taken showing the platform switch concept used to better maintain the alveolar bone crest (Fig 11). To address the parafunction, a light occlusal contact in centric occlusion and complete disclusion in lateral and protrusive excursions were performed. In addition, a Hawley bite appliance with anterior platform was prescribed as a nightguard.

The 18-month follow-up revealed no clinically significant findings. The patient's esthetics and function were satisfactory.

DISCUSSION

In the last decade, studies revealed conflicting results concerning the long-term survival and success rates of short implants.^{6,14} **[Au: There is no ref 14; but see query in reference list. Please verify/fix numbering.]** One of the difficulties encountered when evaluating these studies is the subjectivity of the term “short” implants. Most of the studies consider short implants as being less than 10 mm,⁶⁻⁷ while few studies have included implants of 7 mm or less in length.^{8,9}

Implant length is generally selected according to the maximum amount of bone height present at the recipient site. This is based on the principle that longer implants provide better primary stability and a favorable distribution of occlusal forces due to an increased total surface area.^{10,11} However, an important difference exists between total surface area and functional surface area. Total surface area represents the overall surface area of the implant, while a functional surface area represents the area that transfers the compressive and tensile loads to bone and does not include the passive portion of the implant.¹⁰ It was illustrated that unlike what occurs with the stresses applied to a natural tooth and the periodontal ligament, stresses around implants are greatest at the crest of the ridge and less **[Au: or “least”?] in the apical portion.**^{10,12,13} Based on this principle, an increased length would simply improve primary stability of the implant during initial placement and enhance osseointegration. On the other hand, a wider diameter implant would increase not only primary stability but also the functional surface area at the crestal bone level, and thus lead to a better distribution of occlusal forces to the surrounding bone. Therefore, short wide-diameter implants should bear functional stresses as effectively as longer implants.

Several parameters need to be evaluated before the placement and restoration of short implants. The type of bone is an important variable when placing implants. Since bone quality is considered a major risk factor for implant failure because of the lack of primary stability, the increased stability provided by the wide diameter would be a consid-

erable advantage especially in the posterior maxilla where bone quality and quantity is often less than ideal. Prosthetic loading of short implants also requires careful planning. Most studies on short implants have reported that these implants can be restored with any type of prosthesis (ie, single crowns, FPDs, and removable prostheses).⁴ However, crown-to-implant ratio, excessive occlusal forces, and presence of cantilevers are some of the risk factors that may lead to an increased stress on the implants and may therefore compromise implant survival.⁵ Other parameters are the distance between the threads (thread pitch) and the depth of the threads. High number of threads and deeper threads provide greater surface area that could compensate for the short length implant.

SUMMARY

The aim of this report was to evaluate and discuss the clinical use of short wide-diameter implants in the posterior maxilla as an alternative treatment modality to sinus bone grafting procedures.

In this case, an existing FPD was replacing the missing maxillary first molar. Therefore the easiest treatment plan would probably have been fabrication of a new FPD. One of the disadvantages of an FPD is the difficulty to maintain good home care. By replacing the missing tooth with a single implant-retained crown, the patient was able to floss her teeth (something she could not do before).

In selected cases, short wide-diameter implants could be used effectively in an area of limited bone height, and therefore represent an appropriate alternative treatment option to bone grafting.

The authors would like to add that although short wide-diameter implants could provide sufficient primary stability and functional surface area, further research on their long-term success in cases of reduced alveolar bone height is still necessary.

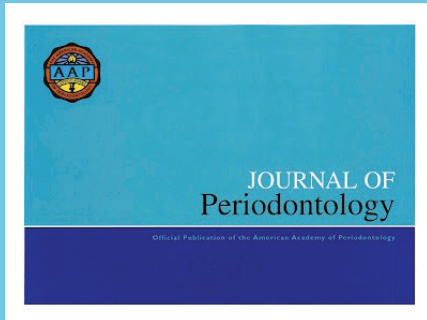
ACKNOWLEDGMENT

The authors would like to thank A. B. Dental Devices for their support.

REFERENCES

1. Kido H, Schulz EE, Kumar A, Lozada J, Saha S. Implant diameter and bone density: Effect on initial stability and pull-out resistance. *J Oral Implantol* 1997;23: 163–169.
2. Maustsushita Y, Kitoh M, Mizuta K, Ikeda H, Suetsugu T. Two-dimensional FEM analysis of hydroxapatite implants: Diameter effects on stress distribution. *J Oral Implantol* 1990;16:6–11.
3. Bahat O, Handelsman M. Use of wide implants and double implants in the posterior jaw: A clinical report. *Int J Oral Maxillofac Implants* 1996;11: 379–386.
4. Gentile MA, Chuang SK, Dobson T. Survival estimates and risk factors for failure with 6 × 5.7-mm implants. *Int J Oral Maxillofac Implants* 2005;20: 930–937.
5. Fugazzotto PA. Shorter implants in clinical practice: Rationale and treatment results. *Int J Oral Maxillofac Implants* 2008;23:487–496.
6. Das Neves FD, Fones D, Bernardes SR, Do Prado CJ, Fernandes Neto AJ. Short implants: An analysis of longitudinal studies. *Int J Oral Maxillofac Implants* 2006;21:86–93.
7. Feldman S, Boitel N, Weng D, Kohles SS, Stach RM. Five-year survival distributions of short-length (10 mm) or less machined-surface and Osseotite implants. *Clin Implant Dent Relat Res* 2004;6:16–23.
- ?? Friborg B, Grondahl K, Lekholm U, Branemark PI. Long-term follow-up of severely atrophic edentulous mandibles reconstructed with short Branemark implants. *Clin Implant Dent Relat Res* 2000;2:184–189. [Au: This reference was not numbered. Should it be? or omit?]
9. Ten Bruggenkate CM, Asikainen P, Foitzik C, Krekeler G, Sutter F. Short (6 mm) nonsubmerged dental implants: Results of a multicenter clinical trial of 1 to 7 years. *Int J Oral Maxillofac Implants* 1998;13: 791–798.
9. Misch CE, Steigenga J, Barboza E, Misch-Dietsh F, Cianciola LJ, Kazor C. Short dental implants in posterior partial edentulism: A multicenter retrospective 6-year case series study. *J Periodontol* 2006;77: 1340–1347.
10. Lum LB. A biochemical rationale for the use of short implants. *J Oral Implantol* 1991;17:126–131.
11. Holgrem ET, Seckinger RJ, Kilgren LM, Mante F. Evaluating parameters of osseointegrated dental implants using finite element analysis: A 2-dimensional comparative study examining the effects of implant diameter, implant shape and load direction. *J Oral Implantol* 1998;24:80–88.
12. Misch CE. Implant design considerations for the posterior regions of the mouth. *Implant Dent* 1999;8:376–386.
13. Roos J, Sennerby L, Lekholm U, Jemt T, Grondahl K, Albrektsson T. A qualitative and quantitative method for evaluating implant success: A 5-year retrospective analysis of the Branemark implant. *Int J Oral Maxillofac Implants* 1997;12:504–514.

Published in Periodontal magazine,
volume 82, issue 5



07

Characterization of five different implant surfaces and their effect on osseointegration: a study in dogs

Paulo G. Coelho,* Estevam A. Bonfante, Roberto
S. Pessoa, Charles Marin, Rodrigo Granato,
Gabriela Giro, Lukasz Witek, Marcelo Suzuki



Superior Implant Technology

Characterization of Five Different Implant Surfaces and Their Effect on Osseointegration: A Study in Dogs

[AQ1] Paulo G. Coelho,* Estevam A. Bonfante,† Roberto S. Pessoa,‡ Charles Marin,§ Rodrigo Granato,§ Gabriela Giro,‡ Lukasz Witek,* and Marcelo Suzuki||

[AQ2] **Background:** Chemical modification of implant surface is typically associated with surface topographic alterations that may affect early osseointegration. This study investigated the effects of controlled surface alterations in early osseointegration in an animal model.

Methods: Five implant surfaces were evaluated: 1) alumina-blasted; 2) biologic blasting; 3) plasma; 4) microblasted-resorbable blasting media (microblasted RBM); and 5) alumina-blasted/acid-etched (AB/AE). Surface topography was characterized by scanning electron microscopy and optical interferometry, and chemical assessment by x-ray photoelectron spectroscopy. The implants were placed in the radius of six dogs, remaining 2 and 4 weeks in vivo. After euthanization, specimens were torqued-to-interface failure, and non-decalcified processed for histomorphologic, bone-implant contact, and bone area fraction occupied evaluation. Statistical evaluation was performed by one-way analysis of variance ($P < 0.05$) and post hoc testing by the Tukey test.

Results: The alumina-blasted surface presented the highest average surface roughness and mean root square of the surface values, the biologic blasting the lowest, and AB/AE an intermediate value. The remaining surfaces presented intermediate values between the biologic blasting and AB/AE. The x-ray photoelectron spectroscopy spectra revealed calcium and phosphorus for the biologic blasting and microblasted RBM surfaces, and the highest oxygen levels for the plasma, microblasted RBM, and AB/AE surfaces. Significantly higher torque was observed at 2 weeks for the microblasted RBM surface ($P < 0.04$), but no differences existed between surfaces at 4 weeks ($P > 0.74$). No significant differences in bone-implant contact and bone area fraction occupied values were observed at 2 and 4 weeks.

Conclusion: The five surfaces were osseointegrative and resulted in high degrees of osseointegration and biomechanical fixation. *J Periodontol* 2011;82:■■■■-■■■■.

KEY WORDS

[AQ3] **Histology; osseointegration; torque.**

Over the last four decades, clinical oral implantology has shown high survival rates over time (often exceeding 95% over 10 years^{1,2}), and has been regarded as one of the most successful treatment modalities in dentistry. Such high success rates have been attributed to the excellent biocompatibility of titanium, which allows for intimate bone interaction at the optical microscopy resolution, regarded as osseointegration.³⁻⁵

Although high survival rates have been reported for endosseous devices, current research has emphasized implant design modification at various length scales (i.e., nanogeometry, microgeometry, and macrogeometry) to improve the early host-implant tissue response.⁶ Such a potential decrease in healing time may result in reduction in treatment time frames through prosthetic restorations that could be placed in occlusal function at early implantation times.⁶⁻⁸

Among implant design modifications attempting to improve the host-implant response, implant surface modifications have been the most investigated.³⁻⁸ The rationale for surface modification lays in the fact that it is the first part of the implant to interact with biofluids, potentially altering the cascade of events that leads to bone healing and intimate apposition with the device.⁹

Several reviews cover the large number of possibilities included in implant

* Department of Biomaterials and Biomimetics, New York University, New York, NY.

† Department of Prosthodontics, University of São Paulo, Bauru School of Dentistry, Bauru, SP, Brazil.

‡ Department of Oral Diagnosis and Surgery, Universidade Estadual Paulista Júlio de Mesquita Filho, Faculdade de Odontologia de Araraquara, Araraquara, SP, Brazil.

§ Department of Dentistry, Universidade Federal de Santa Catarina, Florianópolis, SC, Brazil.

|| Department of Prosthodontics, Tufts University School of Dental Medicine, Boston, MA.

surface modifications, and it is the general consensus that both rough surfaces (over smooth turned surfaces) and surface chemistry (additions of calcium-phosphorus-based bioceramics in various forms over non-coated surfaces) favor the early host-implant response.⁴⁻⁶ From a historical perspective, dental implant surfaces evolved from the as-turned smooth surfaces toward textured rough surfaces, and recent research points toward chemical modification of moderately rough surfaces.^{4-6,10,11}

From a temporal standpoint, both topographic and chemical surface modifications have drawn attention,^{4-6,10,11} because both have shown promising results in *in vitro*¹² and *in vivo* models¹³⁻²⁰ relative to their moderately rough predecessors. Improvements have been achieved by alterations in surface wettability,²¹ impregnation of calcium and phosphorus onto the titanium oxide layer,¹⁸ deposition of discrete bioactive ceramics,^{19,20,22} and through minor incorporation of other chemical elements, such as fluoride.^{11,23} Because changes in surface chemistry typically result in surface texture during processing, controlling such variables to determine their relative effects in healing is a challenging task, and the largest direct comparison between various surfaces in a suitable *in vivo* model is desirable. Thus, the present study biomechanically and histomorphometrically evaluated the effect of various surface modifications in an animal model.

MATERIALS AND METHODS

The implants used in this study were screw-type implants with 3.75 mm of diameter and 8 mm in length provided by the manufacturer.[¶] A total of 75 implants were used and divided into five groups according to surface treatment: 1) alumina-blasted; 2) biologic blasting; 3) plasma; 4) microblasted resorbable blasting media (microblasted RBM); and 5) alumina-blasted/acid-etched (AB/AE). Three implants from each group were used for surface characterization.

Surface Characterization

The surface characterization was accomplished with three different methods ($n = 3$ implants per surface). First, scanning electron microscopy[#] was performed at various magnifications under an acceleration voltage of 15 kV to observe surface topography in the different groups.

The second step was to determine the roughness parameters by optical interferometry^{**} (IFM). Three implants of each surface were evaluated at the flat region of the implant cutting edges (three measurements per implant) and arithmetic mean of the absolute values of the surface height within the sampling area (S_a) and root mean square of the surface departures within the sampling area (S_q) parameters

determined.^{24,25} To separate roughness from waviness and shape for digital three-dimensional measurements, on a micrometer scale, a high-pass gaussian filter of $250 \times 250 \mu\text{m}$ was used. After data normality verification, statistical analysis at 95% level of significance was performed by one-way analysis of variance.

The third procedure was the surface-specific chemical assessment performed by x-ray photoelectron spectroscopy (XPS). The implants were inserted in a vacuum transfer chamber and degassed to 10 to 7 torr. The samples were then transferred under vacuum to the XPS spectrometer.^{††} Survey spectra were obtained using a 165-mm mean radius concentric hemispherical analyzer operated at constant pass energy of 160 eV for survey and 80 eV for high-resolution scans. The take off angle was 90 degrees and a spot size of $150 \times 150 \mu\text{m}$ was used. The implant surfaces were evaluated at various locations (three per implant).

Animal Model and Surgical Procedure

After approval of the Ethics Committee for Animal Research at the Federal University of Santa Catarina, Florianópolis, Brazil, six mongrel dogs were acquired and remained for 2 weeks in the animal facility before the first surgical procedure.

For surgery, three drugs were administered until general anesthesia achievement by intramuscular injection: 1) atropine sulfate (0.044 mg/kg); 2) xilazine chlorate (8 mg/kg); and 3) ketamine chlorate (15 mg/kg). The implantation site was the radius epiphysis, and the right limb of each animal provided implants that remained for 4 weeks *in vivo*, and the left limb provided implants that remained 2 weeks *in vivo*.

For implant placement, the surgical site was shaved with a razor blade and was followed by application of antiseptic iodine solution. An incision of ~5 cm through the skin and periosteum was performed and the periosteum was elevated for bone exposure.

Sequential drills were used following the manufacturer's recommendation under abundant saline irrigation at 1,200 rpm. The implants were placed in an interpolated distribution to minimize bias from different implantation sites (sites 1 to 5 from proximal to distal) along the radial epiphysis for torque and histomorphometric evaluation.

After placement the healing caps were inserted and sutured in layers with vicryl 4-0^{‡‡} for periosteum and nylon 4-0^{§§} for skin was performed. The animals

¶ Ti-6Al-4V, AB-Dental, Nir-galim, Israel.

Philips XL 30, Eindhoven, The Netherlands.

** Phase View 2.5, Palaiseau, France.

†† Kratos Axis 165 multi-technique, Kratos Analytical, Chestnut Ridge, NY.

‡‡ Ethicon Johnson, Miami, FL.

§§ Ethicon Johnson.

stayed in the animal care facility and received antibiotics (benzyl penicillin benzathine, 20,000 IU/kg) and anti-inflammatory (ketoprofen 1% 1 ml/5 kg) medications to control pain and infection. Euthanasia was performed after 4 weeks by anesthesia overdose and the limbs were retrieved by sharp dissection.

For torque testing, the radius was adapted to an electronic torque machine equipped with a 500-Ncm torque load cell.^{||||} Custom machined tooling was adapted to each implant's internal connection and the bone block was carefully positioned to avoid specimen misalignment during testing. The implants were torqued in a counterclockwise direction at a rate of ~0.196 radians per minute until a 10% decrease in maximum value was recorded, and a torque versus displacement curve was recorded for each specimen. The rationale for this procedure was to minimize interface damage before histologic procedures.^{13,14}

The implants in bone were then referred to histomorphometric analysis. The implants in bone were reduced to blocks and then immersed in 10% buffered formalin solution for 24 hours. The blocks were then washed in running water for 24 hours, and gradually dehydrated in a series of alcohol solutions ranging from 70% to 100% ethanol. After dehydration, the samples were embedded in a methacrylate-based resin^{¶¶} according to the manufacturer's instructions. The blocks were then cut into slices (~300 μ m thickness) aiming the center of the implant along its long axis with a precision diamond saw,^{##} glued to acrylic plates with an acrylic-based cement, and a 24-hour setting time was allowed before grinding and polishing. The sections were reduced to a final thickness of ~30 μ m by means of a series of abrasive papers^{***} (400, 600, 800, 1,200, and 2,400) in a grinding/polishing machine^{†††} under water irrigation.²⁶ The sections were then stained with toluidine blue and referred to optical microscopy for histomorphologic evaluation.

The bone-implant contact (BIC) was determined at $\times 50$ to $\times 200$ magnification^{†††} by means of computer software.^{§§§} The regions of BIC along the implant perimeter were subtracted from the total implant perimeter, and calculations were performed to determine the BIC. The bone area fraction occupied (BAFO) between threads in trabecular bone regions was determined at $\times 100$ magnification by means of computer software. The areas occupied by bone were subtracted from the total area between threads, and calculations were performed to determine the BAFO (reported in percentage values of bone area fraction occupied).²⁷

Preliminary statistical analyses showed no effect of implant site (i.e., there were no consistent effects of positions 1 to 5 along the radius) on all measurements. Therefore, site was not considered further in

the analysis. Statistical evaluation of torque to interface fracture, BIC, and BAFO was performed by one-way analysis of variance. Statistical significance was indicated by *P* levels <5%, and post hoc testing used the Fisher LSD test.

[AQ4]

RESULTS

Electron micrographs of all implant surfaces are presented in Figures 1 and 2 and their representative 250 \times 250 μ m IFM three-dimensional reconstructions are shown in Figure 3. Their respective *Sa* and *Sq* values are presented in Figure 4A. The surface texture observed at intermediate and high magnification levels (Figs. 1 and 2) and the IFM reconstruction (Fig. 3) revealed morphologic differences among groups. Although similar morphology was observed for the alumina-blasted, microblasted RBM, and AB/AE surfaces, scanning electron micrographs showed that the biologic-blasting presented rough regions from the grit-blasting procedure along with flat regions with the original as-machined grooves. The plasma group surface morphology presented a rough surface with rounded morphology compared to the other groups (Figs. 1E and 1F). Residual blasting media particles were only observed on the alumina-blasting (Figs. 1A and 1B) and biologic-blasting surfaces (Figs. 1C and 1D).

The IFM measurements presented significant differences for both *Sa* and *Sq* values (Figs. 4A and 4B), where the alumina-blasted surface presented the highest, the biologic-blasting the lowest, and AB/AE the intermediate value. The other surfaces presented intermediate values between the biologic-blasting and AB/AE (non-significant between groups) (Figs. 4A and 4B).

The XPS spectra evaluated the presence of aluminum, phosphorus, calcium, nitrogen, titanium, carbon, V, oxygen, and sodium for the different surfaces (Figs. 4A and 4C). The highest aluminum concentration was observed for the alumina-blasting surface. The highest calcium and phosphorus concentration was observed for the biologic-blasting surface, followed by the microblasted RBM at much lower concentrations and all other surfaces without the presence of these chemical elements. No titanium was detected for the plasma-treated surface, and the second lowest titanium value was observed for the biologic-blasting surface. The highest carbon values were observed for the plasma and alumina-blasting surfaces, and the highest oxygen levels were observed for the plasma,

[AQ5]

|||| Test Resources, Minneapolis, MN.

¶¶ Technovit 9100, Heraeus Kulzer, Wehrheim, Germany.

Isomet 2000, Buehler, Lake Bluff, IL.

*** SiC abrasive papers, Buehler.

††† Metaserv 3000, Buehler.

††† Leica DM2500M, Leica Microsystems, Wetzlar, Germany.

§§§ Leica Application Suite, Leica Microsystems.

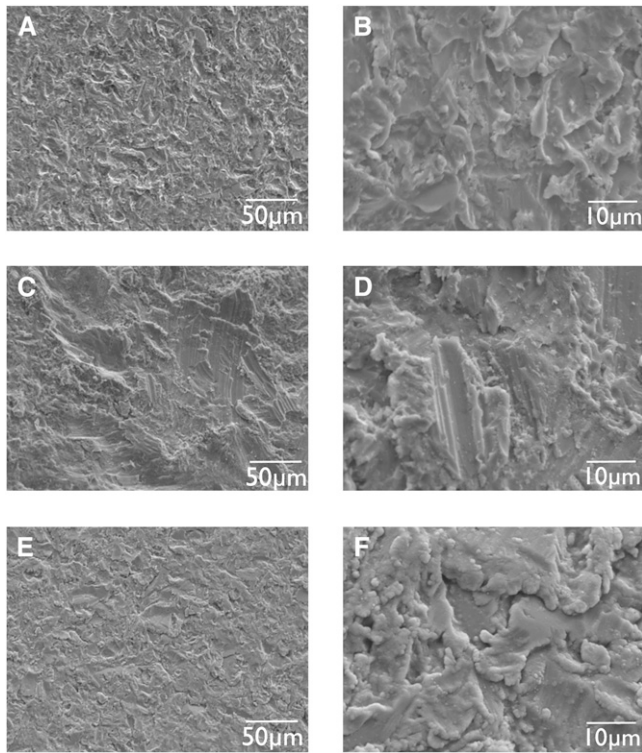


Figure 1.

Scanning electron micrographs of the alumina-blasting (**A** and **B**), biologic-blasting (**C** and **D**), and plasma (**E** and **F**) surfaces.

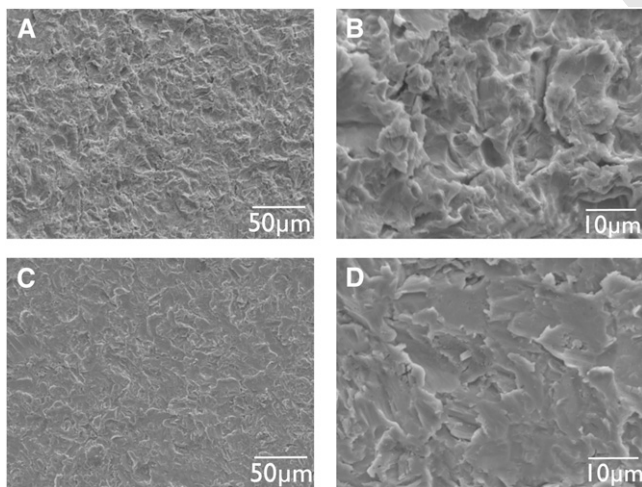


Figure 2.

Scanning electron micrographs of the microblasted RBM (**A** and **B**) and AB/AE (**C** and **D**) surfaces.

microblasted RBM, and AB/AE surfaces (Figs. 4A and 4C).

The animal surgical procedures and follow-up demonstrated no complications regarding procedural conditions, postoperative infection, or other clinical concerns. No implants were excluded from the study

because of clinical instability immediately after euthanization.

The biomechanical testing results showed that significantly higher torque to interface fracture occurred for the microblasted RBM surface relative to others at 2 weeks ($P < 0.04$), but that at 4 weeks no differences were observed between surfaces ($P > 0.74$) (Figs. 5A and 5B).

The non-decalcified sample processing after controlled torque testing showed intimate bone contact with all implant surfaces at regions of cortical and trabecular bone. Higher magnification of the bone-implant interface region showed that the non-decalcified sections obtained after biomechanical testing presented minimal morphologic distortion because of mechanical testing bone disruption (Fig. 6).

Qualitative evaluation of the toluidine blue-stained thin sections revealed no morphologic differences between surfaces at 2 weeks (Figs. 6A through 6C) and 4 weeks (Figs. 6D through 6F) *in vivo*, where intimate contact between cortical (Figs. 6A, 6B, 6D, and 6E) and trabecular (Figs. 6C and 6F) bone was observed. In addition, different healing patterns were observed at different regions along the implant bulk, depending on the interplay between implant geometry and surgical instrumentation dimensions.

At the region of the implant where the inner thread diameter was larger or equal the final surgical drilling dimension allowing intimate contact between implant surface and cortical bone occurred immediately after implantation, substantial bone remodeling in proximity with the implant surface occurred between 2 (Fig. 6A) and 4 (Fig. 6D) weeks *in vivo* for all groups. Although at 2 weeks *in vivo* old bone remodeling was observed along with regions of newly formed woven bone (Fig. 6A), at 4 weeks substantial woven bone was observed in proximity with the implant surface (Fig. 6D).

At regions where a healing chamber was formed because of the formation of a space between the outer diameter of the surgical instrumentation and the inner diameter of the implant thread, woven bone formation was observed throughout the space of the chamber and directly onto the implant surface at 2 weeks *in vivo* (Fig. 6B). At 4 weeks, initial woven bone replacement by lamellar bone was observed throughout the healing chamber (Fig. 6E).

At trabecular bone regions, newly formed woven bone was observed at 2 weeks (Fig. 6C), and initial woven bone replacement by lamellar bone was observed at 4 weeks (Fig. 6F) at regions in proximity with all implant surfaces.

The histomorphometric results demonstrated no significant differences between surfaces for both BIC and BAFO at 2 and 4 weeks *in vivo* (BIC $P > 0.26$ and $P > 0.09$, respectively; BAFO $P > 0.94$ and $P > 0.09$, respectively; Figs. 5C through 5F).

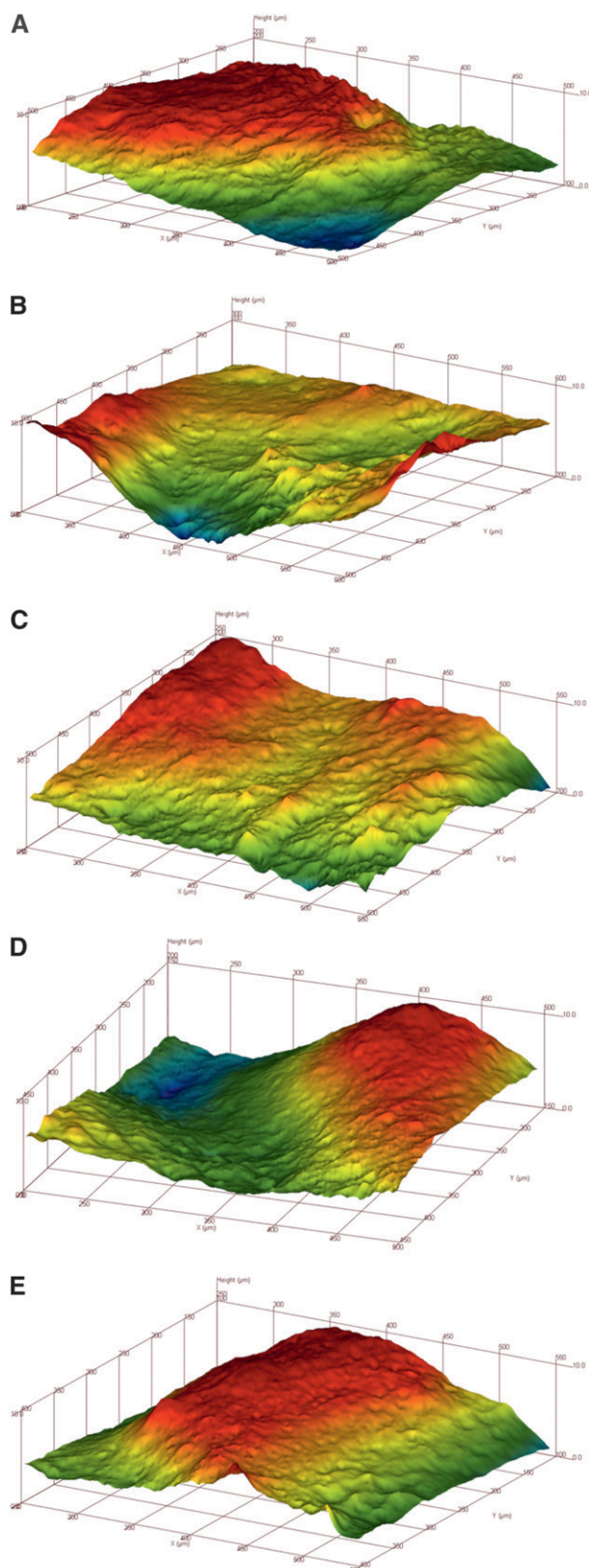


Figure 3. IFM three-dimensional reconstructions of the alumina-blasting (A), biologic-blasting (B), plasma (C), microblasted RBM (D), and AB/AE (E) surfaces.

A	XPS Spectra								IFM	
	Al2p	P2p	Ca2p	N1s	Ti2p	C1s	V2p3	O1s	Na1s	
Alumina Blasted	5.89	-	-	1.12	4.72	52.72	0.12	32.95	0.52	
Biological Blasting	0.55	8.55	12.7	0.37	1.33	38.57	0.06	37.64	0.09	
Plasma	1.49	-	-	0.31	-	48.96	0.03	48.05	0.53	
Microblasted RBM	2.96	2.57	0.67	0.89	7.17	36.59	0.34	47.03	1.43	
AB/AE	1.54	-	-	0.87	8.31	37.48	0.25	49.53	1.03	
									Sa (μm)	Sq (μm)
									2.66 (0.42)	3.41 (0.38)
									0.92 (0.38)	1.17 (0.47)
									1.13 (0.40)	1.50 (0.51)
									1.53 (0.51)	1.80 (0.60)
									1.88 (0.49)	2.29 (0.60)

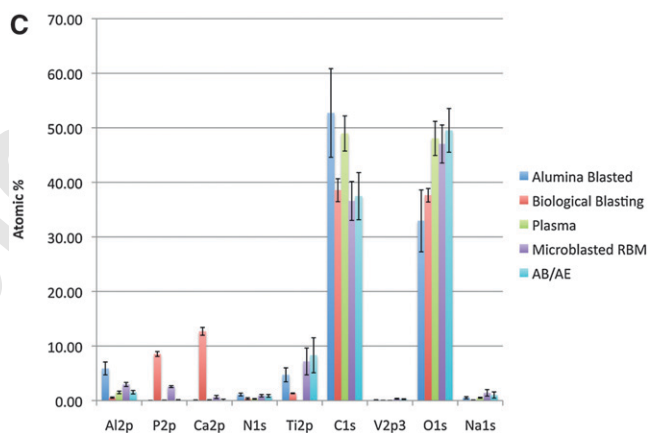
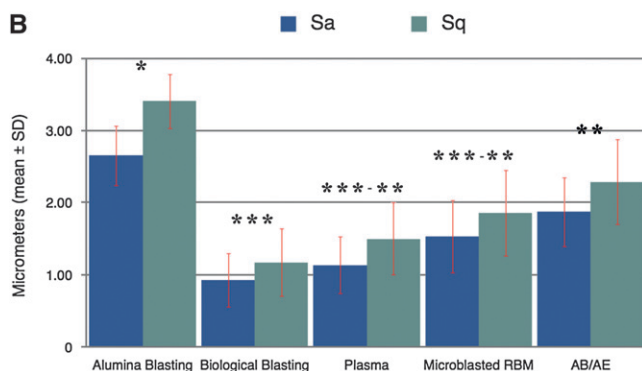


Figure 4.

(A) Average chemical composition for the different surfaces as observed in the XPS spectra and the statistics summary for the Sa and Sq values (mean ± SD). (B) Roughness parameters Sa and Sq (mean ± SD) for the different surfaces. The number of asterisks denotes statistically homogeneous groups. (C) Surface atomic compositions for the different implant surfaces (mean ± SD).

DISCUSSION

Implant surfaces have evolved from the smooth as-machined (as-turned) surfaces toward the now considered standard rough surfaces fabricated by a variety of methods, which include all those used to fabricate the different surfaces evaluated in the present study.⁶ Compared to published data, the obtained surface roughness values in the present study were higher because of the larger filter size used during IFM measurements (the smaller the filter, the lower the Sa and Sq values obtained²⁸). Nonetheless, the relative differences among groups are in agreement with previously published work.^{4,5} Although

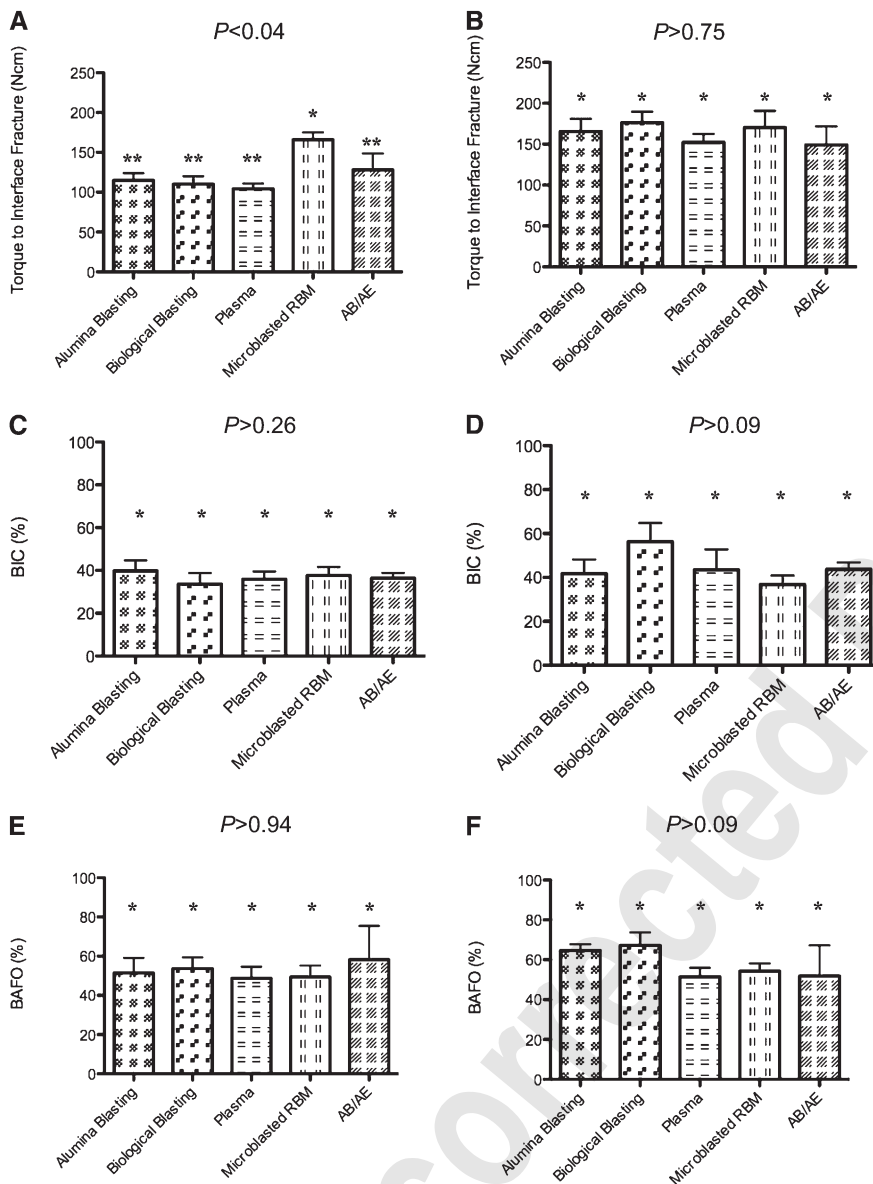


Figure 5.

Torque-interface fracture statistics summary (mean \pm 95% confidence interval [CI]) for the different surfaces at (A) 2 weeks and (B) 4 weeks in vivo. BIC statistics summary (mean \pm 95% CI) for the different surfaces at (C) 2 weeks and (D) 4 weeks in vivo. BAFO statistics summary (mean \pm 95% CI) for the different surfaces at (E) 2 weeks and (F) 4 weeks in vivo. The number of asterisks denotes statistically homogeneous groups.

the alumina-blasting group presented a textured surface along with blasting media particles embedded on the surface, the AB/AE surface presented a reduced surface roughness without evidence of particle embedding in the surface, demonstrating the effectiveness of acid-etching on further cleaning the surface after blasting procedures.

Specific to the incorporation of calcium- and phosphorus-based bioactive ceramics, although both the biologic-blasting and microblasted RBM surfaces were blasted with resorbable blasting media, the

blasting machinery and subsequent surface cleaning differences resulted in different textures and chemistries. First, because of the lower hardness of RBM compared to alumina, lower degrees of roughness were observed compared to both alumina-blasting and AB/AE samples. Second, observation of the electron micrographs for the biologic-blasting and microblasted RBM revealed more consistent spatial distribution of texture for the microblasted RBM surface, which unlike the biologic-blasting group did not show regions where machining grooves were apparent between textured regions. Third, different post-blasting procedures resulted in calcium-phosphorus particles throughout the biologic blasting surface and high degrees of calcium and phosphorus on its surface chemistry spectrum, and chemical impregnation¹⁰ of calcium and phosphorus elements on the microblasted RBM surface.

Although no detail was provided regarding the plasma source composition and temperature for the plasma group, it is apparent from the electron micrographs that the surface was previously blasted and that the texture was affected by the plasma processing. Such statements can be rationalized because rounded structures were observed in the plasma group compared to sharp defined peaks and valleys observed in all other groups. In addition, a substantial chemical shift was achieved by such a method, where titanium was not detected

along with increased carbon and oxygen in the surface composition. This chemical shift may have originated from a substantial increase in the surface oxide layer, or possibly by a high surface energy characteristic that may have readily adsorbed carbon-based species from the atmosphere during sample preparation.

The torque-interface fracture results showed high biomechanical fixation values for all implant surfaces at 2 weeks (significantly higher for the microblasted RBM compared to other surfaces), and a

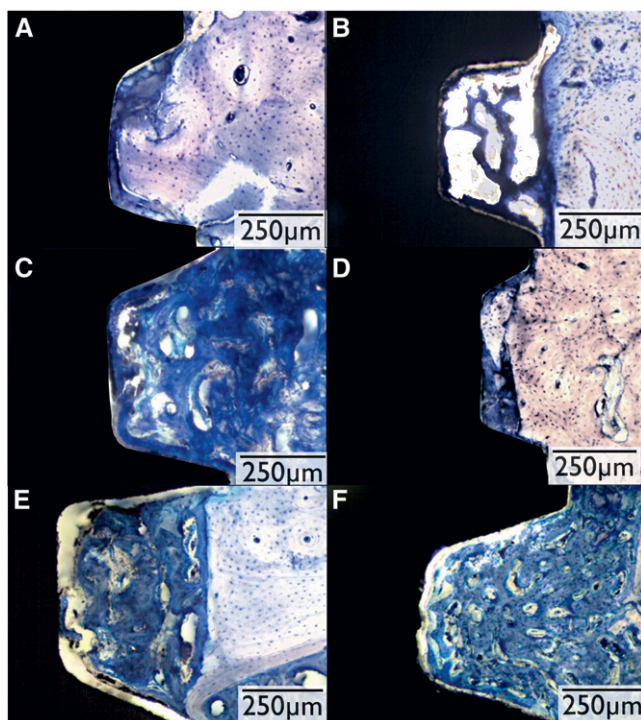


Figure 6.

Representative histologic section for all groups at 2 and 4 weeks in vivo: (A and D, respectively) at a region where intimate contact between implant surface and cortical bone occurred immediately after placement, (B and E, respectively) region where healing chamber formation occurred between implant thread and cortical bone, and (C and F, respectively) trabecular bone region.

general increase for all groups at 4 weeks (no significant differences among groups). Such result at 2 weeks showed that the microblasted RBM surface roughness and chemistry combination favored the early host-implant response, and that shortly after this observation period, no difference was evident because of the osseoconductive and biocompatible properties of other surfaces. The low degree of mechanical disruption between bone and implant observed in the histology slides after mechanical testing was likely caused by the proper specimen alignment and the slow controlled torque rate. Thus, mechanical disruption was observed only in a few histologic sections and did not compromise the histomorphologic and histomorphometric evaluations.^{13,14,17}

In general, results from the histologic sections showed that all of the surfaces investigated were biocompatible and osseoconductive, presenting bone in close contact with the implant surface at regions of cortical and trabecular bone. From a morphologic standpoint no differences were observed between all surfaces investigated. Woven bone was observed around all surfaces at 2 weeks, and initial replacement of woven bone by lamellar bone was observed

for all surfaces at 4 weeks. No detrimental effect caused by blasting media particle presence on the surface was observed for the alumina-blasting and microblasted RBM groups at both implantation times.

Specific to different regions of the implant and its relationship with the surgical drilling dimensions, different healing patterns were observed throughout the implant length. At regions where intimate contact between cortical bone and implant surface existed immediately after placement, an appositional bone healing was observed.^{16,27,29} Such healing pattern comprises interfacial remodeling with subsequent woven bone apposition in close contact with the implant surface,^{16,27,29} as observed sequentially for all groups at 2 and 4 weeks. This type of configuration typically results in high degrees of implant primary stability.²⁷

However, when the interplay between implant geometry and surgical drilling dimensions resulted in healing chamber formation, an intramembranous-like healing pattern was observed.^{16,27,29} Healing chambers have been previously shown to be rapidly filled with woven bone throughout the volume occupied by the blood clot immediately after placement for osseointegration achievement.^{16,17,27,29,30} In agreement with previous studies, the present results showed that in regions where healing chambers formed between implant and cortical bone, rapid woven bone filling occurred before or at 2 weeks, and initial remodeling comprising initial woven bone replacement by lamellar bone was observed by 4 weeks implantation time. The same morphologic evolution trend was observed at regions of trabecular bone.³¹

Although no significant differences were observed for both BIC and BAFO, a general increase was observed from 2 to 4 weeks in vivo, revealing that the time frames investigated in the present study were within the dynamic healing phases that occur at early implantation times. Within groups, the highest increase in BIC and BAFO values over time was observed for the biologic-blasting group, which at 4 weeks presented the highest mean values for BIC and BAFO among all surfaces evaluated. This observation was likely caused by the effect of higher amounts of calcium and phosphorus elements on the surface relative to the other groups, suggesting that their presence resulted in alteration in bone healing dynamics after implantation.^{17-20,32}

CONCLUSIONS

The association of the implant macrogeometry and associated surgical technique with five different osseoconductive surfaces resulted in high degrees of osseointegration and biomechanical fixation. Although insight can be provided by evaluating five surfaces with distinct texture and chemistry, pinpointing

which of the surface parameters accounted for the differences in biomechanical and histomorphometric results is not possible, and experimental studies controlling these variables are warranted.

ACKNOWLEDGMENT

The authors report no conflicts of interest related to this study.

REFERENCES

1. Chuang SK, Tian L, Wei LJ, Dodson TB. Predicting dental implant survival by use of the marginal approach of the semi-parametric survival methods for clustered observations. *J Dent Res* 2002;81:851-855.
2. Chuang SK, Wei LJ, Douglass CW, Dodson TB. Risk factors for dental implant failure: A strategy for the analysis of clustered failure-time observations. *J Dent Res* 2002;81:572-577.
3. Albrektsson T, Gottlow J, Meirelles L, Ostman PO, Rocci A, Sennerby L. Survival of NobelDirect implants: An analysis of 550 consecutively placed implants at 18 different clinical centers. *Clin Implant Dent Relat Res* 2007;9:65-70.
4. Albrektsson T, Wennerberg A. Oral implant surfaces: Part 1 — Review focusing on topographic and chemical properties of different surfaces and in vivo responses to them. *Int J Prosthodont* 2004;17:536-543.
5. Albrektsson T, Wennerberg A. Oral implant surfaces: Part 2 — Review focusing on clinical knowledge of different surfaces. *Int J Prosthodont* 2004;17:544-564.
6. Coelho PG, Granjeiro JM, Romanos GE, et al. Basic research methods and current trends of dental implant surfaces. *J Biomed Mater Res B Appl Biomater* 2009; 88:579-596.
7. Jimbo R, Ono D, Hirakawa Y, Odatsu T, Tanaka T, Sawase T. Accelerated photo-induced hydrophilicity promotes osseointegration: An animal study. *Clin Implant Dent Relat Res* 2009; in press.
8. Jimbo R, Sawase T, Baba K, Kurogi T, Shibata Y, Atsuta M. Enhanced initial cell responses to chemically modified anodized titanium. *Clin Implant Dent Relat Res* 2008;10:55-61.
9. Jimbo R, Sawase T, Shibata Y, et al. Enhanced osseointegration by the chemotactic activity of plasma fibronectin for cellular fibronectin positive cells. *Biomaterials* 2007;28:3469-3477.
10. Dohan Ehrenfest DM, Coelho PG, Kang BS, Sul YT, Albrektsson T. Classification of osseointegrated implant surfaces: Materials, chemistry and topography. *Trends Biotechnol* 2010;28:198-206.
11. Kang BS, Sul YT, Oh SJ, Lee HJ, Albrektsson T. XPS, AES and SEM analysis of recent dental implants. *Acta Biomater* 2009;5:2222-2229.
12. Moura CC, Souza MA, Dechichi P, Zanetta-Barbosa D, Teixeira CC, Coelho PG. The effect of a nanothickness coating on rough titanium substrate in the osteogenic properties of human bone cells. *J Biomed Mater Res A* 2010;94:103-111.
13. Coelho PG, Cardaropoli G, Suzuki M, Lemons JE. Early healing of nanothickness bioceramic coatings on dental implants. An experimental study in dogs. *J Biomed Mater Res B Appl Biomater* 2009;88:387-393.
14. Coelho PG, Lemons JE. Physico/chemical characterization and in vivo evaluation of nanothickness bioceramic depositions on alumina-blasted/acid-etched Ti-6Al-4V implant surfaces. *J Biomed Mater Res A* 2009;90:351-361.
15. Coelho PG, Marin C, Granato R, Suzuki M. Histomorphologic analysis of 30 plateau root form implants retrieved after 8 to 13 years in function. A human retrieval study. *J Biomed Mater Res B Appl Biomater* 2009;91:975-979.
16. Coelho PG, Suzuki M, Guimaraes MV, et al. Early bone healing around different implant bulk designs and surgical techniques: A study in dogs. *Clin Implant Dent Relat Res* 2010;12:202-208.
17. Granato R, Marin C, Suzuki M, Gil JN, Janal MN, Coelho PG. Biomechanical and histomorphometric evaluation of a thin ion beam bioceramic deposition on plateau root form implants: An experimental study in dogs. *J Biomed Mater Res B Appl Biomater* 2009; 90:396-403.
18. Marin C, Granato R, Suzuki M, Gil JN, Piattelli A, Coelho PG. Removal torque and histomorphometric evaluation of bioceramic grit-blasted/acid-etched and dual acid-etched implant surfaces: An experimental study in dogs. *J Periodontol* 2008;79:1942-1949.
19. Mendes VC, Moineddin R, Davies JE. The effect of discrete calcium phosphate nanocrystals on bone-bonding to titanium surfaces. *Biomaterials* 2007;28: 4748-4755.
20. Mendes VC, Moineddin R, Davies JE. Discrete calcium phosphate nanocrystalline deposition enhances osteoconduction on titanium-based implant surfaces. *J Biomed Mater Res A* 2009;90:577-585.
21. Buser D, Broggini N, Wieland M, et al. Enhanced bone apposition to a chemically modified SLA titanium surface. *J Dent Res* 2004;83:529-533.
22. Orsini G, Piattelli M, Scarano A, et al. Randomized, controlled histologic and histomorphometric evaluation of implants with nanometer-scale calcium phosphate added to the dual acid-etched surface in the human posterior maxilla. *J Periodontol* 2007;78:209-218.
23. Mendonça G, Mendonça DB, Aragão FJ, Cooper LF. Advancing dental implant surface technology — From micron- to nanotopography. *Biomaterials* 2008;29:3822-3835.
24. Leach R. Surface topography characterisation. In: [AQ6] *Fundamental Principles of Engineering Nanometrology*. William Andrew; 2009:211-258.
25. Stout K, Sullivan P, Dong W, et al. [AQ7] *Development of Methods for the Characterisation of Roughness in Three Dimensions*. Penton Press; 2000.
26. Donath K, Breuner G. A method for the study of undecalcified bones and teeth with attached soft tissues. The Säge-Schliff (sawing and grinding) technique. *J Oral Pathol* 1982;11:318-326.
27. Leonard G, Coelho P, Polyzos I, Stassen L, Claffey N. A study of the bone healing kinetics of plateau versus screw root design titanium dental implants. *Clin Oral Implants Res* 2009;20:232-239.
28. Wennerberg A, Albrektsson T. Suggested guidelines for the topographic evaluation of implant surfaces. *Int J Oral Maxillofac Implants* 2000;15:331-344.
29. Berglundh T, Abrahamsson I, Lang NP, Lindhe J. De novo alveolar bone formation adjacent to endosseous implants. *Clin Oral Implants Res* 2003;14: 251-262.

30. Coelho PG, Granato R, Marin C, Bonfante EA, Janal MN, Suzuki M. Biomechanical and bone histomorphologic evaluation of four surfaces on plateau root form implants: An experimental study in dogs. *Oral Surg Oral Med Oral Pathol Oral Radiol Endod* 2010;109:e39-e45.
31. Quaranta A, Iezzi G, Scarano A, et al. A histomorphometric study of nanothickness and plasma-sprayed calcium-phosphorous-coated implant surfaces in rabbit bone. *J Periodontol* 2010;81:556-561.
32. Meirelles L, Melin L, Peltola T, et al. Effect of hydroxyapatite and titania nanostructures on early in vivo bone response. *Clin Implant Dent Relat Res* 2008;10:245-254.

Correspondence: Dr. Estevam A. Bonfante, Al. Octávio Pinheiro Brisola, 9-75, Bauru 17012-901, SP, Brazil. Fax: 55-14-32342566; e-mail: estevamab@gmail.com.

Submitted August 21, 2010; accepted for publication September 29, 2010.

Uncorrected Proof

Published in The journal of biomedical
materials research B: applied biomaterials,
August 2012 volume 100b, issue 6

**Journal of
Biomedical Materials Research**
PART B

08

Characterization and in vivo evaluation of laser sintered dental endosseous implants in dogs

Lukasz Witek, Charles Marin, Rodrigo Granato,
Estevam A. Bonfante, Felipe Campos, Julio
Bisinotto, Marcelo Suzuki, Paulo G. Coelho



Superior Implant Technology

Characterization and *in vivo* evaluation of laser sintered dental endosseous implants in dogs

Lukasz Witek,¹ Charles Marin,² Rodrigo Granato,² Estevam A. Bonfante,² Felipe Campos,³ Julio Bisinotto,³ Marcelo Suzuki,⁴ Paulo G. Coelho^{1,5}

¹Department of Biomaterials and Biomimetics, New York University, New York, New York

²Postgraduate Program in Dentistry, UNIGRANRIO University - School of Health Sciences, Duque de Caxias, RJ, Brazil

³Department of Oral and Maxillofacial Surgery, Universidade Federal de Uberlândia, Uberlândia, MG, Brazil

⁴Department of Prosthodontics, Tufts University School of Dental Medicine, Boston, Massachusetts

⁵Department of Periodontology and Implant Dentistry, Director for Research, New York University College of Dentistry, New York, New York

Received 28 October 2011; revised 25 March 2012; accepted 31 March 2012

Published online 12 June 2012 in Wiley Online Library (wileyonlinelibrary.com). DOI: 10.1002/jbm.b.32725

Abstract: Laser metal sintering has shown promising results, but no comparison with other commercially available surface has been performed. This study sought to evaluate the biomechanical and histological early bone response to laser sintered implants relative to alumina-blasted/acid-etched (AB/AE). Surface topography was characterized by scanning electron microscopy and optical interferometry. Surface chemistry was assessed by x-ray photoelectron spectroscopy. Beagle dogs ($n = 18$) received 4 Ti-6Al-4V implants (one per surface) in each radius, remaining for 1, 3, and 6 weeks ($n = 6$ dogs per evaluation time) *in vivo*. Bone-to-implant contact (BIC) and bone area fraction occupancy (BAFO) were evaluated. Biomechanical evaluation comprised torque-to-interface failure. The laser sintered surface presented higher S_a and S_q than AB/AE. Chemistry

assessment showed the alloy metallic components along with adsorbed carbon species. Significantly higher torque was observed at 1 ($p < 0.02$) and 6 week ($p < 0.02$) for the laser sintered, whereas at 3 week no significant differences were observed. Significantly higher BIC and BAFO was observed for the Laser Sintered ($p < 0.04$, and $p < 0.03$, respectively) only at 1 week, whereas no significant differences were observed at 3 and 6 weeks. The laser sintered implants presented biocompatible and osseointegrative properties and improved biomechanical response compared with the AB/AE surface only at 1 and 6 weeks *in vivo*. © 2012 Wiley Periodicals, Inc. *J Biomed Mater Res Part B: Appl Biomater* 100B: 1566–1573, 2012.

Key Words: dental implant, biomechanical, laser, histology

How to cite this article: Witek L, Marin C, Granato R, Bonfante EA, Campos F, Bisinotto J, Suzuki M, Coelho PG. 2012. Characterization and *in vivo* evaluation of laser sintered dental endosseous implants in dogs. *J Biomed Mater Res Part B* 2012;100B:1566–1573.

INTRODUCTION

Research trends have emphasized toward implant design modifications capable of improving the early host implant tissue response¹ and therefore hastening healing time. The main benefit would be the potential reduction in treatment time frames through prosthetic restorations that could be placed in occlusal function earlier than originally recommended protocols.^{1–3}

Among implant design modifications attempting to improve the host-to-implant response, implant surface modifications have been extensively investigated.^{1–6} The rationale for surface modification lies upon the fact that it is the first part of the implant to interact with biofluids, which potentially alters the cascade of events that leads to bone healing and intimate apposition with the device.⁷ Several reviews cover the large number of possibilities included in implant surface modifications, and it is a general consensus that both rough surfaces (over smooth turned surfaces) and

surface chemistry (additions of Ca-P-based bioceramics in various forms over noncoated surfaces) may favor the early host-to-implant response.^{1,5,6,8}

Whereas implant surface texturing is usually accomplished after the implant device is milled to its desired stock shape, surface roughness may be tailored by its fabrication method such as in laser metal sintering.⁹ The process is based on rapid prototyping, where the constructed CAD file is built by a metal forming procedure with a high-power laser beam focused on a metal powder bed and programmed to fuse particles creating a thin metal layer. The process continues until the apposition of layers results in the final shape of the 3D projected device.^{10,11} The resulting surface is porous with functionally graded structures where a gradient of porosity is observed perpendicular to the long axis, high porosity at the surface and the constituting core material that may be selected to suit the device's intended use. In addition, a repeated porous pattern with

Correspondence to: E. A. Bonfante; e-mail: estevamab@gmail.com

interconnected pore network has been described after the laser sintering process,¹² potentially improving osseointegration.¹³ Since the graded structure decreases the discrepancy between the elastic modulus of titanium and that of surrounding bone, a desirable reduction in the interface stress has also been claimed.¹¹

The laser sintering process has a wide range of applications for producing temporary or permanent implantable devices, especially when a design is needed to provide an implant's proper structural and biological function.¹⁴ Although the existing *in vitro*¹² and *in vivo* data^{9,15} on laser metal sintering shows promising results, qualitative and quantitative histological comparisons with other commercially available implant surfaces along with biomechanical testing is yet to be understood. Thus, the present study biomechanically (torque-to-interface failure) and histomorphometrically evaluated the effect of laser sintering compared to alumina-blasted/acid-etched implant (AB/AE) surface modifications in the early bone response in a beagle model. We have hypothesized that the intricate surface topography resulting from laser sintering would improve early biomechanical and histomorphometric parameters compared with an AB/AE implant surface.

MATERIALS AND METHODS

The implants used in this study were Ti-6Al-4V screw type implants with 3.75 mm of diameter and 10 mm in length provided by the manufacturer (AB-Dental, Nir Galim, Israel). A total of 86 implants were used and divided in two groups according to surface treatment: Laser Sintered (experimental) and Alumina-Blasted/Acid-Etched (AB/AE) (control) ($n = 38$ per group). The remaining implants ($n = 10$) were used for surface characterization. Specific detail regarding the processing parameters of the surfaces was not provided from the manufacturer. It has been suggested that while high throughput fabrication may be achieved, all dimensional tolerances must be observed during the post fabrication steps, as well as the potential void inclusion during the sintering process.¹¹

Surface characterization

The surface characterization was accomplished utilizing three different methods. First, scanning electron microscopy (SEM) (Philips XL 30, Eindhoven, The Netherlands) was performed at various magnifications under an acceleration voltage of 15 kV to observe the different groups' surface topography ($n = 1$ per group).

The second step was to determine the roughness parameters by optical interferometry (IFM) (Phase View 2.5, Palaiseau, France). Three implants of each surface were evaluated at the flat region of the implant cutting edges (three measurements per implant) and S_a (arithmetic average high deviation) and S_q (root mean square) parameters determined. A filter size of $250 \times 250 \mu\text{m}^2$ was utilized. Following data normality verification, statistical analysis at 95% level of significance was performed by one-way ANOVA.

The third procedure was the surface specific chemical assessment performed by x-ray photoelectron spectroscopy

(XPS). The implants were inserted in a vacuum transfer chamber and degassed to 10^{-7} torr. The samples were then transferred under vacuum to a Kratos Axis 165 multitechnique XPS spectrometer (Kratos Analytical, Chestnut Ridge, NY). Survey spectra were obtained using a 165 mm mean radius concentric hemispherical analyzer operated at constant pass energy of 160 eV for survey and 80 eV for high resolution scans. The take off angle was 90° and a spot size of $150 \times 150 \mu\text{m}^2$ was used. The implant surfaces were evaluated at various locations (three per implant).

In vivo model and surgical procedure

The *in vivo* study comprised of 18 adult male beagles of ~ 1.5 years old. The study was approved by the Ethics Committee for Animal Research at the École Nationale Vétérinaire d'Alfort (Maisons-Alfort, Val-de-Marne, France). The beagles remained in the facility for 2 weeks prior to the surgical procedures.

For surgery, three drugs were administered until general anesthesia achievement by intramuscular injection. The drugs were atropine sulfate (0.044 mg/kg), xylazine chlorate (8 mg/kg), and ketamine chlorate (15 mg/kg). The implantation site was the radius epiphysis. Batches of six beagles were utilized for each evaluation time *in vivo*, where each animal received one implant of each group in each radii (one limb provided sample for biomechanical testing and the other for histologic evaluation).

For implant placement, the surgical site was shaved with a razor blade followed by application of antiseptic iodine solution. An incision of ~ 5 cm through the skin and periosteum was performed and the periosteum was elevated for bone exposure.

Sequential drills were utilized following the manufacturer's recommendation at 1200 rpm under abundant saline irrigation. The different implant groups were alternately placed from proximal to distal at distances of 1 cm from each other along the central region of the bone. The starting implant surface was also alternated between dogs to minimize bias in the torque and histomorphometric evaluation.

After placement the healing caps were inserted and sutured in layers with vicryl 4-0 (Ethicon Johnson, Miami, FL) for periosteum and nylon 4-0 (Ethicon Johnson, Miami, FL) for skin. The dogs stayed in animal care facility and received antibiotic (Benzyl Penicilin Benzatine 20.000 UI/Kg) and anti-inflammatory (Ketoprofen 1% 1 mL/5 kg) medication to control the pain and infection. Euthanasia was performed after 1, 3, and 6 weeks by anesthesia overdose and the limbs were retrieved by sharp dissection.

Torque testing was performed immediately after euthanasia. The radius was adapted to an electronic torque machine equipped with a 500 Ncm torque load cell (Test Resources, Shakopee, MN). Custom machined tooling was adapted to each implant's internal connection and the bone block was carefully positioned to avoid specimen misalignment during testing. The implants were torqued in counter clockwise direction at a rate of ~ 0.196 radians/min and a torque versus displacement curve was recorded for each specimen.

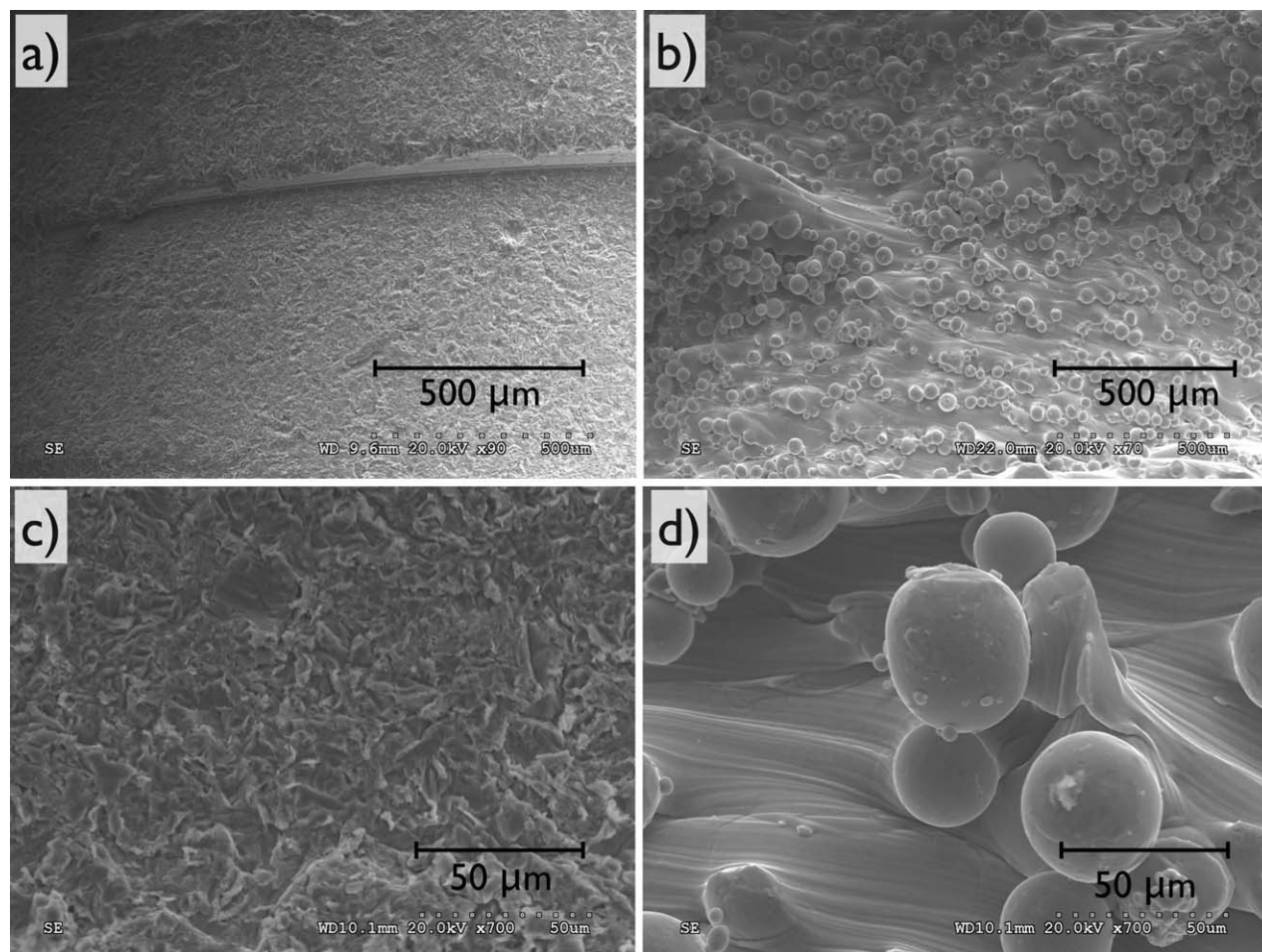


FIGURE 1. SEM of Alumina-Blasted/Acid-Etched (a and c) and Laser Sintered (b and d) presented different surface roughness morphology, which can be seen at low and high magnification.

Histomorphometric analysis

The implants in bone were reduced to blocks and immersed in 10% buffered formalin solution for 24 h. The blocks were then washed in running water for 24 h, and gradually dehydrated in a series of alcohol solutions ranging from 70 to 100% ethanol. Following dehydration, the samples were embedded in a methacrylate-based resin (Technovit 9100, Heraeus Kulzer GmbH, Wehrheim, Germany) according to the manufacturer's instructions. The blocks were then cut into slices ($\sim 300\ \mu\text{m}$ thickness) aiming the center of the implant along its long axis with a precision diamond saw (Isomet 2000, Buehler, Lake Bluff), glued to acrylic plates with an acrylate-based cement, and a 24 h setting time was allowed prior to grinding and polishing. The sections were then reduced to a final thickness of $\sim 30\ \mu\text{m}$ by means of a series of SiC abrasive papers (400, 600, 800, 1200, and 2400) (Buehler, Lake Bluff, IL) in a grinding/polishing machine (Metaserv 3000, Buehler, Lake Bluff, IL) under water irrigation.¹⁶ The sections were then toluidine blue stained and referred to optical microscopy for histomorphologic evaluation.

The bone-to-implant contact (BIC) was determined at $50\times$ to $200\times$ magnification (Leica DM2500M, Leica

Microsystems GmbH, Wetzlar, Germany) by means of a computer software (Leica Application Suite, Leica Microsystems GmbH, Wetzlar, Germany). The regions of bone-to-implant contact along the implant perimeter were subtracted from the total implant perimeter, and calculations were performed to determine the BIC. The bone area fraction occupied (BAFO) between threads in trabecular bone regions was determined at $100\times$ magnification (Leica DM2500M, Leica Microsystems GmbH, Wetzlar, Germany) by means of computer software (Leica Application Suite, Leica Microsystems GmbH, Wetzlar, Germany). The areas occupied by bone were subtracted from the total area between threads, and calculations were performed to determine the BAFO (reported in percentage values of bone area fraction occupied).¹⁷

Preliminary statistical analyses showed no effect of implant site (i.e., there were no consistent effects of positions 1 and 2 along the radius) on all measurements. Therefore, site was not considered further in the analysis. Statistical evaluation of torque, BIC, and BAFO was performed by Friedman's test. Statistical significance was indicated by *p*-levels less than 5%.

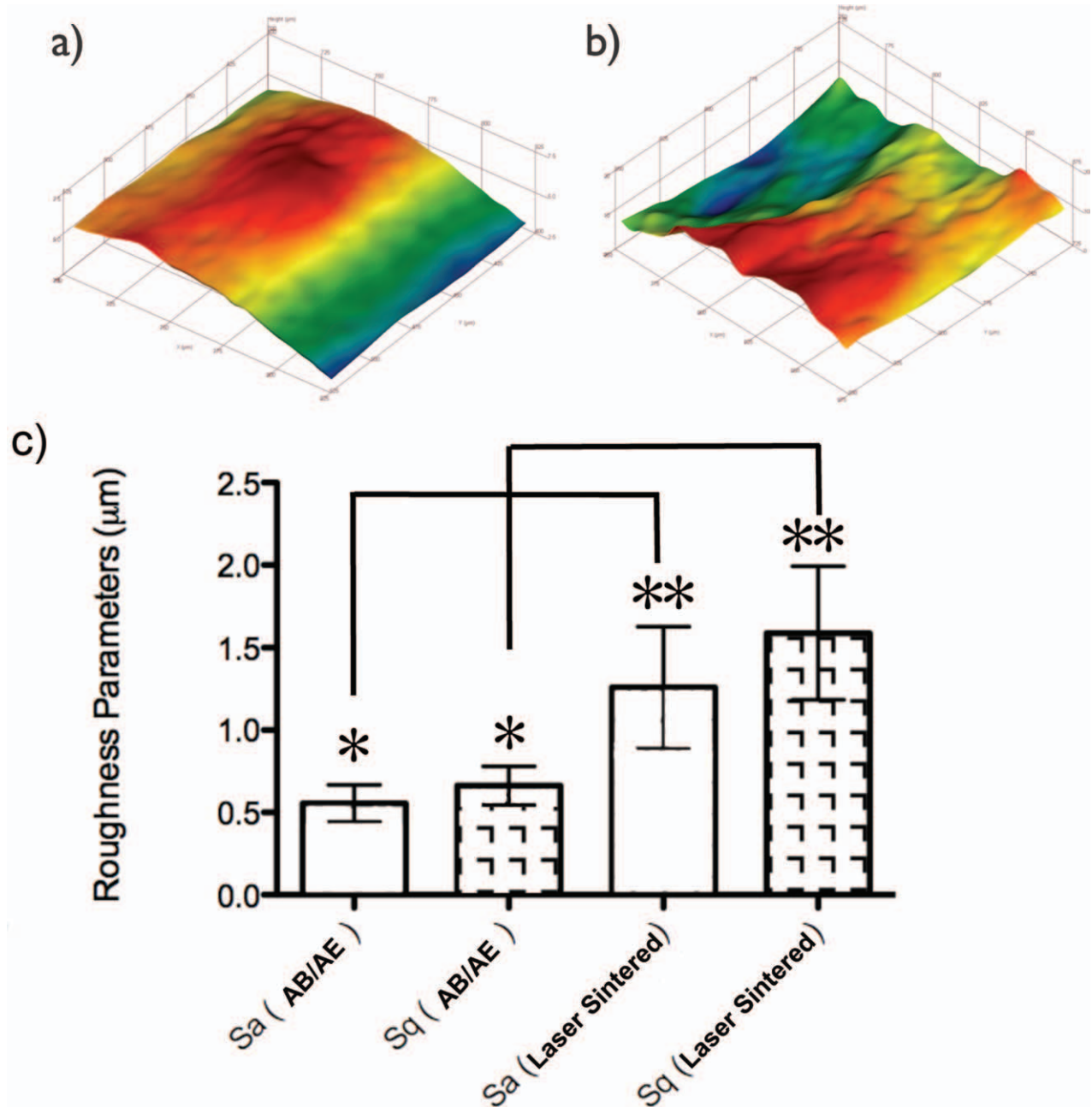


FIGURE 2. (a, b) Representative IFM reconstruction (filter size of $250 \times 250 \mu\text{m}^2$) of the AB/AE and laser sintered implants, respectively, (c) Bar graph (mean 95% CI) representing the surface roughness parameters, S_a and S_q also illustrating a significant difference, $p < 0.02$ (asterisks represent statistically homogenous groups. [Color figure can be viewed in the online issue, which is available at wileyonlinelibrary.com.]

RESULTS

Surface characterization

Implant surfaces' electron micrographs are presented in Figure 1 and their representative $250 \mu\text{m} \times 250 \mu\text{m}$ IFM

three-dimensional reconstructions, in Figure 2(A,B). Their respective S_a and S_q values are presented in Figure 2(C,D). The surface texture observed at intermediate and high magnification levels (Figure 1), as well as the IFM

TABLE I. X-Ray Photoelectron Spectroscopy Atomic Percentages for the AB/AE and Laser Sintered Implants

	Al2p	C1s	O1s	Ti2p	V2p3
AB/AE	3.43 (1.2)	31.82 (4.2)	45.3 (3.3)	13.21 (2.2)	0.43 (0.15)
Laser sintered	2.88 (0.9)	42.1 (3.8)	35.09 (2.8)	10.64 (3.2)	0.21 (0.11)

Mean (\pm SD).

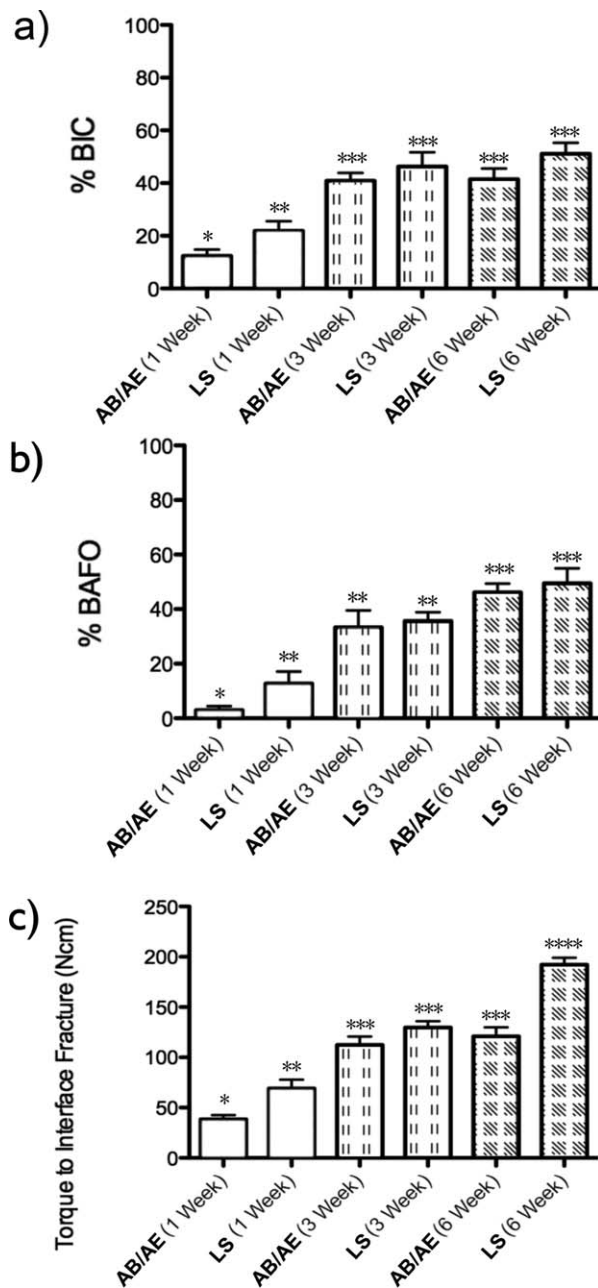


FIGURE 3. (a) Bone-to-implant contact ($p < 0.02$), (b) Bone area fraction occupancy ($p < 0.02$), and (c) Torque to interface failure ($p < 0.01$) statistics summary (mean \pm 95% CI) for the different implants and times *in vivo* (asterisks represent statically homogenous groups).

reconstruction [Figure 2(A,B)] revealed morphologic differences between the two groups. The IFM measurements presented significant differences for both S_a and S_q values [Figure 2(C)], where the experimental (laser sintered) implant presented the higher values. Mean S_a and S_q values were $0.56 \mu\text{m}$ ($0.11 \mu\text{m}$, 95% CI) and $0.66 \mu\text{m}$ ($0.11 \mu\text{m}$, 95% CI) for AB/AE and $1.26 \mu\text{m}$ and $1.59 \mu\text{m}$ for Laser Sintered, respectively ($0.35 \mu\text{m}$ and $0.38 \mu\text{m}$, 95% CI).

The XPS spectra demonstrated the presence of Al, C, O, Ti, and V for the different surfaces (Table I). The highest aluminum concentration was observed for the AB/AE likely

due to the alumina blasting procedure. Higher O, Ti, and V concentrations were observed for the AB/AE surface. Conversely, higher C values were detected for the experimental (laser sintered) surface (Table I).

***In vivo* model**

The animal surgical procedures and follow-up demonstrated no complications regarding procedural conditions, postoperative infection, or other clinical concerns. No implants were excluded from the study due to clinical instability immediately after the euthanization.

The biomechanical testing showed that significantly higher torque to interface fracture was observed for the experimental surface relative to control at 1 week ($p = 0.011$), but that at 3 weeks no differences were observed between surfaces ($p = 0.129$). At 6 weeks, a significantly higher removal torque ($p < 0.002$) was observed for the experimental surface in comparison to the control (Figure 3).

The nondecalcified sample processing showed intimate bone contact with all implant surfaces at regions of cortical and trabecular bone (Figure 4). Qualitative evaluation of the toluidine blue stained thin sections revealed no morphologic differences between surfaces at 1 and 3 weeks *in vivo*, where intimate contact between cortical and trabecular bone was observed. In addition, different healing patterns were observed at specific regions along the implant bulk, depending on the interplay between device geometry and surgical instrumentation dimensions (Figure 4).

At the region of the implant where the inner thread diameter was larger or equal the final surgical drilling dimension allowing intimate contact between implant surface and cortical bone immediately after implantation, substantial bone remodeling in proximity with the implant surface occurred between 1 [Figure 4(A,D)] and 3 [Figure 4(B,E)] weeks *in vivo* for all groups. While at 1 week *in vivo* old bone remodeling was observed along with regions of newly formed woven bone [Figure 4(A,D)], at 3 weeks substantial woven bone was observed in proximity with the implant surface [Figure 4(B,E)].

At regions where a healing chamber was formed due to the formation of a space between the outer diameter of the surgical instrumentation and the inner diameter of the implant, woven bone formation was observed throughout the space of the chamber and directly onto the implant surface at 3 weeks *in vivo* [Figure 4(B,E)]. At 6 weeks, woven bone replacement by lamellar bone was observed throughout the healing chamber [Figure 4(C,D)] in both groups.

At trabecular bone regions, newly formed woven bone was observed at 3 weeks [Figure 4(B,E)], and its replacement by lamellar bone was observed at 6 weeks [Figure 4(C,F)] at regions in proximity with all implant surfaces.

The histomorphometric results demonstrated a significant difference between experimental groups for BIC at 1 week *in vivo* ($p < 0.04$) with the laser sintered having a higher value, whereas the 3 and 6 weeks *in vivo* exhibited no significant differences between groups [$p > 0.40$ and $p > 0.11$, respectively – Figure 3(A)]. The same trend was observed for BAFO, where a significant difference was

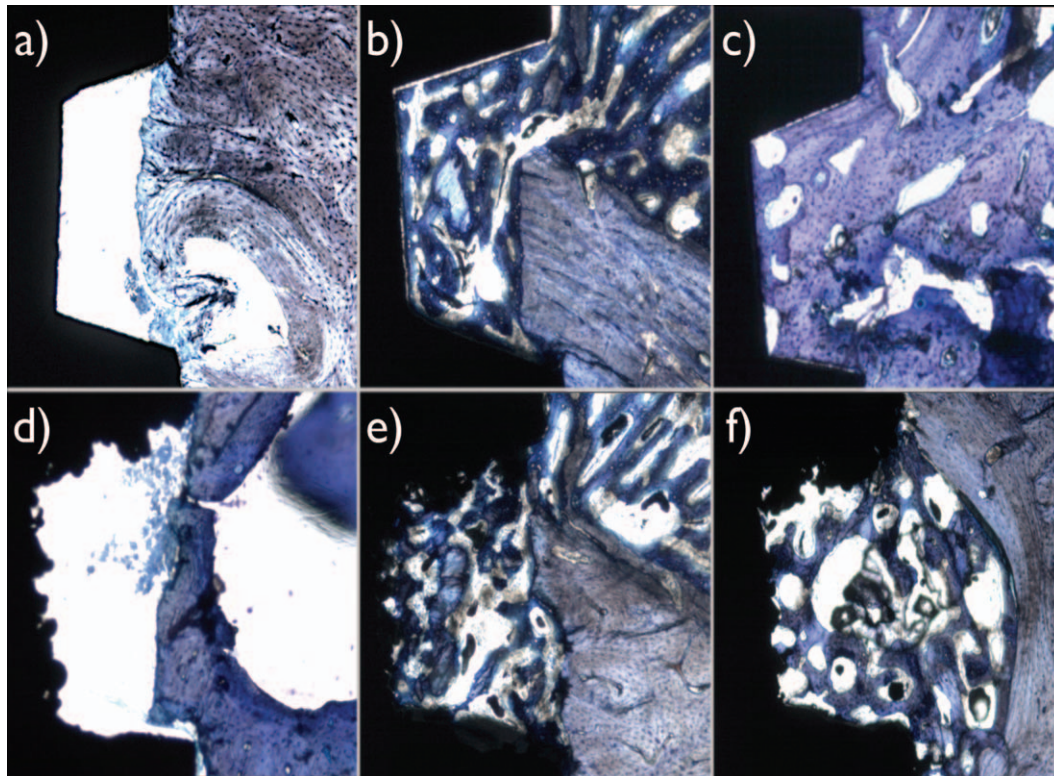


FIGURE 4. Optical micrographs at the top depicting 1, 3, and 6 weeks observation period for AB/AE implant surface (a, b, and c) and the same time points at the bottom for laser sintered (d, e, and f). [Color figure can be viewed in the online issue, which is available at wileyonlinelibrary.com.]

observed at 1 week (significantly higher for laser sintered, $p < 0.03$), but not at 3, and 6 weeks *in vivo* [$p > 0.70$, and $p > 0.60$, respectively—Figure 3(B)].

DISCUSSION

Both histomorphometric parameters evaluated in this study were significantly higher for the laser sintered compared with the AB/AE only in the first week evaluation with values being not significantly different at the subsequent observation periods (3 and 6 weeks *in vivo*). As per the imaging results, the three-dimensional surface configuration of the laser sintered implant may have provided larger surface area during the early stages of wound healing with increased blood clot retention compared to the AB/AE. General BIC and BAFO measurements were in agreement with the biomechanical results, where torque was significantly higher for the laser sintered at 1 week and then not significantly different to the AB/AE at 3 weeks. At 6 weeks when more time was allowed for early bone healing, the histomorphometric results remained not significantly different between groups whereas significantly higher torque was observed for the experimental relative to the control implant group. The 6 weeks results for BIC and BAFO contrasting with torque-to-interface failure test is in agreement with the claim that static osseointegration histomorphometric parameters may fail to represent the bone/implant interface mechanical properties. From a clinical standpoint, lower BIC and BAFO may be preferred on a higher mechanical property bone implant interface compared with a higher

BIC and BAFO on a lower mechanical property bone that may yield reduced stability.¹

The implant surface physical characterization showed that both arithmetic mean of the absolute values of the surface height within the sampling area and the root mean square of the surface departures were significantly higher for the laser sintered relative to AB/AE surface. It is possible that the observed 1 week significantly higher torque for the laser sintered relative to the AB/AE is likely a function of the higher resistance to torque provided by the increased surface texture of the former, and should not be suggestive as a motivation for immediate loading since the following observation period (3 weeks) revealed no statistical difference in torque between groups. At early observation periods, such as 1 week, torque resistance seems to be highly influenced by surface topography since osseointegration process is at its very initial stage.¹⁸ The similar results obtained at 3 weeks may be elucidated by the described early bone healing events shown for screw-root form implants with healing chambers where intense bone remodeling and resorption is observed at the regions where the interplay between surgical techniques and implant macrodesign allows an intimate contact between bone and implant.^{17,19–22} Because at 3 week woven bone was under formation at healing chamber regions and bone resorption was occurring at the implant outer threads, torque levels were similar irrespective of implant group. However, with initial lamellar bone formation in the healing chamber region, the significant increase in torque values at 6 week

for the laser sintered suggests that the surface topography was an important factor for improved bone response. The S_a mean value (1.26 μm) for the laser sintered fell within the moderately rough range, shown to provide the strongest bone response compared to minimally rough (S_a 0.5–1 μm) surfaces such as the AB/AE (0.56 μm).²³

From a temporal standpoint, both topographic and chemistry surface modifications have drawn attention,^{1,5,6,24,25} as both have been showing promising results *in vitro*²⁶ and *in vivo*^{27–35} relative to their moderately rough predecessors. As for implant physical modifications at the nanometric scale, the resulting surface configuration that can be tailored on a laser sintered implant for improved bone response is yet to be understood. Several processing parameters seem to have an effect on the final surface topography of laser sintered implants and likely on its osseointegrative properties, such as the power rating of the laser, the diameter of the laser beam focus, the scanning speed, the average particle size of the starting material powder, the process atmospheric conditions and others.³⁶ Nonetheless, our surface chemistry results are suggestive that only biocompatible elements along with adsorbed carbon species were present at the surface indicating that the fabrication technique was suitable for biomedical applications. Therefore, future investigation with variations in such processing parameters along with surface physico-chemical characterization and *in vivo* experimentation is warranted.

An *in vitro* study comparing acid-etched and laser sintered titanium surfaces has shown improved osteoblastic differentiation, production of bone morphogenetic protein, vascular endothelial growth factor and specific bone proteins for the laser sintered likely due to the controlled porous topography.³⁷ Although a clinical short-term comparison of AB/AE and laser sintered microimplants have reported significantly higher bone density in the threaded area for the laser sintered surface, no differences in BIC or in bone density outside the threaded area measurements were detected.³⁸ Therefore, several temporal evaluations became key to understanding the potential differences in healing events between different surfaces.

Although several animal models, such as the rabbit, pig, sheep, goat, and others could suit *in vivo* research, the canine model has shown close similarity in bone composition to that of human,³⁹ and has been indicated as one of the most appropriate for the testing of implant materials.⁴⁰ Differences in remodeling rate must be acknowledged and have been reported for example between the canine model and human.⁴¹

Our postulated hypothesis that laser sintered implants would improve early biomechanical and histomorphometric parameters compared to an AB/AE implant surface was partially accepted, since only higher torque to interface failure was observed at 1 and 6 week, but no differences were found for BIC and BAFO.

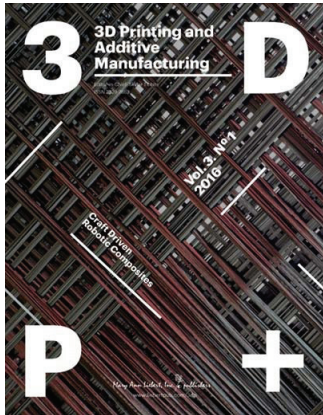
REFERENCES

- Coelho PG, Granjeiro JM, Romanos GE, Suzuki M, Silva NR, Cardaropoli G, Thompson VP, Lemons JE. Basic research methods

- and current trends of dental implant surfaces. *J Biomed Mater Res B Appl Biomater* 2009;88:579–596.
- Jimbo R, Ono D, Hirakawa Y, Odatsu T, Tanaka T, Sawase T. Accelerated photo-induced hydrophilicity promotes osseointegration: An animal study. *Clin Implant Dent Relat Res* 2011;13:79–85.
- Jimbo R, Sawase T, Baba K, Kurogi T, Shibata Y, Atsuta M. Enhanced initial cell responses to chemically modified anodized titanium. *Clin Implant Dent Relat Res* 2008;10:55–61.
- Albrektsson T, Gottlow J, Meirelles L, Ostman PO, Rocci A, Sennerby L. Survival of NobelDirect implants: An analysis of 550 consecutively placed implants at 18 different clinical centers. *Clin Implant Dent Relat Res* 2007;9:65–70.
- Albrektsson T, Wennerberg A. Oral implant surfaces. I. Review focusing on topographic and chemical properties of different surfaces and *in vivo* responses to them. *Int J Prosthodont* 2004;17:536–543.
- Albrektsson T, Wennerberg A. Oral implant surfaces. II. Review focusing on clinical knowledge of different surfaces. *Int J Prosthodont* 2004;17:544–564.
- Jimbo R, Sawase T, Shibata Y, Hirata K, Hishikawa Y, Tanaka Y, Bessho K, Ikeda T, Atsuta M. Enhanced osseointegration by the chemotactic activity of plasma fibronectin for cellular fibronectin positive cells. *Biomaterials* 2007;28:3469–3477.
- Wennerberg A, Albrektsson T. On implant surfaces: A review of current knowledge and opinions. *Int J Oral Maxillofac Implants* 2010;25:63–74.
- Mangano C, Piattelli A, Raspanti M, Mangano F, Cassoni A, Iezzi G, Shibli JA. Scanning electron microscopy (SEM) and X-ray dispersive spectrometry evaluation of direct laser metal sintering surface and human bone interface: A case series. *Las Med Sci* 2011;26:133–138.
- Lopez-Heredia MA, Sohler J, Gaillard C, Quillard S, Dorget M, Layrolle P. Rapid prototyped porous titanium coated with calcium phosphate as a scaffold for bone tissue engineering. *Biomaterials* 2008;29:2608–2615.
- Traini T, Mangano C, Sammons RL, Mangano F, Macchi A, Piattelli A. Direct laser metal sintering as a new approach to fabrication of an isoelastic functionally graded material for manufacture of porous titanium dental implants. *Dent Mater* 2008;24:1525–1533.
- Xue W, Krishna BV, Bandyopadhyay A, Bose S. Processing and biocompatibility evaluation of laser processed porous titanium. *Acta Biomater* 2007;3:1007–1018.
- Li JP, de Wijn JR, Van Blitterswijk CA, de Groot K. Porous Ti6Al4V scaffold directly fabricating by rapid prototyping: preparation and *in vitro* experiment. *Biomaterials* 2006;27:1223–1235.
- Bertol LS, Júnior WK, Silva FP, Aumund-Kopp C. Medical design: Direct metal laser sintering of Ti-6Al-4V. *Mater Des* 2010;31:3982–3988.
- Mangano C, Mangano F, Shibli JA, Luongo G, De Franco M, Brigguglio F, Figliuzzi M, Eccellente T, Rapani C, Piombino M, Macchi A. Prospective clinical evaluation of 201 direct laser metal forming implants: Results from a 1-year multicenter study. *Las Med Sci* 2012;27:181–189.
- Donath K, Breuner G. A method for the study of undecalcified bones and teeth with attached soft tissues. The Sage-Schliff (sawing and grinding) technique. *J Oral Pathol* 1982;11:318–326.
- Leonard G, Coelho P, Polyzois I, Stassen L, Claffey N. A study of the bone healing kinetics of plateau versus screw root design titanium dental implants. *Clin Oral Implants Res* 2009;20:232–239.
- Löberg J, Mattisson I, Hansson S, Ahlberg E. Characterisation of titanium dental implants i: Critical assessment of surface roughness parameters. *Open Biomater J* 2010;2:18–35.
- Berglundh T, Abrahamsson I, Lang NP, Lindhe J. De novo alveolar bone formation adjacent to endosseous implants. *Clin Oral Implants Res* 2003;14:251–262.
- Bonfante EA, Granato R, Marin C, Suzuki M, Oliveira SR, Giro G, Coelho PG. Early bone healing and biomechanical fixation of dual acid-etched and as-machined implants with healing chambers: An experimental study in dogs. *Int J Oral Maxillofac Implants* 2011;26:75–82.
- Coelho PG, Suzuki M, Guimaraes MV, Marin C, Granato R, Gil JN, Miller RJ. Early bone healing around different implant bulk

- designs and surgical techniques: A study in dogs. *Clin Implant Dent Relat Res* 2010;12:202–208.
22. Marin C, Granato R, Suzuki M, Gil JN, Janal MN, Coelho PG. Histomorphologic and histomorphometric evaluation of various endosseous implant healing chamber configurations at early implantation times: A study in dogs. *Clin Oral Implants Res* 2010;21:577–583.
 23. Wennerberg A, Albrektsson T. Effects of titanium surface topography on bone integration: A systematic review. *Clin Oral Implants Res* 2009;20(Suppl 4):172–184.
 24. Kang BS, Sul YT, Oh SJ, Lee HJ, Albrektsson T. XPS, AES and SEM analysis of recent dental implants. *Acta Biomater* 2009;5:2222–2229.
 25. Dohan Ehrenfest DM, Coelho PG, Kang BS, Sul YT, Albrektsson T. Classification of osseointegrated implant surfaces: Materials, chemistry and topography. *Trends Biotechnol* 2010;28:198–206.
 26. Moura CC, Souza MA, Dechichi P, Zanetta-Barbosa D, Teixeira CC, Coelho PG. The effect of a nanothickness coating on rough titanium substrate in the osteogenic properties of human bone cells. *J Biomed Mater Res A* 2010;94:103–111.
 27. Coelho PG, Cardaropoli G, Suzuki M, Lemons JE. Early healing of nanothickness bioceramic coatings on dental implants. An experimental study in dogs. *J Biomed Mater Res B Appl Biomater* 2009;88:387–393.
 28. Coelho PG, Lemons JE. Physico/chemical characterization and in vivo evaluation of nanothickness bioceramic depositions on alumina-blasted/acid-etched Ti-6Al-4V implant surfaces. *J Biomed Mater Res A* 2009;90:351–361.
 29. Coelho PG, Marin C, Granato R, Suzuki M. Clinical device-related article: Histomorphologic analysis of 30 plateau root form implants retrieved after 8 to 13 years in function. A human retrieval study. *J Biomed Mater Res B Appl Biomater* 2009;91:975–979.
 30. Coelho PG, Suzuki M, Guimaraes MV, Marin C, Granato R, Gil JN, Miller RJ. Early bone healing around different implant bulk designs and surgical techniques: A study in dogs. *Clin Implant Dent Relat Res* 2010;12:202–208.
 31. Granato R, Marin C, Suzuki M, Gil JN, Janal MN, Coelho PG. Biomechanical and histomorphometric evaluation of a thin ion beam bioceramic deposition on plateau root form implants: An experimental study in dogs. *J Biomed Mater Res B Appl Biomater* 2009;90:396–403.
 32. Granato R, Marin C, Suzuki M, Gil JN, Janal MN, Coelho PG. Biomechanical and histomorphometric evaluation of a thin ion beam bioceramic deposition on plateau root form implants: an experimental study in dogs. *J Biomed Mater Res B Appl Biomater* 2009;90:396–403.
 33. Marin C, Granato R, Suzuki M, Gil JN, Piattelli A, Coelho PG. Removal torque and histomorphometric evaluation of bioceramic grit-blasted/acid-etched and dual acid-etched implant surfaces: An experimental study in dogs. *J Periodontol* 2008;79:1942–1949.
 34. Mendes VC, Moineddin R, Davies JE. The effect of discrete calcium phosphate nanocrystals on bone-bonding to titanium surfaces. *Biomaterials* 2007;28:4748–4755.
 35. Mendes VC, Moineddin R, Davies JE. Discrete calcium phosphate nanocrystalline deposition enhances osteoconduction on titanium-based implant surfaces. *J Biomed Mater Res A* 2009;90:577–585.
 36. Hollander DA, von Walter M, Wirtz T, Sellei R, Schmidt-Rohlfing B, Paar O, Erli HJ. Structural, mechanical and in vitro characterization of individually structured Ti-6Al-4V produced by direct laser forming. *Biomaterials* 2006;27:955–963.
 37. Mangano C, De Rosa A, Desiderio V, d'Aquino R, Piattelli A, De Francesco F, Tirino V, Mangano F, Papaccio G. The osteoblastic differentiation of dental pulp stem cells and bone formation on different titanium surface textures. *Biomaterials* 2010;31:3543–3551.
 38. Shibli JA, Mangano C, D'Avila S, Piattelli A, Pecora GE, Mangano F, Onuma T, Cardoso LA, Ferrari DS, Aguiar KC, et al. Influence of direct laser fabrication implant topography on type IV bone: A histomorphometric study in humans. *J Biomed Mater Res A* 2010;93:607–614.
 39. Aerssens J, Boonen S, Lowet G, Dequeker J. Interspecies differences in bone composition, density, and quality: Potential implications for in vivo bone research. *Endocrinol* 1998;139:663–670.
 40. Pearce AJ, Richards RG, Milz S, Schneider E, Pearce SG. Animal models for implant biomaterial research in bone: A review. *Eur Cells Mater* 2007;13:1–10.
 41. Bloebaum RD, Ota DT, Skedros JG, Mantas JP. Comparison of human and canine external femoral morphologies in the context of total hip replacement. *J Biomed Mater Res* 1993;27:1149–1159.

Published: Volume 3, number 1, 2016 in:



Enhanced Osteoblast Response to Porosity and Resolution of Additively Manufactured Ti-6Al-4V Constructs with Trabeculae-Inspired Porosity

Alice Cheng, Aiza Humayun, Barbara D. Boyan, Zvi Schwartz

ABSTRACT | The addition of porosity to the traditionally used solid titanium metal implants has been suggested to more closely mimic the natural mechanical properties of bone and increase osseointegration in dental and orthopedic implants. The objective of this study was to evaluate cellular response to three-dimensional (3D) porous Ti-6Al-4V constructs fabricated by additive manufacturing using laser sintering with low porosity (LP), medium porosity (MP), and high porosity (HP) with low resolution (LR) and high resolution (HR) based on a computed tomography scan of human trabecular bone. After surface processing, construct porosity ranged from 41.0% to 76.1%, but all possessed micro-/nanoscale surface roughness and similar surface chemistry

containing mostly Ti, O, and C. Biological responses (osteoblast differentiation, maturation, and local factor production) by MG63 osteoblast-like cells and normal human osteoblasts favored 3D than two-dimensional (2D) solid constructs. First, MG63 cells were used to assess differences in cell response to 2D compared to LR and HR porous 3D constructs. MG63 cells were sensitive to porosity resolution and exhibited increased osteocalcin (OCN), vascular endothelial growth factor (VEGF), osteoprotegerin (OPG), and bone morphogenetic protein 2 (BMP2) on HR 3D constructs than on 2D and LR 3D constructs. MG63 cells also exhibited porosity-dependent responses on HR constructs, with up to a 6.9-fold increase in factor production on LP-HR and MP-HR constructs than on HP-HR

constructs. NHOs were then used to validate biological response on HR constructs. NHOs exhibited decreased DNA content and alkaline phosphatase activity and up to a 2.9-fold increase in OCN, OPG, VEGF, BMP2, and BMP4 on 3D HR constructs than on 2D controls. These results indicate that osteoblasts prefer a 3D architecture than a 2D surface and that osteoblasts are sensitive to the resolution of trabecular detail and porosity parameters of laser-sintered 3D Ti-6Al-4V constructs. **Acknowledgements:** This study was supported by A.B. Dental.

Abstract accepted to AADR/CADR Annual Meeting (2016).



3D-printed implants support stem cell differentiation and vertical bone growth

A. Cheng, David J. Cohen, MD, Barbara D. Boyan, PhD, K. Sahingur, Zvi Schwartz, PhD, DMD.

ABSTRACT | Objectives: The objective of this study was to fabricate laser sintered constructs with a trabecular-inspired porosity and characterize the biological response in vitro and in vivo. **Methods:** A CT scan of human trabecular bone was overlaid on itself 24 times to create porous 3D constructs. Constructs were laser sintered from Ti-6Al-4V powder and were 15mm in diameter and 5mm in height, including a 1mm solid base. 2D controls were 1mm in height solid disks. Human mesenchymal stem cells (hMSCs) were plated on constructs and evaluated for osteoblastic differentiation, maturation and local factors after 3, 6 and 9 days, and mineralization after 8w. Implants were 6.5mmx3.5mm and 2mm in height with an arch for mechanical testing.

Solid, 3D and 3D implants with DBX putty were placed on athymic nude rat calvaria for 10w to assess osseointegration. **Results:** Porosity of 3D constructs for cell culture was $57\pm1\%$, and porosity of implants was $67\pm3\%$. Mostly Ti, O and C were present on material surfaces. Contact angle on 2D surfaces was $62\pm18^\circ$ and solid implants was $47\pm17^\circ$. All constructs possessed micro-/ nano-scale topographies. Markers for osteoblastic differentiation, maturation and local factor production were elevated on 3D constructs compared 2D controls, and this was sustained over 9d of culture. After 8w, hMSCs produced mineral content on 3D constructs as verified by SEM and LCM imaging. Mechanical pullout testing of implants on rat calvaria showed significantly higher force at

failure for 3D and 3D-DBX implants compared to 2D implants; however, no differences were observed between 3D and 3D+DBX implants. MicroCT indicated vertical bone growth into both 3D and 3D+DBX implants that did not significantly differ from each other. Histology corroborated microCT observations. **Conclusions:** Laser sintered 3D implants sustain osteoblastic differentiation of hMSCs and induce vertical bone growth in an animal model without the use of exogenous factors. **Acknowledgements:** This study was supported by A.B. Dental.



Trabecular Porosity Implants with Surface Roughness Induce Vertical Bone Growth without the Use of a Bone Substitute

David J. Cohen, MD, Ryan M. Clohessy, Barbara D. Boyan, PhD, Zvi Schwartz, DMD, PhD.


ABSTRACT | Introduction: Over 1 million joint replacement surgeries are performed in the United States each year, and approximately 20% of these procedures require the use of bone graft substitutes to aid in implant osseointegration [1,2]. The objective of this study was to analyze bone growth and mechanical integration of solid and 3D porous implants in a novel rat cranial onlay model, with and without the use of a bone substitute. The overall hypothesis was that 3dimensional (3D) trabecularinspired porosity is able to increase bone growth and mechanical pullout force of the implant compared to homogenous round holes in 2D implants. The hypothesis of the first study was that rough implant surfaces and the use of demineralized bone matrix putty (DBX) on laser sintered

implants would increase bone growth into homogeneous holes and mechanical pullout strength. The hypothesis of the second study was that trabecularinspired, interconnected porosity of laser sintered implants would be able to achieve similar vertical bone growth compared to porous implants with DBX, and that mechanical pullout force of porous implants would increase compared to solid implants.

Methods: In the first experiment, disks 5mm in diameter and 1mm in height with twelve evenly spaced 0.5mm holes were manufactured using laser sintering from Ti6Al4V powder (EOS Systems). "Smooth" disks were polished with sandpaper, while "Rough" disks were blasted with calcium phosphate and acid etched to induce micro/ nanoroughness.

In the second experiment, "Solid" constructs 6.5mm in length, 3.5mm in width and 2mm in height were manufactured and surface processed using the same methods as for "Rough" disks. "Porous" constructs were manufactured in the same dimensions, with a trabecularinspired porosity of 5mm in length surrounded by 0.75mm solid supports on each end. The trabecular porosity design was taken from a CT template of human femoral head superimposed upon itself 24 times, with a total interconnected porosity of $67\% \pm 3\%$.

Implants used for mechanical testing included a 1mm diameter thick arch that spanned across the implant. Athymic nude male rats (n=8 for each group) approximately 78 weeks old (200250g) were purchased from Harlan



Laboratories. After cranial incision, the periosteum was lifted. Pilot holes were drilled in the calvarium at the site of implant placement (between the coronal and sagittal cranial sutures) to allow for stem cell infiltration during healing. For both “DBX” groups, DBX was applied underneath and above disks before implantation. Implants were secured by a pursestring suture closing the periosteum, and then the outer skin flap was suture closed. Animals were harvested after 10 weeks for microCT analysis of bone growth, mechanical pullout testing and scanning electron microscopy of implants and calvaria after mechanical testing. Animal experiments were approved by the Institutional Animal Care and Use Committee at Virginia Commonwealth University. One way ANOVA with Bonferroni postcorrection to Student’s test was used to analyze data, with $p < 0.05$ indicating significance.

Results: In the first study, no statistically significant differences were observed for bone to implant contact for Smooth, Rough or DBX groups.

However, vertical bone ingrowth into pores was significantly higher for DBX disks than for Smooth or Rough disks. Pullout testing revealed significantly higher force at failure for DBX disks compared to Smooth and Rough disks. Electron micrographs of calvaria and implants after mechanical testing showed bone nodules on the surface of Smooth group calvaria that did not remain in implant holes after testing. In contrast, bone was found incorporated into implant holes for Rough and DBX groups after testing, with additional bone nodule formation observed on DBX group calvaria. In the second study, bone to implant contact was significantly decreased for Porous and DBX groups compared to for the Solid group.

Discussion: Although Rough disk implants had higher bone to implant contact and mechanical testing values compared to Smooth disk implants, the differences were not statistically significant. The DBX group had superior bone ingrowth into disk holes and mechanical pullout force compared to both Rough and Smooth disk implants,

indicating that including holes in a 2D construct is not sufficient to induce bone growth without the use of a bone substitute. However, for 3D construct implants with a trabecularinspired porosity, no differences were seen for bone to implant contact or mechanical pullout force between Porous and DBX groups. This suggests that implant integration is porosity dependent, and that a trabecularinspired porosity can enhance vertical bone growth compared to homogenous round holes. Because bone to implant contact is not an indicative measure of implant success in 3D porous implants, we combined it with other metrics such as vertical bone growth and mechanical pullout testing.

Significance: This study indicates that trabecular boneinspired porosity produced by laser sintering Ti6Al4V can induce vertical bone growth, even without the use of a bone substitute.

Acknowledgements: This study was supported by A.B. Dental.

Abstract accepted to AADR/CADR Annual Meeting (2015).



Subperiosteal microtextured titanium-alloy implants lead to osteointegration outside bone envelopes

Sharon L. Hyzy, MS, David J. Cohen, MD, Barbara D. Boyan, PhD, Zvi Schwartz, PhD, DMD.

ABSTRACT | Objectives: Additive-manufacturing (AM) offers the ability to tailor implants to individual patients and with specific surface treatments may be osteogenic. This could be beneficial for producing more effective treatment of edentulous mandibles in cases that can't be restored conventionally. This study assessed effects of three bone treatment regimens on bone formation around AM-fabricated titanium-aluminum-vanadium (Ti6Al4V) implants in rat and rabbit models.

Methods: Ti6Al4V disks and wrap implants were produced by AM and acid-etched to create a specific microsurface.

5.0mm disks with 0.05mm holes were implanted subperiosteally on the calvaria of male Sprague-Dawley rats. Prior to insertion, bone was treated by in-situ

decalcification (no treatment; 24% EDTA; or 37% phosphoric acid) (n=6/group).

Animals were euthanized at 35 and 70d. Wrap implants were surgically affixed to left tibias of 30 New Zealand White rabbits. Animals were euthanized at 1w (n=3), 3w (n=16), or 6w (n=11). Fixed samples were analyzed by microCT and histology.

Results: Osteointegration was found on the base of the disks and bone infiltration into implant holes was achieved at 35 and 70d. Bony ingrowth varied within each treatment group, but no difference was found between groups. No new bone was observed in the wrap implants at 1w. At 3w bone formed outside the envelope and cartilage-in-transition-to-bone was found. At 6w bone formed between implant and cortical bone

with full osteointegration. Bone-implant contact increased, and was significantly higher at 6w compared to earlier times.

Conclusion: Ti6Al4V implants with specific surface roughness allow for osteogenesis and osteointegration, and the potential for bone to grow into a void space without use of bone graft substitutes. These data indicate that if implants are tailored to the individual's mandible, there is a high chance for osteointegration, indicating potential new modes of treatment and restoration in cases of mandibular bone deficiency.

Acknowledgements: This study was supported by A.B. Dental.

Abstract accepted to EuroPerio 2015 Conference.



3D Porous Ti6Al4V Constructs Produced by Additive Manufacturing Capture Human Trabecular Bone Structure and Promote Osteoblast Differentiation and Mineralization

Alice Cheng, Aiza Humayun, Barbara D. Boyan, Zvi Schwartz

ABSTRACT | Aim: The aim of this study was to characterize three-dimensional (3D) porous Ti6Al4V constructs fabricated by additive manufacturing from a human trabecular bone template using laser sintering, and evaluate biological response to these constructs.

Material and Methods: 2D control and 3D porous Ti6Al4V constructs were manufactured using laser sintering to produce constructs with low, medium and high porosity (LP, MP, HP) with low and high trabecular bone detail (LD, HD). Material characterization included contact angle (2D only), micro-computed tomography, x-ray photoelectron spectroscopy, laser confocal microscopy, and scanning electron microscopy. MG63 cells were seeded (6x10⁴ cells/construct) and harvested 24h after confluence

on tissue culture polystyrene to assess response. hMSCs were seeded (2x10⁶ cells) on MP-HD constructs with and without collagen coatings and cultured for 8w in growth or osteogenic medium to assess mineralization.

Results: Open porosity of constructs ranged from 41-76%. All constructs had similar surface micro- and nano-roughness after processing. Surface chemistry consisted mostly of O, C and Ti. 2D disks had a contact angle of 62°. MG63 cells had decreased DNA content and alkaline phosphatase activity and increased osteocalcin and BMP2 on 3D constructs in comparison to 2D. Vascular endothelial growth factor, BMP2 and BMP4 were highest on MP-HD constructs. Mineral content was observed on MP-HD constructs after 8w with and without the

presence of a collagen coating.

Conclusion: 3D Ti6Al4V constructs produced by additive manufacturing to mimic trabecular bone with varying porosity differentially affect osteoblast response and induce hMSC mineralization, even in the absence of osteogenic media supplements.

chondrocytes mature into a thin layer of bone, spreading from the implant holes. At 6 weeks, the bone establishes significant contact on the outward facing sides of the implant and has achieved good contact with the inward sides.

Acknowledgements: This study was supported by A.B. Dental.



IADR

International Association
for Dental Research

Human Osteoblasts Are Sensitive to Porosity of High-Resolution, Additively-Manufactured 3D Constructs

Alice Cheng, Aiza Humayun, Barbara D. Boyan, Zvi Schwartz

ABSTRACT | The objective of this study was to analyze effects of porosity on proliferation and maturation of normal human osteoblasts (NH0st) using 3D titanium-aluminum-vanadium (Ti6Al4V) constructs fabricated by additive manufacturing based on a high-resolution human trabecular bone CT.

Methods: 2D (15mmx1mm) and 3D (15mmx5mm) Ti6Al4V constructs were manufactured from CT scans of human femoral trabecular bone using laser sintering in low, medium and high porosities (LP/MP/HP). Surfaces were grit-blasted and acid-etched to achieve micro and nanoscale roughness. Porosity, surface chemistry, topography and compressive modulus were characterized on 3D constructs, and wettability was analyzed on 2D surfaces. MG63 osteoblast-like

cells and NH0st cells were seeded at 60,000 cells/construct/well and harvested 24h after confluence on TCPS. DNA, alkaline phosphatase specific activity (ALP), osteocalcin (OCN) and bone morphogenetic proteins 2 and 4 (BMP2/BMP4) were analyzed as markers for osteoblast proliferation, differentiation, maturation, or local factor production. Data were analyzed by ANOVA with Bonferroni post-test ($n=6$ /variable).

Results: 3D constructs contained mostly O, C and Ti on their surfaces. 2D contact angle was $62 \pm 19^\circ$. Surfaces had microscale roughness with homogeneous nanoscale features. Total porosity ranged from 41.0 ± 0.3 to $76.1 \pm 0.8\%$. For MG63 and NH0st cells, DNA decreased on 2D surfaces compared to TCPS, and decreased on LP and MP constructs compared

to 2D. MG63 ALP increased on 2D surfaces compared to TCPS, but decreased on 3D constructs. NH0st cell ALP decreased on all surfaces compared to TCPS. For both MG63 and NH0st cells, OCN was increased on 3D constructs compared to TCPS and 2D; BMP2 and BMP4 increased on LP and MP constructs compared to TCPS, 2D and HP.

Conclusions: Osteoblasts exhibited greater differentiation, maturation and local factor production in a human trabecular bone-like 3D environment compared to 2D, and this depended on porosity.

Acknowledgements: This study was supported by A.B. Dental.



Characterization of and Cell Response to 3D Laser Sintered Implants

Alice Cheng, Sharon L. Hyzy, MS, David J. Cohen, MD, Barbara D. Boyan, PhD, Zvi Schwartz, PhD, DMD.PhD, DMD.

ABSTRACT | Objectives: Although most dental implants meet or exceed a 95% success rate over a 5 year period, compromised patients such as smokers, diabetics and the elderly have a much higher rate of implant failure due to poor osseointegration. Porous titanium implants have been introduced as a way of increasing mechanical interlocking and early bone integration. The objective of this study was to characterize and evaluate cell response to 3D porous titanium implants manufactured using laser sintering with porosity comparable to that of human trabecular bone.

Methods: CT scans were conducted of femoral heads obtained from hip replacements. 3D titanium disks 15mm in diameter

and 4mm in height were manufactured from CT scan templates using laser sintering with commercially pure titanium powder. Micro and nanoscale roughness were created by acid etching. Porosity, wettability, surface chemistry and topography were characterized. DNA, alkaline phosphatase specific activity (ALP), osteocalcin (OCN) and bone morphogenetic protein 4 (BMP4) were analyzed as markers for proliferation and enhancement of an osteoblastic environment of MG63 cells plated on surfaces. Data were analyzed by ANOVA with Bonferroni post-hoc test (n=6/variable).

Results: Low, medium and high porosity surfaces were confirmed with total porosity values of 16.2%, 38.5% and 70.0%, respectively. Nanoscale roughness was

superimposed on microrough surfaces after treatment, and all surfaces were hydrophilic. Surface chemistry contained titanium, oxygen and carbon as the three most prevalent elements. DNA decreased with increasing porosity. ALP decreased with increasing porosity, while OCN exhibited the opposite trend. BMP4 also increased with increasing porosity, suggesting that a higher porosity is more favorable for osteoblastic differentiation.

Conclusion: Laser sintering is able to produce 3D porous implants based on a CT template scan of human bone. These surfaces show increased cell response on highly porous surfaces, suggesting improved osseointegration of laser sintered surfaces for dental implants.

Acknowledgements: This study was supported by A.B. Dental.



Implantation of an Osteoconductive Additive Manufactured Titanium Alloy Implant Leads to Osteointegration Outside the Bone Envelope in Rats and Rabbits

David J. Cohen, MD, Alexander Whitehead, Sharon L. Hyzy, MS, Barbara D. Boyan, PhD, Zvi Schwartz, DMD, PhD.

ABSTRACT | Introduction: The number of discharges of patients with spinal fusion surgery for back problems has steadily increased over the past decade. There remains a need for a cage implant that will enable more effective osteointegration. Additive manufacturing offers the ability to tailor implants to individual patients and, with different surface treatment applications, may be osteoinductive. This capability could be particularly beneficial in producing more effective cage implants for interbody spinal fusion. In the present study, additive manufacturing was used to create a titanium alloy surface with a specific roughness to determine its osteogenic capacity in both a rat and rabbit model.

Methods: 5 mm disks were generated by laser sintering

Ti6Al4V alloy powder. The resulting disks were grit blasted and then acid etched, subjected to a cleaning protocol and then sterilized via gamma radiation. In the first study, the discs were implanted subperiosteally on the surface of the calvaria of male Sprague Dawley rats under institutional approval of Virginia Commonwealth University (Richmond). Three treatment groups (n=6) were established to determine the effect of pretreating the implantation site via in situ decalcification. Following elevation of a periosteal flap, multiple 0.3mm holes were drilled into the marrow space of the left parietal bone. Exposed bone around these holes was left untreated, treated with 24% EDTA for five minutes, or 37% phosphoric acid for 1 minute. The disks were placed over the holes and the flap

was sutured over the disk. Animals were euthanized at 35 and 70 days. In the second study, additively manufactured titanium alloy wrap implants (Figure 1b) were grit blasted, acid etched, cleaned and sterilized as above.

Implants were surgically affixed to the left tibia of 30 New Zealand White rabbits under institutional approval at the Medical University of Lodz (Lodz, Poland). Animals were euthanized at two weeks (n=3), three weeks (n=16), or six weeks (n=11) after surgery. All fixed samples from both studies were scanned by microCT and bone implant contact calculated. Samples were then embedded in resin and ground samples prepared. Twenty-eight of the wrap implant samples remained intact and viable after histologic processing and were then stained



with Stevenel's Blue along with all 48 disk implant samples. Samples were photographed using Zen 2012 Blue Edition software with an AxioCam MRc5 camera and Axio Observer Z.1 microscope (Carl Zeiss Microscopy, Oberkochen, Germany). Bone implant contact (BIC) was calculated by dividing the bone contact perimeter by the total perimeter of the implant. Base and side BICs of the wrap implants were also calculated by measuring the bone facing sides (base) of the implant and outward facing sides of the implant. Statistics were derived using a oneway ANOVA test with a Tukey's posttest for significance and $p < 0.05$ considered significant.

Results: In the first study, osteointegration was present on the base of the disks and bone infiltration into the implant holes was achieved at both 35 and 70 days as observed by both microCT and histomorphometric analysis. There was variability in the amount of bony ingrowth within each pretreatment group. No difference was seen between the treatment groups at either 35 or 70 days. In the second

study, wrap implants exhibited increased osteointegration on all on all sides with time. Total bone implant contact increased at each time point, and was significantly higher after six weeks compared to earlier time points, demonstrated both by microCT analysis and histomorphometric measurements. At one week, no new bone or cartilage was present. At three weeks, cartilage infiltrated the implant in areas and a thin layer of bone was observed growing from the implant holes. At 6 weeks, bone had established significant contact on the external side of the implant and demonstrated good contact with the osseous side of the implant. In addition, new bone was observed outside the bone envelope.

Discussion: Using a titanium alloy implant with a specific surface roughness allows for good osteoconduction and osteointegration, as well as the potential for bone to grow into a void space without the use of a bone graft substitute. In rats, there was no difference seen in pretreatment of the bone surface

prior to implantation. However, all treatment groups showed vertical growth of bone into the holes of the implant after 70 days demonstrating the osteoconductive ability of the implant material. The titanium wrap used in rabbits allowed for osteointegration as early as 6 weeks, as well as the creation of vertical growth through the implant holes. These results suggest that this approach may enable consistent vertical growth of bone during implant placement allowing for better results following spinal fusion surgery.

Significance: Biomaterials are used in spine fusions, with varying material properties. However, additive manufacturing allows titanium alloy implants to be tailored to the space and a specific surface applied to allow osteoconduction and osteointegration of bone, potentially allowing a void space to be filled without the use of a bone graft substitute.

Acknowledgements: This study was supported by A.B. Dental.



Sustained Response of Human Mesenchymal Stem Cells on Additively Manufactured 3D Porous Ti6Al4V

A. Cheng, A. Humayun, Barbara D. Boyan, Zvi Schwartz, PhD, DMD.

ABSTRACT | Introduction: Titanium and its alloys are commonly used materials in dental and orthopedic implants due to their desirable mechanical properties and ability to osseointegrate with bone. However, implant success rates are reduced dramatically for compromised patients, including smokers, diabetics and those with low bone density.


Implant design can be optimized with surface roughness and porosity to achieve a more desirable biological response. In this study, additive manufacturing was used to produce Ti6Al4V 3D constructs with porosities based on a human trabecular bone template, and human mesenchymal stem cell (hMSC) response was analyzed over a period of 8 weeks on these constructs to determine the effect of the 3D environment on biological

response in comparison to a 2D environment.

Materials and Methods: Ti6Al4V powder was used to laser sinter 2D and porous constructs based on a trabecular bone template captured from a computed tomography (CT) scan of a human femoral head. Constructs were subsequently blasted with calcium phosphate and pickled in nitric acid. X-ray photoelectron spectroscopy (XPS), scanning electron microscopy (SEM) and laser confocal microscopy (LCM) were used to analyze chemistry, topography and roughness, respectively. Contact angle was performed on 2D surfaces and microCT on 3D constructs. Surfaces were gamma sterilized for cell culture and seeded with 60,000 hMSCs per construct for 3, 6 and 9 days to analyze DNA (proliferation),

alkaline phosphatase specific activity (ALP, early osteoblast differentiation), osteocalcin (OCN, late osteoblast differentiation) and vascular endothelial growth factor (VEGF, blood vessel formation). Porous constructs were seeded with 2 million hMSCs for 8 weeks in osteogenic medium (OM), OM with bone morphogenetic protein 2 (BMP2) and OM with a collagen I coating (COL1) on the surface, and mineralization was analyzed by SEM, LCM and energy dispersive x-ray (EDX).

Results and Discussion: Sintered constructs had mostly Ti, O and C present on their surfaces, and SEM and LCM revealed a homogenous combined micro-/nanoroughness as a result of surface treatment. Contact angle on 2D surfaces was 62 ± 18 . Porous constructs had



interconnected porosity ($57.3 \pm 0.8\%$). DNA and ALP were decreased on 3D constructs compared to TCPS and 2D controls at 3, 6 and 9 days. In contrast, OCN and VEGF were increased on 3D constructs compared to TCPS and 2D controls at 3, 6 and 9 days. For all three groups, DNA increased at 6 and 9 days compared to at 3 days. For TCPS, ALP decreased at 6 and 9 days compared to at 3 days, while there were no significant differences in ALP over time for 2D and 3D constructs. OCN levels were relatively stable over 3, 6, and 9 days for all groups. For TCPS, VEGF was increased at day 9 compared to days 3 and 6, while there were no significant changes for 2D surfaces. For 3D constructs, VEGF was increased in a time dependent manner (day 9 > day 6 > day 3). SEM and OsteoImage

hydroxyapatite staining of cells cultured for 8 weeks showed mineral deposition on all 3D constructs. EDX analysis revealed Ca:P ratios of 1.68, 1.50 and 1.41 for OM, BMP2 and COL1 groups, respectively.

Conclusions: Additively manufactured 3D Ti6Al4V constructs with porosity in the likeness of human trabecular bone sustain osteoblastic differentiation of hMSCs over time compared to 2D controls, and mineral deposition occurred by 8 weeks. Ca:P ratios suggest dystrophic calcification when OM alone was used; but physiological mineralization in cultures treated with BMP2 or grown on COL1 coated surfaces. These results suggest that a 3D environment with tailored porosity and surface roughness can enhance biological response and may

improve osseointegration clinically.

Acknowledgements: This study was supported by A.B. Dental.



Response to Laser Sintered 3D Porous Trabecular Titanium Constructs Occurs in a Cell Maturation Dependent Manner


Alice Cheng, Sharon L. Hyzy, MS, David J. Cohen, MD, Barbara D. Boyan, PhD, Zvi Schwartz, PhD, DMD.

ABSTRACT | Introduction: Titanium and its alloys are commonly used materials in orthopaedic implants due to their strong mechanical properties and ability to osseointegrate with bone. However, a stiffness mismatch between solid titanium and human bone results in stress shielding and bone resorption around implants [1]. Porous implants have been designed to better match the mechanical properties of bone, but pores are largely pre-defined and homogenous with limited surface processing [2]. Additive manufacturing such as laser sintering is a bottom-up approach to creating custom orthopaedic implants [3]. In this study, we use trabecular bone as a biological template for laser sintering 3D Ti6Al4V porous constructs with combined micro-/nano-roughness,

and analyze both human mesenchymal stem cell (hMSC) and osteoblast (MG63) response to these constructs.

Methods: 3D laser sintered (3DLS) constructs 15mm in diameter and 5mm in height with a 1mm solid base were manufactured from Ti-6Al4V particles 25-45µm in diameter with the EOS Ytterbium fiber laser system, a wavelength of 1054nm, continuous power of 200W, scanning rate of 7m/s and laser spot size of 0.1mm. Solid 2D, low, medium and high porosity (LP, MP, HP, respectively) constructs were manufactured with high detail by replicating a processed computed tomography scan of human trabecular bone. Constructs were further blasted with calcium phosphate particles and etched in 0.3N HNO₃ to produce a micro-rough surface. Constructs were

further pickled in a bath of 1:1 20 g/L NaOH:H₂O₂ and then in 65% HNO₃ to clean surfaces and induce nano-roughness. Chemistry, wettability, total and open porosity, surface roughness, surface topography and compressive modulus were characterized using x-ray photoelectron spectroscopy (XPS), sessile drop contact angle (on 2D surfaces only), laser confocal microscopy, scanning electron microscopy (SEM) and compression testing. MG63 osteoblast or hMSC cells were plated on three different porosity 3D constructs with TCPS, 2D used as control at a seeding density of 60,000 cells/well and harvested 24 hours after confluence to analyze DNA, alkaline phosphatase specific activity (ALP), osteocalcin (OCN), and vascular endothelial growth factor (VEGF).



Results: Total percent porosity (avg \pm SD) for LP, MP and HP constructs was $54.2 \pm 0.9\%$, $59.5 \pm 0.5\%$ and $72.2 \pm 0.9\%$, respectively. Total and open porosity values were not significantly different. XPS showed mainly oxygen, carbon and titanium in the oxide layer, which was similar among all sintered constructs. An elevated presence of nitrogen was seen on 2D surfaces compared to 3D constructs, and other trace elements included phosphorous, calcium and sulfur. Contact angle of 2D proxy surfaces was $62 \pm 18^\circ$. Surface micro roughness (S_a , avg \pm SD) was $4.0 \pm 0.6 \mu\text{m}$ for 2D surfaces and did not statistically differ from roughness of 3D constructs. Peak to valley roughness (S_z) was $34.1 \pm 4.7 \mu\text{m}$ for 2D surfaces and was only lower than HP constructs, which had an S_z value of $37.6 \pm 7.9 \mu\text{m}$. Micro-CT revealed different macro-topographies for constructs with varying porosity (Fig 1a), SEM micrographs revealed different macro-topographies for constructs with varying porosity, while surface roughness induced by post processing at the micro- and

nano-surface were similar with all construct (Fig 1b). For MG63 cells, DNA decreased on 2D, LP, MP and HP constructs compared to TCPS and decreased on LP and MP constructs compared to 2D. DNA for HP was significantly higher than LP and MP constructs. ALP activity was significantly elevated on 2D and decreased on LP and MP constructs compared to TCPS, decreased on LP, MP and HP constructs compared to 2D, and increased on HP compared to LP and MP constructs. OCN was increased on LP and MP constructs compared to both TCPS and 2D, and decreased on HP compared to LP and MP constructs (Fig 1c, top). VEGF was increased on MP and HP constructs compared to TCPS, 2D and LP constructs, and decreased on HP compared to MP constructs. For hMSC cells, DNA decreased on all sintered constructs compared to TCPS. ALP activity was reduced on all sintered constructs compared to TCPS, and LP, MP and HP constructs compared to 2D. OCN was increased on LP, MP and HP constructs compared to both TCPS and 2D sintered surfaces (Fig 1c,

bottom). VEGF was increased on all sintered constructs compared to TCPS control.

Discussion: Laser sintering was able to produce 2D and 3D porous Ti6Al4V constructs with low, medium and high porosities from a human trabecular bone template. Surface processing induced a combined micro-/nano- roughness on surfaces that has been previously perceived as favorable for osteoblast differentiation. A decrease in cell proliferation and increase in differentiation markers for both MG63 and hMSCs shows a favorable osteoblastic response to sintered constructs, although a reduced response was seen with hMSC cells compared to MG63 cells. Cell response also favored 3D constructs compared to 2D controls, suggesting structural parameters such as porosity, strut thickness and curvature may all contribute to osteoblast differentiation and maturation.

Acknowledgements: This study was supported by A.B. Dental.

Abstract accepted to 92nd Meeting of the Virginia Academy of Science In response to the Call for Presentation Title



Laser sintered titanium surfaces mimic trabecular bone structure and induce osteoblast differentiation in a porosity-dependent manner

Alice Cheng, Sharon L. Hyzy, MS, David J. Cohen, MD, Barbara D. Boyan, A. Humayun, PhD, Zvi Schwartz, PhD, DMDSchwartz, PhD, DMD.PhD, DMD.

ABSTRACT | An increasing number of orthopaedic and dental implants are being implanted and must successfully serve a longer lifespan. Selective laser sintering (SLS) is a form of additive manufacturing that can produce customized, porous titanium alloy implants with high resolution. We created 3D titanium surfaces with low, medium and high porosity based on a human trabecular bone template, which were further blasted and pickled to induce combined micro-/nano-roughness. We characterized the porosity (41-76%), surface chemistry (Ti, O and C being the three most prominent elements), wettability (62 ± 18 degrees), roughness and topography (showing combined micro-/nano-roughness). We then analyzed MG63 osteoblast response to surfaces. Cell viability

on surfaces with varying porosity was not significantly different. DNA (proliferation) and alkaline phosphatase specific activity (early osteoblast differentiation) decreased with increasing porosity, and osteocalcin (late osteoblast differentiation), osteoprotegerin (bone remodeling), VEGF (blood vessel formation), and BMP2, 4 (factors for creating an osteogenic environment) increased with increasing porosity. The most favorable cell response was shown on high porosity, high resolution surfaces. The results of the present study indicate that surface modification and three dimensional structure can enhance bone apposition and osseointegration.

Acknowledgements: This study was supported by A.B. Dental.



Laser Sintered 3D Porous Titanium Scaffolds Provide Appropriate Surface Properties for Improved Osteoblast Response

Alice Cheng, Sharon L Hyzy, David J Cohen, Barbara D Boyan, Zvi Schwartz

ABSTRACT | Titanium is a commonly used material for dental and orthopaedic implants that has good mechanical properties and high biocompatibility. However, osseointegration (close apposition of implant with bone) is greatly reduced in aging patients, diabetics, or smokers. Additive manufacturing provides complete control over implant porosity, which contributes to osseointegration, and cannot be achieved through traditional manufacturing methods. In this study, we used direct metal laser sintering to produce 3D porous titanium surfaces that mimic human trabecular bone porosity and have micro/nanoroughness. Surfaces 15mm in diameter and 4mm in height were manufactured in titanium from a human trabecular bone computed tomography template,

characterized with contact angle, xray photoelectron spectroscopy, laser confocal microscopy and microcomputed tomography, and analyzed for osteoblast (bone cell) response. 3D printed surfaces of commercially pure titanium can be customized with porosity ranging from 1570% open porosity, are hydrophilic, and have a combined micro and nanoroughness that has shown to be favorable for osteoblast differentiation and osseointegration. MG63 osteoblastlike cells were plated on surfaces and assayed for protein 24 hours after reaching confluence. Osteoblast response showed decreased DNA content and alkaline phosphatase activity (early marker of osteoblast differentiation) on surfaces with increasing porosity whereas osteocalcin, a marker

of welldifferentiated osteoblasts was increased. BMP4, a factor for creation of an osteogenic environment, increased with increasing porosity and compared to 2D control surfaces. Our results indicate that laser sintering can be used to custom manufacture implants with varying porosity and surface properties that increase osteoblast response, which may increase osseointegration in vivo.

Acknowledgements: This study was supported by A.B. Dental.



Wrap Implant

A. Cheng, A. Humayun, Barbara D. Boyan, Zvi Schwartz, PhD, DMD.

ABSTRACT | Introduction:

Edentulous patients (those lacking teeth) require one of two approaches to augmentation: inserting a vertical bone graft, or subperiosteally anchoring a device on which an implant can be attached. Bone grafts have had unpredictable results and can undergo resorption over time, compromising implant stability and success. As of the subperiosteal approach, current materials have not proven to directly integrate with the bone, in a process termed osseointegration. Therefore, we used additive manufacturing to create a titanium alloy surface with a specific roughness to determine if it would be osseoinductive in a challenging rabbit model over six weeks.


Materials and Methods: Additively manufactured titanium alloy wrap

implants (Figures 1 and 2) were acid etched and grit blasted and surgically affixed to the left tibia of 30 New Zealand White rabbits under institutional approval at the Medical University of Lodz (Lodz, Poland). Animals were euthanized at two weeks (n=3), three weeks (n=16), or six weeks (n=11) after surgery. Fixed samples were scanned by microCT and bone-implant contact calculated. Samples were then embedded in resin, and ground samples prepared. 28 of the implant samples remained intact and viable after processing and were then stained with Stevenel's Blue. Samples were photographed using Zen 2012 Blue Edition software with an AxioCam MRc5 camera and Axio Observer Z.1 microscope (Carl Zeiss Microscopy, Oberkochen, Germany). Bone-implant contact

(BIC) was calculated by dividing the bone contact perimeter by the total perimeter of the implant. Base and side BICs were also calculated by measuring the bone-facing sides (base) of the implant and outward facing sides of the implant. Statistics were derived using a one-way ANOVA test with a Tukey's post-test for significance and $p < 0.05$ considered significant.

Results and Discussion:

Osseointegration of the implants increased on all sides over time. Total BIC increased at each time point examined, and was significantly higher after 6 weeks than the earlier time points, both by microCT and histomorphometric measurements. Base and side BICs increased over time. At 2 weeks, cartilage can be seen growing toward the implant in areas where direct contact does not exist. After



3 weeks, the chondrocytes mature into a thin layer of bone, spreading from the implant holes. At 6 weeks, the bone establishes significant contact on the outward facing sides of the implant and has achieved good contact with the inward sides.

Conclusions: Here we demonstrate that using a titanium alloy implant with a specific surface roughness allows for satisfactory osseosynthesis and osseointegration, as well as the creation of vertical dimension without a bone graft. The use of the titanium wrap allows for osseointegration as early as 6 weeks after placement. These results suggest that this approach may be a novel way to achieve consistent vertical augmentation during implant placement, decreasing healing time and

allowing implants to be loaded sooner.

Acknowledgements: This study was supported by A.B. Dental.



Osseointegration Capability of Direct Metal Laser Sintered Titanium Implants With Unique Surface Characterization: An In Vitro and In Vivo Evaluation

Sharon L. Hyzy, David J. Cohen, Ryan Clohessy, Alice Cheng, Barbara D. Boyan, Zvi Schwartz


ABSTRACT | Introduction: More than 500,000 dental implants are placed each year in the United States. Success rates are 95% for healthy patients, but are dramatically reduced in the elderly and compromised patients. Titanium (Ti) is commonly used as a dental implant material because of its good biocompatibility and mechanical strength. Ti implant surfaces modified with combined micro- and nano-scale surface roughness and with high wettability have greater osteoblast differentiation and improved bone-implant contact in comparison to smooth implants. As an alternative to traditional, subtractive manufacturing methods, additive manufacturing methods such as laser sintering have increased efficiency and decreased waste, while maintaining good spatial

resolution of 3D implant features. Additive manufacturing methods combined with simple surface treatments of grit blasting and acid etching can produce a unique implant. The purpose of this study was to analyze effects of a 3D laser sintered titanium implant surface with combined micro-/nano-roughness and wettability in vitro and in a novel in vivo model of bone formation and osseointegration.

Materials and Methods:

Disks 15mm in diameter were manufactured using direct metal laser sintering. Ti alloy particles (24-45 μm diameter) were sintered with an ytterbium laser using a spot size of 0.1mm at 1054nm, continuous power of 200W, and a scanning rate of 7m/s. Disks that were machined (M), laser sintered machined (M-LST), laser sintered blasted with CaPO₄ (LST), and

acid etched LST (A-LST) were used for in vitro studies. The disk surfaces were characterized for topography with scanning electron microscopy (SEM), roughness with laser confocal microscopy, and wettability with sessile drop contact angle. MG63 osteoblast-like cells were plated at 20,000 cells per surface and assayed for DNA, alkaline phosphatase (ALP) specific activity, osteocalcin (OCN), BMP2, VEGF, FGF2, and integrins $\alpha 2$ and $\alpha 1$ (ITGA2, ITGB1). Implants 3.7mm in diameter and 8mm in height were implanted in 8 male New Zealand white rabbits (4 \pm 0.25kg) to evaluate osseointegration. A-LST implants were placed in the right femur and machined/ CaP blasted clinically used implant was placed in the contralateral leg. Morphometric analysis of bone-implant contact and mechanical



testing were performed after 3 and 6 weeks' post-operative. Tensile testing was performed with an MTS Insight 30 using a custom fabricated sample holder opposite a 30 KN load cell at 1mm/min.

Results and Discussion:

Microtopographic features were visible by SEM on LST surfaces, while A-LST surfaces had nanotopographic features overlaid on microtopographic surfaces visible at high magnification. Quantitative roughness (Ra) values of $3.37 \pm 0.62\mu\text{m}$ and peak-to-valley height (Sz) of $62.74 \pm 9.81\mu\text{m}$ were obtained for LST disks. LST surfaces were also hydrophilic, exhibiting contact angle of 34 ± 7 degrees. DNA was higher on all surfaces compared to the M group. ALP was higher on LST and A-LST compared to machined disks. OCN increased in a surface

roughness-dependent manner. BMP2 and ITGA2 were higher on all surfaces compared to M, and higher on LST and A-LST compared to M-LST. VEGF increased on LST and A-LST compared to M group only. FGF2 increased on LST and A-LST compared to both M and M-LST. ITGB1 increased on all surfaces compared to M, and A-LST compared to M-LST. MicroCT analysis of bone-implant contact of implants retrieved after 6 weeks of implantation revealed no significant differences between control and experimental implant groups in the superior cortical, inferior cortical or trabecular bone. Histomorphometric analysis demonstrated significant difference in bone-implant contact between the A-LST vs M-LST in the cortical portion implants retrieved at three weeks, as well as in the cortical

and total bone-implant contact of implants retrieved at 6 weeks. Mechanical testing demonstrated no significant difference at the force of failure between the M-LST and A-LST during pull out testing.

Conclusions: We produced implants by additive manufacturing that, after surface treatment by grit blasting and acid etching, yielded a unique surface with combined micro-/nano-roughness and lower wettability than conventional implants. These surfaces enhanced osteoblast response, induced cells to produce local factors in vitro and improved the osseointegration process in vivo.

Acknowledgements: This study was supported by AB Dental.

Acknowledgements: This study was supported by A.B. Dental.



Osteoblast Response and Osseointegration of Direct Metal Laser Sintered Titanium Implants

Sharon L. Hyzy, David J. Cohen, Alice Cheng, Barbara D. Boyan, Zvi Schwartz

ABSTRACT | Statement of Purpose:

Dental implants are placed in over 500,000 people each year in the United States, most of which are successful [1]. However, dental implant failure rates increase dramatically for the elderly, patients with diabetes, a history of smoking, or are otherwise compromised [2]. Titanium is a commonly used material in dental implants, with good biocompatibility and mechanical strength. It has been shown that titanium implant surfaces modified with combined micro and nano surface roughness increase osteoblast differentiation, which can lead to improved implant osseointegration [3]. However, traditional manufacturing methods produce surfaces that require a series of additional treatments to induce roughness. 3D additive manufacturing methods such as

laser sintering have increased efficiency and decreased waste, while maintaining good spatial resolution. The purpose of this study was to analyze effects of a 3D laser sintered titanium alloy implant surface with combined micro-/nano-roughness in vitro and in a novel in vivo model.

Methods: Disks 15mm in diameter and 1mm in height and screws 3.7mm in diameter and 8mm in height were manufactured using direct metal laser sintering. Titanium alloy (Ti6Al4V) particles 24–45 μm in diameter were sintered with a ytterbium laser spot size of 0.1mm at 1054nm, continuous power of 200W and scanning rate of 7m/s. Surfaces were characterized for topography with scanning electron microscopy (SEM), chemistry with x-ray photoelectron spectroscopy (XPS) and energy

dispersive x-ray spectroscopy (EDX), roughness with laser confocal microscopy, and wettability with sessile drop contact angle. Machined disks (M), laser sintered machined disks (M-LST), laser sintered disks blasted with CaPO_4 (LST) and laser sintered disks blasted with CaPO_4 particles and acid etched (A-LST) were used for in vitro studies. MG63 osteoblast-like cells were cultured at 20,000 cells per surface and assayed for DNA, alkaline phosphatase (ALP) specific activity, osteocalcin (OCN), bone morphogenetic protein 2 (BMP2), vascular endothelial growth factor (VEGF), fibroblast growth factor 2 (FGF2), integrins α_2 and β_1 (ITGA2, ITGB1). OCN, OPG and BMP2 were also analyzed from normal human osteoblast (NHOB) cultures. For in vivo studies, 8 male New Zealand white rabbits

4±0.25kg in weight were implanted with a laser sintered implant in the left femur and a control implant in the contralateral bone. Micro-computed tomography (micro-CT) was used to analyze bone-to-implant contact after 6 weeks of implantation. After production, SEM revealed LST surfaces had a rough microtopography, while A-LST surfaces also included a fine nanotopography at high magnification. Quantitative roughness (Ra) values of 3.37±0.62µm and peak-to-valley height (Sz) of 62.74±9.81µm were obtained for LST disks. LST surfaces were also hydrophilic, exhibiting contact angle of 34±7 degrees. XPS analysis showed that titanium (87.8±0.5%), aluminum (8.3±0.7%) and vanadium (3.9±0.2%) were the three most dominant elements, although calcium and phosphorous were also revealed through EDX analysis of A-LST surfaces due to the surface treatment. For MG63 cells, DNA was elevated on all surfaces compared to the M group. ALP activity was increased on LST

and A-LST compared to both M and M-LST. OCN increased on all groups with increasing surface roughness. BMP2 and ITGA increased on all surfaces compared to M, and increased on LST and A-LST compared to M-LST. VEGF increased on LST and A-LST compared to the M group only. FGF2 increased on LST and A-LST compared to both M and M-LST. ITB1 increased on all surfaces compared to M, and A-LST compared to M-LST. Expression of OCN, OPG and BMP2 by NHOST cells increased in a roughness-dependent manner on M, M-LST, LST and A-LST surfaces. Micro-CT analysis of bone-to-implant contact of implants retrieved after 6 weeks of implantation revealed no significant differences between control and experimental implant groups in the superior cortical, inferior cortical or trabecular bone, although differences may have been obscured by the implant shadowing.

Conclusions: 3D laser sintering is a method of producing titanium alloy surfaces and implants that are inherently hydrophilic and can be modified for varying

surface roughness. Surfaces with combined micro-/nano-roughness enhanced osteoblast response and have potential for increased osseointegration in vivo.

References: 1 American Academy of Implant Dentistry
2 Moy PK. Int J Oral Max Impl. 2005;20(4):569-577.

3 Gittens RA. Biomaterials. 2011;32(13):3395-3403

Acknowledgements: This study was supported by A.B. Dental.



Osteoblast Response to 3D Porous Titanium Manufactured by Laser Sintering with Multi-Scale Roughness Mimicking Trabecular Bone

Alice Cheng, Sharon L. Hyzy, MS, David J. Cohen, MD, Barbara D. Boyan, PhD, Zvi Schwartz, PhD, DMD.

ABSTRACT | Introduction:


Although it has been shown that multi-scale roughness is able to increase osteoblast response in vitro and osseointegration in vivo, many solid orthopaedic implant materials such as titanium (Ti) have different mechanical properties than bone, contributing to stress shielding in addition to decreased osseointegration for at-risk patients [1, 2].

Varying macro/micro porosity allows the implant to be tailored to better mimic the host bone's mechanical properties, and has been shown to reduce stress shielding in clinical cases [1]. However, top-down or bulk manufacturing methods do not provide complete control over an implant's porosity, shape and size. Selective laser sintering achieves a micro-scale resolution

that can be manufactured from the bottom-up, producing porous surfaces that are further able to be roughened by chemical treatment to enhance osseointegration [3]. In this study, we used laser sintering combined with chemical treatment to manufacture Ti scaffolds with multi-density trabecular-like porosity from original patient CT scans of trabecular bone, and study their effect on osteoblast proliferation and differentiation.

Methods: CT scan of a human femur retrieved from a hip replacement procedure was used to create a porosity template for disk production. Original bone porosity was rotated and superimposed upon itself 12, 24 or 36 times to create disks with high, medium and low porosities, respectively. Porous disks 15mm in diameter and 5mm

in height were produced with commercially pure grade 2 titanium particles 24-45 μm in diameter with a ytterbium fiber laser system, wavelength of 1054 nm, continuous power of 200W, scanning rate of 7 m/s, and laser spot size of 0.1mm. After production, disks were blasted with CaPO₄ particles, acid etched with HNO₃ and rinsed in distilled water and methanol. Finally, disks were pickled in a mixture of NaOH and H₂O₂, then with HNO₃ before rinsing in distilled water and drying for 24 hours. Scanning electron microscopy (SEM) was used to evaluate surface topography, x-ray photoelectron spectroscopy (XPS) to evaluate the surface chemistry, contact angle on the underside of disks as a proxy for surface wettability, laser confocal microscopy (LCM) to evaluate macro- and micro-roughness,



and microCT to evaluate porosity. MG63 osteoblast-like cells were seeded on disks at a plating density of 60,000 cells/disk and cultured until confluence on a TCPS control, without the use of differentiation media. DNA, alkaline phosphatase specific activity (ALP) and bone morphogenetic protein 4 (BMP4) were measured as markers of osteoblast proliferation, differentiation and production of osteogenic factors. All measurements were performed with at least $n=6$ per disk and significance is noted at $p<0.05$ according to 1way ANOVA with Bonferroni correction.

Results: SEM images visually confirmed differences in porosity at the macro scale, while showing similar roughness for high and medium porosity groups at the micro-scale. Nano-scale features were formed on surfaces after pickling treatment. XPS showed high levels of oxygen, carbon and titanium on all surfaces, followed by trace amounts of nitrogen, calcium, phosphorus and aluminum. Contact angle results showed neutral to moderate hydrophilicity on

high porosity surfaces, and high hydrophilicity on medium and low porosity surfaces. microCT evaluations revealed porosities of $65.2\% \pm 3.3\%$ for high porosity samples, $27.6\% \pm 1.8\%$ for medium porosity samples, and $7.4\% \pm 0.8\%$ for low porosity samples. Osteoblast growth on the different surfaces showed significantly decreased DNA with decreasing porosity when compared to TCPS. ALP activity was lower on high and medium porosity surfaces and similar on high porosity surfaces when compared to TCPS. BMP4 level was similar to TCPS with a significance increase in BMP level as porosity decreased.

Discussion: Characterization of 3D scaffold (porous) Ti disks revealed similar topography at the micro- scale, while roughness, chemistry, wettability and porosity varied at the macro-scale. Surface treatment was able to induce roughness at the micro- and nano-scale, which has been shown to be desirable for increasing osteoblast proliferation and differentiation [2, 4]. These results indicate that the combination of macro three

dimensional structure with the correct micro/nano-roughness decreases cells proliferation and increases cell differentiation concomitant with increased local factor production, indicating induction of bone formation and osseointegration.

Significance: Selective laser sintering allows implant design and porosity to incorporate the patient's own bone structure through a CT scan. This method has the ability to produce customized implants for patients with 3D structure and correct porosity, while reducing material waste in the manufacturing process. Moreover, surface treatment to induce micro- and nano-roughness on implants result in the combination of macro and micro/nano structure, which will support osteoblastic differentiation, increased production of local factors important for creating an osteogenic environment and as a whole will enhance bone formation and osseointegration.

Acknowledgements: This study was supported by A.B. Dental.



termis

Porosity and Surface Features of Additively Manufactured “Trabecular Titanium” Constructs Affect Osteoblast Phenotype

Alice Cheng, Aiza Humayun, David J. Cohen, Barbara D. Boyan, Zvi Schwartz

ABSTRACT | Problem: Decreased osseointegration in compromised patients leads to dental and orthopaedic implant failure. Porous implants have shown good biological response but porosity is difficult to customize.

Objective: To investigate the effect of porosity and surface features of 3D Ti-6Al-4V constructs manufactured from a trabecular bone template.

Methodology: Human trabecular bone was used as a template to laser sinter low (LP), medium (MP) and high porosity (HP) constructs with low (LD) and high detail (HD). Ti-6Al-4V disks had 15mm diameter and 5mm height, and micro-/nano-roughness after surface treatment. Compressive modulus, surface chemistry, porosity, topography, roughness and wettability were analyzed. MG63 cells were

analyzed for DNA, protein, alkaline phosphatase specific activity (ALP), osteocalcin (OCN), vascular endothelial growth factor (VEGF) and bone morphogenetic protein 2 (BMP2).

Results: Construct porosities ranged from 41% to 76% with complete interconnectivity. Surface roughness at the micro-scale was not significantly different among 3D constructs. O, C, and Ti were most common surface elements. Contact angle on 2D surfaces was 62 degrees. Osteoblast response increased for HD constructs compared to 2D and 3DLD. DNA and ALP activity was decreased on HDLP and HDMP constructs, while OCN, VEGF and BMP2 were elevated. 3DHD constructs showed more than a sevenfold increase in expression of certain factors when compared to TCPS and 2D

controls, indicating the effect of 3D, porosity and structure detail on cell response.

Significance: Laser sintering can produce 3D porous Ti-6Al-4V constructs with trabecular bone detail. Surface and structural features enhance osteoblast response, suggesting osseointegration in vivo.

Disclosures: ZS is a consultant for AB Dental.

Acknowledgements: This study was funded by AB Dental and the National Science Foundation.



TEL +972-8-8531388 | FAX +972-8-8522562 | www.ab-dent.com